NON-LINEARITIES IN METAL CONTACTS AT MICROWAVE FREQUENCIES

by

F. ARAZM

A thesis presented for the degree of Doctor of Philosophy in the Department of Electronic and Electrical Engineering, University of Sheffield.

September 1978

CONTENTS

ABSTRACT

Starting with a comprehensive literature survey, the work reported in the thesis consists of a mathematical analysis and then measurements of the 3rd- and 5th-order intermodulation products produced by the non-linearities of a large number of various metal contacts.

The experimental study concentrated on the intermodulation products generated at the contacting faces between similar and dissimilar metals and included contact materials of copper, beryllium copper, brass, oxygen free copper, oxygen free nickel, mild steel, stainless steel (EN58B), duraluminium and twelve home-made steels with various compositions.

The measurements were carried out for the first time at L-band frequencies on a good experimental arrangement.

The fundamental excitation frequencies were $f_1 \approx 1.3$GHz and $f_2 \approx 1.7$GHz and the 3rd- and 5th-order intermodulation products were $2f_2 - f_1 \approx 2.1$GHz and $3f_2 - 2f_1 \approx 2.5$GHz respectively.

The quantitative studies were mainly concerned with the variation of the 3rd- and 5th-order intermodulation product levels with the power levels of the fundamental signals and with the axial force applied to the contact.

ACKNOWLEDGEMENTS

The investigations reported here have been carried out in the Department of Electronic and Electrical Engineering at the University of Sheffield.

The author is indebted to Professor F.A. Benson, for the facilities provided in the laboratories of his Department and for his patience and constant guidance throughout his supervision of this project.

A debt of gratitude is acknowledged to Dr. J.M. West of the Department of Metallurgy for his valuable advice in electroplating. The author wishes also to acknowledge a debt of gratitude to Dr. A.R. Entwishe of the Department of Metallurgy for his technical advice in electropolishing the test sample pairs.

Grateful thanks are due to Dr. J. Beach of the Department of Metallurgy for his invaluable help in arranging for the production of various special steels. The author wishes to thank Mr. G. Glossop for analysing the many various samples of test materials.

The author's gratitude is also extended to :

(i) Messrs. H. Flower, A.W. Clarke and all their colleagues, in particular Mr. J. O'Neill in the Departmental workshops for their skill and technical advice in the construction of certain items of equipment and many test sample pairs required for the study.

(ii) Mr. E. Needham of the Department of Metallurgy for the production of various steels.

(iii) Mrs. D. Grayhurst for her patience and diligence in typing the thesis swiftly and accurately.

LIST OF PRINCIPAL SYMBOLS

f	Frequency
B	Magnetic flux density
H	Magnetic field intensity
C_i	Constant where $i = 1,2,...$
$f_{I.P.} = \sum_{i=1}^{n} C_i f_i$	I.P. frequency
a_k	Constant where $k = 1,2,...$
$N = \sum_{i=1}^{n} \lvert C_i \rvert$	Integer, order of I.P.
n	Integer, number of inputs of a non-linear device
L	Integer
C_p	Integer, where $p = 1,2,...,n$
q_p	Integer, where $p = 1,2,...,n$
k	Positive integer
s	Insulating film thickness
S	Axial force (N)
ψ	Work function of metal electrode (vacuum level of metal)
η	Fermi level
ϕ	Barrier height at the interface of metal and insulator (distance between bottom of the insulator conduction band and the Fermi level and the metal)
J	Tunnel current density
V	Voltage across the film
ν	Poisson's ratio
ε_r	Relative dielectric constant
μ_r	Relative permeability
ρ	Electrical resistivity
R_o	Characteristic resistance of a transmission line
$\omega = 2\pi f$	Angular frequency

LIST OF ABBREVIATIONS

I.P.	Intermodulation product
V.H.F.	Very high frequency
U.H.F.	Ultra high frequency
L-band	1GHz to 2GHz
S-band	2GHz to 4GHz
C-band	4GHz to 6GHz
R.F.	Radio frequency
C.L.A.	Central line average
B.P.F.	Band pass filter
T.E.M.	Transmerse electromagnetic mode
W	Watt
mW	Milli-Watt
μW	Micro-Watt
dB	10^{-1} Bel
dBm	10 log(1mW/1)
dBW	10 log(1W/1)
kHz	10^{3}Hz
MHz	10^{6}Hz
GHz	10^{9}Hz
P.T.F.E.	Polytetrafluorethylene
λ_{air}	Wavelength in free space
W_{arm}	Width of an arm of the rat-race
W_{ring}	Width of the ring of the rat-race
Z_{arm}	Input impedance of an arm of a rat-race
Z_{ring}	Impedance of the ring of a rat-race
P	Magnitude of R.F. power (W)
p	Magnitude of R.F. power (dBW)
$P_{I.P.}$	Magnitude of I.P. (W)
$P_{I.P.}$	Magnitude of I.P. (dBW)

CHAPTER 1

1. INTRODUCTION AND SURVEY OF PREVIOUS WORK

1.1 Introduction

The ease of installation and other mechanical considerations have made the use of coaxial cables very popular in modern military communication, particularly aboard ship or aircraft as the feeder system, short jumper connectors etc.

There are many different sources of non-linear generation of components that may cause interference to the reception of wanted signals in a co-located transmitter-receiver system. Such sources may be associated with the transmitter power amplifier, multicouples, antennas and of course coaxial cable feeder systems and associated connectors especially "rusty" connectors due to their inherent non-linear properties at microwave frequencies.

In general, if n different unmodulated fundamental frequencies, f_1, f_2, ...f_n are incident upon a device with a non-linear characteristic, then not only harmonics of each different frequency are produced but also an infinite number of intermodulation products (I.P.'s) are generated. The non-linearity may be non-linear B-H characteristics of steel or non-linear i-v characteristics of contacts or semi-conductors.

An I.P. is defined as :

$$f_{I.P.} = \sum_{i=1}^{n} c_i f_i$$

where c_i is an integer which can be positive, negative or zero.

Then

$$\sum_{i=1}^{n} |c_i|$$

signifies the order of the I.P., therefore for n different unmodulated fundamental frequencies there are an infinite number of I.P.'s. As an example the number of 3rd-order I.P.'s with n fundamental frequencies is given by n^3-n^2.

For narrow-band systems where the upper and the lower frequency limits are not too far apart, the even-order I.P.'s, such as 2nd-order will fall well outside the bandwidth. However, the lower odd-order I.P.'s will present the greatest problem in narrow-band systems, causing nuisance interference with the reception signals. Hence the frequencies at which they occur must be excluded from a frequency assignment plan. In a frequency-agile system which is essential for U.H.F. and microwave frequency communication, the planning of frequency assignments can be prohibitively complicated as a result of such restrictions.

The object of this project was, firstly, to construct a basic microwave circuit, suitable for measurement of I.P.'s at L-band frequencies, and secondly to reduce the residual level (residual level is defined as the I.P. power level observed when there is a single piece, see Fig.4.1, at the test location) with the use of coaxial cables having silver-plated wire-braided outers as dummy loads. The experimental work was concerned with the investigation of I.P. generation at metal-to-metal interfaces of a large number of metals under various surface conditions such as mechanically and electrically polished, electro-plated.

This thesis reports measurement of 3rd- $(2f_2-f_1)$ and 5th- $(3f_2-2f_1)$ order I.P.'s resulting from two unmodulated fundamental signals f_1 = 1.296GHz and f_2 = 1.698GHz.

1.2 Survey of Previous Investigations

This section is devoted to the presentation of a brief outline of the work reported and conclusions drawn by previous investigators in the general field of interference due to intermodulation products in the V.H.F., U.H.F. and microwave frequency regions. At first a brief survey is given of various methods for evaluating I.P.'s at the output of a non-linear device without memory.

1.2.1 Survey of various methods for evaluating I.P.'s

In seeking to evaluate the output of a non-linear device it is necessary to distinguish between those non-linearities which can be defined with reasonable accuracy by a limited order polynomial, and those which are discontinuous.

1.2.1.1 Sea Ronald, G.[1]

The output of the non-linear device as a power series function of the input, which consists of a sum of cosine waves of different frequencies is expressed by Sea. He has derived an equation which gives the amplitude of any particular frequency component in the output of a non-linear device described by a power series (see Appendix I). For higher-order polynomials and multiple inputs a simple programmable method has been described which applies some mathematical hygiene to the more straightforward approach.

1.2.1.2 Bennett, W.R.[2]

A method of computing I.P. at the output of a non-linear device with discontinuous characteristics by means of multiple

Fourier series is described by Bennett. His analysis applied specially to the case of two frequencies applied to a modulator of the "cut-off" type; i.e. a modulator which operates by virtue of its being insensitive to input changes throughout a particular range of values. Using a trigonometric integral method for a simple rectifying characteristic when two frequencies are applied, a general equation which gives the amplitude of any particular frequency component is derived by Bennett (see Appendix II). In Appendix II, the case of no noise for a half-wave linear rectifier is mentioned.

1.2.2 Survey of previous studies

This section presents a brief outline of the work reported and conclusions drawn by previous investigators in the V.H.F., U.H.F. and microwave frequency regions.

1.2.2.1 Foster, D.E.[3]

Foster has investigated the types of interference encountered in radio reception and concluded that the interference of signals from two or more radio stations was caused by some agencies external to the receiver and termed this "External Cross-Modulation". He observed that the generation of I.P.'s arising from multiple radio signals present in a locality were enhanced by the presence of power wiring, poor connection between two metallic bodies such as lighting or in piping or even in an antenna. He also obtained expressions for various components of the output when a non-linear medium was subjected to signals having two different frequencies.

1.2.2.2 Ebel, A.J.[4]

Ebel has given an account of the sources of I.P.'s in the high frequency radio communication band. He has measured

I.P.'s generated from fundamental frequencies of 580kHz and 1370kHz with powers of 5000W and 250W respectively.
He concluded that :

1. The most "spurious radiation" in the field of two strong signals was generated in the receiving antenna system. The solution to the problem seemed to be an antenna system balanced against the ground either using a loop or a matched transmission line.
2. The probability of a receiving antenna generating I.P.'s depends on the extent of the non-linearity of the impedance, the effective heights of the conductors and the impedance of the conductor at intermodulation frequency as well as upon the field product.

1.2.2.3 Blake, K.W.[5]

Blake carried out a series of experiments aboard a ship. The number of workable channels available in the band was much smaller than was the case ashore, where grouped transmitters and receivers were set up on well separated sites. He concluded that, this was due to the generation of 3rd-order I.P.'s. Experiments carried out proved that the effect was due to external cross-modulation arising in parts of the ship's structure such as loose antenna rods which acted as non-linear conductors, and not, as he initially thought, by the close proximity of the antennas. He reported that the levels of interference vary as much as 26dB in 2 hours. Blake also observed that generation of the interference signals due to corroded metals could be reproduced by touching any two pieces of corroded metals together and the effect is significant if the length of these corroded joints approached a half wavelength or multiple thereof.

1.2.2.4 Reiffen, B. and Grazel, A.I.[6]

Reiffen and Grazel measured 2nd-, 3rd-, 4th- and 5th-order I.P.'s generated in a passive U.H.F. transmission system at moderate power levels. They observed that since 2nd- and 3rd-order I.P.'s did not qualitatively behave in the same way with the power level, their levels were approximately of the same order of magnitude ranging from -140dB to -110dB below the input power levels, with each signal giving 100W. The 4th-order I.P. was not detectable, while the 5th-order was at -160dB below the fundamental frequency power level.

The authors reported that physical metal-to-metal contacts were the primary source of generation of I.P.'s and loose connector-cable interfaces were the source of I.P. generation in cable-connector assemblies.

1.2.2.5 Löw, V.W.[7]

A comprehensive investigation for I.P.'s generated due to the non-linear behaviour at metallic contacts has been undertaken by Löw. He measured the 3rd-order $(2f_1-f_2)$ I.P. for signal frequencies f_1 = 4.021GHz and f_2 = 4.156GHz at input power levels of about 4W from each source.

Löw measured I.P.'s generated at metal-to-metal interfaces of silver, gold, copper and aluminium, investigating the effect of contact pressure and the amplitude of the current flowing through the contact on the I.P.'s power level. He divided the contacts into two groups according to their geometric form, namely surface contacts and point contacts.

Löw's experimental and theoretical work led to the following conclusions :

1. The level of I.P.'s increase by increasing input power level.

2. At practically zero contact load, all metal-to-metal contacts generated high 3rd-order I.P.'s (80-90dB below input power) and an increase in contact load resulted in a sharp (for silver-to-silver) or a gradual (for aluminium-to-aluminium) decrease of I.P.'s.
3. The amplitude of the 3rd-order I.P.'s for small and medium contact load (i.e. between 0∿9N) is proportional to the cube root of the contact load and inversely proportional to the size of the current carrying contact area.
4. The 3rd-order I.P.'s power was proportional to the cube of the input signal level (provided $P_{10} = P_{01}$).
5. Among the materials examined, silver contacts produced the lowest I.P. power and aluminium contacts produced the largest distortion level.
6. Separation and repositioning the contacts at the same contact load and signal level, changed the I.P. level to about 60dB.
7. Soldered joints were I.P. free.
8. Flexible waveguide and waveguide flanges generated I.P.'s of peak levels -90dB under various conditions.

1.2.2.6 Rutz-Philipp, E.M.[8]

For the investigation of interference phenomena, Rutz-Philipp has derived the equivalence between the lumped-element and a microwave circuit. He has related interference phenomena on ships and other vehicles to corroded joints on support structures and reported that such joints exhibit frequency conversion properties similar to the property of

non-linear resistive elements. He assumed the i/v characteristic of a non-linear resistive element can be approximated by an exponential function and then he expressed the functional relationship between the current and the generator voltage as a power series (see Appendix III). He evaluated $H_k(z)$ (see Appendix III.4) for typical values of the constants γ, I_o of a non-linear resistor and for typical values of a linear resistor $R = 2R_o$ in the circuit and found that :

1. The magnitude of polynomials $H_k(z)$ is determined by all three constant parameters, γ, I_o and $2R_o$.
2. The polynomials are not all positive but alternate between positive and negative values. For a small value of k they are positive and very small and become larger as k increases, reach a maximum value, decrease and become negative. Then when k is further increased, the polynomials $H_k(z)$ go through negative and positive cycles of increasing amplitude.
3. In the series representation of the Fourier coefficients of current components (see Appendix III.6), where the polynomials $H_k(z)$ are weighted by the contributions of the amplitudes of the incident waves, $(E_{10} \& E_{01})$, to the current components, the weighting factors have the effect of damping the alternating cycles of positive and negative values of the polynomials.
4. The current component at the lower order intermodulation frequencies will always be larger than the current component at the higher order intermodulation frequencies.

5. The power at the lower order intermodulation frequencies increases faster than the power at the higher order intermodulation frequencies.
6. The maximum power at the lower order I.P.'s will be obtained at a higher incident power level than the maximum of power at the higher order I.P.

1.2.2.7 Cox, R.D.[9]

Cox measured 3rd-, 5th- and 7th-order I.P.'s generated in the waveguide circuitry of a 6GHz diversity communication system. His investigation was concentrated on the effect of transmitter frequency separation. According to Cox's observation I.P.'s generated in ferrite components, attenuators and dummy loads were steady, whereas loose metal-to-metal surfaces and contacts such as in waveguide joints or loose protruding screws used for tuning or impedance matching in waveguides produced strong and erratically changing I.P. levels. In his investigation he used two transmitters each having an output power between 1W and 1.5W. For most of the ferrite components, he examined the 3rd-order I.P.'s level was steady at about -90dBm when using two 1W transmitters, whereas for the same amount of input power, I.P. powers as high as -25dBm were detected in loose waveguide joints, tuning and matching scre s. Cox concluded that I.P. levels are independent of changes in transmitter frequency and its frequency separation.

1.2.2.8 Mason, H.P.[10]

Field tests concerning I.P.'s have been undertaken in the past by Mason. He carried out a series of experiments on board a ship and observed that the residual I.P. levels

present in naval communication complexes varied considerably from day to day. He attributed these variations to the changing atmospheric conditions such as humidity, temperature and pressure. He also pointed out that the main source of non-linearity causing the generation of I.P.'s was the corrosion layers between the parts of the hull and super-structure of the ship.

1.2.2.9 Ebenezer, D.R. and Betts, J.A.[11,12]

A general investigation of intermodulation interference caused by the external environment in a mobile communication system was carried out by Ebenezer and Betts with the H.F. range. They measured 3rd-order I.P.'s at 7.5MHz, 11.4MHz, 2.7MHz and 9.0MHz, where f_1 = 1.2MHz and f_2 = 5.1MHz were the fundamental frequencies. They also carried out a laboratory based study which was mainly concerned with the generation of I.P.'s in clean (non-oxidized) ferromagnetic specimens. Studies were carried out to observe the effect of surface preparation and slight changes to chemical composition of structural steels, especially those used in ship construction, on the generation of I.P.'s.

They pointed out that two major mechanisms in the external environment were responsible for the production of I.P.'s.

(i) Non-linear B-H characteristics of steels.

(ii) Non-linear characteristics of metal-oxide films between metal-to-metal interfaces.

Results of laboratory investigations led to the following conclusions :

1. Composition of steel plays an important role in the generation of I.P.'s. A reduction of 10-15dB could be achieved by using special steels. Addition of small quantities of Cr and Ni in steels e.g. a 3% Cr - 3% Ni steel, improved the 3rd-order I.P. level by 10-12dB. Small additions of Si and Al had negligible effect upon the I.P.'s level.
2. I.P.'s were linearly dependent on the bulk of steel, i.e. a larger amount of steel produces a higher level of I.P.'s.
3. Conducting coating on steel caused a considerable decrease in I.P. level. A coating thickness of 5.08×10^{-3}mm (0.2×10^{-3}in.) of Cd caused a reduction of 10-15dB and a 101.6×10^{-4}mm (4×10^{-4}in.) thick coating of Zn reduced the 3rd-order I.P.'s level by 25dB.
4. The presence of surface corrosion increased the level of I.P.'s. An oxidized metal-to-metal interface in a high current density situation, caused a dramatic increase in the overall I.P.'s levels.

1.2.2.10 Bayrak, M. and Benson, F.A.[13,14]

A detailed investigation of I.P.'s generated by non-linear effects in coaxial connector mating faces, coaxial cable to connector interfaces, coaxial cable braided outer conductors and contacting faces between similar and dissimilar metals under various conditions have been made by Bayrak and Benson at S-band frequencies. They measured 3rd-order I.P.'s $(2f_2-f_1)$ and 5th-order I.P.'s $(3f_2-2f_1)$, resulting from two fundamental signals about a centre frequency of 3GHz with a

minimum frequency separation of 400MHz. An experimental set-up was designed and constructed with a view to isolate the sources of intermodulation products and assess the variation of their amplitudes under various conditions. In the case of metallic contacts, contact materials of copper, brass, beryllium-copper, nickel, aluminium, stainless steel and mild-steel were used, also electroplated metal contacts of gold, silver, rhodium, copper and tin were tested. They studied metal-to-metal contacts under three groups according to their geometric construction, namely surface contacts, spherical and point contacts. They also carried out a few preliminary measurements on a variety of waveguide components.

Bayrak and Benson drew the following conclusions from their work :

1. Among the materials tested, mild steel, aluminium and stainless steel exhibited the strongest 3rd-order and 5th-order I.P.'s in the case of similar and dissimilar metal-to-metal contacts.
2. The lowest I.P.'s levels were generated with copper, brass, beryllium copper and nickel contacts.
3. Dissimilar contacts of steels or aluminium with any other materials examined generated I.P.'s, which were either high or of an intermediate value.
4. Similar or dissimilar metal-to-metal contacts of electroplated gold, silver, rhodium, copper or tin did not exhibit strong I.P.'s.
5. The largest 3rd- and 5th-order I.P. power levels were obtained for a very low contact load, regardless of the contact shape or composition of the specimens used.

6. The I.P. power levels were more susceptible to variation in contact load for the point contacts than in the case of surface or spherical contacts.
7. In general, surface contacts generated lower I.P. power levels than any other types of contacts.
8. A properly soldered similar or dissimilar metal-to-metal contact did not generate any detectable I.P. power.
9. Oxidized metal surface produced higher I.P. levels than their unoxidized counterparts.
10. The variation of I.P. power level with the total R.F. power level does not obey the predicted variation using "polynomial approximation technique" but any increase and/or decrease in R.F. power level causes increase and/or decrease respectively in the I.P. power level.
11. Non-linearity in the contact resistance has the most responsibility for generation of I.P.'s when currents of different frequencies flow partially or fully through them.
12. Solid jacketed cables with single-wire inner conductors did not exhibit detectable I.P.'s.
13. Braided cables with low filling factors generated strong erratic I.P. levels, particularly under flexed conditions.
14. The cable connector transitions, connector mating junctions and waveguide flange interfaces are the most serious of generating I.P.'s power levels along a transmission line.

1.2.2.11 Sanli, H.[15]

Sanli carried out a continuation of Bayrak's work. He measured the 3rd- and 5th-order I.P.'s in S-band frequencies. Primarily, Sanli improved Bayrak's measuring set up by bringing down the residual level with the use of a coaxial cable having silver-plated wire-braided outers as dummy loads instead of commercially available loads. His investigation included the generation of I.P. at metal-to-metal interfaces under various surface conditions, such as mechanically polished, electropolished, oxidized etc.

The following conclusions were drawn from his study :

1. The behaviour of point and spherical contacts, strongly suggests that high current densities are involved to generate strong I.P.'s.
2. Mechanically micro-polishing or electro-polishing of the contacting faces improved non-linearity greatly, especially in steels and nickel contacts.
3. The power level of I.P. is proportional to power "n" of R.F. power level. The value of "n" is different for each material and is also dependent on axial force. For materials tested "n" varied between $2 \sim 3$ for both 3rd- and 5th-order I.P.'s.
4. The non-linear process which caused the generation of I.P.'s in the metallic contacts was resistive and not capacitive.
5. High conducting oxide films are the most serious cause of non-linearity.
6. Material which has composite multi-layer oxide films is more susceptible to I.P. generation.

Sanli's work further confirmed most of the observations made by Bayrak, with the only contradiction that nickel was among the materials which generated a very high level of I.P. powers.

CHAPTER 2

2. MEASURING EQUIPMENT

2.1 Introduction

Third- and fifth-order I.P.'s generated at contacts due to the simultaneous application of two fundamental signals at L-band frequencies centred on 1.5GHz were measured by using the microwave circuit illustrated in Fig.2.1. The basic principles underlying the measurement of I.P.'s using the system are self-explanatory. The input power delivered by the two L-band power signal sources is attenuated by at least 6dB in the "power combining unit" which consists of two rat-races connected in cascade before reaching the test sample location.

2.2 Measuring Circuit Components

2.2.1 Microwave signal generator

Two "Airborne Instruments Laboratory" (AIL) type 125 power signal sources were utilized as drive equipment covering the frequency range 0.2GHz to 3GHz. Each signal source provided a maximum power output of approximately 12W at 1.3GHz and 1.7GHz. Throughout the I.P. measurements reported in this thesis, the signal sources were in the continuous working (CW) mode tuned to the frequencies 1.698GHz and 1.296GHz. These frequencies are referred to as the fundamental signal frequencies.

The following technical data are supplied by the manufacturer :

(i) The nominal R.F. output impedance of these units is 50Ω.

(ii) Harmonics: Second 40dB down from fundamental.

Third 46dB down from fundamental.

Signal-to-noise ratio 60dB.

(iii) Stability: The power output variation will not exceed ±0.05dB/hour.

The output frequency variation will not exceed ±40 parts per million/hour.

(iv) Nominal load V.S.W.R. for normal operation is 1.5 to 1. Performance is not seriously degraded for load S.W.R.'s as great as 3 to 1.

2.2.2 Detector

A Hewlett-Packard spectrum analyser shown in Fig.2.1 was used as a sensitive detector for all measurements of intermodulation signals. The analyser's R.F. and I.F. sections form a highly sensitive super-heterodyne receiver with spectrum-scanning capabilities over the frequency range of 10MHz to 40GHz in 14 frequency bands. The analyser presents a calibrated CRT display up to 2GHz wide.

R.F. section 8555A
I.F. section 8552B
Display section 141T

In this work, a logarithmic scale of the display was utilized to allow absolute power levels to be read in "dB", having a sensitivity of -117dBm.

The following input specifications are provided by the manufacturer :

Input impedance: 50Ω nominal (0.01-18GHz)

Reflection coefficient < 0.130 (1.30 S.W.R.) for input R.F. attenuator setting > 10dB.

Maximum input power level: peak or average power +10dBm (1.0$V_{a.c.}$ peak) incident on mixer, + 33dBm incident on input attenuator.

For this work, care should be taken not to apply the maximum allowable input power to the mixer diode, when it can be driven into non-linear operation, resulting in spurious responses in the form of harmonics in the case of single input, and harmonics and I.P.'s in the case of multiple frequency inputs.

2.2.3 Tunable band pass filters

Two similar "System Donner type DB-745-1000" band-pass filters with tuning range 1-2GHz indicated as B.P.F.1 and B.P.F.2 in Fig.2.1 and one "Telonic Industries Inc. type TTA 3000-5-5-EE" band-pass filter with tuning range 2- GHz (B.P.F.3 in Fig.2.1) were used.

The B.P.F.1 and B.P.F.2 filters were introduced for the following reasons :

1. To transmit the fundamental signals derived from the two power signal sources unattenuated into the power combining unit.
2. To block transmission of power from one signal source to another.
3. To filter out effectively the 2nd- and 3rd-harmonics of the power sources.

The B.P.F.3 filter was required to pass only the desired intermodulation signal to be detected and to improve the isolation between the power sources and the detector. This filter consisted of iris-coupled, 0.05dB Chebyschev designed cavities in 5 sections permitting a selection of filtering characteristics from 2-4GHz. Each section is capacity loaded to tune over a 2 to 1 range and the inherent high Q provided a minimum insertion loss.

Each filter was tested for loss using a network analyser. Graphs 2.1, 2.2 and 2.3 show typical attenuation/frequency characteristics obtained for the band-pass filters B.P.F.2, B.P.F.1 and B.P.F.3 at spot frequencies.

2.2.4 Coaxial dummy loads

The test bench shown in Fig.2.1 required three suitable dummy loads to dissipate the total power injected simultaneously into the system by the two L-band power signal sources. It has been observed by a number of previous investigators[13,14,15] that a non-linear dummy load can generate high levels of harmonics, predominantly odd harmonics, and I.P.'s which can easily mask the I.P.'s generated by the test samples. Owing to the critical nature of the tests to be made, it was necessary to find a suitable dummy load which does not, by itself, produce any detectable intermodulation level with the maximum input power, so that the maximum available sensitivity of the spectrum analyser can be utilized. Also the characteristic impedance of the load must be compatible with the rest of the circuit. Initially, three similar commercial loads, "Birds Electronic Ltd. model 81B termaline coaxial resistor" were used as dummy loads. These loads at maximum incident power (about 2W from each R.F. power source upon the sample) in the absence of a test sample in the circuit gave rise to a 3rd-order I.P. level of about -110dBW. However, further improvement of the residual level was found to be necessary. Therefore, throughout the experimental work three long lengths (100m each) of UR(M)43 silver-plated copper wire-braided coaxial cables were used as dummy loads. The test results showed that the residual level was improved by 15dB bringing the residual level down to -125dBW. This improvement

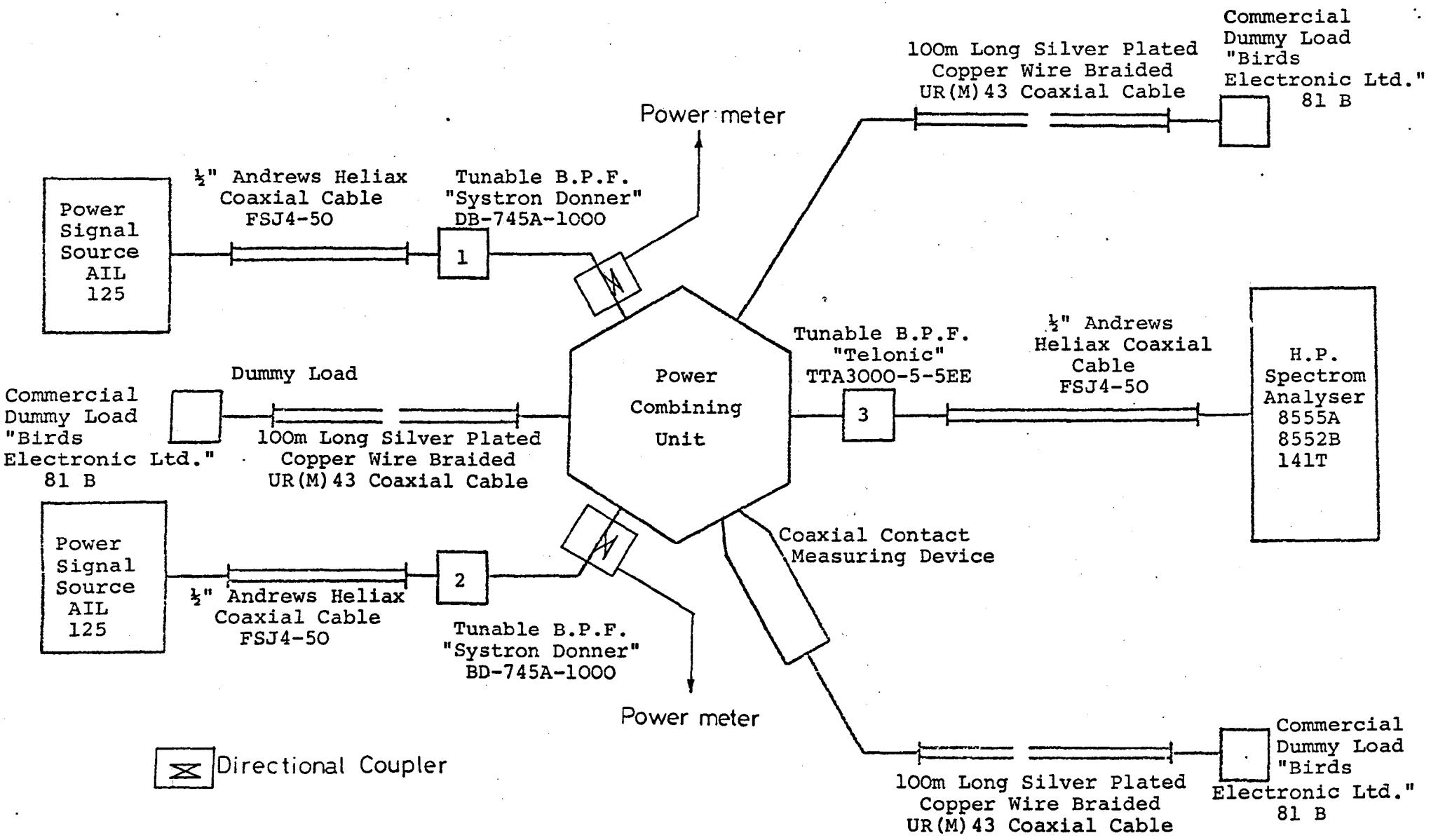

FIG. 2.1. Block Diagram of Test-Bench

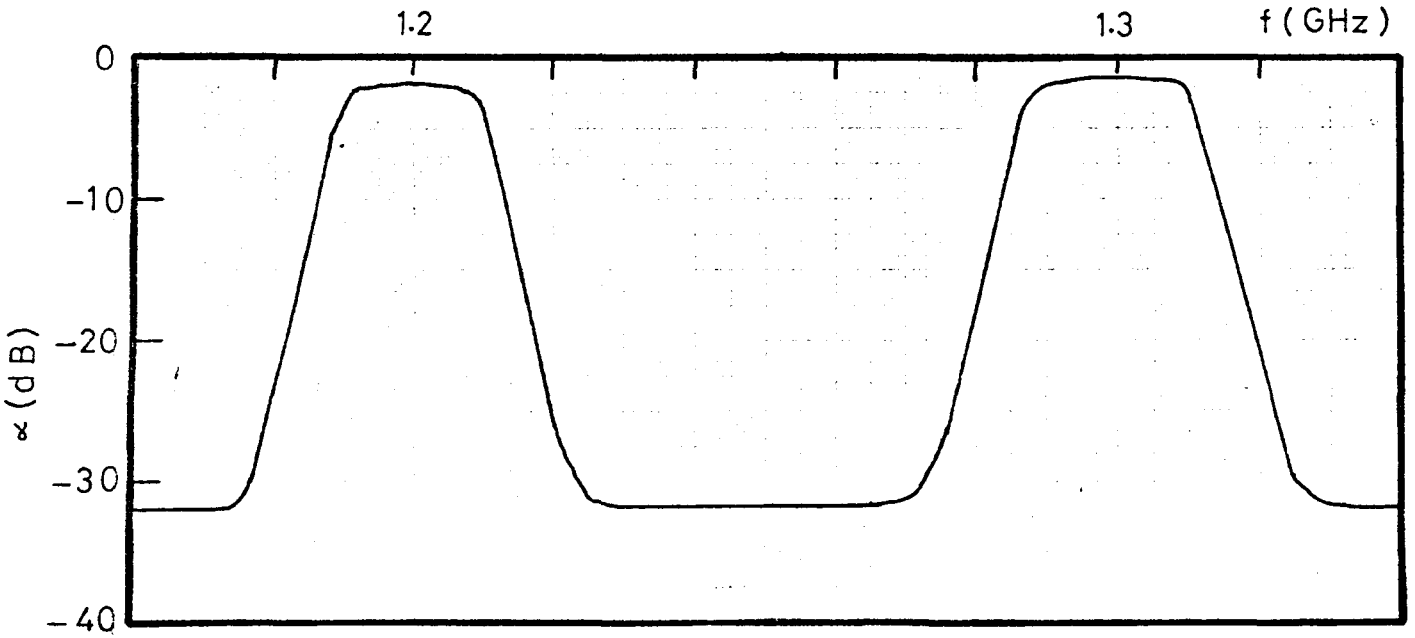

Graph 2-1 Band pass filter 2

Attenuation vs frequency at spot frequencies

f =1·2 & f=1·3 GHz

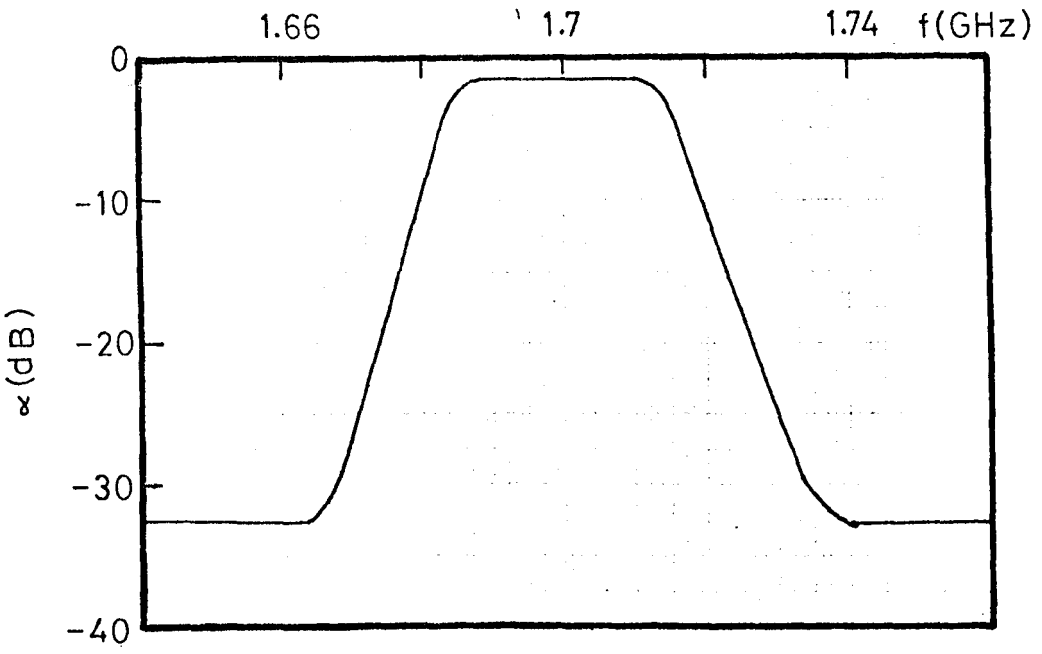

Graph 2-2 Band pass filter 1
Attenuation vs frequency at
spot frequency f=1·7 GHz

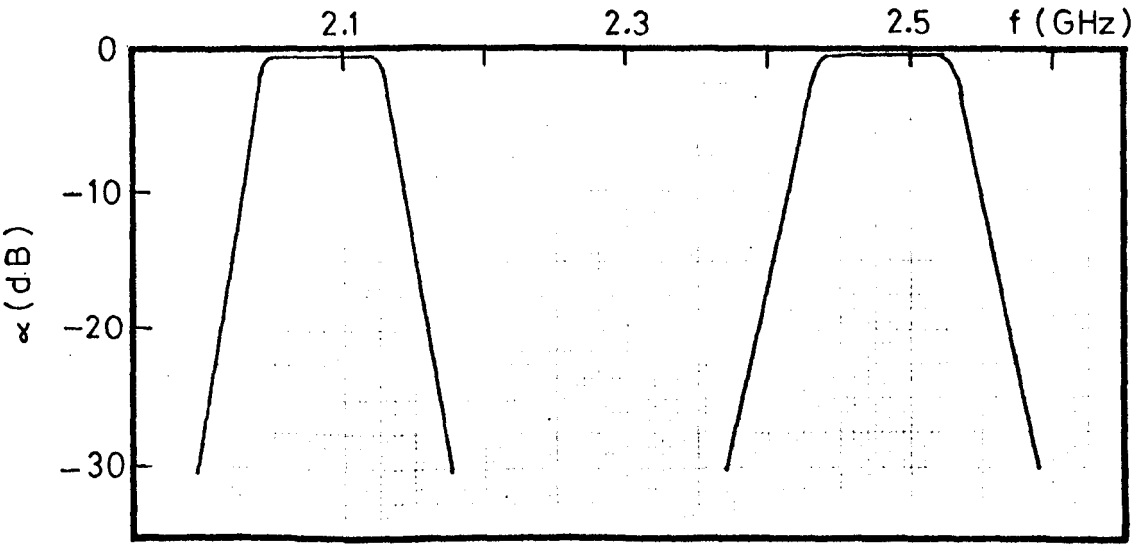

Graph 2-3 Band pass filter 3
Attenuation vs frequency at spot
frequencies f=2.1 & f=2.5 GHz

itself generating any comparable intermodulation signal. The unit consisted of two cascaded hybrid-rings (rat-races) and sandwiched between two brass plates as illustrated in Fig.2.2. A rat-race consists of a transmission line ring of three half wavelengths, circumference (3 $\lambda g/2$) as illustrated in Fig.IV.1 and is thus frequency sensitive.

The design and assembly procedure of the hybrid-ring is given in Appendix IV. Theoretical and experimental treatments appear in the literature[16,17] characterising the various aspects of the hybrid-rings and hence only the description of the operation of the unit will be given here.

Assume that the rat-race shown in Fig.IV.1 is lossless. An incident wave, which the rat-race is designed for, at port "1" divides equally at the junction between the input arm and main ring, half the power travelling round the circuit in a clockwise direction and the rest in an anti-clockwise direction. At port "4" both the clockwise and anti-clockwise waves have travelled a further 3 $\lambda g/4$ and are thus in phase, and an output can be obtained from this port. At port "2", the clockwise wave has travelled a distance of $\lambda g/4$, and the anti-clockwise wave has travelled a distance of 5 $\lambda g/4$. The phase difference between the waves is therefore 2π and hence an output can be obtained at port "2" which is in antiphase to the output of port "4". By the same reasoning, cancellation of fields occur at port "3" and there is zero output at this port. By reciprocity the algebraic sum of two signals incident at port "1" and port "3" simultaneously appears at pot "2" and the algebraic difference appears at port "4".

In summary, a rat-race is a 3dB directional coupler with symmetrical coupling properties. A complete balance

between the arms may be obtained only at the frequency for which the ring is designed.

Referring to Fig.2.2, two fundamental signals at nominal frequencies 1.698GHz (f_2) and 1.296GHz (f_1) are injected simultaneously into the ports "1" and "3" respectively of rat-race (1) and the remaining four ports are properly terminated by good matching terminations. Half of the power from each source will combine vectorially in port "A", while the other halves combine at port "2" to be dissipated into the dummy load. The power at port "A" will travel towards the rat-race (2) and will be divided equally between ports "4" and "6" at port "B". The power arriving at port "6" will be transmitted into the test sample and then to the matched dummy load for dissipation, while that arriving at port "4" will be dissipated in the matched dummy load connected at that port. No input power will thus reach the port "5" of the rat-race (2). The intermodulation products generated at the non-linear test sample connected at port "6" will be injected back into the ring of rat-race (2) and will be split equally between port "B" and port "5". The portion of the intermodulation signal arriving at port "5" is detected by a spectrum analyser.

2.2.6.1 Electrical performance of power combining unit

The degree of coupling, isolation etc., between the ports, and also normalized input impedance and voltage reflection coefficients at input ports "1" and "3" of the power combining unit when it was connected to the coaxial-contact-measuring device (see section 2.2.7), were measured. The measurements were undertaken by means of a network analyser and a single-piece made of brass was put in the test sample

pair location while other ports were terminated to appropriate loads of 50Ω.

Graph 2.4(a) illustrates the isolation between input ports ("1" and "3") and detector in the frequency range 1 to 2GHz.

Graph 2.4(b) illustrates the insertion loss between input ports ("1" and "3") and port "6" where the test sample pairs are connected in the frequency range 1 to 2GHz.

Graph 2.5(b) illustrates isolation between input ports "1" and "3" in the frequency range 1 to 2GHz.

Graphs 2.5(a), 2.6(a) and 2.6(b) illustrate the attenuation between port "5" and three other ports ("2", "4" and "6") in the frequency range of 0.5 to 1GHz, 1 to 2GHz and 2 to 4GHz respectively. It was evident that the unit could be successfully operated at the design frequency of 1.5GHz, though the properties of the unit still hold reasonably well over the range 0.9 to 2.6GHz.

The coupling and isolation between any two ports of the power combining unit could be easily obtained in dB's at any desired frequency from 0.5 to 4GHz from Graphs 2.4, 2.5 and 2.6.

To measure the normalized input impedance and voltage reflection coefficients at each of the two input ports, the remaining five ports were again terminated with appropriate loads of 50Ω.

Photographs (a) and (b) of Fig.2.3 represent the normalized input impedance in polar form at two input ports, "1" and "3" respectively. In this measurement the frequency was swept between 1 to 2GHz. The voltage reflection

coefficients were measured at two input ports "1" and "3" and three spot frequencies, 1.3, 1.5 and 1.7GHz and the corresponding V.S.W.R.'s were calculated. These results are summarised in Table 2.1.

Table 2.1

f(GHz)	Port "1"		Port "3"	
	S_{11}	V.S.W.R.	S_{33}	V.S.W.R.
1.3	$0.05\angle+110^{\circ}$	1.1	$0.19\angle110^{\circ}$	1.47
1.5	$0.08\angle-160^{\circ}$	1.174	$0.08\angle55^{\circ}$	1.174
1.7	$0.06\angle-110^{\circ}$	1.128	$0.08\angle145^{\circ}$	1.174

It is evident that the V.S.W.R. of the whole system which consists of the power combining unit in cascade with the coaxial contact measuring device is less than 1.5 to 1 which is the nominal load V.S.W.R. of signal sources for normal operation.

From the fact that the voltage reflection coefficients at the two input ports "1" and "3" were not equal, it was necessary to produce a chart to give a direct reading of the incident power on the test sample versus the output power of each signal source.

Referring to Fig.2.1, assume that the magnitude of the output power of each power source is P_A and P_B respectively. These powers are attenuated in passing through junction cables, filters and the power combining unit to the sample and also reflected because of mismatches.

The incident powers P_{10} and P_{01} (see section 3.6 for notation) on the test sample from sources A (f_1 = 1.3GHz) and

B (f_2 = 1.7GHz) respectively, were measured against P_A and P_B, the output power from each source. Graph 2.7 illustrates P_{10} and P_{01} vs. P_A and P_B and Fig.2.4 shows the block diagram for this measurement. In this figure P_{in} represents P_{10} or P_{01} and P_{source} represents P_A or P_B. In this measurement a single piece (reference sample), made of brass was located in the coaxial contact measuring device.

2.2.7 Coaxial contact measuring device

To investigate the I.P.'s generated at metallic contacts, a coaxial contact measuring device was used. This device was capable of measuring, firstly, the variation of I.P. with the contact pressure between two metals at a constant incident power, and secondly, the variation of I.P. with the incident power upon the test sample with a constant contact pressure between the metals. It was also easy to dismantle so that different samples of contacting metals could be quickly inserted and removed. This device had an air dielectric coaxial line with a characteristic impedance of 50Ω and a normal working frequency of 1.5GHz. The diameters of the conductors of the coaxial transmission line were chosen so that the line had a characteristic impedance of 50Ω and a cut-off frequency of 5.5GHz. Then since the cut-off wavelength $\lambda_c \approx \pi(r_i + r_o)$ [20] where $2r_i$ and $2r_o$ are the outer diameter of the inner conductor and the inner diameter of the outer conductor respectively and also the nominal characteristic impedance is :

$$Z_o = 138\sqrt{\frac{\mu_r}{\epsilon_r}} \log \frac{r_o}{r_i}$$

by selecting $\mu_r = \epsilon_r = 1$, $Z_o = 50\Omega$ and $\lambda_c = 54.54$mm (or $f_c \approx 5.5$GHz) it was found that $2r_i = 10.5$mm and $2r_o = 24.14$mm.

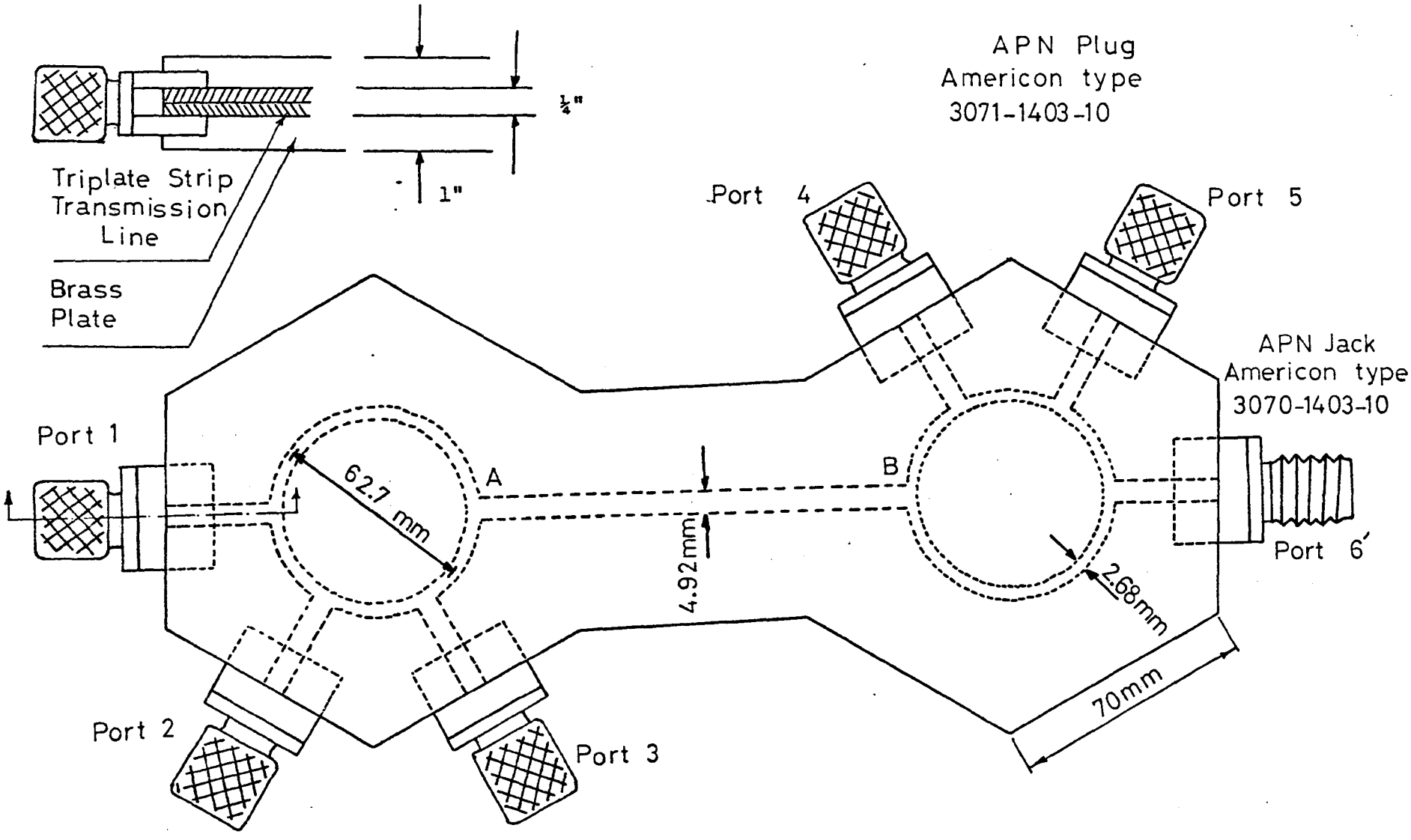

FIG. 2.2

Power Combining Unit Centre Frequency at 1.5GHz.

a)

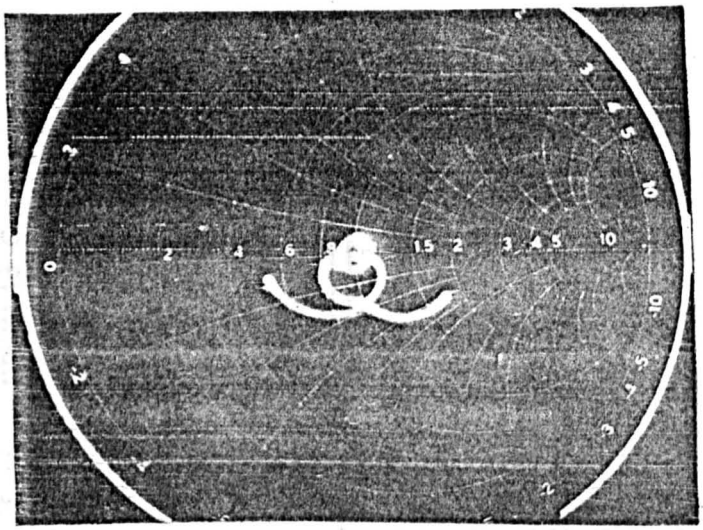

b)

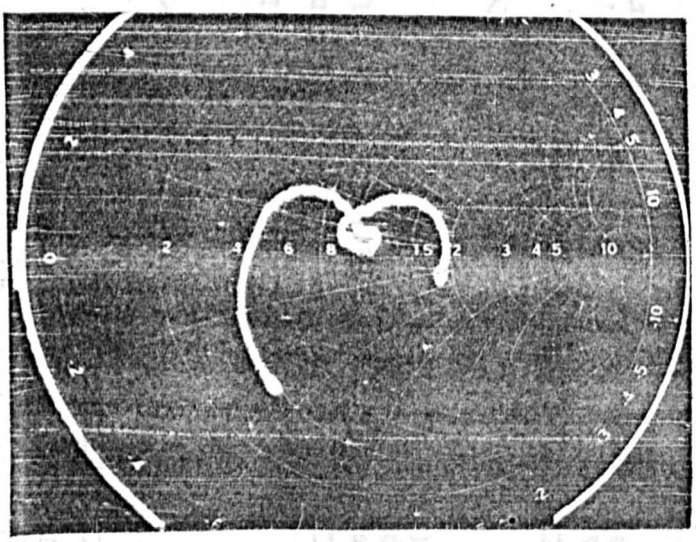

FIG. 2.3 Normalized Input Impedance at
a) port "1" b) port "3"
f=1-2 GHz

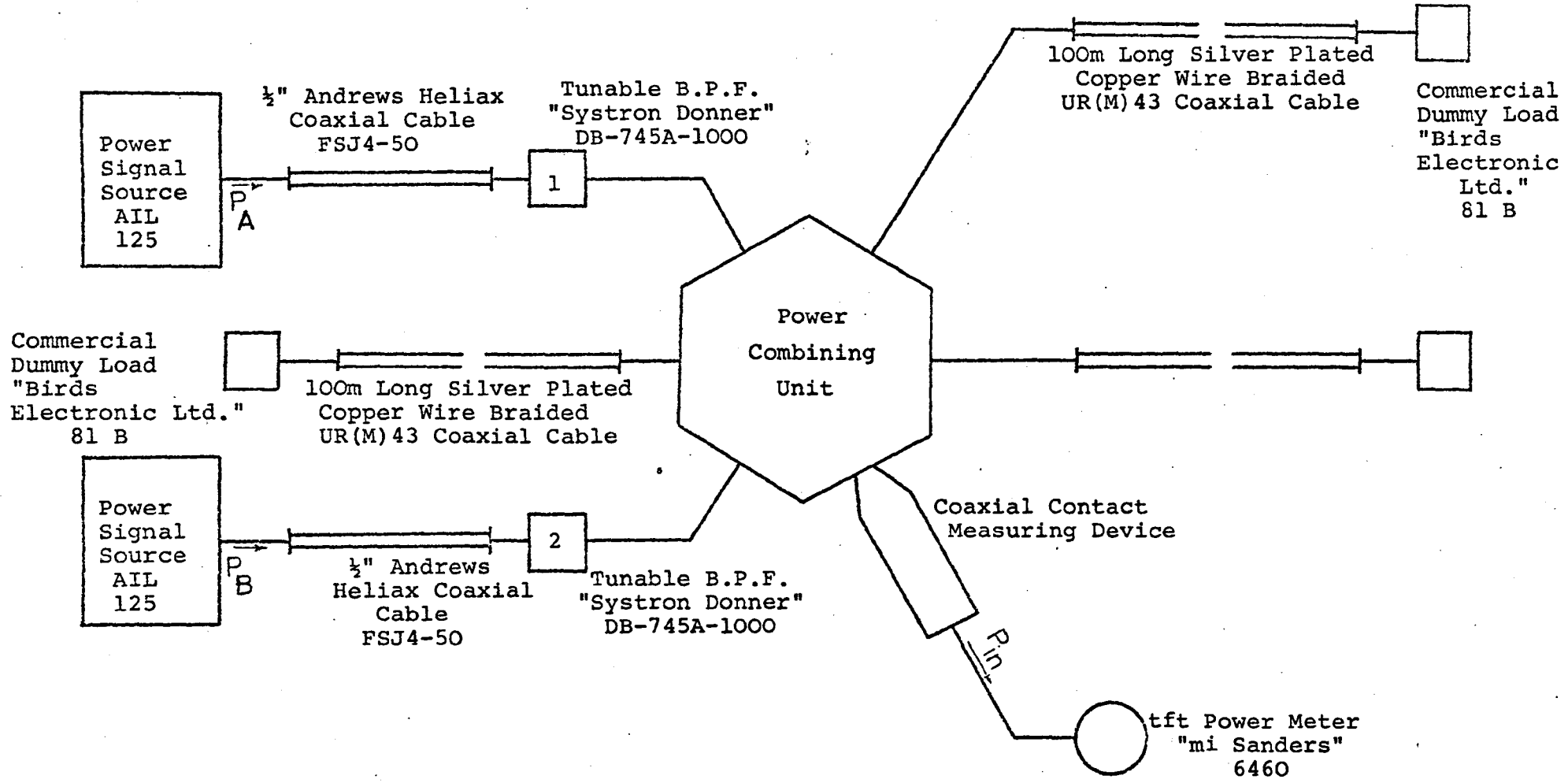

FIG. 2.4. Set Up for Measuring P_{in} vs P_{source}.

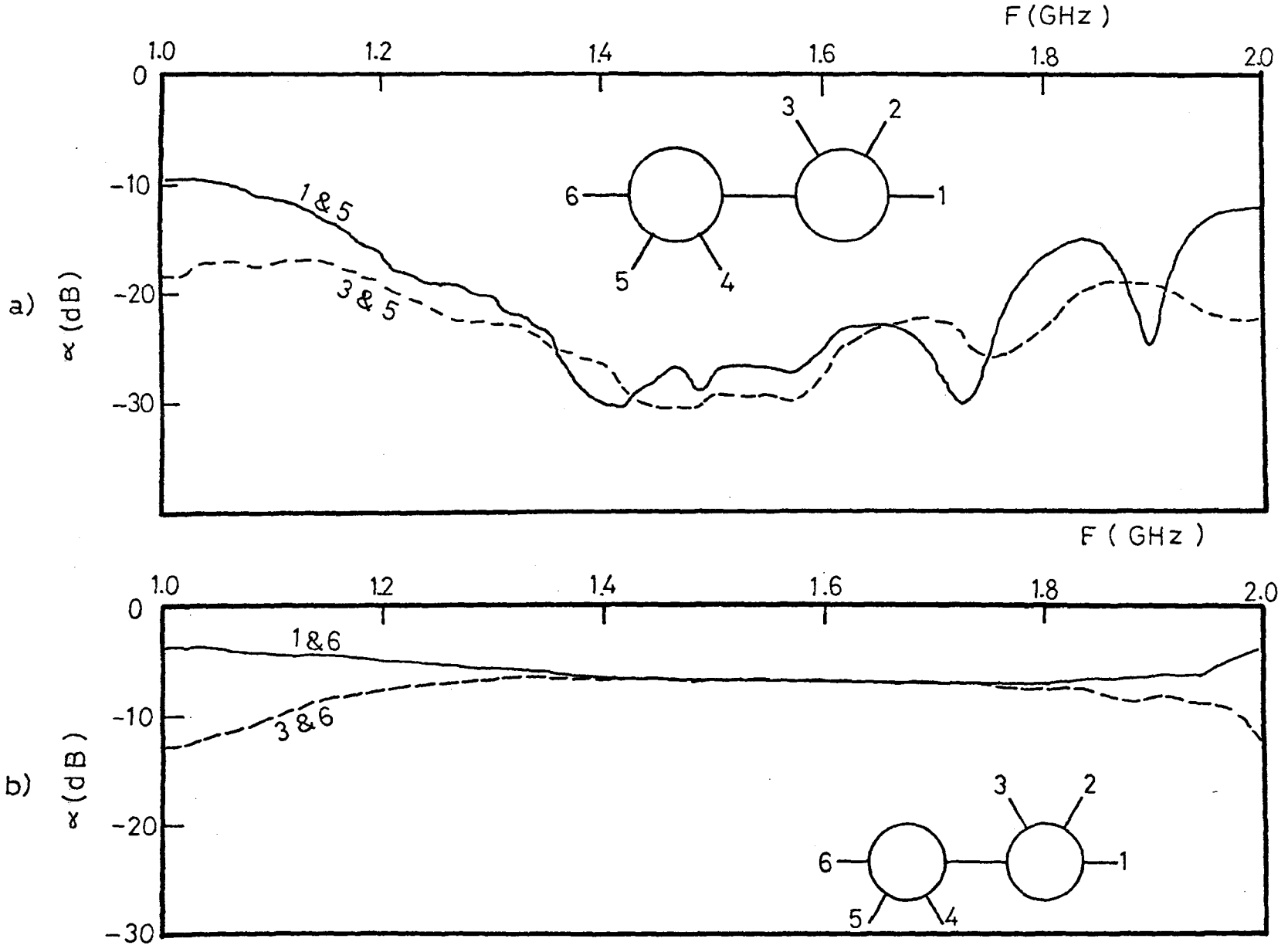

Graph 2.4 Power Combining Unit a) Isolation b) Attenuation

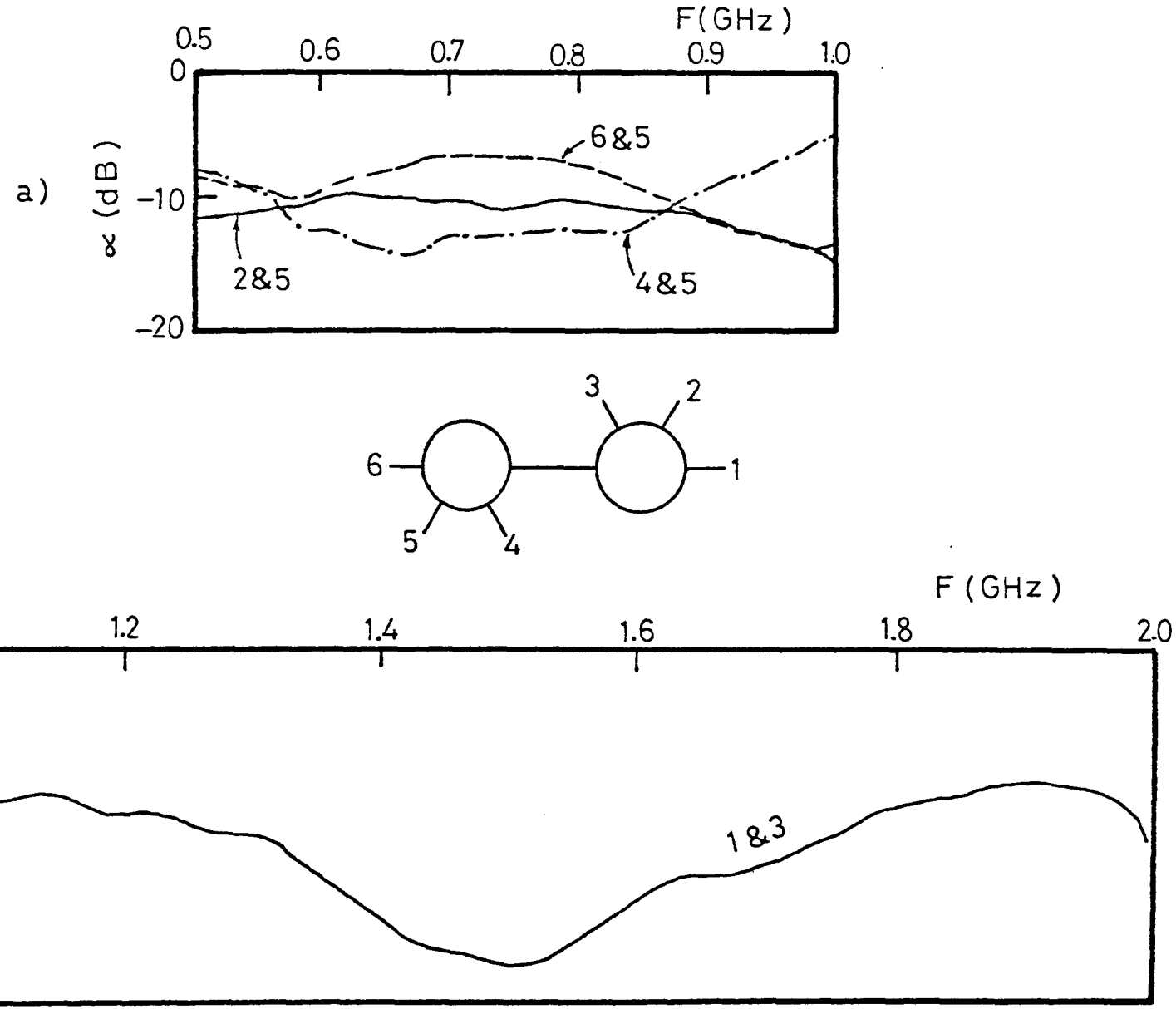

Graph 2.5 Power Combining Unit a) Attenuation b) Isolation

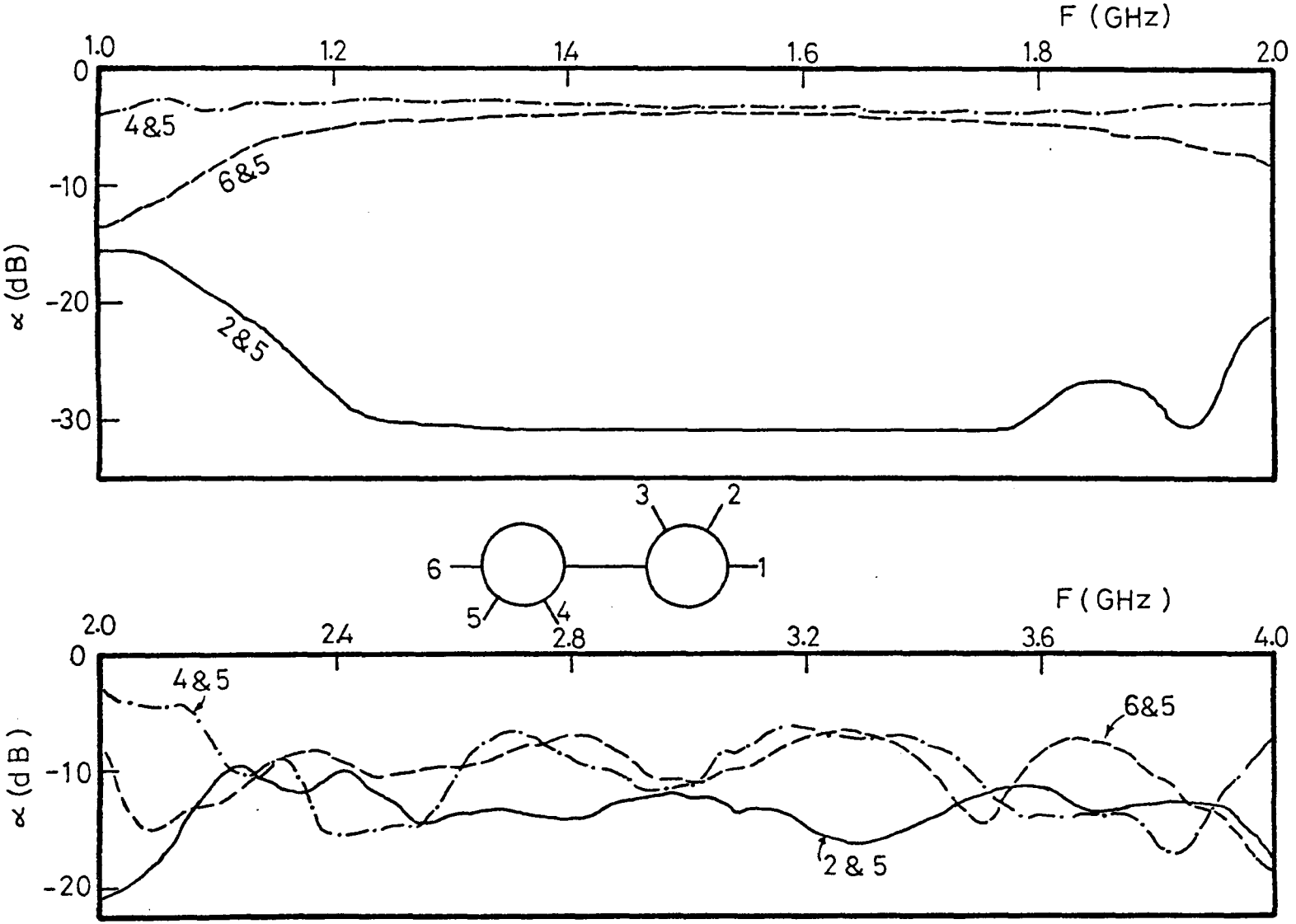

Graph 2.6 Power Combining Unit Attenuation vs Frequency

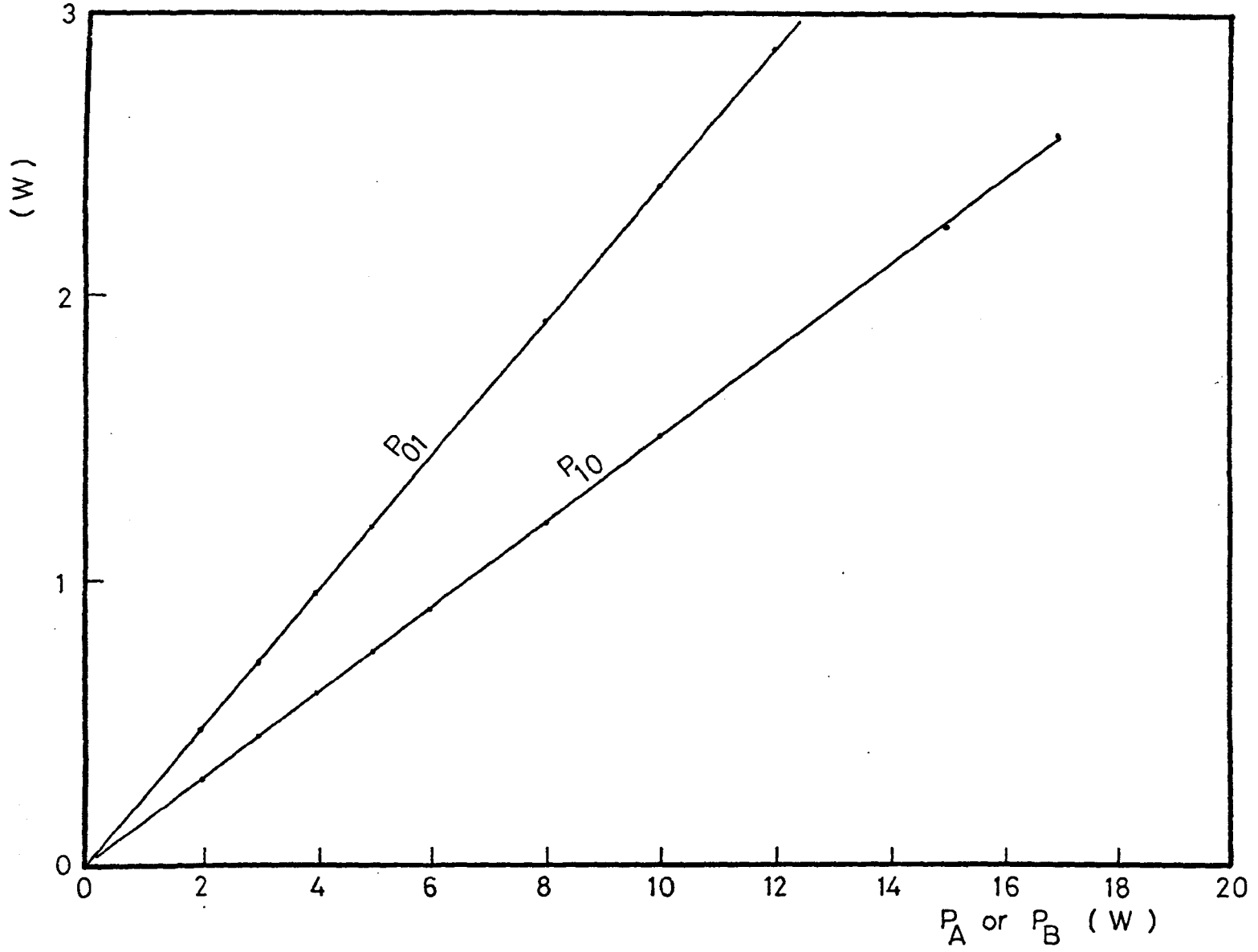

Graph 2.7 Incident Powers P_{10} & P_{01} vs Output Powers of Signal Sources

Since the conductor diameters of the device and of the coaxial N-type connectors are different, it was necessary to use some matching technique to reduce mismatch in going from one dimension to another. Therefore a taped section of line was designed. It was evident that the longer the taper length the better the uniformity of the line, and yet a taper which is too long yields unnecessary high wall losses. Therefore, after consulting the literature[20], the lengths of the tapered sections at the end of the device were chosen to have a wavelength (at 1.5GHz, λ = 200mm) as shown in Figs.2.5 and 2.7. All metallic sections, except the bellows (see Fig.2.5), of the device were made of brass.

The inner conductor of this device is in two sections, a stationary section (see Fig.2.7) and a sliding section (see Fig.2.5), which incorporates a bellow in the middle of the solid inner conductor. The outer conductor also consists of two sections, the main outer conductor body (see Fig.2.6) and a sliding section (see Fig.2.5). The stationary section is soldered to the power combining unit via an "APN Jack, Americon type 3070-1403-10". The two sliding sections were locked together via an "APN Jack-to-plug" adaptor. The bellows were carefully soldered to the inner conductor at each end and then the outer faces of the grooves were sprayed with P.T.F.E. to a thickness of not more than 0.01mm to eliminate the possibility of metal-to-metal contacts if the grooves accidentally become fully compressed. The bellows unit was of type FC10* with a spring rate of 32.44Lb/In and a compression stroke of 0.112 x 2.8mm which was, for a minimum

---

* Purchased from "Servometer Corporation".

lifetime of 100,000 cycles. Therefore the maximum allowable axial force was about 17N.

Since metal-to-metal contacts between the outer surfaces of the sliding section and the inner surface of the main outer conductor body (sliding section housing shell) were to be avoided to prevent any unwanted intermodulation signal, it was decided to spray a P.T.F.E. dielectric coating of thickness of 0.08mm over the outer surface of the sliding section. The immediate advantage of spraying P.T.F.E. was its ease of application since it has lower friction. Finally, Eccofoam dielectric resin was moulded in the region between the inner and outer conductor at the input and the output sections as shown in Figs.2.5 and 2.7.

Each of the test sample pairs was screwed at location "T" in Figs.2.5 and 2.7. After establishing the initial metal-to-metal contact of the test sample pairs, any slight movement of the sliding section into the main outer conductor body will exert a compression on the bellows and hence an axial force on the test sample junction. The magnitude of this axial force was obviously a function of the axial compression applied to the bellows. The movement of the sliding section was controlled by the pressure control nut (Fig.2.8). The compression of the bellows was measured by a "Baty" dial gauge, Model D5 (accurate to ±0.01mm up to a maximum displacement of 8mm) and from the calibration chart for the bellows (see Graph 2.8) the pressure could be interpolated.

However a P.T.F.E. dielectric coating prevents good electrical contact between the sliding section and the main outer conductor body at the output of the device which would

cause a large discontinuity in the current flow and hence the field propagation through the device. To overcome this an attempt was made to improve the situation over the frequency range considered by a double quarter-wave transformer (see Fig.2.6). The dielectric constant of the P.T.F.E. (2.04) was taken into account when designing the quarter-wave sections.

2.2.7.1 Calibration of exerted axial load for direct force reading

Calibration of the axial force exerted against compression of the bellows was achieved by the arrangement illustrated in Fig.2.8. A short length of an aluminium bar with a small diameter and a weight of W_1 was attached to the dial gauge to enable the laoding of variable weights (W) for the compression of the bellows. The return spring of the dial gauge was released so that its movable shaft would not exert any unwanted axial force on the bellows. A thin aluminium disc of weight W_2 was screwed to the brass inner conductor protruding from the top of the bellows to support the loading weights. A thin, low friction, tapered P.T.F.E. bush was introduced between the inner conductor and the main outer conductor body of the device to ensure an accurate axial compression of the bellows. The dial gauge was fixed to the main outer conductor body. The sliding section was supported by the pressure-control-nut. The calibration was then as follows :

The vertical position of the dial gauge was first adjusted so that the end of the thin aluminium bar was in contact with the aluminium disc. In this position there is no axial force on the bellows, apart from that due to the weights, W_1, W_2 and W_3 (see Fig.2.8). The estimated sum

$\Delta W = W_1 + W_2 + W_3$ was about 33×10^{-2}N ($\simeq$ 33gr-wt). After zeroing the scale of the dial gauge a 1N (100gr-wt) was gently loaded onto this aluminium bar which in turn pushed the aluminium disc and hence compressed the bellows. The amount of compression was then recorded from the scale in millimetres. The loaded weights were increased up to 15N with 1N increments and readings taken of the loading in N. The procedure was repeated eleven times to plot the calibration chart of Graph 2.8. The axial force "S" in Graph 2.8 is given in Newton's, when 1kg-wt = 9.81N. For a given value of load, the average, maximum and minimum compressions are shown in the graph. This graph approximately increases with linearity.

The maximum error introduced into the reading of the axial force interpolated directly from the chart for a given value of compression was suspected to be not more than ±8% over the whole range.

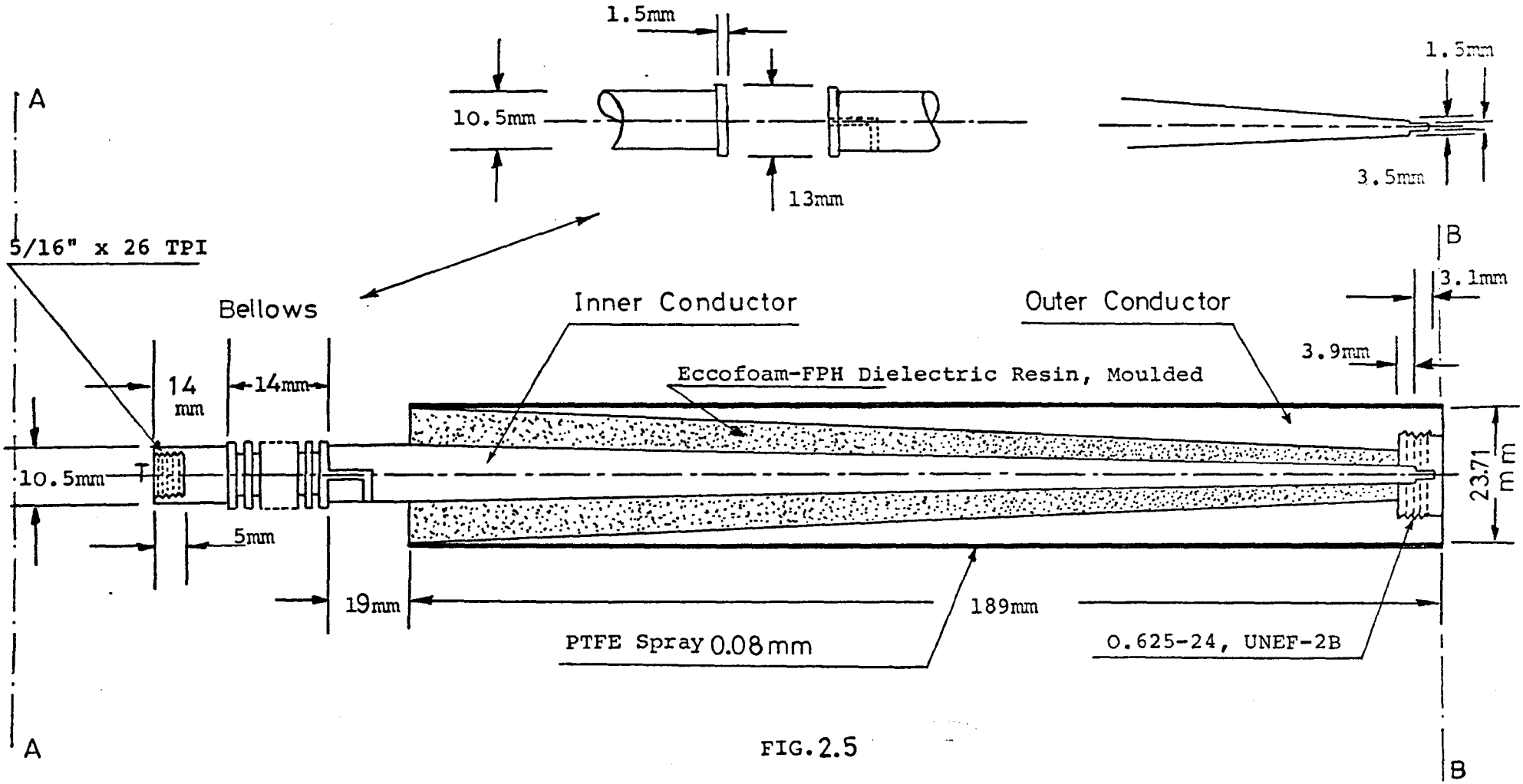

FIG. 2.5

Coaxial Contact Measuring Device Sliding Section

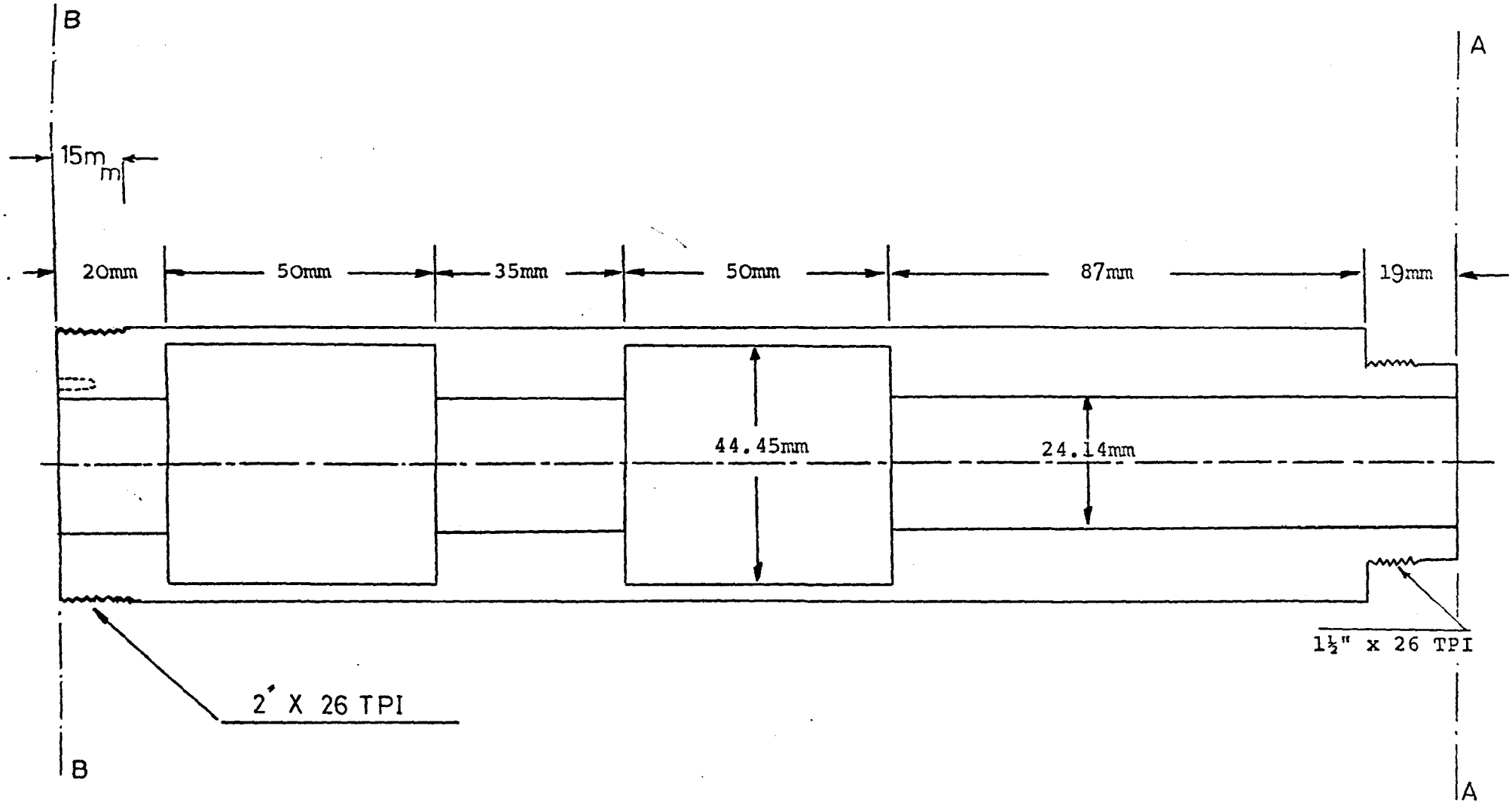

FIG. 2.6

Coaxial Contact Measuring Device, Sliding Section Housing Shell

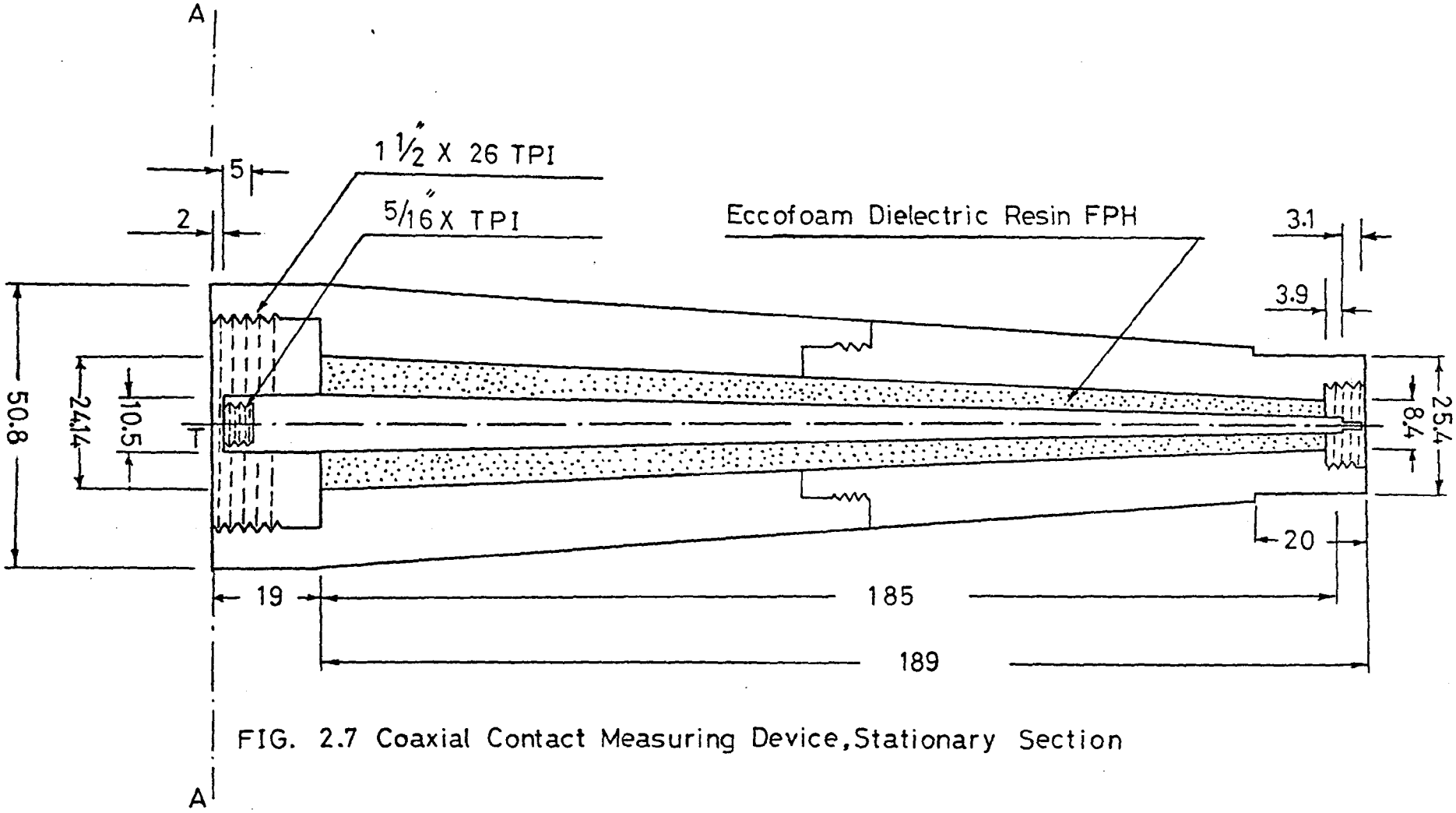

FIG. 2.7 Coaxial Contact Measuring Device, Stationary Section

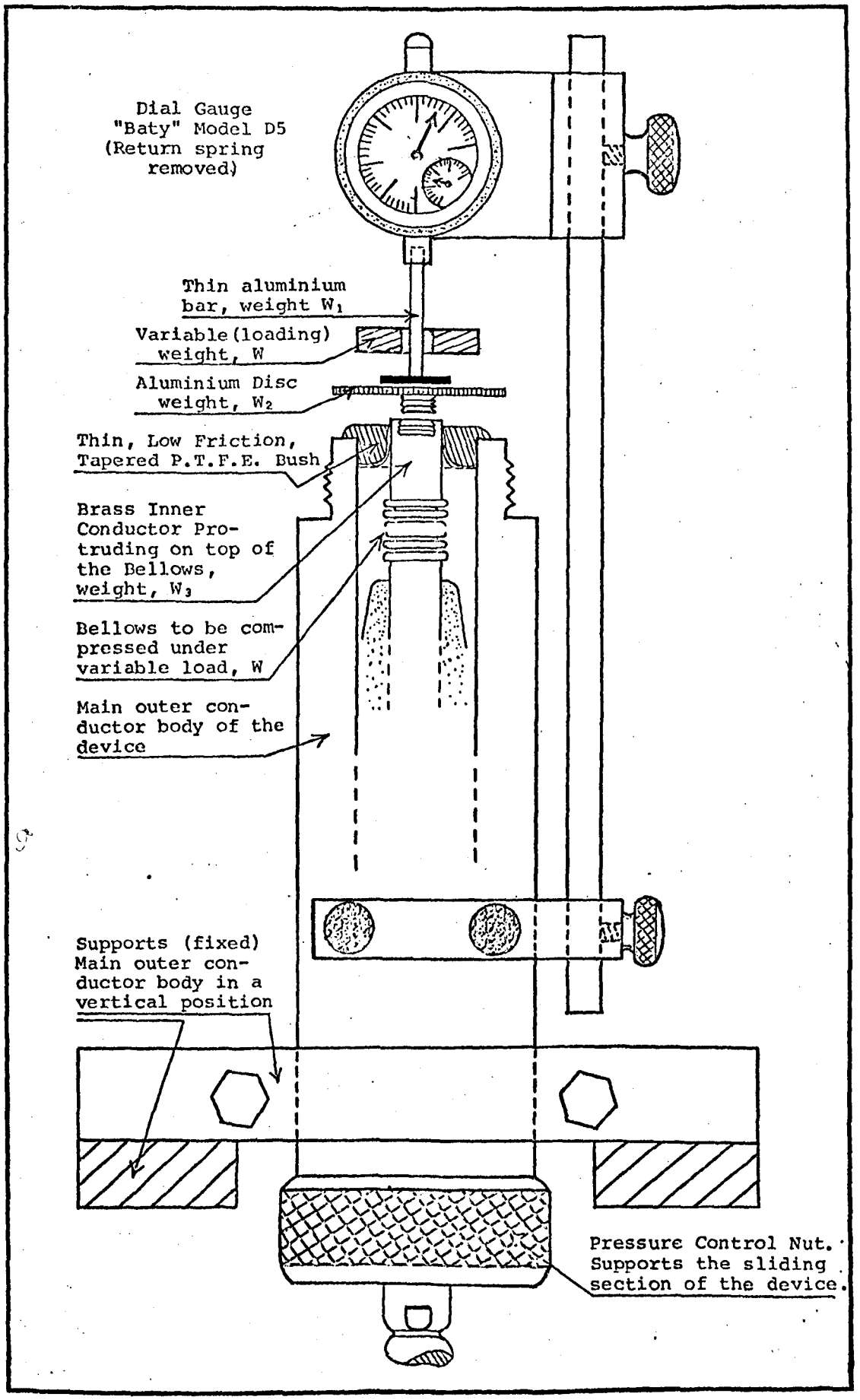

Fig. 2-8 Set Up for Calibration of Coaxial-Contact-Measuring-Device

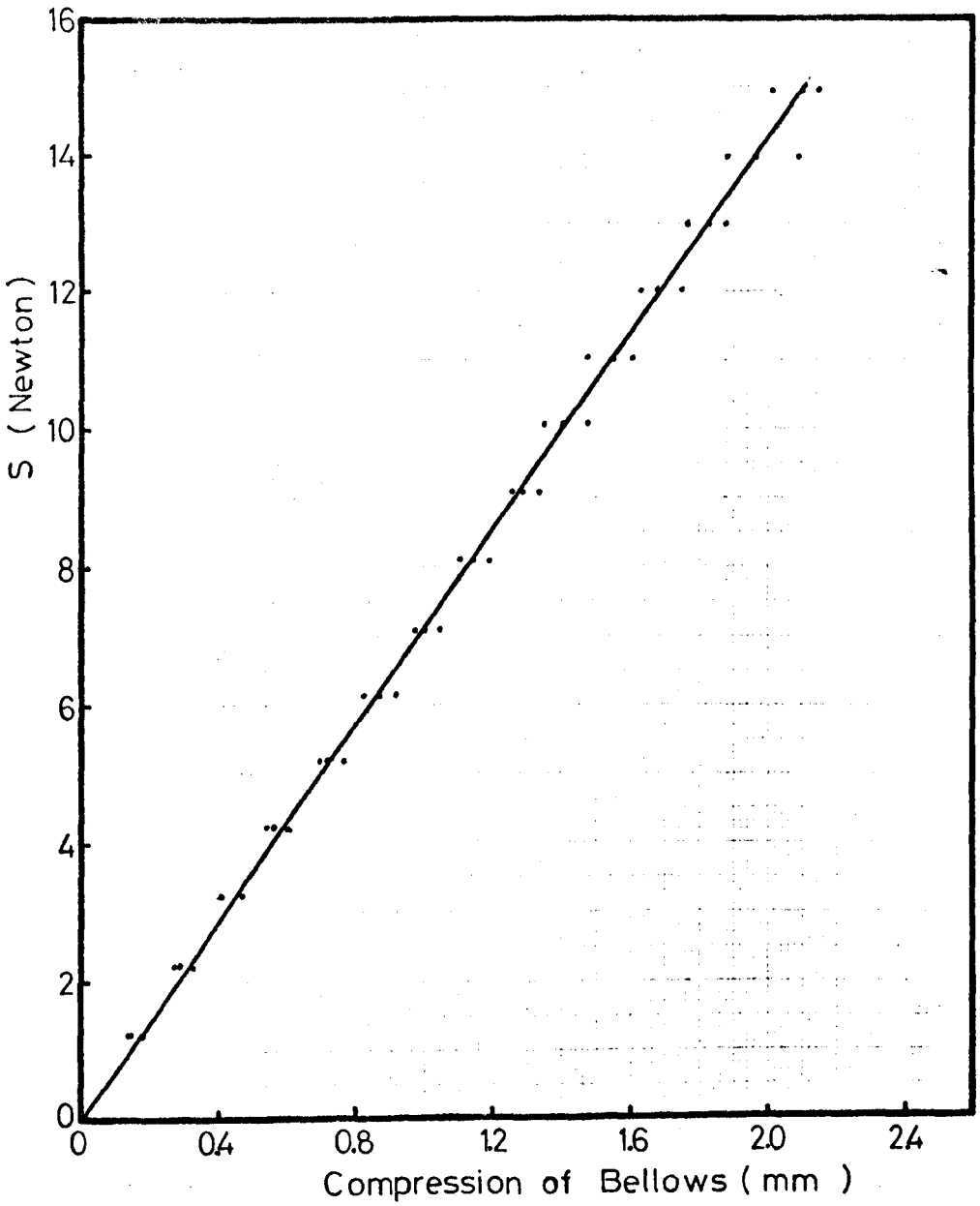

Graph 2-8 Loading vs Compression
Calibration Chart for
Coaxial_Contact_Measuring_Device

CHAPTER 3

3. THEORETICAL TREATMENTS

3.1 Introduction

When two metallic electrodes are brought together, since all metallic surfaces contain oxide films (insulated), then at low axial force they are actually separated by an insulating film of thickness 's'. The Fermi levels of a system of conductors (similar or dissimilar electrodes) in thermal equilibrium must be coincident and also the equilibrium conditions require that the top of the energy gap of the insulator be positioned above the Fermi level, and below the vacuum level (work function) of electrodes. Thus the action of the insulator is to introduce a new potential barrier between the electrodes by lowering the potential barrier existing between the two electrodes by an amount $\psi-\phi$, where ϕ is the distance between the bottom of the insulator conduction band and the Fermi level of the metal electrodes (see Fig.3.1).

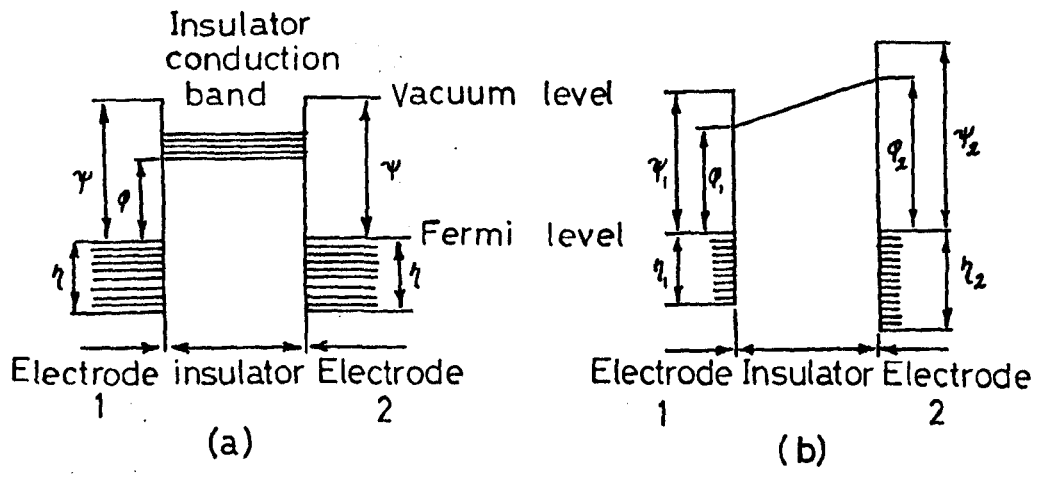

Fig.3.1 Energy diagram of potential barrier between (a) similar electrodes, and (b) dissimilar electrodes.

The abrupt change in the potential barrier at the metal-insulator interface is an ideal model. In actual fact, the barrier changes smoothly as a result of the image force. The image force is the result of polarization of the metal surface when an electron is approaching a flat metal surface and the image potential can be derived using the mirror image method. Fig.3.2 depicts the energy diagram of a rectangular barrier with the image potential superimposed for two similar electrodes.

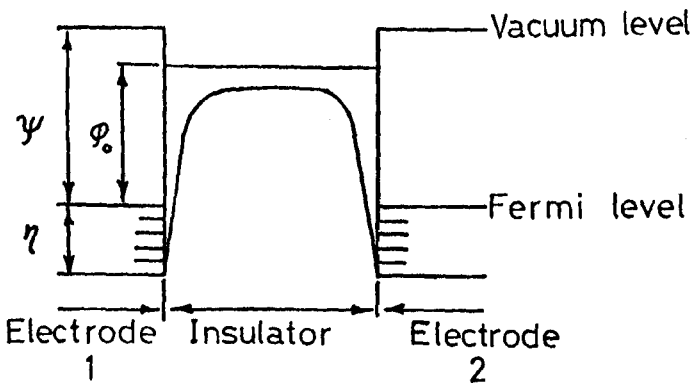

Fig.3.2 Effect of image force on a rectangular barrier.

The electronic current can flow through the insulating region between the two electrodes if :

(i) The electrons in the electrodes have enough thermal energy to surmount the potential barrier and flow in the conduction band.

(ii) The barrier is thin enough to permit its penetration by the electric tunnel effect.

The phenomenon of particles, here electrons, penetrating a potential hill is called 'tunnel effect'.

3.2 Tunnelling Through Thin Insulating Films

The electric tunnel effect between similar and dissimilar electrodes separated by a thin insulating film (neglecting the space charge effect), using a trapezoidal barrier (neglecting image force) and image force, has been studied by Simmon[21,22].

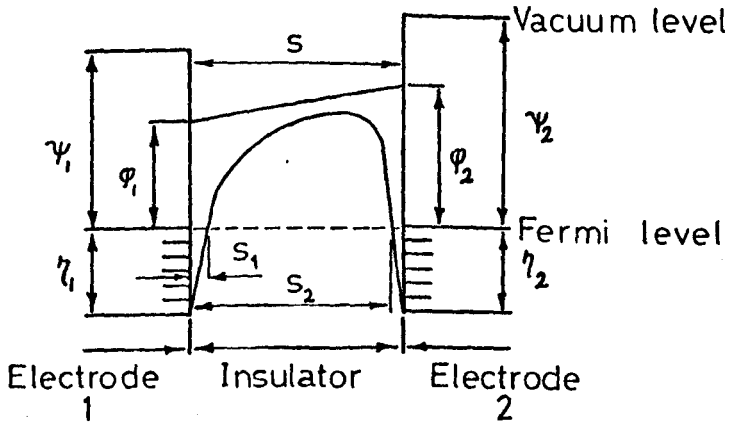

Fig.3.3 Energy diagram of the asymmetric potential barrier.

He has derived formulae for J-V characteristics for similar and dissimilar junctions separated by thin insulator films at low (V≈0), intermediate ($V < \phi_o/e$) and high ($V > \phi_o/e$) voltage ranges due to tunnel effect. In practical terms, when J is expressed in A/cm^2, ϕ_o in V, and s (separation between electrodes), s_1, s_2 (see Fig.3.3) in Å, for the symmetric potential barrier (similar electrodes) with an image force he gives :

$$J = (6.2 \times 10^{10}/\Delta s^2)\ \{\phi_I \exp(-1.025\ \Delta s\ \phi_I^{\frac{1}{2}}) - (\phi_I + V)\ \exp[-1.025\ \Delta s(\phi_I + V)^{\frac{1}{2}}]\}$$

where $\phi_I = \phi_o - (V/2s)(s_1+s_2) - (5.7/2\varepsilon_r \Delta s)\,\mathrm{Ln}[s_2(s-s_1)/s_1(s-s_2)]$

and
$$\left.\begin{aligned} s_1 &= 3/\varepsilon_r\phi_o \\ s_2 &= s[1 - 23/(3\phi_o\varepsilon_r s + 20 - 2V\varepsilon_r s)] + 3/\varepsilon_r\phi_o \end{aligned}\right\} V < \phi_o$$

$$\Delta s = s_2 - s_1 \qquad (3.2\text{-}1)$$

ε_r is the dielectric constant of the insulator. It is evident that if we have a single circular contact with radius "a", we can determine the I-V characteristic of the contact, i.e. in the case of a similar metal-to-metal contact we have :

$$a = 1.1445 \sqrt[3]{\frac{S}{E}\, r(1-\nu^2)} \qquad (3.2\text{-}2)$$

when we have considered an elastic deformation and S is axial force, E is modulus of elasticity of electrodes and ν is Poisson's ratio of electrodes. (See Fig.3.4).

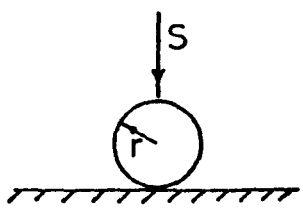

Fig.3.4 Contact positions.

Then we get :

$$I = J \times (\pi a^2) \qquad (3.2\text{-}3)$$

Since we can expand (3.2-1) in series of V we can write :

$$I = \sum_{i=0}^{\infty} a_i V^i \qquad (3.2\text{-}4)$$

For a simple case without image force by expanding the radical of the exponents and the exponents themselves and neglecting the term V of the fourth order and higher from literature[21] eqn.27, we get :

$$J = \frac{3}{2} \frac{e^2 (2m)^{\frac{1}{2}}}{h^2 sA} \exp(-A\sqrt{\phi}) \left[\pm bV + cV^3\right] \qquad (3.2\text{-}5)$$

where $A = 2s\sqrt{\frac{2m}{h^2}}$

$$b = \frac{A\sqrt{\phi}}{2} - 1$$

$$c = \frac{A^3 e^2}{192\sqrt{\phi}} - \frac{A^2 e^2}{64\phi} - \frac{Ae^2}{64\phi^{3/2}}$$

where m is mass of electron, e is charge of electron and h is Planck's constant.

3.3 Thermionic Effect

Emission-limited current flow between closely spaced parallel metal electrodes has been studied by Simmons[24]. He has compared the thermionic J-V characteristic with the tunnel J-V characteristic and concluded that for a temperature of 300k, and for a barrier thickness less than 40Å, the tunnel J-V characteristic, for similar and dissimilar electrodes, predominates. His derivations are based on neglecting the space-charge limited effects which is satisfied for insulators only a few tenths of an angstrom thick. In the case of dissimilar electrodes, the thermionic current flow between the electrodes is polarity sensitive, the greater current flowing when the electrode of the lower work function is at a negative potential. In this case the junction is rectifying very strongly and the rectification increases with decreasing temperature.

3.4 Analysis of Contact in Coaxial Contact Measuring Device

To investigate the I.P.'s generated at metallic contacts, the metal-to-metal contact takes place at the inner conductor of the coaxial contact measuring device (see Fig.3.5).

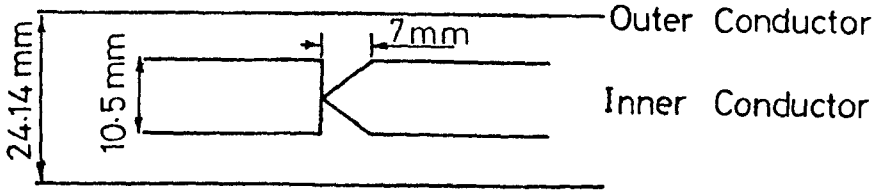

Fig.3.5 Position of metal-to-metal contact in a coaxial contact measuring device.

The outer and inner diameters have been chosen so that we have only the TEM mode (see section 2.2.7) therefore we consider the circuit as a simple transmission line.

The effect of double discontinuities at the inner conductor can be neglected, since the spacing between discontinuities is much less than twice the separation between the transmission line conductors[25, Section F, p.697].

The J-V characteristic shown in eqn.(3.2-1), because of the following reasons may not satisfy the actual contact in the coaxial contact measuring device :

1. The current lines are constricted and also because of skin effect, there is no longer a uniform current distribution.
2. There are two distinctly different metal-insulator interfaces in the case of dissimilar electrodes. In the case of a similar metal-to-metal junction, the surface states at the interface will differ

significantly, and could also contribute to electrical asymmetry.

3. There is the plausible assumption that the dielectric constant ϵ_r varies slightly throughout the oxide film. This would result in an asymmetric barrier in a symmetrical junction which would give rise to an asymmetric electrical behaviour.

3.4.1 Skin effect in a current constriction

This effect arises from an induction by its own magnetic field on an alternating current. Here we are concerned with the skin effect in a current constriction. For computing its order of magnitude we may take an example.

If the electrodes are made of iron, according to eqn. (3.2-2), with r = 0.1cm, ν = 0.3, E = $20 \times 10^8 gr/cm^2$ at S = 10gr the radius of the contact area is a = 0.88×10^{-3}cm. Then a.c. resistance (R_{ac}) of the constriction can be approximately calculated from d.c. resistance (R_{dc}) of the constriction. We have[26, eqn.11.09] :

$$\frac{R_{ac}}{R_{dc}} \approx \frac{a}{10^3} \sqrt{\frac{f}{\rho}} \, \mathrm{Ln} \, \frac{\pi r_i}{2a} + \frac{1}{4} \qquad (3.3\text{-}1)$$

At f = 1.5GHz where $2r_i$ = 10.5mm and $\rho = 10^{-7}\Omega$cm, this ratio is about 7.64. Since d.c. resistance of the constriction[26] is (see Appendix V) :

$$R_{dc} = \frac{\rho}{2a} \qquad (3.3\text{-}2)$$

or $R_{dc} = 11.35 \times 10^{-3}\Omega$, therefore R_{ac} is about 0.087Ω which is negligible compared with a load resistance of 50Ω.

3.5 The Source of Non-Linearity

The problems involved in the contacts as used in telecommunication circuits are mainly related to the properties of surface films as well as the bulk material itself. When two fresh metals are brought together, they are actually separated (insulated) by a thin oxidized layer of thickness s. If the electric field built up in the insulator is less than 10^6V/cm (this value was determined by Holm[26] which must be built up before fritting can occur), or in other words the insulator is not fritted or damaged (fritting or damage of an oxide layer can be done mechanically by increasing the axial force or electrically by increasing the electric field inside the insulator), then the non-linear J-V characteristics described in Sections 3.2 and 3.3 are responsible for producing I.P.'s. Let us take an example; suppose the electrodes are aluminium with a thickness of Al_2O_3, s = 5Å. According to equation (3.2-2) when S = 10gr, r = 0.1cm, $E = 7 \times 10^8 gr/cm^2$ and $\nu = 0.36$, the radius of a single spot is $\alpha = 1.23 \times 10^{-3}$cm and the contact area is $A_c = 4.75 \times 10^{-6} cm^2$. Therefore the capacitance between two electrodes when the dielectric constant of Al_2O_3 is about 8, will be $C = 8\varepsilon_0 \frac{A_c}{s} \simeq 6.72 \times 10^{-11}$F, then at f = 1.5GHz we can obtain :

$$\frac{1}{\omega C} \simeq 1.57\Omega \qquad (3.5\text{-}1)$$

At the same time when the thickness is less than 40Å the tunnel effect predominates then with $\varepsilon_r = 8$ and $\phi_0 = 4$eV[21] the tunnel resistivity is $\sigma = 7.5 \times 10^{-7} \Omega\text{-cm}^2$, then the tunnel resistance is :

$$R_t = \frac{\sigma}{A_c} < 0.16\Omega \qquad (3.5\text{-}2)$$

Comparing eqns. (3.5-1) and (3.5-2) suggests that for this thickness ($s = 5\mathring{A}$) of the insulator the J-V tunnel characteristic is the source of non-linearity where V is the voltage drop between two electrodes.

On the other hand when fritting can occur, it provides the possibility of metallic contact. Then by current flowing through the contact construction, the contact is heated and the constriction resistance differs from that of the unheated constriction. In general if V is the voltage drop between two electrodes and I is the current we have :

$$V = R_t I \tag{3.5-3}$$

Then if $R_c(T_o)$ is the unheated constriction resistance, according to equation (3.3-2) we have

$$R_c(T_o) = \frac{\rho}{2a} \tag{3.5-4}$$

Then the contact voltage U, which could be measured by cross rods[21] is :

$$U = (R_c + R_t)\ I \tag{3.5-5}$$

For a metal where thermo-electric effect is ignored, the relation between contact voltage and super-temperature T_m at the contact (in similar metal-to-metal contact) or at very close contact to the interface (in dissimilar metal-to-metal contact)[21] is :

$$T_m^2 - T_o^2 = \frac{U^2}{4L} \tag{3.5-6}$$

which is independent of the shape or size of the conductor or of the flowing current, provided, of course, there is no flow of energy across the bounding surface of the conductor. The

Lorenz constant* L according to Weidemann-Franz law is :

$$\lambda\rho = LT \tag{3.5-7}$$

where λ is thermal conductivity of metal, ρ is resistivity and T is absolute temperature in metal. In this case (i.e. when fritting has occurred) V = 0 and we have[21] :

$$\frac{R_c(T_m)}{R_c(T_o)} = \left[-\frac{T_o\sqrt{L}}{U/2}\tan^{-1}\frac{U/2}{T_o\sqrt{L}}\right] \tag{3.5-8}$$

where $R_c(T_m)$ is the heated constriction resistance at absolute temperature T_m.

It is evident from eqn. (3.5-8) that the constriction resistance is a non-linear source. Even if the thermo-electric effect is not neglected, such as with nickel, Holm[21,pp.81-84] through some examples has shown this non-linearity. Usually both phenomena, the tunnel effect and fritting, appear in all kind of contacts.

3.6 Power Conversion in Non-Linear Resistive Element

In Section 3.5 it was shown whether a thin insulator is fritted or not, the non-linear resistance or actually the non-linear current/voltage across the junction is responsible for producing I.P.'s. The non-linear current/voltage across the contact can be shown as a series :

$$i = \sum_{i=1}^{\infty} a_i v^i \tag{3.6-1}$$

In the following derivation, it is assumed that the generator voltage in the circuit is composed of two sine waves (i.e. at the frequency f_1 and f_2 where $f_2 > f_1$) that are not harmonically related.

---

* The numerical value of "L" in Weideman-Franz law is about 2.45×10^{-8} $\frac{W\text{-}\Omega}{degree^2}$

A schematic diagram of the circuit is presented in Fig.3.6. In this figure r represents a non-linear element.

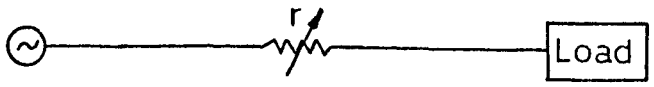

Fig.3.6 Schematic presentation of a contact that functions as a non-linear resistive element.

When the incident powers of two sine waves at fundamental frequencies (f_1 and f_2) upon the non-linear element are P_{10} and P_{01} respectively, it is possible to establish and equivalent circuit to Fig.3.6, as shown in Fig.3.7. In Sections 3.4 and 3.5 it was determined that the non-linear resistance is negligible compared to the load resistance. Therefore :

$$e(t) = E_{10}\cos(2\pi f_1 t) + E_{01}\cos(2\pi f_2 t + \phi) \qquad (3.6\text{-}2)$$

where

$$E_{10} = \sqrt{8R_o P_{10}}$$
$$E_{01} = \sqrt{8R_o P_{01}} \qquad (3.6\text{-}3)$$

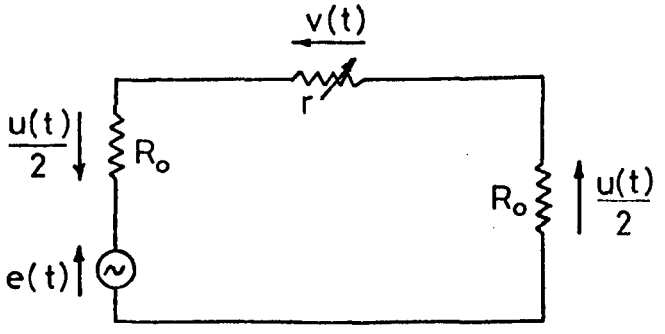

Fig.3.7 Lumped-element circuit equivalent to Fig.3.6, where non-linear resistor is in series with two linear load resistors.

The voltage drop across the non-linear resistor is :

$$v(t) = V_{10}\cos(2\pi f_1 t) + V_{01}\cos(2\pi f_2 t + \phi) \qquad (3.6\text{-}4)$$

By putting eqn.(3.6-4) into eqn.(3.6-1), it is simple to realize[1] that i(t) which is a periodic function of time can be represented by the Fourier series :

$$i(t) = \frac{1}{2} \sum_{m=-\infty}^{\infty} \sum_{n=-\infty}^{\infty} I_{mn} \, e^{j2\pi(mf_1 + nf_2)t} \qquad (3.6\text{-}5)$$

where $I_{m,n} = I_{-m,n}$, since current is real.

This current produces a voltage drop across the linear resistance $2R_o$, which in its turn can be presented by the Fourier series :

$$u(t) = \frac{1}{2} \sum_{m=-\infty}^{\infty} \sum_{n=-\infty}^{\infty} U_{mn} \, e^{j2\pi(mf_1 + nf_2)t} \qquad (3.6\text{-}6)$$

From Fig.3.7 :

$$e(t) = u(t) + v(t) \qquad (3.6\text{-}7)$$

$$u(t) = 2R_o \, i(t) \qquad (3.6\text{-}8)$$

Therefore from eqns. (3.6-6) and (3.6-7), the total voltage across the non-linear resistor is

$$v(t) = \frac{1}{2} \sum_{m=-\infty}^{\infty} \sum_{n=-\infty}^{\infty} (E_{mn} - U_{mn}) e^{j2\pi(mf_1 + nf_2)t} \qquad (3.6\text{-}9)$$

where $E_{mn} = 0$ when m or $n \neq 0$ or ± 1.

Equation (3.6-9) can be written as :

$$v(t) = \frac{1}{2} \sum_{m=-\infty}^{\infty} \sum_{n=-\infty}^{\infty} V_{mn} \, e^{j2\pi(mf_1 + nf_2)} \qquad (3.6\text{-}10)$$

By comparing eqns. (3.6-9) and (3.6-10) one can obtain :

$$V_{10} = E_{10} - U_{10} \qquad (3.6\text{-}11)$$

$$V_{01} = E_{01} - U_{01} \qquad (3.6\text{-}12)$$

$$V_{mn} = -U_{mn} \text{ (when m or } n \neq 0 \text{ or } \pm 1) \qquad (3.6\text{-}13)$$

The total power delivered to the linear load resistors is :

$$P_t = \frac{1}{2} \sum_{m=-\infty}^{\infty} \sum_{n=-\infty}^{\infty} U_{mn} I_{mn} = R_o \sum_{m=-\infty}^{\infty} \sum_{n=-\infty}^{\infty} I_{mn}^2 \qquad (3.6\text{-}14)$$

In fact the incident power $P_{in} = P_{10} + P_{01}$ reaches the point where the non-linear element (resistor) is located. One part of this power is reflected back which is negligible since the non-linear resistance is very small compared to the load resistance. One part of the incident power which is transferred to the output is :

$$P_{out} = \frac{1}{4} (U_{10} I_{10} + U_{01} I_{01}) = \frac{1}{2} R_o (I_{10}^2 + I_{01}^2) \qquad (3.6\text{-}15)$$

Another part of the incident power (P_{in}) which is observed by a non-linear resistor is :

$$P_{absorbed} = \frac{1}{2} (V_{10} I_{10} + V_{01} I_{01}) \qquad (3.6\text{-}16)$$

This part of the power can be converted to waves at the intermodulation frequencies. In fact it is assumed that the non-linear resistor acts as a converter which can be represented as the infinite current sources all connected in parallel to r.

The power at the intermodulation frequency ($mf_1 + nf_2$) that is guided by the circuit is :

$$P_{mn} = \frac{1}{2} U_{mn} I_{mn} = R_o I_{mn}^2 \qquad (3.6\text{-}17)$$

The amplitudes of the 3rd- and 5th-order I.P.'s current, $I_{-1,2}$ and $I_{-2,3}$ are given in Appendix VI.

When two incident powers are equal ($P_{10} = P_{01}$ and $P_{in} = 2P_{10}$) it can be shown that :

$$I_{10} = I_{01} \approx \sqrt{\frac{P_{in}}{R_o}} \qquad (3.6\text{-}18)$$

If eqn. (3.6-1) is a convergent series so that $a_i >> a_{i+1}$ then :

$$V_{10} = V_{01} \approx \frac{1}{a_1}\sqrt{\frac{P_{in}}{R_o}} \qquad (3.6\text{-}19)$$

From Appendix IV parts 3 and 4, where $V_{10} = V_{01} = V$, the amplitude of the 3rd- and 5th-order I.P.'s current are approximately :

$$\begin{aligned} I_{-1,2} &\approx 0.75\ a_3 V^3 \\ I_{-2,3} &\approx 0.625\ a_5 V^5 \end{aligned} \qquad (3.6\text{-}20)$$

From eqns. (3.6-17), (3.6-19) and (3.6-20) one can obtain :

$$\begin{aligned} P_{-1,2} &\approx \left(\frac{0.75}{R_o}\right)^2 \left(\frac{a_3}{a_1^3}\right)^2 P_{in}^3 \\ P_{-2,3} &\approx \left(\frac{0.625}{R_o^2}\right)^2 \left(\frac{a_5}{a_1^5}\right)^2 P_{in}^5 \end{aligned} \qquad (3.6\text{-}21)$$

If $p_{in} = 10 \log P_{in}$, $p_{-1,2} = 10 \log P_{-1,2}$, $p_{-2,3} = 10 \log P_{-2,3}$ and $R_o = 50\Omega$ then :

$$\begin{aligned} p_{-1,2} &\approx -36.5 + 20 \log\left|\frac{a_3}{a_1^3}\right| + 3p_{in} \\ p_{-2,3} &\approx -72 + 20 \log\left|\frac{a_5}{a_1^5}\right| + 5p_{in} \end{aligned} \qquad (3.6\text{-}22)$$

By the same reasoning when two incident powers are not equal, one can obtain :

$$\begin{aligned} P_{-1,2} &= 8\left(\frac{0.75}{R_o}\right)^2 \left(\frac{a_3}{a_1^3}\right)^2 P_{10}\, P_{01}^2 \\ P_{-2,3} &= 32\left(\frac{0.625}{R_o^2}\right)^2 \left(\frac{a_5}{a_1^5}\right)^2 P_{10}^2\, P_{01}^3 \end{aligned} \qquad (3.6\text{-}23)$$

3.7 Two Back-to-Back Diodes as a Non-Linear Element

A theoretical quantitative investigation of I.P.'s, because of unexpected phenomena occurring at the metal-to-metal interface, is very complicated. In the following two back-to-back diodes are assumed to be the non-linear element in the lumped circuit shown in Fig.3.7, and by establishing a relationship

between output and input of this kind the amplitudes of the 3rd- and 5th-order I.P.'s are calculated.

In this case, the current/voltage characteristic of each diode can be approximated by an exponential function :

$$\begin{aligned} i &= -i_{01}\,\{\exp[-\gamma_1 v_1(t)] - 1\} \\ i &= i_{02}\,\{\exp[-\gamma_2 v_2(t)] - 1\} \end{aligned} \qquad (3.7\text{-}1)$$

when $v = v_1 + v_2$, then the relationship between i and e (see Fig.3.7) is :

$$\frac{(1 + i/i_{02})^{\gamma_1}}{(1 - i/i_{01})^{\gamma_2}} = \exp[-\gamma_1\gamma_2 (e - 2R_o i)] \qquad (3.7\text{-}2)$$

If a symmetric junction is assumed, then, $i_{01} = i_{02} = I_o$ and $\gamma_1 = \gamma_2 = \gamma$, therefore :

$$u = 2R_o I_o \tanh[-\frac{\gamma}{2}(e - u)] \qquad (3.7\text{-}3)$$

Since expanding u vs e is very complicated, the relationship between output u(t) and input e(t) referring to Fig.3.8, may be approximated as :

$$\begin{aligned} u(t) &= e(t) \quad \text{for} \quad -E_1 \leqslant e \leqslant +E_1 \\ &= E_1 \quad \text{for} \quad e \geqslant E_1 \\ &= -E_1 \quad \text{for} \quad e \leqslant -E_1 \end{aligned} \qquad (3.7\text{-}4)$$

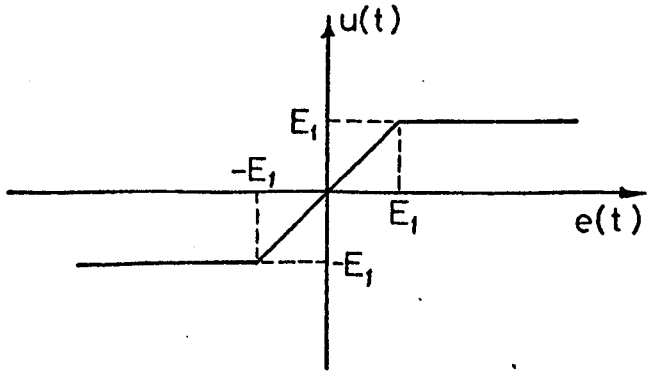

Fig.3.8 Output-input relationship of discontinuous type.

It is assumed that the constant of proportionality is unity since its only effect is to multiply the entire solution by a constant. It is convenient to represent the amplitude ratio E_{01}/E_{10} (see eqn.(3.6-2)) by k, and without loss of generality to take :

$$E_{10} > 0 \quad \text{and} \quad 0 \leqslant k \leqslant 1 \tag{3.7-5}$$

Furthermore if the ratio of cut-off amplitude E_1, in Fig.3.8, to E_{10} is assumed by c, for a specified value of k one can show :

$$0 \leqslant c \leqslant 1 + k \tag{3.7-6}$$

since for $c > 1 + k$ there is no I.P. generation.

Referring to eqn.(3.6-2), if $x = 2\pi f_1 t$ and $y = 2\pi f_2 t + \phi$, then the relationship in eqn(3.7-4) becomes :

$$\begin{aligned} u(x,y) &= E_{10}(\cos x + k\cos y) && \text{for} && -c \leqslant \cos x + k\cos y \leqslant +c \\ &= E_1 && \text{for} && \cos x + k\cos y > -c \\ &= -E_1 && \text{for} && \cos x + k\cos y \leqslant -c \end{aligned} \tag{3.7-7}$$

If either x or y is increased or decreased by any multiple of 2π, the value of u(x,y) is unchanged. Hence u(x,y) is a periodic function of x and y. From the above consideration, u(x,y) can be investigated by expanding it in a double Fourier series in x and y, since it satisfies the condition of expansion, thus :

$$U(x,y) = \sum_{m=0}^{\infty} \sum_{n=0}^{\infty} \left[U_{\pm mn} \cos(mx \pm ny) + W_{\pm mn} \sin(mx \pm ny) \right] \tag{3.7-8}$$

where

$$\begin{aligned} U_{\pm mn} &= \frac{1}{2\pi^2} \int_{-\pi}^{\pi} \int_{-\pi}^{\pi} u(x,y) \cos(mx \pm ny)\, dx\, dy \\ W_{\pm mn} &= \frac{1}{2\pi^2} \int_{-\pi}^{\pi} \int_{-\pi}^{\pi} u(x,y) \sin(mx \pm ny)\, dx\, dy \end{aligned} \tag{3.7-9}$$

It is easy to investigate that (see Appendix VII) :

$$W_{\pm mn} = 0$$

$$U_{\pm mn} = 0 \quad \text{for} \quad m+n \quad \text{even}$$

$$U_{mn} = U_{\pm mn} = \frac{4}{\pi^2} \int_{y=0}^{\pi} \int_{x=0}^{\arccos(-k\cos y)} U(x,y) \cos mx \cos ny \, dx \, dy \quad \text{for } m+d \text{ odd} \tag{3.7-10}$$

Referring to Appendix VII, the integration of the right-hand side of eqn.(3.7-10) for the 3rd- and 5th-order I.P.'s can be done numerically. Some results are shown in Graphs 3.1 to 3.6.

The amplitude of the 3rd-order $U_{-1,2}$ and the 5th-order $U_{-2,3}$, when the incident powers at both fundamental frequencies f_1 and f_2 are equal, $k = 1$, for several values of c are plotted in Graph 3.1.

The amplitude of the 3rd-order I.P.'s, $U_{-1,2}$ and $U_{2,-1}$ for three cases: $c = 0.6$, $c = 0.9$ and $c = 1.2$ against k are plotted in Graphs 3.2, 3.3 and 3.4.

The amplitude of the 5th-order I.P.'s $U_{-2,3}$ and $U_{3,-2}$ for $c = 0.6$ against k are plotted in Graph 3.5.

Assuming that there is a bias voltage E_o where $c_o = \frac{E_o}{E_{10}}$, $U_{2,-1}$ for $c = 1$ and three values of $c_o = 0$, 0.4 and 0.8 against k is plotted in Graph 3.6.

Actually Graphs 3.2 to 3.6 show the variation of I.P. levels with the incident power at the fundamental frequency f_1, while the incident power at fundamental frequency f_2 is kept constant.

(a) Since k varies from zero to one, if for instance in Graph 3.2, the amplitude of $U_{-1,2}$ is needed for a value of k greater than one, k_1, it can be obtained

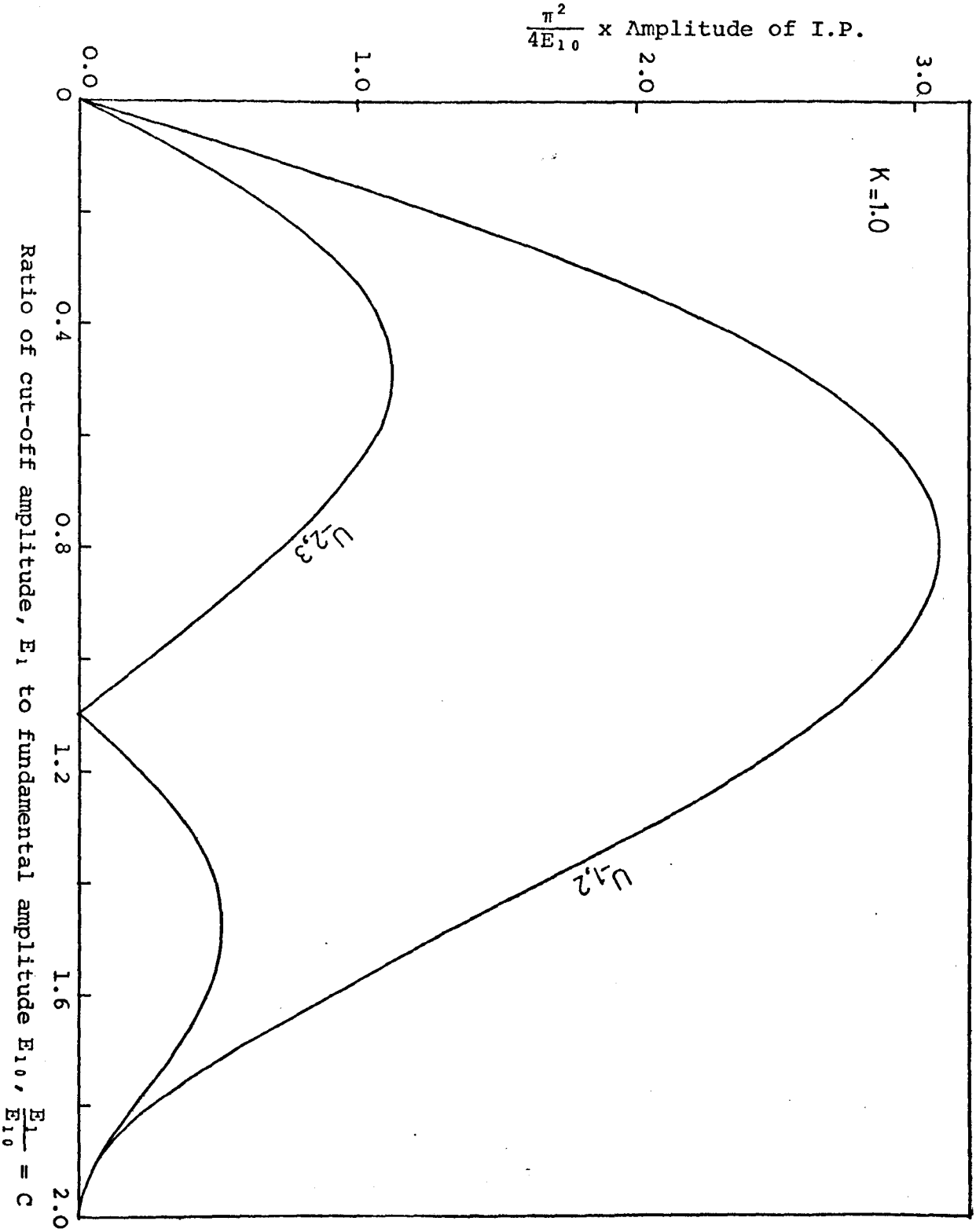

Graph 3.1 Curves showing amplitude of 3rd- and 5th-order I.P.'s at frequencies of $2f_2-f_1$ and $3f_2-2f_1$ when input wave consists of two frequencies f_1 and f_2 with equal amplitude, $\frac{E_{01}}{E_{10}} = k = 1$.

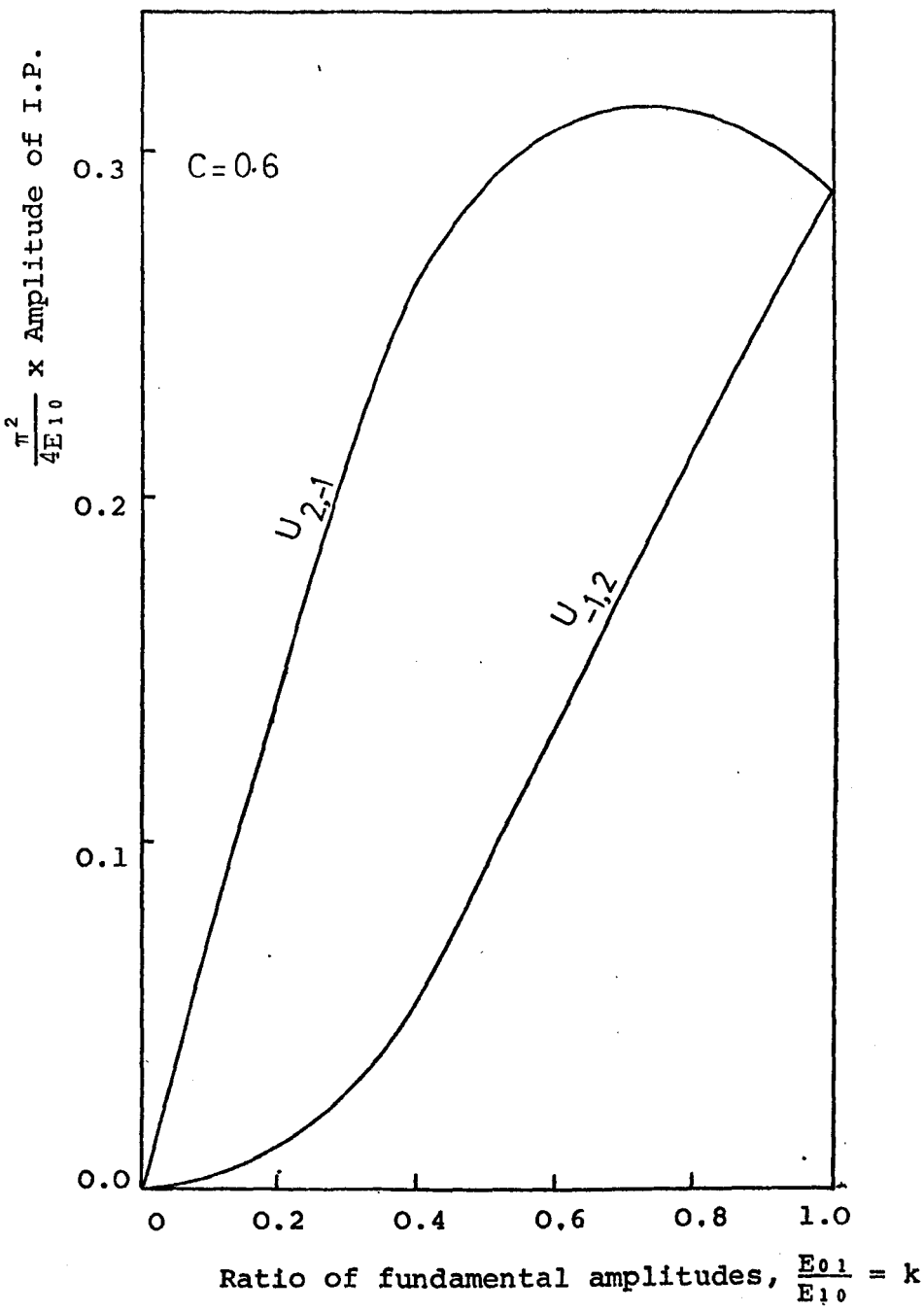

Graph 3.2 Curves showing amplitudes of 3rd-order I.P.'s at frequencies of $2f_1-f_2$ and $2f_2-f_1$ for C = 0.6.

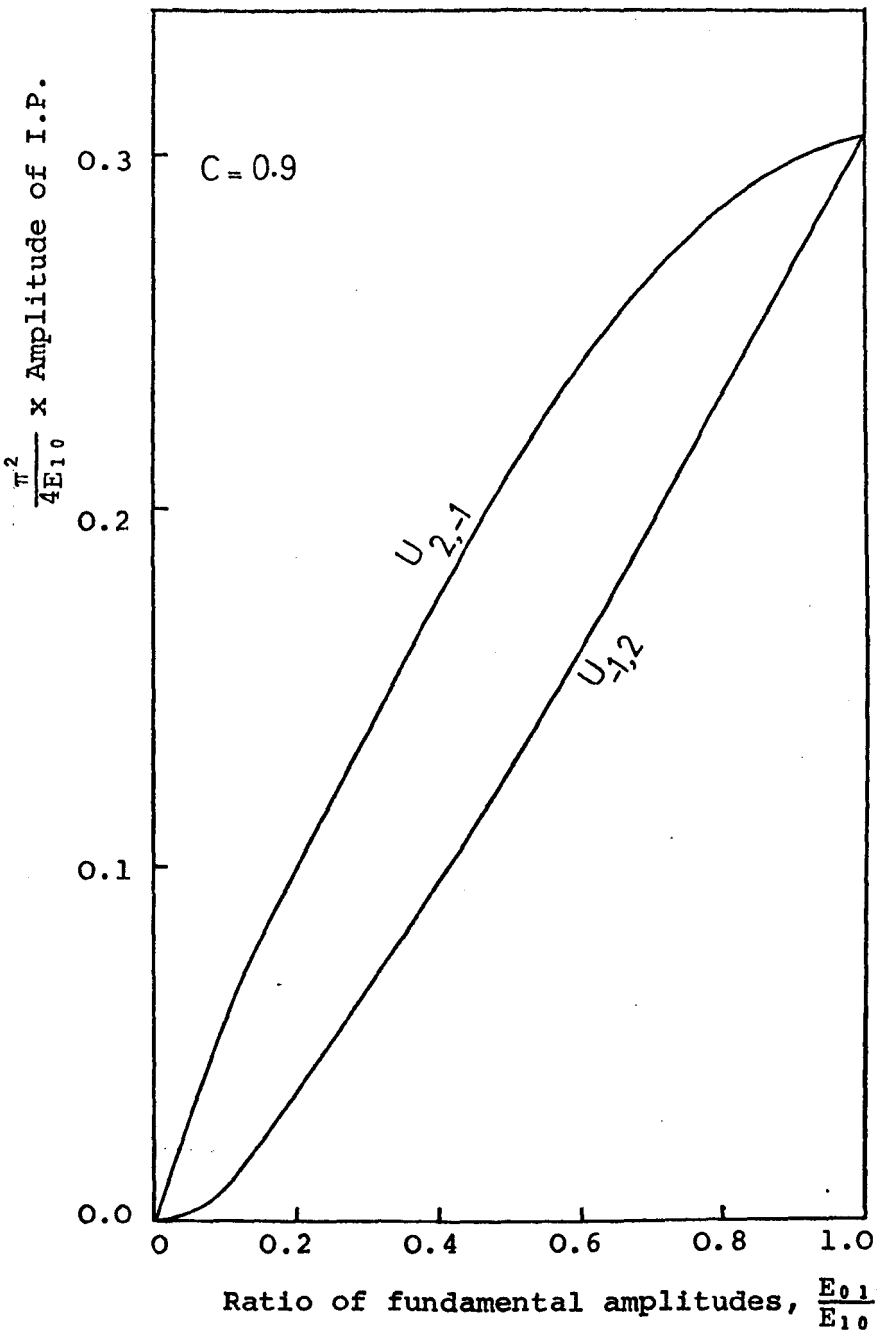

Graph 3.3 Curves showing amplitudes of 3rd-order I.P.'s at frequencies of $2f_1-f_2$ and $2f_2-f_1$ for C = 0.9.

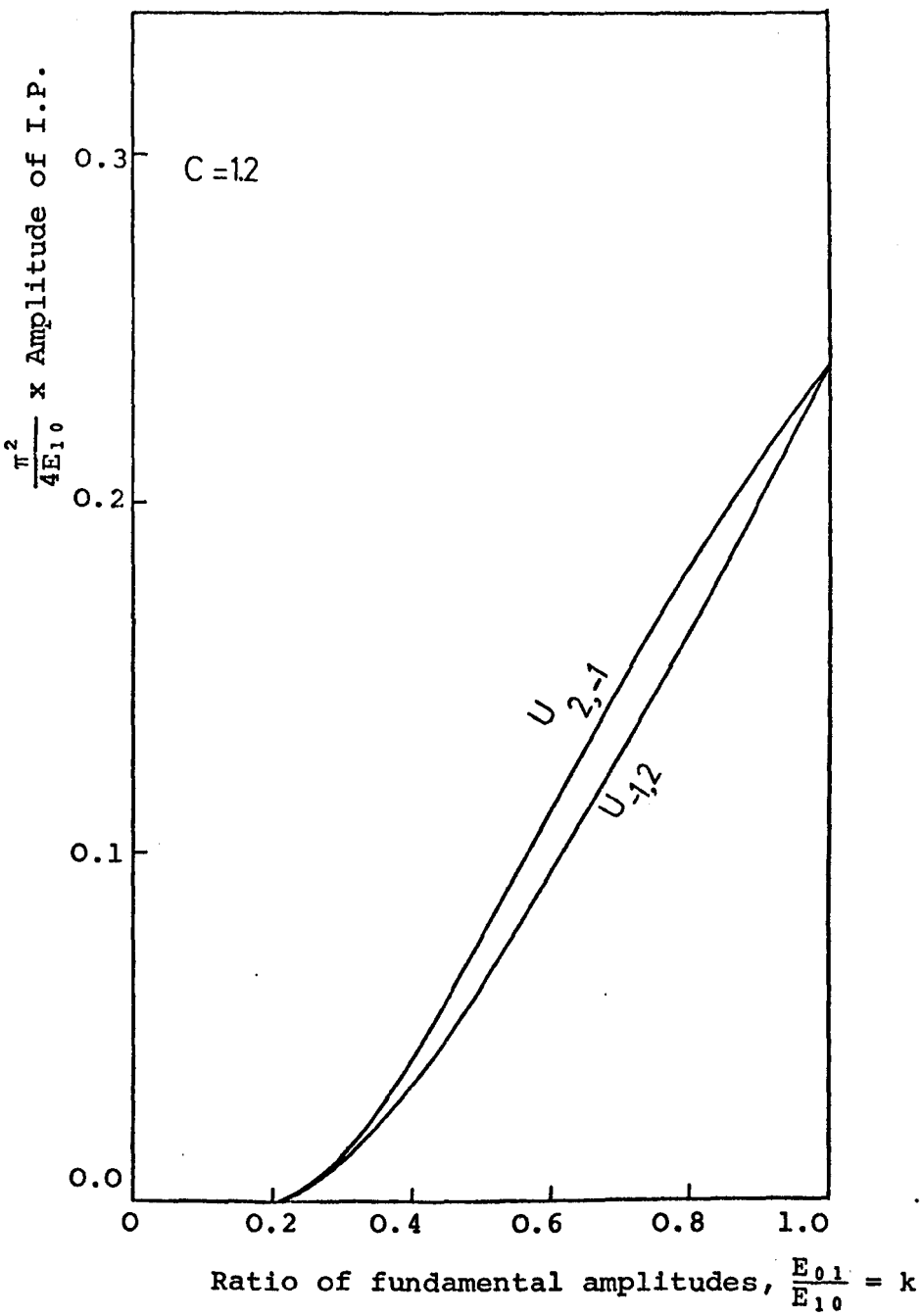

Graph 3.4 Curves showing amplitudes of 3rd-order I.P.'s at frequencies of $2f_1-f_2$ and $2f_2-f_1$ for C = 1.2.

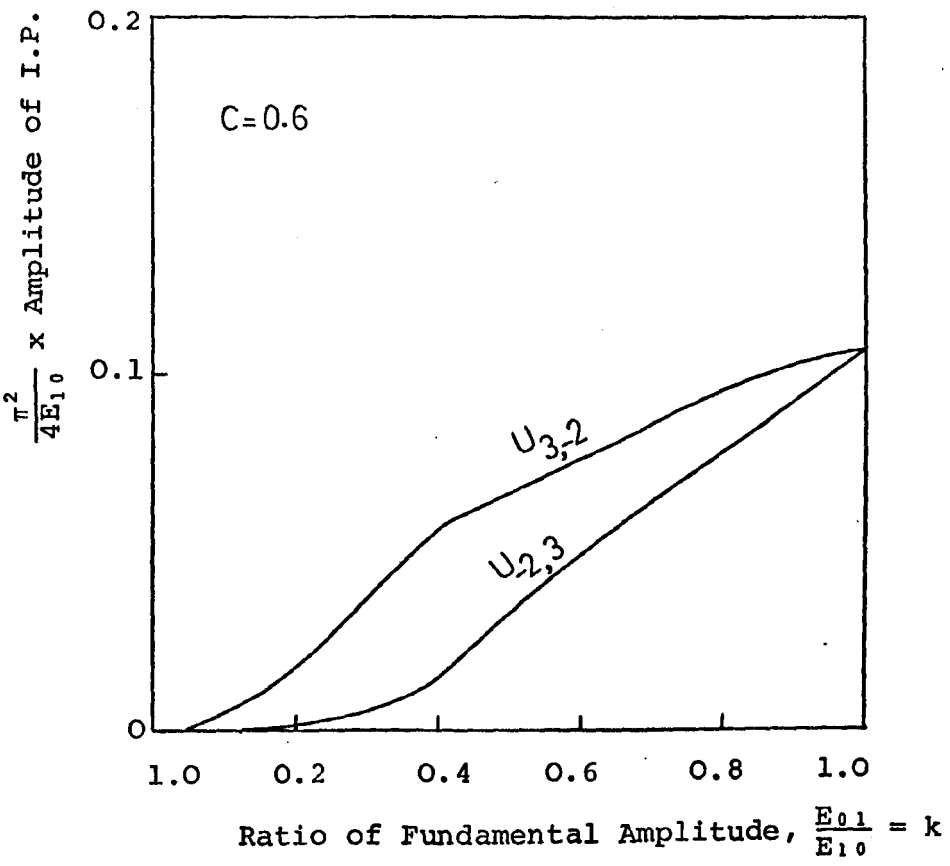

Graph 3.5 Curves showing amplitudes of intermodulation Frequencies $3f_2-2f_1$ and $3f_1-2f_2$ when Input wave consists of two frequencies with C = 0.6.

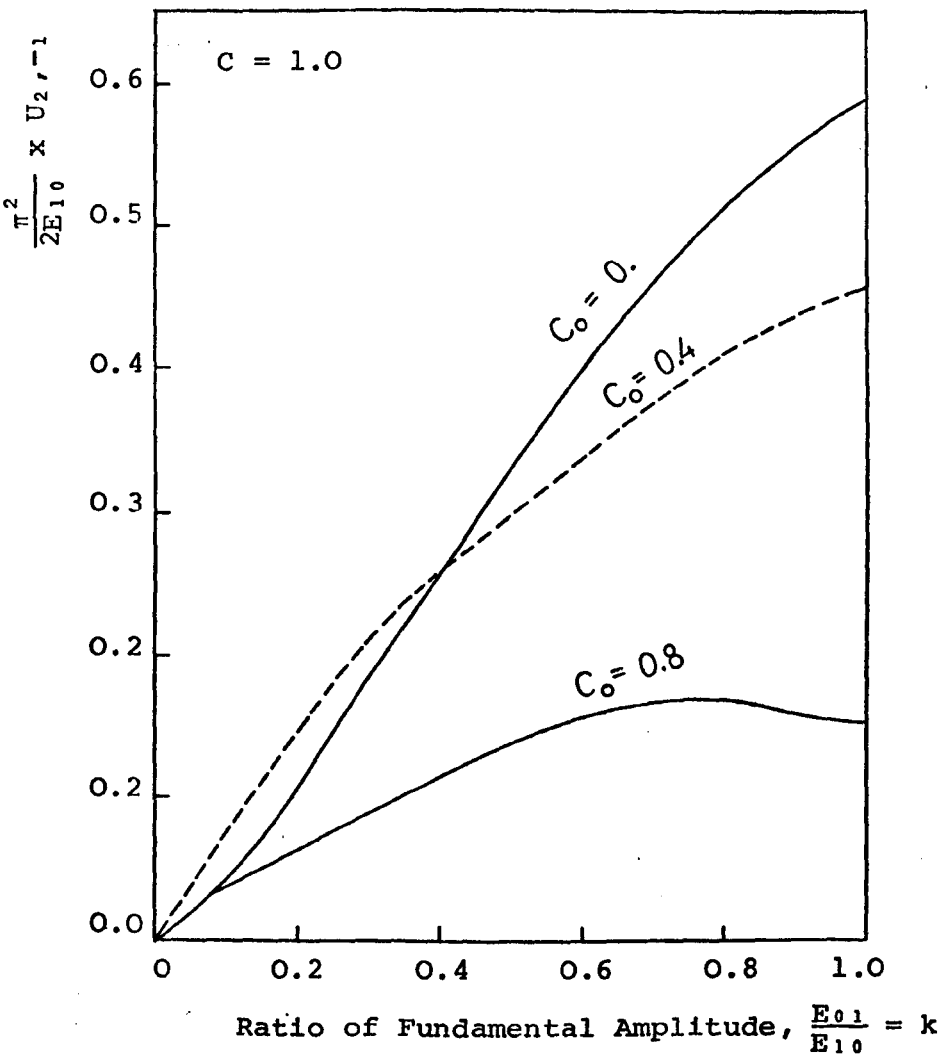

Graph 3.6 Curves showing amplitude of 3rd-order I.P. at frequency of $2f_1-f_2$ for different bias condition, C_o = 0., 0.4 and 0.8, when C = 1.0.

from the value of $U_{2,-1}$ at $k = \frac{1}{k_1}$ when this value is multiplied by k_1.

(b) The variation of U_{mn} against variation of incident power at fundamental frequency f_1, while incident power at fundamental frequency f_2 is kept constant, is equal to variation of U_{mn} against variation of incident power at fundamental frequency f_2, while incident power at fundamental frequency f_1 is kept constant.

When the input consists of only one sine wave :

$$e = E \cos 2\pi ft \qquad (3.7\text{-}11)$$

By considering the relationship of eqn. (3.7-4) and Fig.3.8, it is easy to show :

$$U_n = 0 \quad \text{for} \quad n \quad \text{even}$$

and

$$U_n = \frac{2E}{\pi}\left\{\frac{2c}{n}\sin\left[n \cos^{-1} c\right] - \frac{1}{n+1}\sin\left[(n+1) \cos^{-1} c\right] - \frac{1}{n-1}\sin\left[(n-1) \cos^{-1} c\right]\right.$$

for n odd (3.7-12)

where U_n is the half amplitude of the nth-harmonic at output and the ratio of the cut-off amplitude, E_1 in Fig.3.8, to E, is represented by c, then :

$$0 < c < 1 \qquad (3.7\text{-}13)$$

Since for $c > 1$ there is no harmonic generation.

3.8 Calculation of 5th-Order I.P. Levels from Measured 3rd-Order I.P. Levels

When the amplitude of two incident powers are the same and equal to E, then the amplitude of current of the 5th-order I.P. as a function of E, $I_{-2,3}(E)$, can be expressed as the weighted sum of a number of sample values of $I_{-1,2}(E)$ at

values of E displaced from the particular value under consideration but related to it by constant multipliers[29]. This can be done on the assumption that current in the equivalent circuit shown in Fig.3.7 is represented as a polynomial of the input voltage, i.e.

$$i = \sum_{i=1}^{\infty} a_i e^i \qquad (3.8\text{-}1)$$

In other words it is possible to write :

$$I_{-2,3}(E) = b_1 I_{-1,2}(c_1 E) + b_2 I_{-1,2}(c_2 E) + \ldots + b_n I_{-1,2}(c_n E) \qquad (3.8\text{-}2)$$

The values of b's and c's, by using Appendix VI, parts 3 and 4 (to ease calculation when using parts 3 and 4 of Appendix VI one should replace V by E) for approximations involving from one to six samples are as follows :

n=1 no approximation formula exist

n=2

c_1=1.0379 c_2=0.7677
b_1=0.3665 b_2=-0.9059

n=3

c_1=1.0105 c_2=0.8592 c_3=0.6193
b_1=0.5857 b_2=-0.8236 b_3=-0.3449

n=4

c_1=1.0043 c_2=0.9044 c_3=0.7444 c_4=0.5198
b_1=0.7091 b_2=-0.6787 b_3=-0.4725 b_4=-0.1514

n=5

c_1=1.002 c_2=0.9315 c_3=0.8169 c_4=0.6560 c_5=0.4501
b_1=0.7880 b_2=-0.5453 b_3=-0.4926 b_4=-0.2712 b_5=-0.7589

n=6

c_1=1.0639 c_2=1.0033 c_3=0.9221 c_4=0.8033 c_5=0.6429 c_6=0.4403
b_1=-0.1086 b_2=0.7487 b_3=-0.5636 b_4=-0.4660 b_5=-0.2471 b_6=-0.6821

In Graphs 3.7 and 3.8 measured 5th-order I.P.'s together with those calculated from measured 3rd-order I.P. levels for 3 sample case, n=3, and 2 sample case, n=2, for

stainless steel cast Nos. 3714 and 3716, are plotted.

This calculation at low incident power and when the 3rd-order I.P. levels are constant over a range of total incident power does not give a good approximation.

3.9 Summary

When two metallic electrodes are brought together, they are actually separated by an insulating film (oxidized layers), then the non-linear I-V characteristic of the contact is responsible for the generation of I.P.'s, where the "V" could be the voltage drop between two electrodes or the contact voltage (constriction voltage) or the sum of both. This non-linear characteristic depends on the shape factor of the contact point which in turn is a function of the axial force and mechanical properties of the bulk of the electrodes. For certain electrode members and at a certain axial force, the I-V characteristic depends on temperature at the contact point, thickness of oxidized layers, forbidden energy gap of oxidized layers and their dielectric constant. For insulator thickness less than 40Å, and for a temperature of 300k, the tunnel J-V characteristic for similar and dissimilar electrodes, predominates. For insulator thickness more than 40Å at a temperature of 300k, the thermionic effect predominates and for a thicker insulator, there will be the space-change effect. Therefore, even if the temperature of the contact point does not change by increasing "V", the J-V characteristic resulting from the tunnel effect and thermionic effect[24] is not a simple exponential curve. The fact is, the I-V characteristic becomes complicated when the temperature at the contact is not constant, and even more

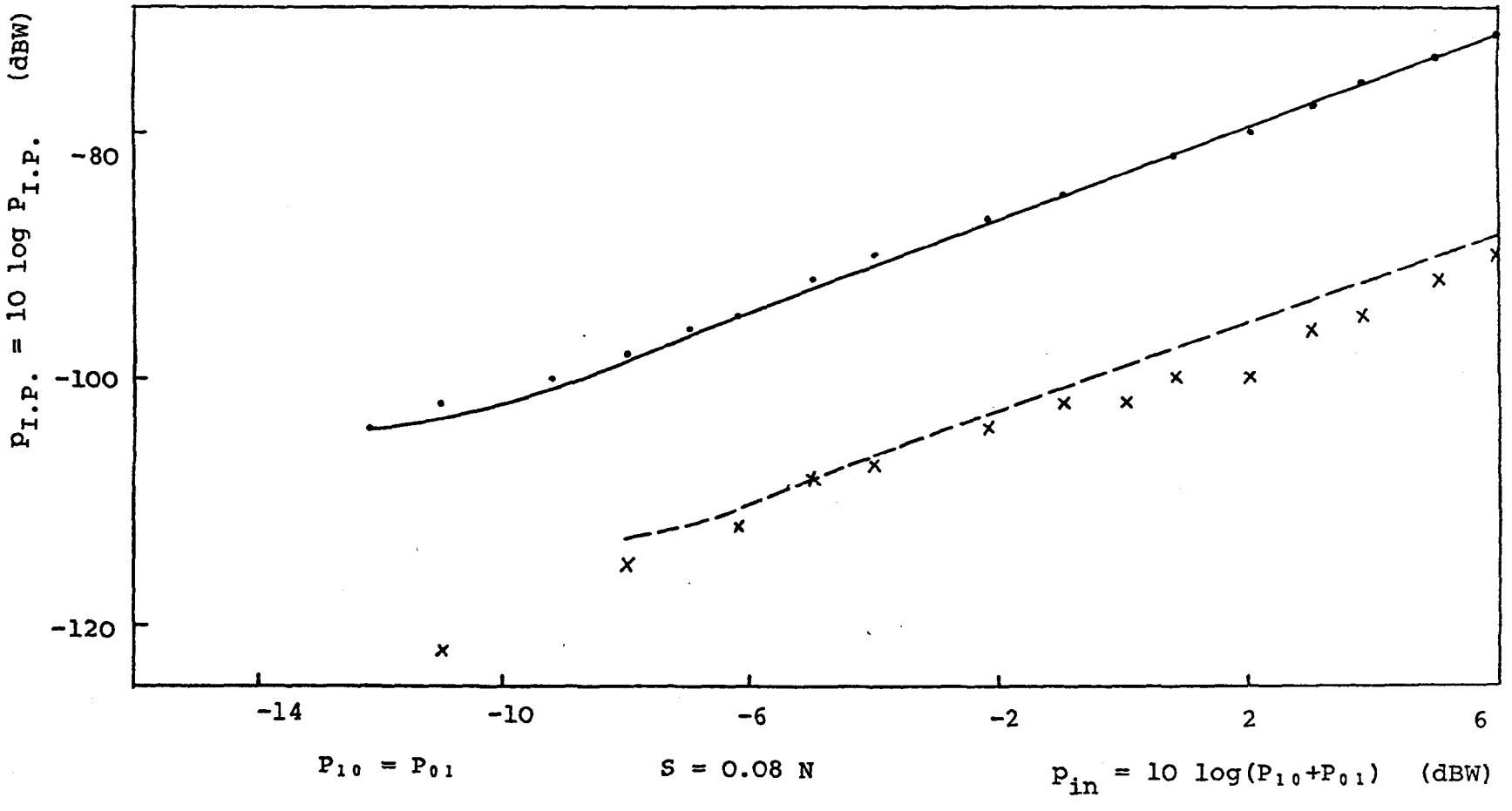

Graph 3.7 Measured 3rd-order and 5th-order I.P. for stainless steel to stainless steel, cast No. 3714, and 3-sample case, 5th-order I.P. calculated from 3rd-order I.P.

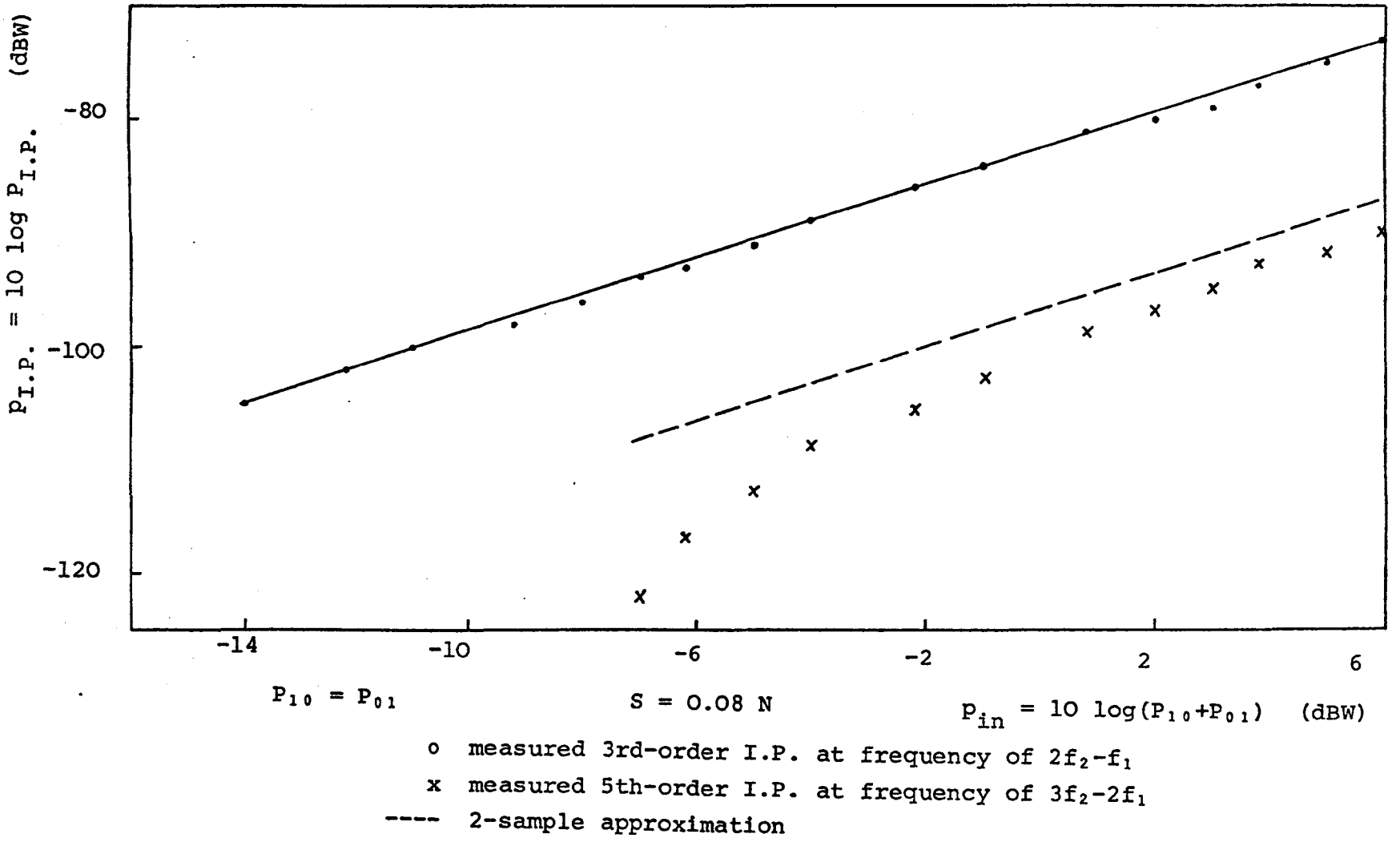

Graph 3.8 Measured 3rd-order and 5th-order I.P. for stainless steel to stainless steel, cast No. 3716, and 2-sample case, 5th-order I.P. calculated from 3rd-order I.P.

complicated when the metal members become more activated at a higher temperature, presenting a changeable behaviour of contact. All of them together make a theoretical treatment very difficult.

CHAPTER 4

4. TECHNIQUES OF MEASUREMENT

4.1 Introduction

The investigations are concerned with the measurement of 3rd-order intermodulation products ($2f_2-f_1$) at a frequency of 2.1GHz and 5th-order intermodulation products ($3f_2-2f_1$) at a frequency of 2.5GHz. The two power sources were operated at frequencies of f_1 = 1.296GHz and f_2 = 1.698GHz respectively.

4.2 Quantitative Investigation

For convenience and clearer representation, the power level of a given intermodulation product, $p_{I.P.}$, was recorded in "dBW" according to the following expressions :

$$p_{I.P.} = 10 \log P_{I.P.} \quad \text{(referring to a level of 1W)}$$

where p_{mn} = power level of I.P. at a frequency of (m+n) in "dBW"

P_{mn} = power level of I.P. at a frequency of (m+n) in "W"

If the measured power levels of the 3rd- and 5th-order intermodulation products by the spectrum analyser were $\alpha_{-1,2}$ and $\alpha_{-2,3}$ both in "dBm", it was estimated that the total power levels of the 3rd- and 5th-order intermodulation products $p_{-1,2}$ and $p_{-2,3}$ both in "dBW" generated at a contact, were 12 and 16dB too low respectively, owing to the following points :

1. Approximately half the intermodulation products power generated by the test sample reaches the power-combining unit. The other half will be absorbed in the dummy load connected to the end of the test sample.

2. The transmission losses take place between ports 6 and 5 of the power combining unit. The transmission losses at 3rd-order intermodulation frequency (≈2.1GHz) and at 5th-order intermodulation frequency (≈2.5GHz) between ports 6 and 5 of the power combining unit according to Graph 2.6(b) are 13dB and 9dB respectively.
3. The transmission losses take place between port 5 of the power combining unit and the spectrum analyser through B.P.F.(3) and the junction cord (Andrew cable of about 1.5m long). These losses for both intermodulation frequencies were estimated to be about 2dB.

Finally by changing the units from "dBm" to "dBW" one can obtain :

$$P_{-1,2}(\text{dBW}) = \alpha_{-1,2}(\text{dBm}) - 12$$
$$P_{-2,3}(\text{dBW}) = \alpha_{-2,3}(\text{dBm}) - 16$$

These 12dB and 16dB differences were taken into account during the measurements of the intermodulation products and corrections have been made to the final results reported here.

The experimental work fell into two categories :

1. Intermodulation products power level variation with incident powers.
2. Intermodulation products power level variation with axial force.

For the measuring of the intermodulation products power level with incident power, the investigation was carried out as follows :

The two power signal sources A and B (see Fig.2.1), were set at frequencies f_1 and f_2 of 1.296GHz and 1.698GHz respectively at which they were calibrated. The two tunable band pass filters, B.P.F.(1) and B.P.F.(2), were then tuned to the appropriate frequencies of f_1 and f_2 respectively. The receiver band pass filter B.P.F.(3) was tuned to the intermodulation product frequency being investigated. Finally the test sample was plugged into the appropriate location in the coaxial contact measuring device (see Figs.2.5, 2.6 and 2.7).

After allowing about 40 minutes for the two power signal sources and the spectrum analyser to warm up, the power levels at both sources were increased according to Graph 2.7, to a maximum value of $P_A \approx 12.6W$ and $P_B = 8W$ (A and B refer to power signal sources of frequencies $f_1 = 1.3GHz$ and $f_2 = 1.7GHz$ respectively) which provided a resultant equal incident power upon the test sample of 1.92W. In some measurements, maximum input power level was limited by the sample itself. Keeping the incident R.F. power upon the test sample equal, readings of 3rd-order I.P. levels were taken as the total incident power upon the test sample varied from a minimum at which the intermodulation signal was detectable to the maximum of $2 \times 1.92W$ and then from the maximum down to a level at which the intermodulation signal level was undetectable on the spectrum analyser. Equal incident power upon the test sample was necessary for comparison of results. If 5th-order I.P.'s could be detected the receiver band pass filter B.P.F.(3) was then tuned to this frequency and a set of measurements was taken of 5th-order power level variations with decreasing incident power upon the test sample.

Owing to the critical nature of the tests to be carried out great care was necessary to minimize the effect of other components on the I.P.'s of interest. Therefore it was necessary to characterise the "residual level" of the measuring circuit when there is a single piece (see Fig.4.1) at the test sample location. This was done before carrying out the measurements of I.P.'s generated by the test sample of different materials, as follows :

By disconnecting the main outer conductor body of the coaxial-contact measuring device (see Fig.2.6), a single piece of the same material as the test sample pairs to be investigated, was inserted into the test sample location by screwing it to the appropriate sections of the inner conductor of the coaxial-contact measuring device. This single piece was prepared with a diameter equal to that of the inner conductor of the coaxial-contact measuring device and a length equal to that of the test sample pairs, as illustrated by Fig.4.1. Good metal contacts at junctions X and Y were established as demonstrated by Fig.4.2. Finally the main outer conductor body of the device was screwed tightly back onto the input section and the 3rd- and 5th-order I.P. power levels were observed over the whole spectrum of R.F. input power.

This procedure was repeated for each different material mentioned in Section 5.1 and further the whole procedure was repeated a number of times as a check of the validity of the results. It was observed that the residual level of the 3rd-order I.P. level was about -125dBW at the maximum incident power (i.e. $P_{10} = P_{01} = 1.92W$ or $P_{in} = 3.84W$). When the input power level decreased, the level of I.P. also decreased, and

measurements of intermodulation power level, over the whole incident power range and the resultant graph were produced. This graph will be referred to as the "residual curve" and included in most of the graphs given in Chapter 6 for comparison reasons.

To confirm that the display obtained on the CRT of the spectrum analyser was due to the I.P.'s generated at the contact (see Fig.4.3), the following checks were made :

1. One of the transmitter frequencies was changed by a known amount, then by observing the change in magnitude and direction of the output frequency, the output signal could be properly identified. Consider for example the measurement of the 3rd-order I.P.'s at the frequency of $2f_2-f_1$ for which the receiver band pass filter B.P.F.(3) was tuned. Keeping f_1 constant and increasing/decreasing f_2 by Δf_2, must cause an increase/decrease of $2\Delta f_2$ in the intermodulation frequency. Similarly, keeping f_2 constant at a given frequency and increasing/decreasing f_1 by Δf_1, must cause a decrease/increase of Δf_1 in the intermodulation frequency.
2. An increase or decrease of power level of either of the signal sources resulted in a corresponding increase or decrease of the level of intermodulation signal observed on the spectrum analyser. Thus, reducing the power level of one of the signal sources to zero should reduce the power level of the intermodulation signal under consideration to

3. During the time of the measurements, if the test specimen was disturbed or the initial set condition of the given test specimen altered by any means, a change in the level of intermodulation signal was observed.
4. When there was no metal-to-metal contact between the two halves of the test sample pairs (see Fig.4.3) at the maximum R.F. incident power level, the 3rd-order intermodulation product power levels at frequency 2.1GHz were approximately equal to the "residual level". There were no detactable 5th-order intermodulation products at frequency 2.5GHz.
5. When the two halves of the test sample pairs were brought together so as to just make contact, strong 3rd- and 5th-order I.P.'s were generated.
6. When one of the contacting metal surfaces of the test sample pair was totally sprayed with a thin P.T.F.E. dielectric coating and then the two halves brought back into contact under the same conditions (i.e. physical metal-to-metal contact was eliminated), the 3rd-order I.P. power levels were again approximately equal to the "residual level" and also no 5th-order I.P.'s were detected.

Owing to the geometrical configuration of a test sample pair as illustrated in Fig.4.3, some power reflection will occur at the discontinuity caused by the test sample in its location in the coaxial-contact measuring device. When the two halves of a test sample pair were in contact, since the length of discontinuity is much less than a wavelength, it was estimated that the power reflection taking place at the

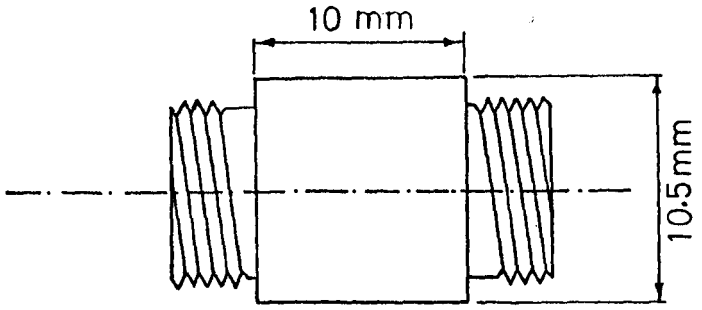

Fig.4.1 Single piece of material.

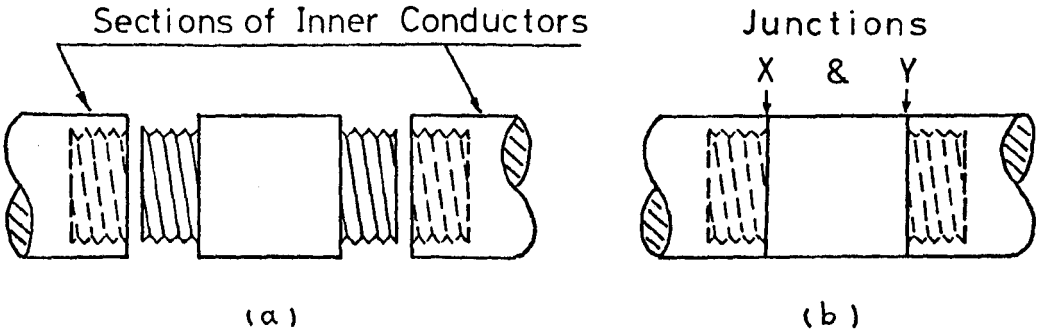

Fig.4.2 Insertion of a single piece of material into the test sample location of a coaxial contact measuring device.

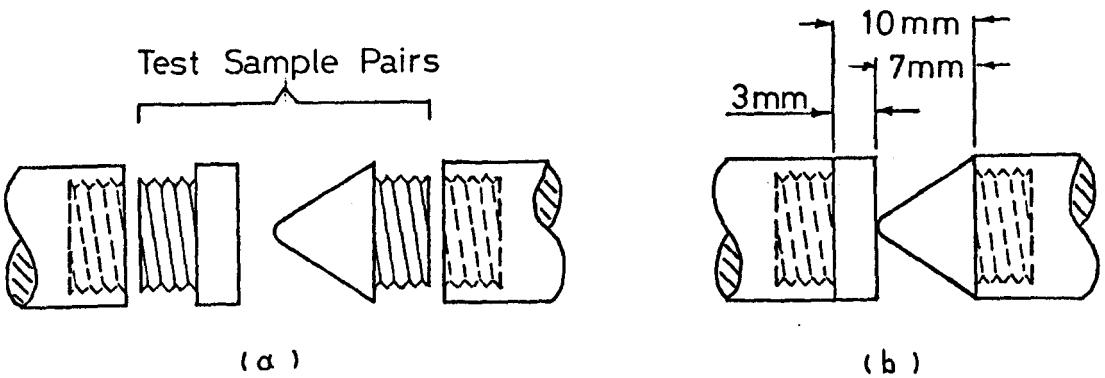

Fig.4.3 Insertion of test sample pairs into the test sample location of a coaxial contact measuring device.

discontinuity was about 1%. This level of power reflection did not seriously degrade the electrical performance of the measuring circuit.

Intermodulation product power level variations with incident power were measured at approximately 0.07N axial force which was established by using an "Avometer" and checking the continuity of the inner conductor and increasing the axial force from zero to 0.07N. After removing the "Avometer" from the circuit, the variation of 3rd-order I.P.'s with increasing and decreasing incident power were measured. Then both input power levels were taken up to 1.92W each and 5th-order I.P. levels with decreasing incident power were measured. Data was then obtained by varying the axial force from 0.07N to about 3.55N (in a few cases up to 5.68N) and recording the respective 3rd- and 5th-order I.P. power levels by tuning the receiver filter to the appropriate frequency while the incident power levels were kept constant at 1.92W each. At an axial force of 3.55N, again the variation of 3rd- and 5th-order I.P. levels with decreasing incident power were measured. Then by increasing the incident power levels up to the maximum value (1.92W each), readings of 3rd- and 5th-order I.P. levels were continued with varying axial force from 3.55N up to 10.65N, while again incident power levels were kept constant at 1.92W. In some cases, however, before establishing initial contact at the test sample junction, the R.F. input power levels of both sources were increased to the maximum value. During this procedure it was observed that when there was no physical contact at the junction, only the "residual level" was detectable on the spectrum analyser. In this situation when

contact had just occurred at approximately zero axial force at the junction, the strongest 3rd- and 5th-order I.P. power levels were observed for all the similar and dissimilar metal-to-metal contacts. These strong I.P. power levels were most susceptible to very large changes, since keeping the contact at zero axial force was impossible. Therefore initial readings were done at 0.07N instead of zero axial force. No measurements were undertaken in the reverse order with respect to axial force (i.e. starting from a maximum value of the axial force to a minimum value or zero), since the calibration of the bellows (see Section 2.2.7.1) used in the coaxial-contact measuring device would no longer apply. In the experiments with increasing axial force, Graph 2.8, which gives a direct reading of axial force in Newton for a given value of compression in mm, was used.

In the second group of measurements (statistical measurements), the same initial procedure was carried out, but only the 3rd-order I.P. power levels generated at the contacts of five test sample pairs of each of seven different materials (see Section 5.1, except oxygen-free copper) and of three test sample pairs of each of twelve different steels (see Table 5.1), were measured at discrete axial force of 0.07N, 0.3555N, 1.42N, 3.55N, 7.1N and 10.65N while the incident power level of each power source upon the test sample was kept constant at 1.92W.

CHAPTER 5

5. TEST SAMPLES AND THEIR ASSEMBLY PROCEDURE

5.1 Test Samples

The generation of intermodulation products at contacts was studied for the following base materials :

Commercial copper	B.S. 1432/3
Commercial hard-brass	B.S. 249
Commercial mild-steel	B.S. 970 dated EN3B
Aluminium alloy (Duraluminium)	B.S. HE30 WP
Stainless-steel	B.S. dated type 321 S20 EN58-B
Half-hard beryllium copper	
O-Nickel (oxygen-free nickel)	
O-Copper	

and twelve steels with different compositions* according to table 5.1.

The experimental study was aimed at the investigation and comparison of intermodulation products generated in several contact materials. Therefore, only one type of geometrical configuration, namely, spherical contact, was used (see Fig. 5.1).

5.2 Mechanical Polishing of Test Samples

In the study of metal-to-metal contacts, the surface finish of the contacting faces of the test sample pairs was obtained by mechanical polishing. It was necessary to obtain

---

*The steels were made in the Metallurgy Department of the University of Sheffield. They were made in small induction vacuum furnace of 1kg capacity. The base iron was pure iron (0.005%C) and alloy additions were commercially pure (99.5%). They were hot rolled at 1150°C from 25mm diameter to 12.5mm diameter.

Table 5.1 Steels made in Metallurgy Dept. of University of Sheffield

Analysis in %

Cast No.	C	S	P	Cr	Mn	Mo	Ni	Si	W	V	Nb	Ti	Co	Al	Cu	Old cast No.
3709RV	0.12	-	-	<0.02	1.7	<0.02	<0.02	0.74	<0.02	<0.02	<0.02	<0.02	0.02	0.027	<0.02	2507
3710RV	0.15	-	-	-	1.78	"	<0.02	1.08	"	"	"	"	<0.02	0.025	"	2508
3711RV/B	0.14	-	-	2.09	1.79	"	2.26	0.34	"	"	"	"	"	0.023	"	2505
3712RV	0.17	-	-	1.84	1.70	"	4.18	0.4	"	"	"	"	"	0.018	"	2506
3713RV	0.21	-	-	2.9	1.63	"	3.00	0.33	"	"	"	"	"	0.014	"	2491
3714RV	0.2	0.041	0.007	<0.02	1.57	"	<0.02	0.31	"	"	"	"	"	0.023	"	2389RV/A
3715RV	0.14	0.046	0.004	0.27	1.59	"	<0.02	0.37	"	"	"	"	"	0.024	"	2389RV/B
3716RV	0.16	0.049	0.005	1.85	1.67	"	0.02	0.35	"	"	"	"	"	0.011	"	2389RV/C
3717RV	0.14	0.048	0.003	15.2	1.87	"	<0.02	0.35	"	"	"	"	"	<0.02	"	2389RV/D
3718RV	0.2	-	-	0.02	1.51	"	0.025	<0.02	"	"	"	"	"	0.050	"	2494
3719RV	0.31	-	-	<0.02	1.66	"	0.04	0.02	"	"	"	"	"	0.070	"	2495
3720RV	0.12	-	-	<0.02	1.7	"	<0.02	0.02	"	"	"	"	"	0.17	"	2496

Fig. 5.1 Geometrical Configuration of Test Sample Pairs

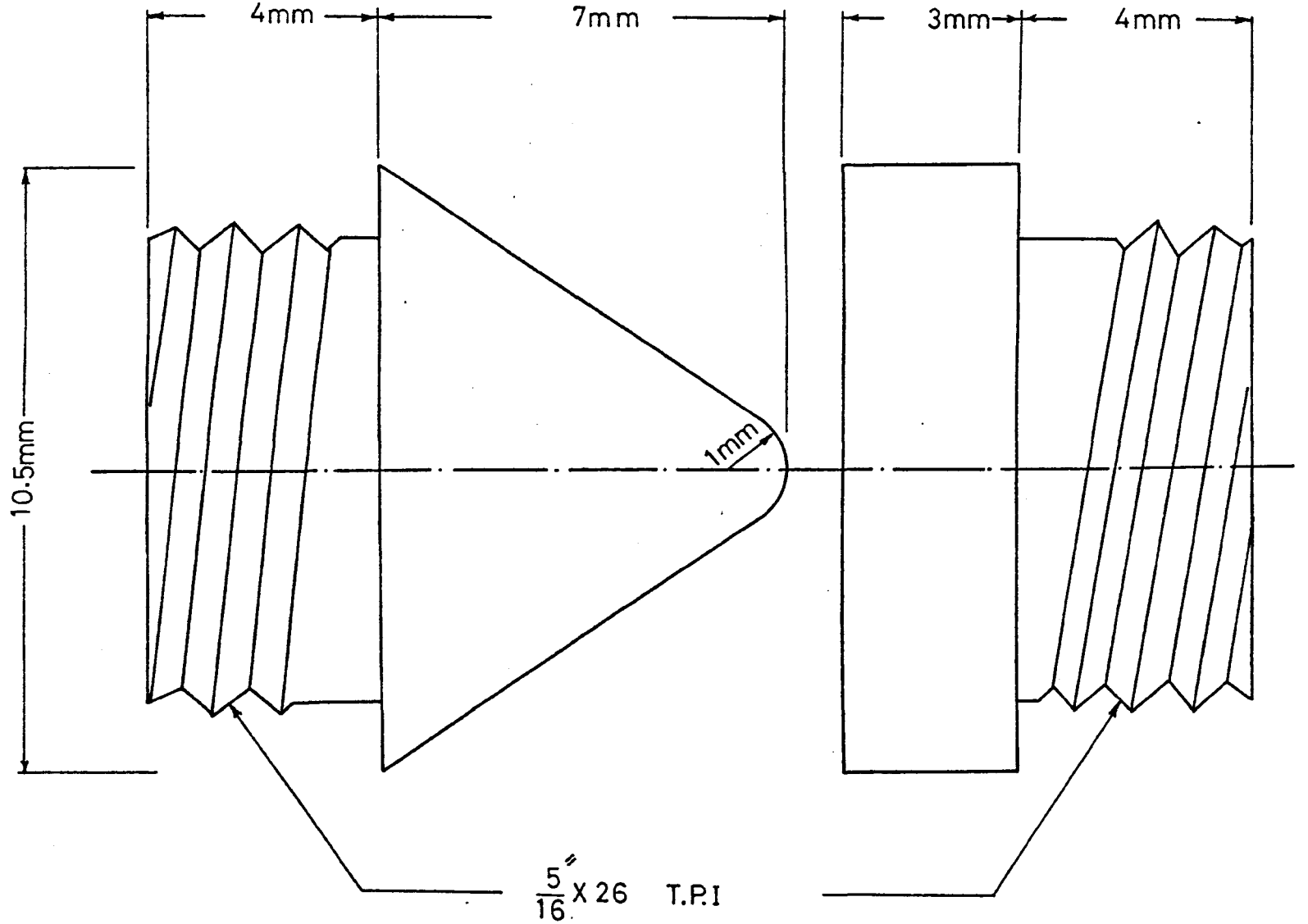

a better surface finish on the specimens to obtain comparable results, since only machined down-to-size samples had very irregular surfaces. Emery cloth, with grain sizes of 600 mesh, was used for mechanical polishing of one half of a test sample pair (flat one, see Fig.4.3), while the spherical one was polished with a polishing cloth (with nap on it) of 4μ (which was the size of the diamond particles in the paste which was rubbed on to the polishing cloth). Then the test sample halves were washed with Teepol (which was a multiple purpose detergent of 50%) and then dried off with Methanol. All the contact surfaces of the specimen were mechanically polished to give a surface roughness of less than 15μ (C.L.A.)*. Similar and dissimilar metal-to-metal contacts were studied by mechanical polishing of the surfaces of test sample pairs.

5.3 Electropolishing of Test Samples

It was necessary to study the effect of surface finish of test sample pairs to know how important the role of contact surface condition is on the contact resistance, which was reported[15] to be the predominant non-linearity generating intermodulation product. Because of perturbation of the structure of test sample pairs caused by mechanical polishing, the contact surfaces of six test sample pairs made of copper, oxygen-free copper, stainless steel (EN58B), mild steel, oxygen-free nickel and aluminium alloy, were electropolished to give a surface roughness of less than 0.3μ (C.L.A.). Since the overall area of one half of the test sample pair (flat one) was about 3.9cm^2 and that of the spherical one was about 3.5cm^2, the operating conditions and bath compositions for the above electropolishing (except aluminium alloy), are given in table

---

* C.L.A. is defined as arithmetical mean deviation, British Standards, Methods for the Assessment of Surface Texture, 1134, Part I, 1972.

IX-1. The contact surfaces of test sample pairs made of aluminium alloy were electropolished by local polishing[30] (Jacquet Method). Local polishing, carried out by means of a pad electrode, with its round tip wrapped in a material which is an electric insulator, was unattacked by the electrolyte, but spongey enough to retain a good quantity of it. This pad is made the cathode and the metal is the anode, connected to the positive pole of a current source. The polishing process, which is restricted to the contact zone (0.5-1cm^2) can be extended as desired by moving the pad. Thus, at an initial voltage of 15-30V, a current of 0.2-0.4A polishes the small area, whereas an ordinary cell would require a much higher current. It is a particular advantage of the process that it is independent of the surface area to be polished and that the value of both voltage and current density can be finally defined for any particular metal and electrolyte. The operation condition, voltage and current of aluminium alloy electropolishing is given in Appendix IX. Similar metal-to-metal contacts were studied by electropolishing of the surfaces of six mentioned test sample pairs.

5.4 Electroplating of Test Samples

A study of electroplated metal contacts was carried out using gold, silver, copper, nickel and cadmium plating to a thickness of approximately 3μ for gold, silver and copper, and 30μ for nickel and cadmium. All test sample pairs electroplated*, were machined from commercial hard brass specified in section 5.1. Before electroplating, the contacting

*Electroplating was kindly performed by J. Townroe & Sons Ltd., Sheffield.

face of the flat surface half, of a test-sample pair, was mechanically polished (with surface roughness of less than 0.3μ C.L.A.) and the spherical half was roughly micro-polished with approximately the same surface roughness of 0.3μ C.L.A.

CHAPTER 6

6. RESULTS

6.1 Introduction

As mentioned in Section 3.9, the non-linear I-V characteristic, or in other words the non-linear contact resistance, is responsible for generation of I.P.'s. The axial force (and not pressure, since the actual area of contact differs from the apparent area of contact) and the geometry of a particular sample at a certain voltage drop "v", determine the contact resistance (see equation (3.2-2) for similar electrodes) which is the sum of the constriction and tunnel resistances for the insulator film (oxidized layers) with a thickness of less than 40Å.

Therefore, the data reported in this chapter is introduced under the following two fundamental groups :

1. Variation of the I.P. power level $p_{I.P.}$, expressed in "dBW" (as defined in Section 4.2), with incident power p_{in}, expressed in "dBW" (see Section 3.6 for notation), when the axial force S is kept constant.
2. Variation of the I.P. power level $p_{I.P.}$, with axial force S, expressed in Newtons, when the incident power P_{in} is kept constant.

The fundamental frequencies were f_1 = 1.296GHz and f_2 = 1.698GHz and measurements were taken for the 3rd-order I.P.'s, $p_{-1,2}$, at a frequency of 2.1GHz, and 5th-order I.P.'s, $p_{-2,3}$, at 2.5GHz. Great care was taken during the assembly of theses measuring circuits to ensure that no significant I.P.'s were present due to the system itself. This was achieved by

minimizing the number of connections involved and whenever possible placing components, such as the coaxial contact measuring device, filters, power sources and power combining unit etc., on shock absorbing material, and as a further precaution, connectors were tightly screwed together. The notation of "residual levels" appearing on the graphs is concerned only with the 3rd-order I.P. as discussed, in detail, in Section 4.2, since there was no detectable 5th-order residual level through the whole range of incident power level.

6.2 Similar Metal-to-Metal Contacts with Mechanically Polished Surface

Variation of 3rd- and 5th-order I.P. levels from similar-to-similar contacts with mechanically polished contact surfaces (see Section 5.2) of eight base materials and twelve different steels (see Section 5.1) were recorded. Measurements were carried out for each test sample pairs according to Section 4.2, i.e. variation of 3rd-order I.P. with increasing and decreasing incident power level at an axial force of 0.08N, variation of 5th-order I.P. with decreasing incident power at the same constant axial force, variation of 3rd- and 5th-order I.P. levels with axial force at total incident power of $2 \times 1.92 = 3.84$W and finally variation of 3rd- and 5th-order I.P. levels with decreasing incident power level at axial force of 3.55N (for a few test sample pairs at axial force of 5.68N which are mentioned below each figure).

6.2.1 Stainless steel-to-stainless steel (EN58B)

Graph 6.1 shows the results for stainless steel (EN58B). The 3rd-order I.P. level (see Graph 6.1a) increased with increasing incident power level up to $P_{in} \approx 0.15$W ($p_{in} \approx -8$dBW) and then decreased slowly up to -74dBW at maximum available

L-Band

Graph 6.1 Stainless Steel-to-Stainless Steel, EN58B, Mechanical Polished

□ 3rd-Order I.P. with Increasing Incident Power

○ 3rd-Order I.P. with Decreasing Incident Power

△ 5th-Order I.P. with Decreasing Incident Power

———Residual level

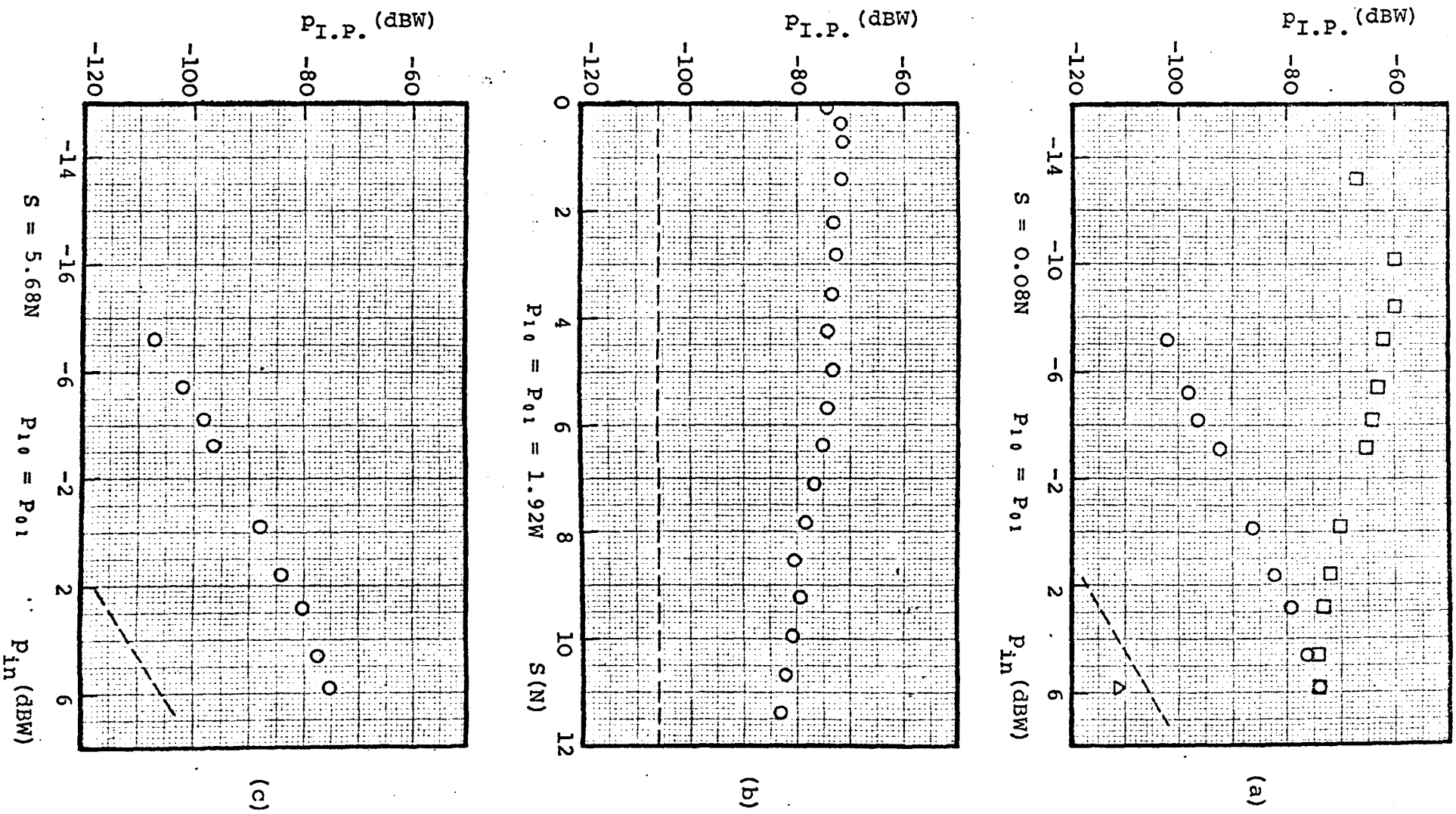

incident power P_{in} = 3.84W. By decreasing the incident power level, the 3rd-order I.P. decreased linearly with a slope of about 2.2 and it was almost repeatable. The 5th-order I.P. was recorded only at maximum input power being 35dB less than the 3rd-order I.P. In this graph, it can be seen that a permanent change occurred in the surface property of contact samples. Variation of 3rd- and 5th-order I.P. levels with axial force (see Graph 6.1b) shows that the maximum I.P. levels were obtained at S = 0 where the actual area of contact is very small and unstable. The 3rd-order I.P. decreased very slowly with increasing axial force, indicating that, the maximum available axial force was not sufficient to break the oxidized layers completely. In Graph 6.1c the variation of 3rd-order I.P. with incident power level at constant axial force of 5.68N is plotted which decreases linearly with a slope of about 2.5.

6.2.2 Mild steel-to-mild steel

The results for the test sample pair made of mild steel are given in Graph 6.2. The almost repeatable 3rd-order I.P. level with incident power level at constant axial force of 0.08N (see Graph 6.2a) indicate that, the maximum available incident power has been harmless to oxidized layers (see Section 6.8) on the test sample pairs and 5th-order I.P. is about 20dB less than 3rd-order I.P. over the whole range of incident power. This almost constant difference in level between the 3rd- and 5th-order I.P. levels strongly suggests that, the undamaged oxidized layers in the same way are responsible for generation of I.P.'s. The difference between 3rd- and 5th-order I.P. levels still remains constant at about 20dB, in Graph 6.2b where I.P.'s level variation is plotted against axial force at

L-Band

Graph 6.2 Mild Steel-to-Mild Steel, Mechanical Polished

□ 3rd-Order I.P. with Increasing Incident Power

○ 3rd-Order I.P. with Decreasing Incident Power

△ 5th-Order I.P. with Decreasing Incident Power

---Residual level

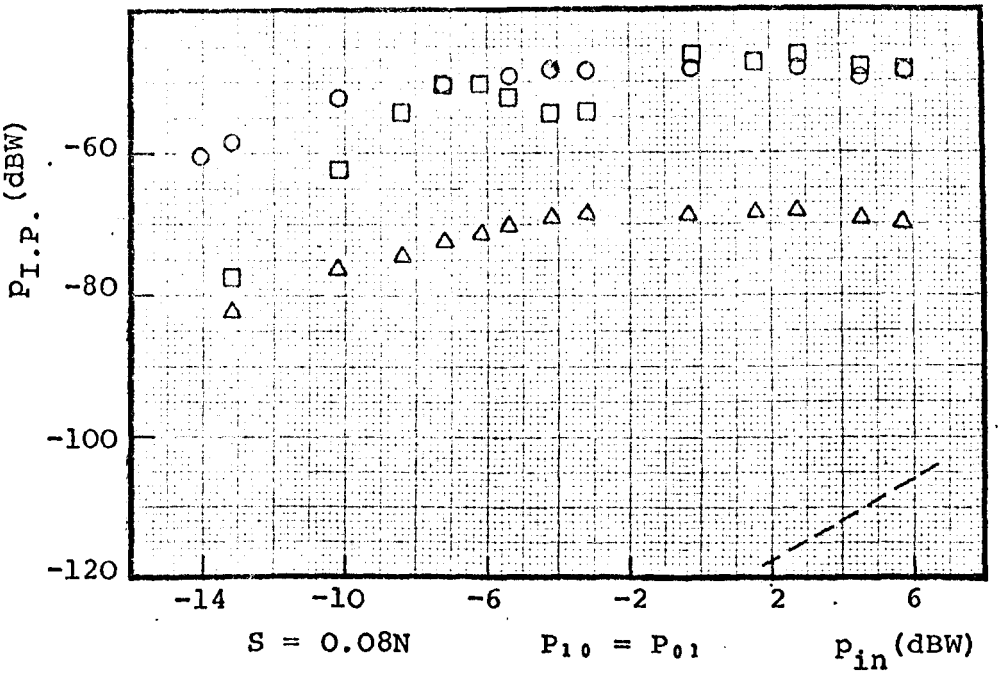

(a)

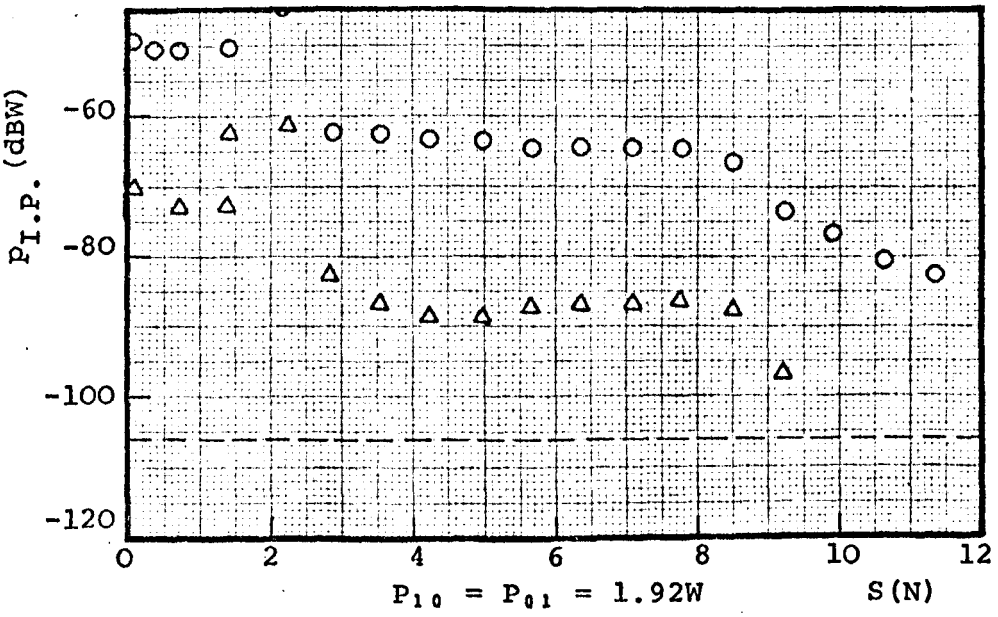

(b)

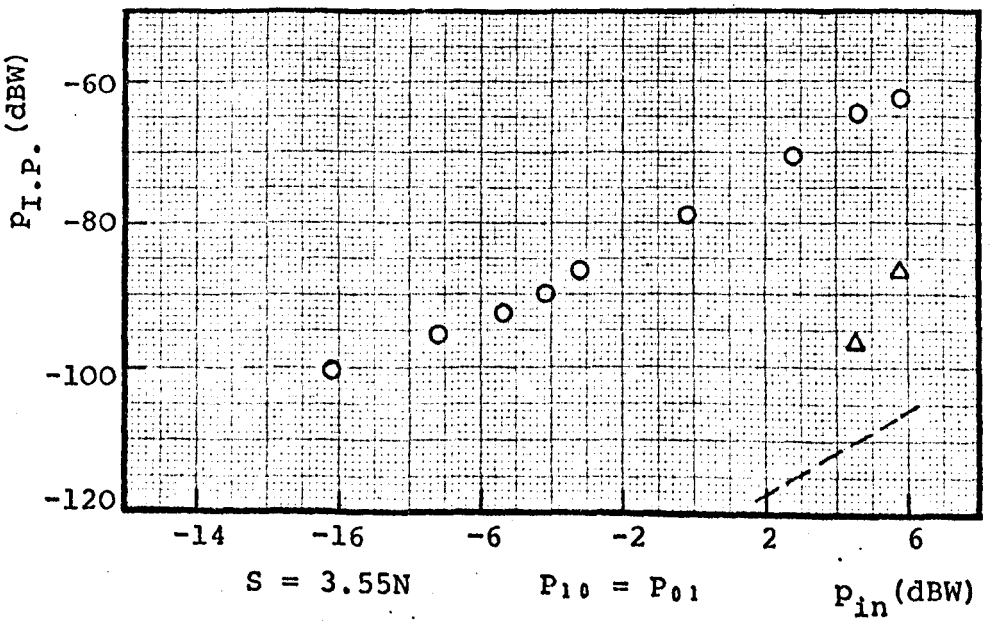

(c)

P_{in} = 3.84W. This graph shows the mechanical breakdown of oxidized layers had occurred in two steps, i.e. S_1 = 2N and S_2 = 8N, but the maximum available axial force was not sufficient to break down the oxidized layers completely establishing perfect metal-to-metal contact. The variation of 3rd-order I.P. level with incident power at constant axial force of 3.55N is nearly linear with a slope of about 2.4 (see Graph 6.2c) indicating that, the first step breakdown of oxidized layers has changed the I-V characteristics of the contact point(s) completely.

6.2.3 Duraluminium-to-duraluminium

Graph 6.3 illustrates the results for 3rd- and 5th-order I.P. levels for duraluminium. Both the 3rd- and 5th-order I.P. levels are plotted with decreasing incident power and show a difference of about 50dB at maximum available incident power, P_{in} = 3.84W and furthermore the 3rd-order I.P. level decreases linearly with a slope of 4.6 at first, down to $P_{in} \approx 0.3$W and then decreases more slowly (see Graph 6.3a). The increase and decrease of 3rd-order I.P. level in Graph 6.3b at S_1 = 3N and S_2 = 5N respectively can be interpreted by relative microslip motion at the interface of a microcontact point and large difference between hardness of Al_2O_3 and the base material itself. The 5th-order I.P. level was not detectable beyond 1N. In Graph 6.3c, both the 3rd- and 5th-order I.P. levels are plotted with decreasing incident power level at constant axial force of 3.55N. The 3rd-order I.P. level decreased linearly with decreasing incident power level with a slope of about 4. The high I.P. levels in Al can be related to the oxide layer on its surface which can be very rapidly formed at the contact

L-Band

Graph 6.3 Duraluminium-to-Duraluminium, Mechanical Polished

□ 3rd-Order I.P. with Increasing Incident Power

○ 3rd-Order I.P. with Decreasing Incident Power

△ 5th-Order I.P. with Decreasing Incident Power

---Residual level

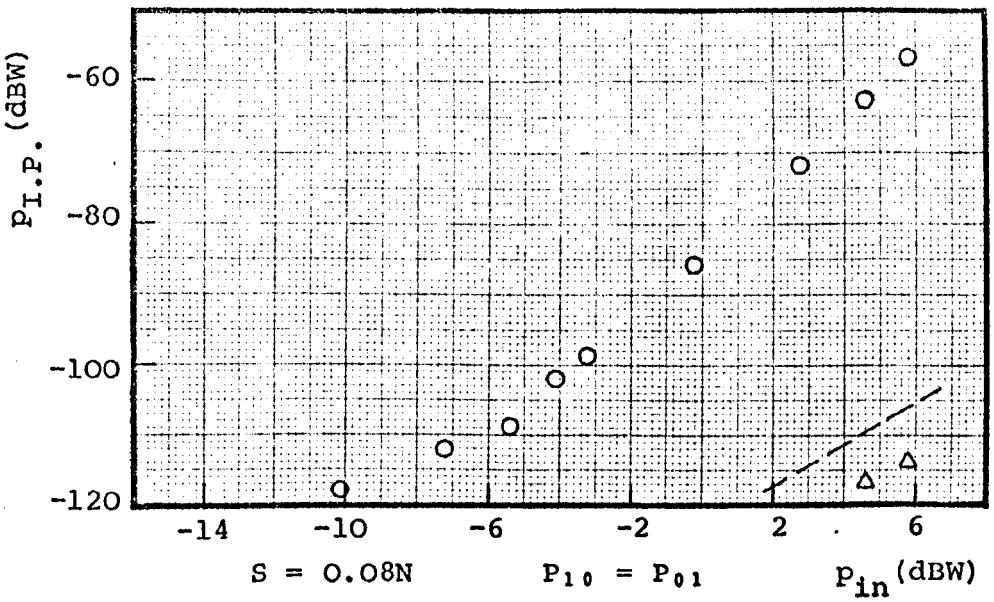

(a)

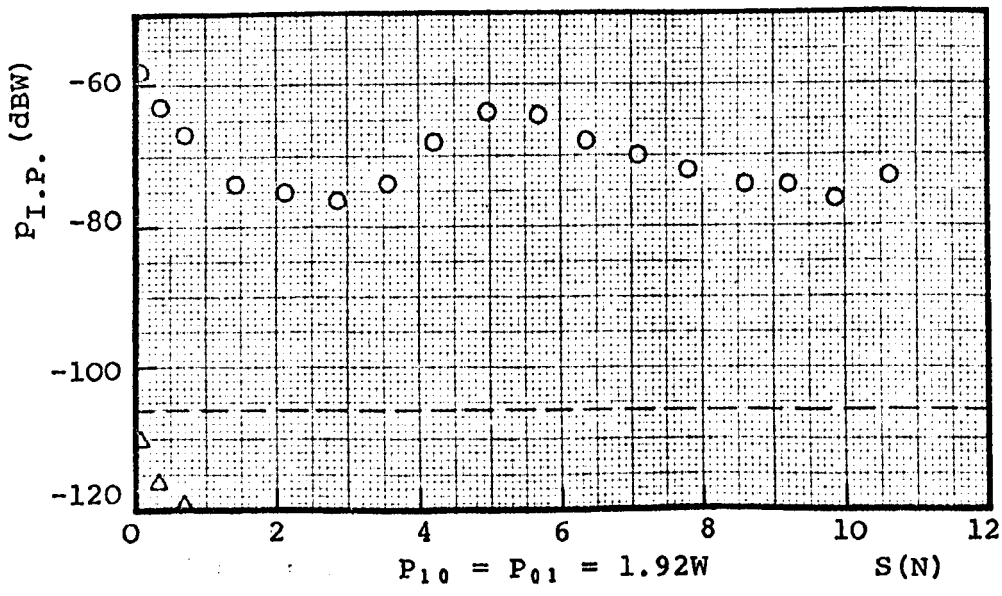

(b)

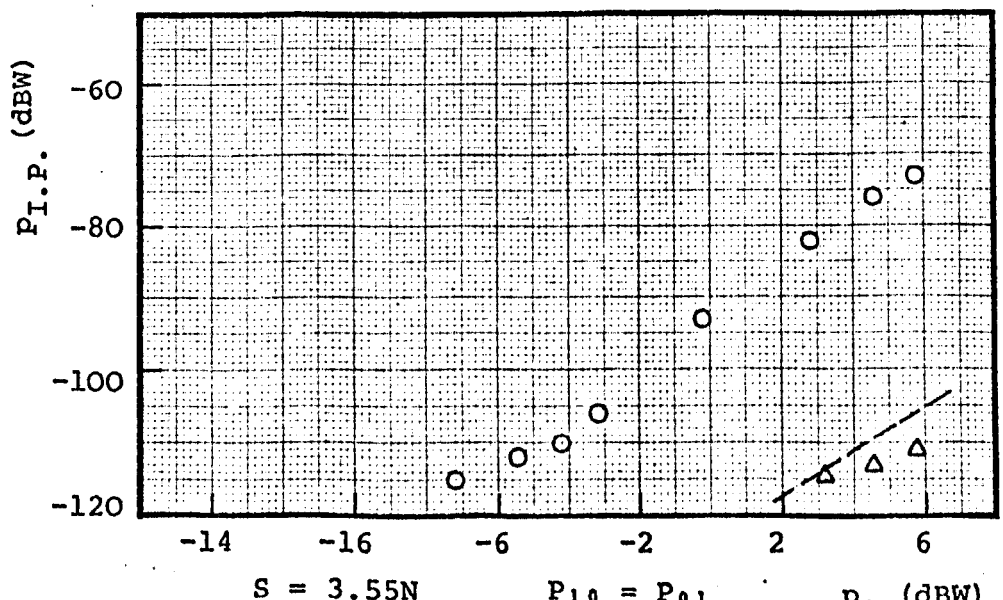

(c)

point with oxygen especially when the temperature at that point is high or the incident power is high.

6.2.4 Oxygen free nickel-to-oxygen free nickel

The results were obtained for both 3rd- and 5th-order I.P. levels and are shown in Graph 6.4. The erratic variation in 3rd-order I.P. level with increase of incident power level (Graph 6.4a) is related to the changeable behaviour of the oxide layers during electric breakdown of the layers. The slope of the 3rd-order I.P. level with decreasing incident power level is about 3.2 and the 5th-order I.P. level is about 30dB less than the 3rd-order I.P. level at P_{in} = 3.84W. Maximum available axial force was not able to produce a perfect metal-to-metal contact (Graph 6.4b) and therefore the 3rd-order I.P. level remains almost unchanged with increasing axial force and so is the slope of 3rd-order I.P. level with decreasing incident power at constant axial force of 5.68N (Graph 6.4c) indicating that, while the surface property of the contact surface is unchanged, the generation of I.P. level is almost repeatable. In other words the non-linear I-V characteristic of the oxide layer is responsible for generation of I.P. levels and undamaged oxide layers almost produce a stable I-V characteristic.

6.2.5 Brass-to-brass

Graph 6.5 shows the test results obtained for test sample pairs made of brass. From Graphs 6.5a and b, it can be seen that the electrical and mechanical breakdown of oxide layers of brass can occur more easily than of oxygen free nickel. The 3rd-order I.P. level increases with increasing incident power level up to $P_{in} \approx 0.5W$ ($p_{in} \approx -3.2dBW$) and then it increases more slowly up to -59dBW at $P_{in} \approx 3.84W$. The slopes of the 3rd- and 5th-order

L-Band

Graph 6.4 Oxygen Free Nickel-to-Oxygen Free Nickel, Mechanical Polished

□ 3rd-Order I.P. with Increasing Incident Power

○ 3rd-Order I.P. with Decreasing Incident Power

△ 5th-Order I.P. with Decreasing Incident Power

---Residual level

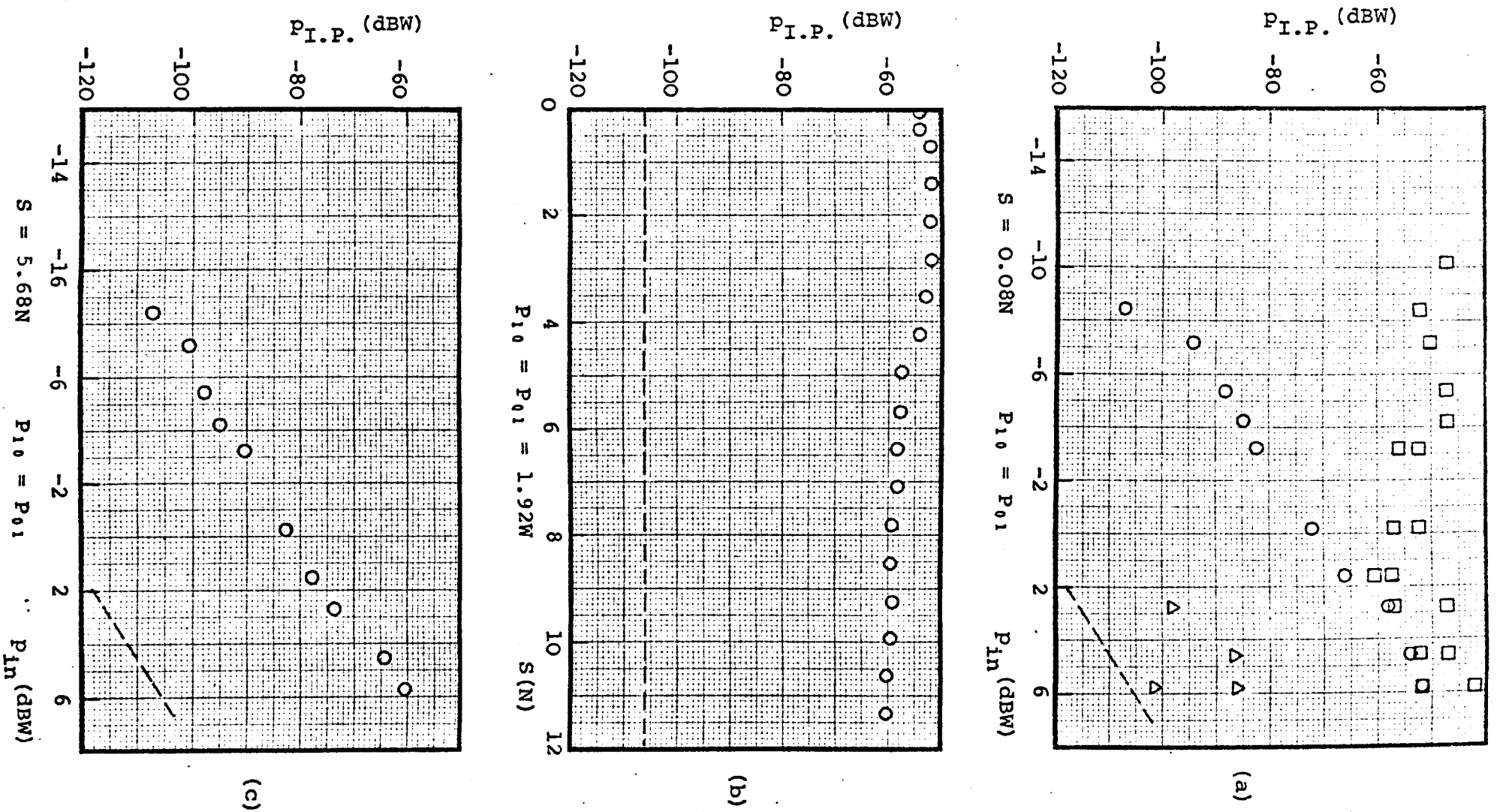

L-Band

Graph 6.5 Brass-to-Brass, Mechanical Polished

□ 3rd-Order I.P. with Increasing Incident Power

○ 3rd-Order I.P. with Decreasing Incident Power

△ 5th-Order I.P. with Decreasing Incident Power

---Residual level

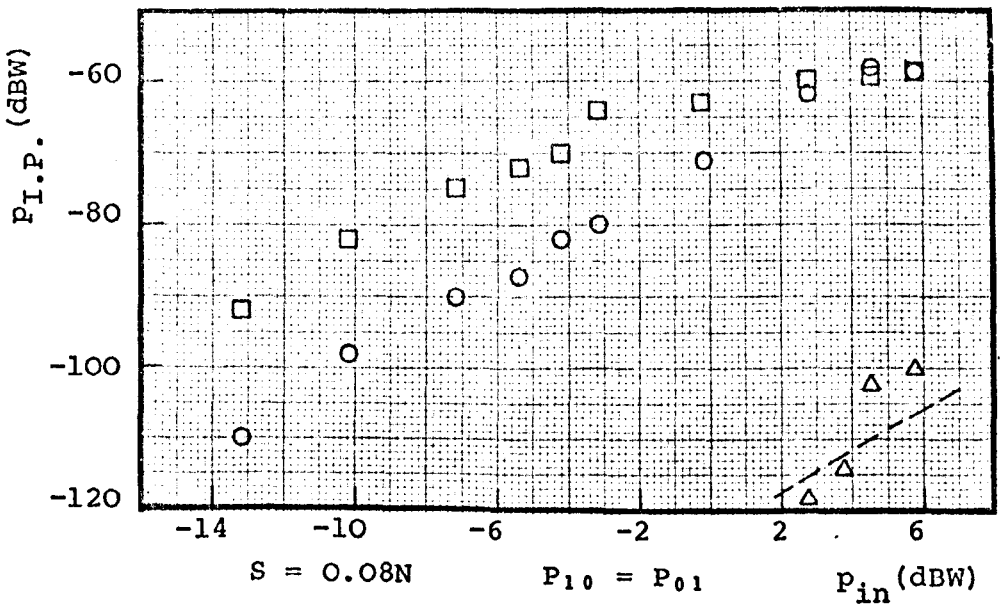

(a)

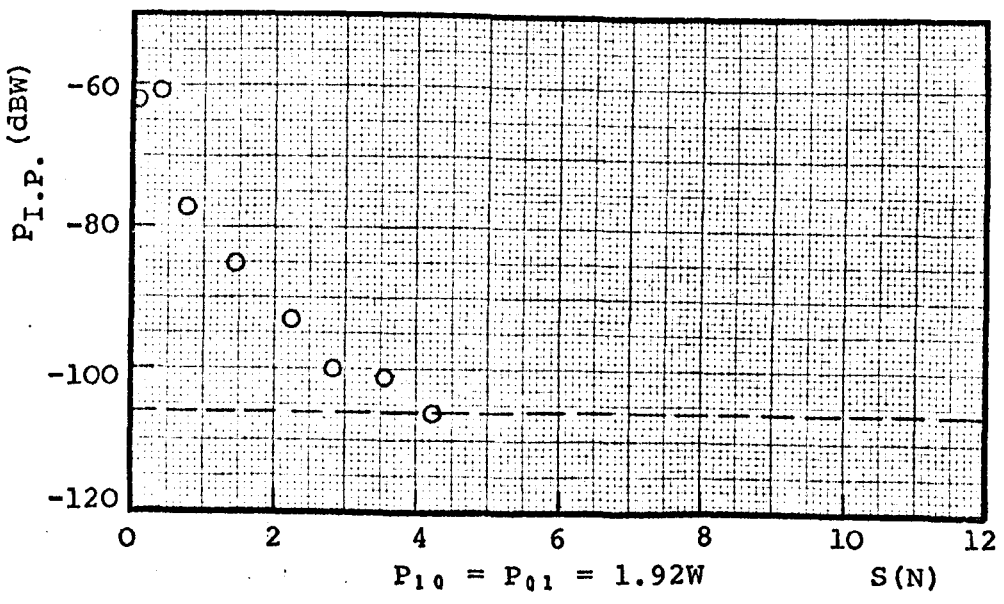

(b)

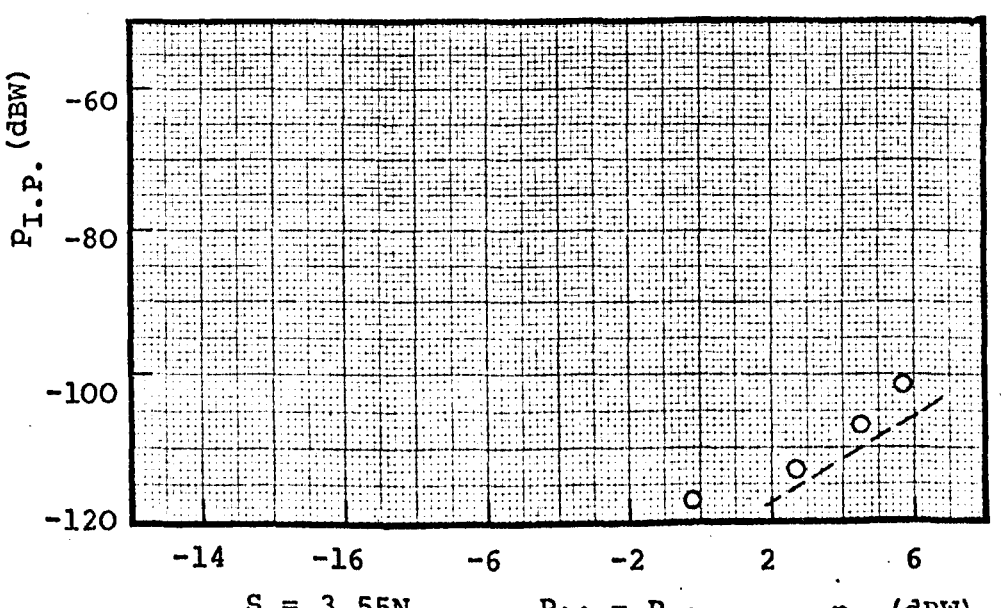

(c)

I.P. levels with decreasing incident power level are about 3 and 6 respectively (Graph 6.5a). The axial force of about 4N was sufficient to breakdown the oxide layers (Graph 6.5b). The slope of the 3rd-order I.P. level with decreasing incident power, where the mechanical breakdown is going to be completed, i.e. at an axial force of 3.55N is almost 3 and repeatable.

6.2.6 Copper-to-copper, beryllium copper-to-beryllium copper, oxygen free copper-to-oxygen free copper

The 3rd-order I.P. level generated at contact point(s) of the test sample pairs made of copper, beryllium copper and oxygen free copper, has its maximum value at axial force of zero but even an axial force of 0.08N is sufficient to produce a perfect metal-to-metal contact, bringing the 3rd-order I.P. level down to residual level. Therefore no graph is produced to show the results. These results show that when the contact surfaces are covered with very thin oxide layers or in other words they are electrically clean, no matter what surface finish (in this case mechanically polished surface) the I.P.'s level fall down to residual level at very low axial force.

6.2.7 Steel-to-steel, 3709 and 3710

Graphs 6.6 and 6.7 show the results obtained for similar steel-to-steel contact of test sample pairs made of steel cast Nos.3709 and 3710 respectively. The electrical breakdown occurs at an incident power level of about 0.5W for both steels (see 3rd-order I.P. level, Graphs 6.6a and 6.7a) and gives a 3rd-order level of -62dBW at incident power of level of P_{in} = 3.84W. The slopes of the 3rd-order I.P. level with decreasing incident power level for both samples are about the same and is nearly 2. The difference between 3rd- and 5th-order I.P. levels at constant axial force of 0.08N through the whole range of incident

L-Band

Graph 6.6 Steel-to-Steel, Cast No. 3709, Mechanical Polished

□ 3rd-Order I.P. with Increasing Incident Power

○ 3rd-Order I.P. with Decreasing Incident Power

△ 5th-Order I.P. with Decreasing Incident Power

---Residual level

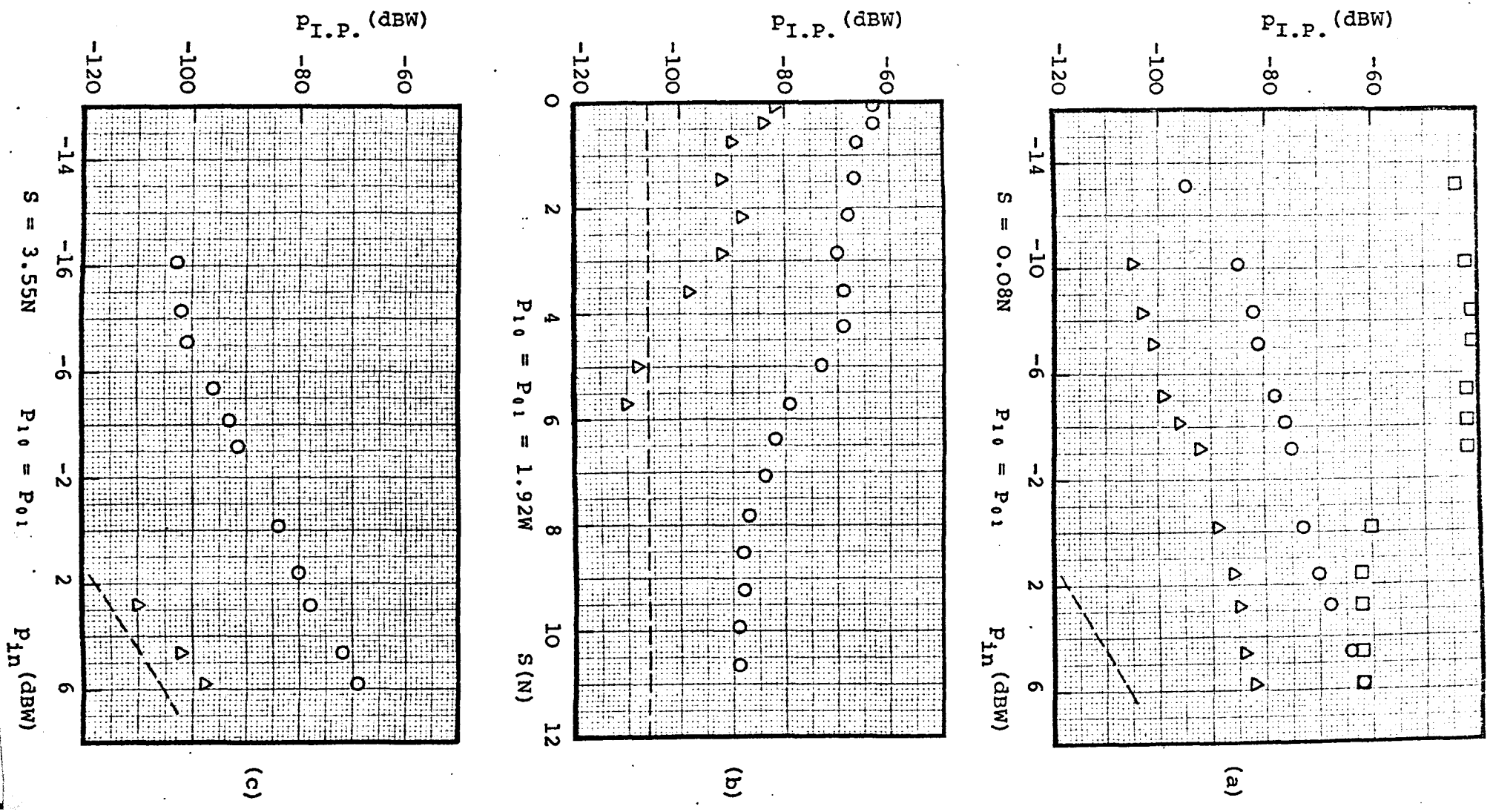

L-Band

Graph 6.7 Steel-to-Steel, Cast No. 3710, Mechanical Polished

□ 3rd-Order I.P. with Increasing Incident Power

○ 3rd-Order I.P. with Decreasing Incident Power

△ 5th-Order I.P. with Decreasing Incident Power

---Residual level

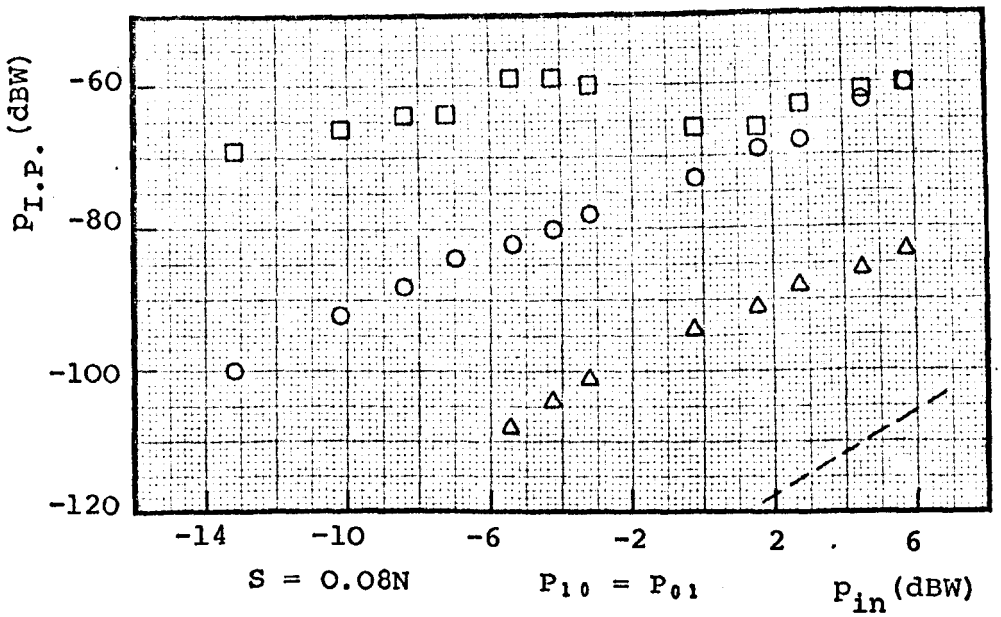

(a)

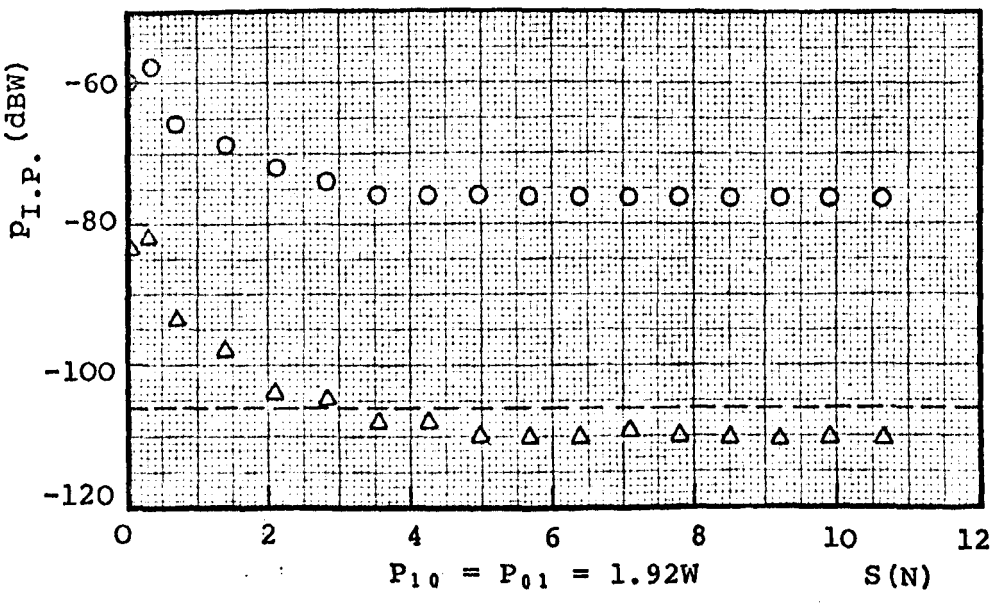

(b)

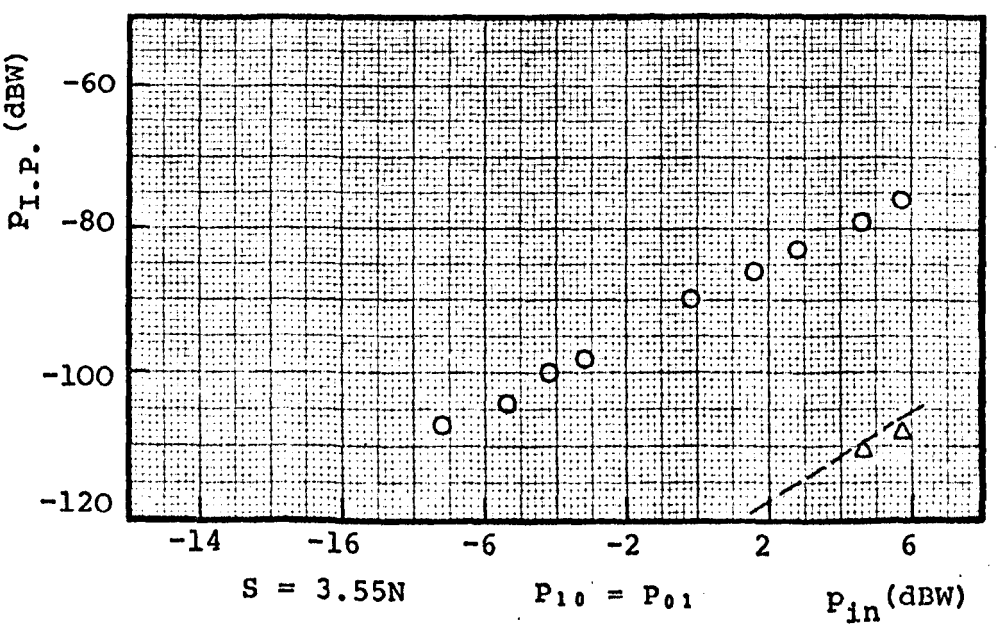

(c)

power level is about 20dB for both samples the 3rd-order I.P. levels being higher than the 5th-order I.P. levels. This difference increases as axial force increases at a constant incident power level of 3.84W (see Graphs 6.6b and 6.7b) to about 30dB indicating that when the better contact is established, by mechanical breakdown when axial force is increasing, the higher order I.P. levels drop down more rapidly. The slope of 2.5 can be seen from almost linear variation of 3rd-order I.P. level with decreasing incident power level for both steels (Graphs 6.6c and 6.7c) at constant axial force of 3.55N. The almost similar results for both steels, 3709 and 3710, could be expected since their compositions were almost alike (see Table 5.1, Section 5.1).

6.2.8 Steel-to-steel, 3711, 3712 and 3713

The results obtained for similar steel-to-steel contacts for three steels with cast Nos. of 3711, 3712 and 3713 are illustrated in Graphs 6.8, 6.9 and 6.10 respectively. These three steels contain Cr and Ni with different percentages. The 3rd- and 5th-order I.P. levels in these three samples are very high and the 3rd-order I.P. level is about -65dBW at maximum available incident power of P_{in} = 3.84W at a constant axial force of 0.08N (see Graphs 6.8a, 6.9a and 6.10a). At an incident power level of about 0.5W a deformation has occurred to the oxide layers between the contact surfaces of these three steels when the incident power was increasing. By decreasing incident power level, both the 3rd- and 5th-order I.P. levels decreased in these three steels and the slope of the 3rd-order I.P. level is about 2. In Graphs 6.8b, 6.9b and 6.10b it can be seen that the maximum available axial force was not sufficient

L-Band

Graph 6.8 Steel-to-Steel, Cast No. 3711, Mechanical Polished

□ 3rd-Order I.P. with Increasing Incident Power

○ 3rd-Order I.P. with Decreasing Incident Power

△ 5th-Order I.P. with Decreasing Incident Power

———Residual level

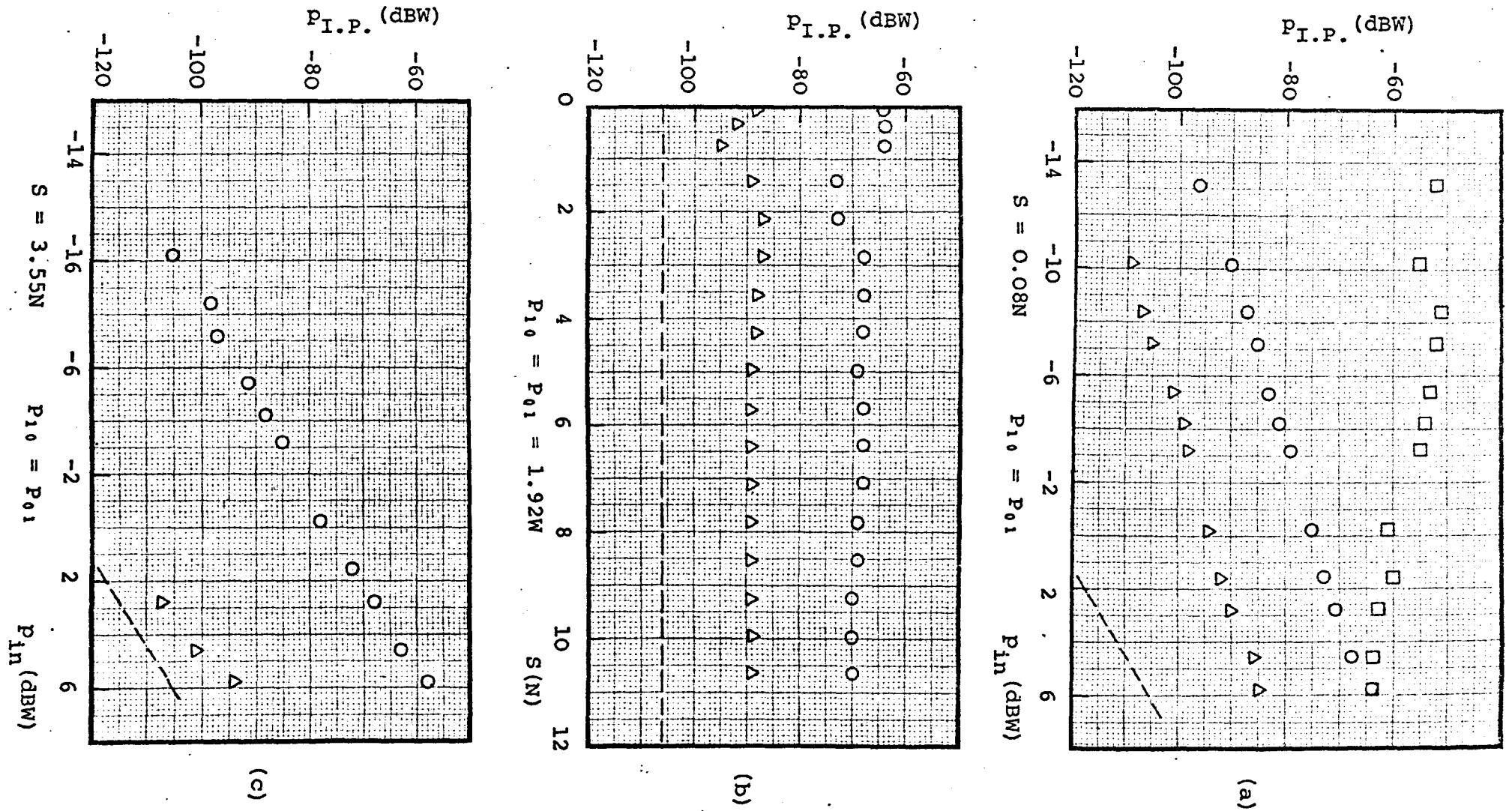

L-Band

Graph 6.9 Steel-to-Steel, Cast No. 3712, Mechanical Polished

□ 3rd-Order I.P. with Increasing Incident Power

○ 3rd-Order I.P. with Decreasing Incident Power

△ 5th-Order I.P. with Decreasing Incident Power

---Residual level

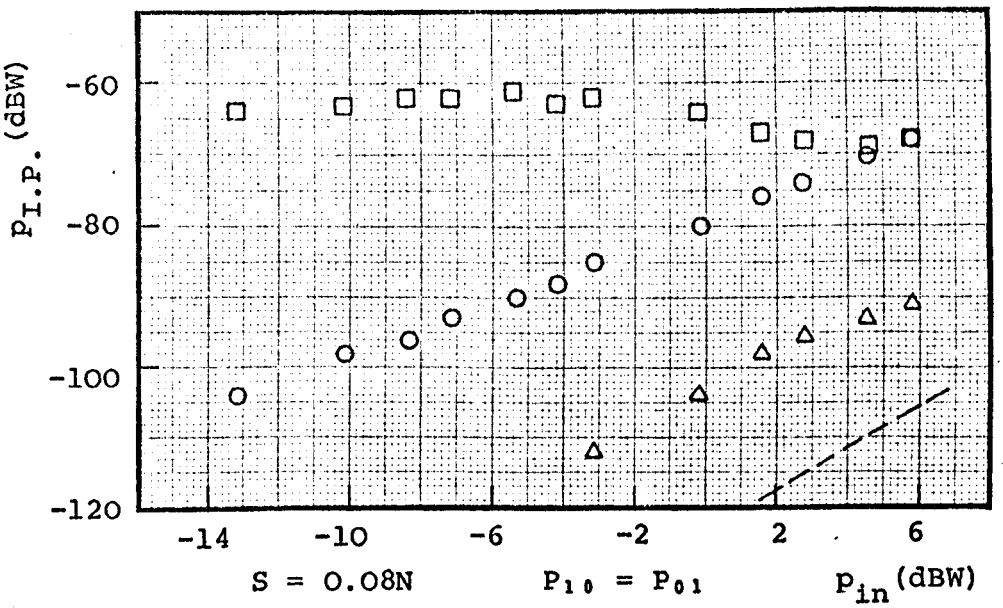

(a)

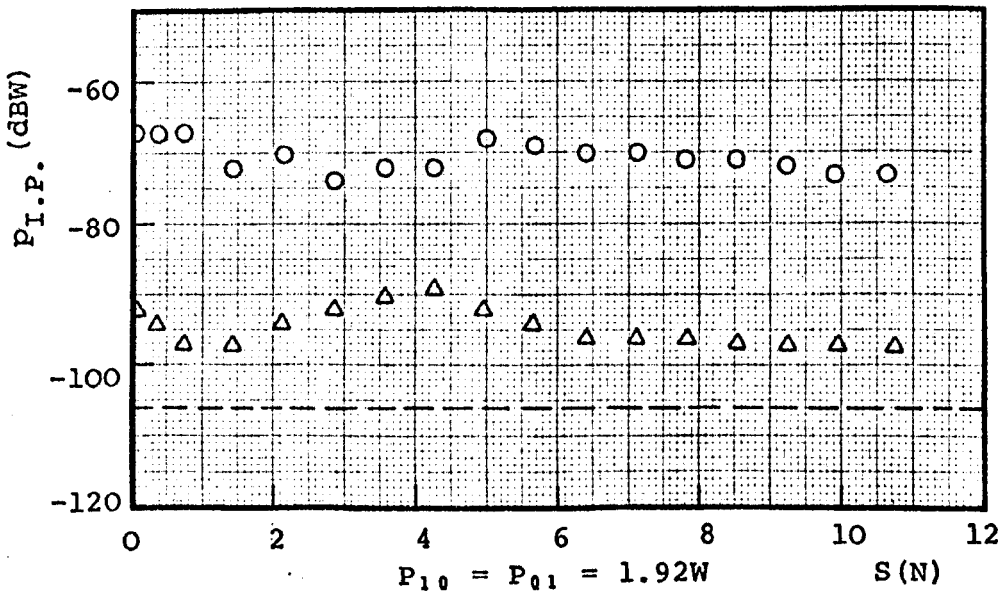

(b)

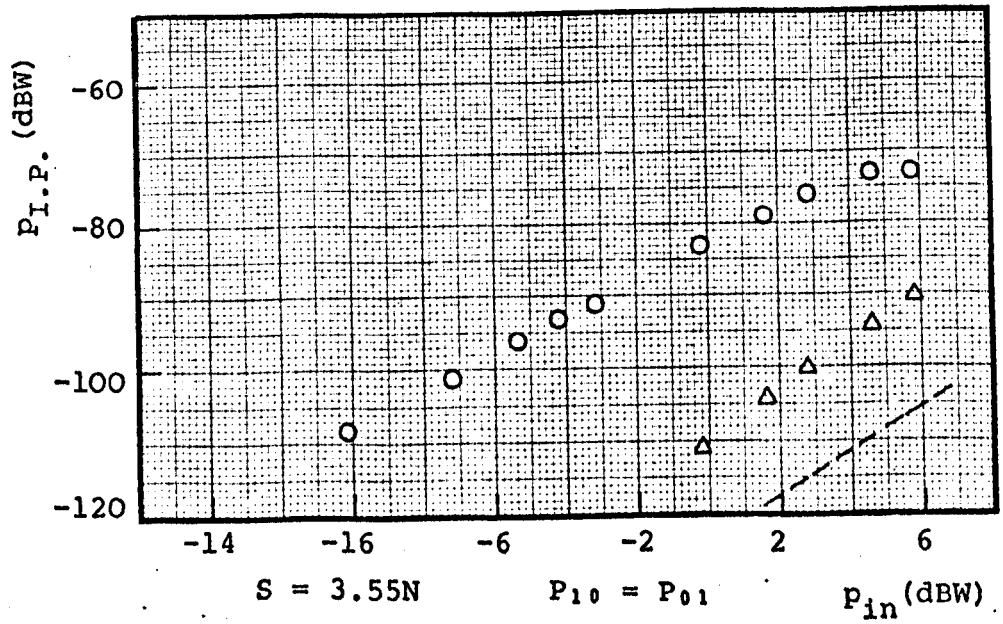

(c)

L-Band

Graph 6.10 Steel-to-Steel, Cast No. 3713, Mechanical Polished

□ 3rd-Order I.P. with Increasing Incident Power

○ 3rd-Order I.P. with Decreasing Incident Power

△ 5th-Order I.P. with Decreasing Incident Power

---- Residual level

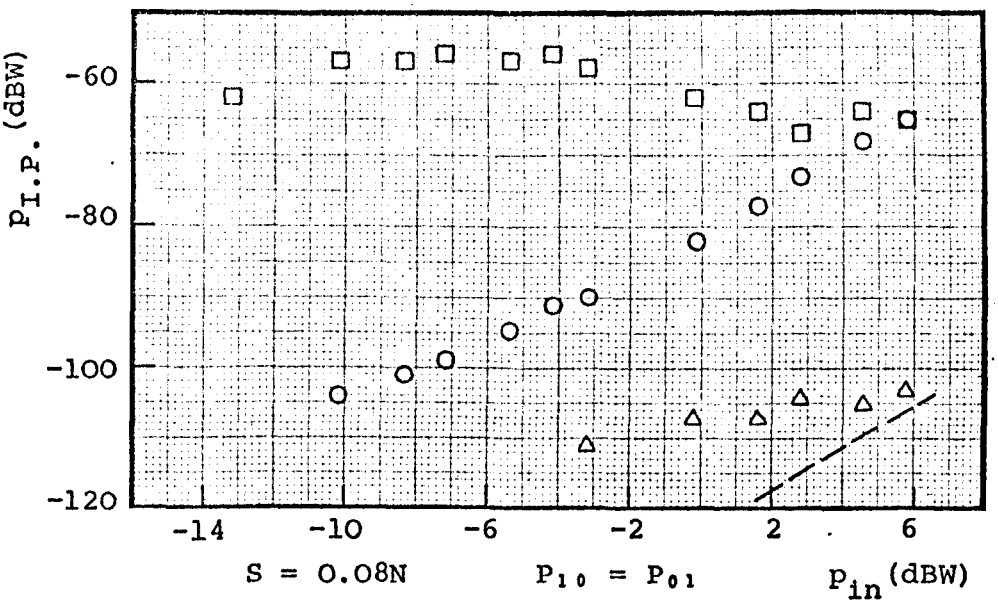

(a)

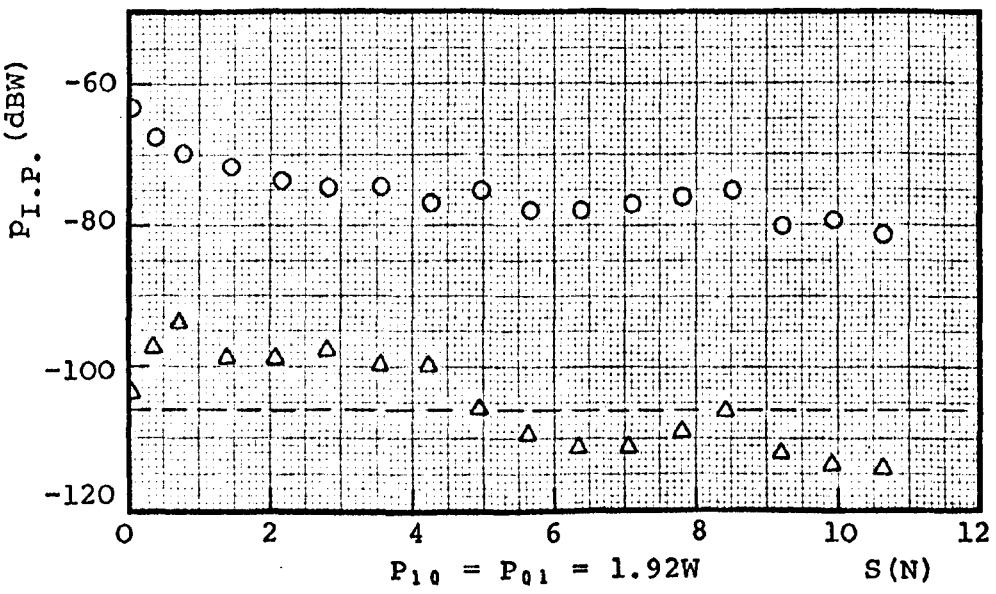

(b)

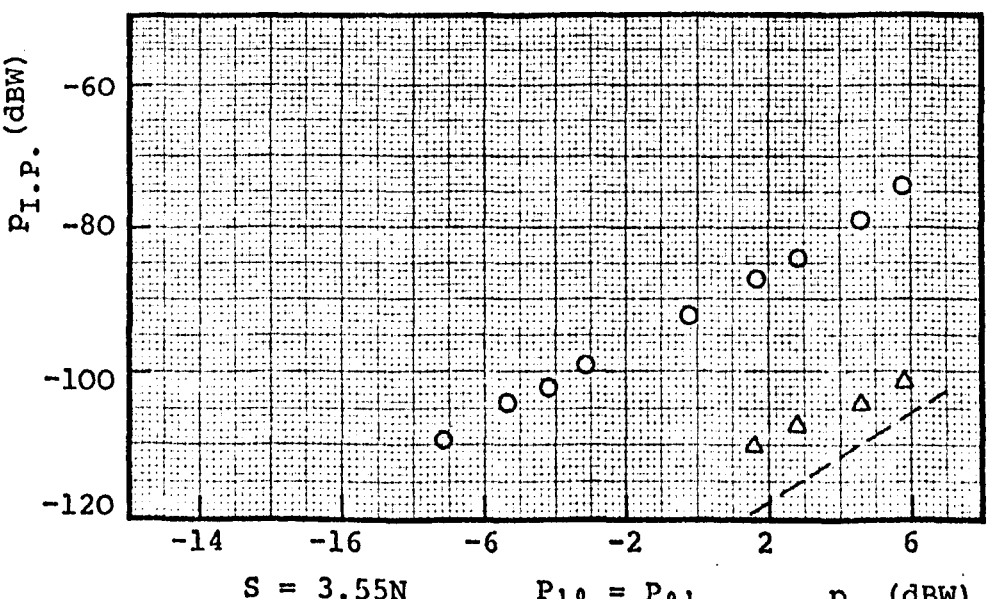

(c)

for a complete mechanical breakdown of oxide layers. The 5th-order I.P. level was between about 20-30dB down to 3rd-order I.P. level. Variation of 3rd- and 5th-order I.P. levels with decreasing incident power level at a constant axial force of 3.55N are plotted in Graphs 6.8c, 6.9c and 6.10c. In the case of steel with cast No. 3711 the contact surfaces were separated and again established at axial force of 3.55N. Therefore the initial condition in surface contacts has been changed and higher 3rd-order I.P. levels were recorded with decreasing incident power indicating that contact surfaces are very important for generation of I.P.'s and since the initial condition has been changed the results cannot be repeatable. The slope of 3rd-order I.P. illustrated in these graphs is about 2.5. From similar behaviour of these three steels it seems that the Cr and Ni content of percentages of those shown in Table 5.1 have little effect on contact surfaces when they are mechanically polished as far as generation of I.P.'s is concerned.

6.2.9 Steel-to-steel, 3714, 3715, 3716 and 3717

Graphs 6.11, 6.12, 6.13 and 6.14 demonstrate the typical 3rd- and 5th-order I.P. levels obtained from similar steel-to-steel, cast Nos. 3714, 3715, 3716 and 3717 respectively. The 3rd-order I.P. level obtained from steel 3714 shown in Graph 6.11a for constant axial force of 0.08N indicate that the maximum incident power level was not sufficient for an electrical deformation on the surface oxide layers at contact point while in the other three steels electrical deformation has occurred at a fairly low incident power of about 0.15W. Increase in carbon content or decrease in Cr content (which means less protection against surface oxidation), in construction of a steel (such as steel 3714 compared with other three steels, see Table 5.1) may

L-Band

Graph 6.11 Steel-to-Steel, Cast No. 3714, Mechanical Polished

□ 3rd-Order I.P. with Increasing Incident Power

○ 3rd-Order I.P. with Decreasing Incident Power

△ 5th-Order I.P. with Decreasing Incident Power

---Residual level

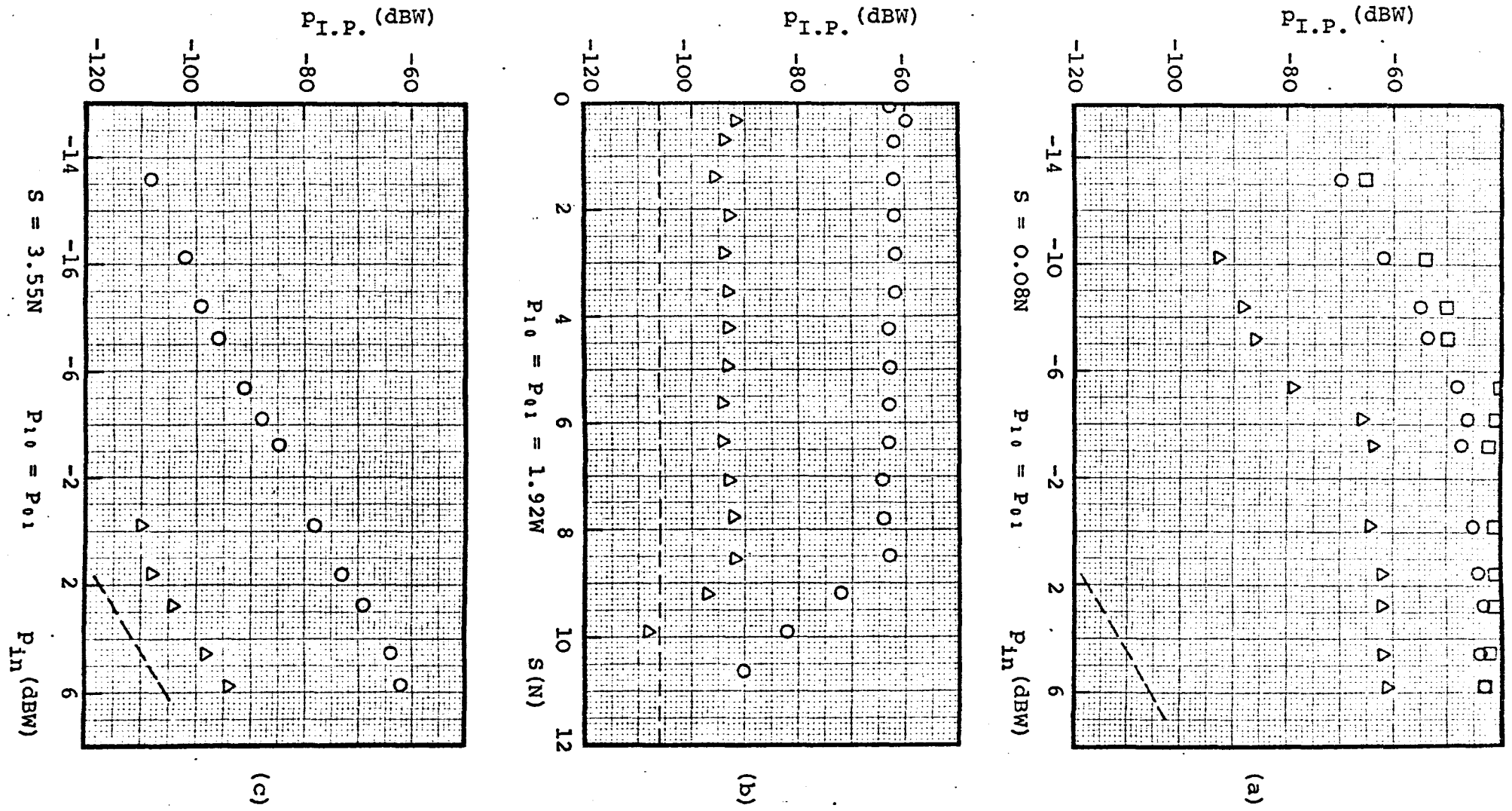

L-Band

Graph 6.12 Steel-to-Steel, Cast No. 3715, Mechanical Polished

□ 3rd-Order I.P. with Increasing Incident Power

○ 3rd-Order I.P. with Decreasing Incident Power

△ 5th-Order I.P. with Decreasing Incident Power

---Residual level

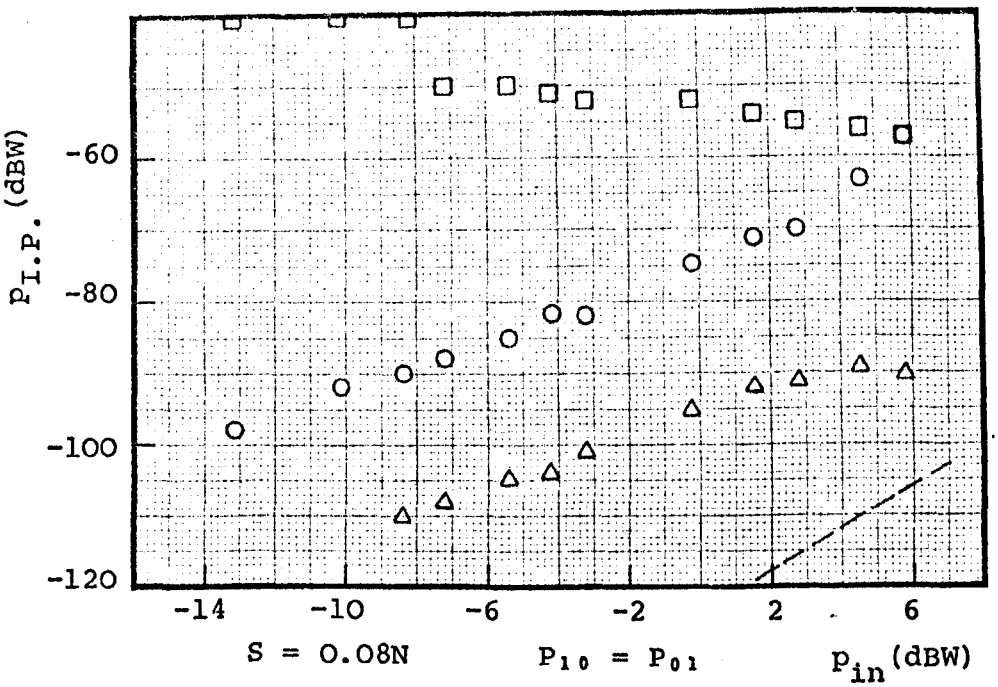

(a)

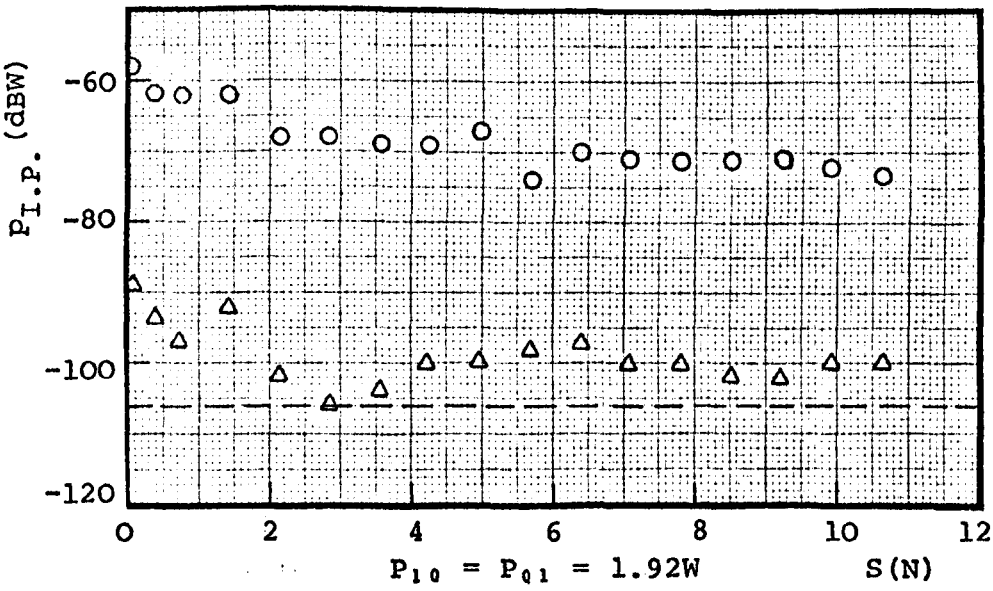

(b)

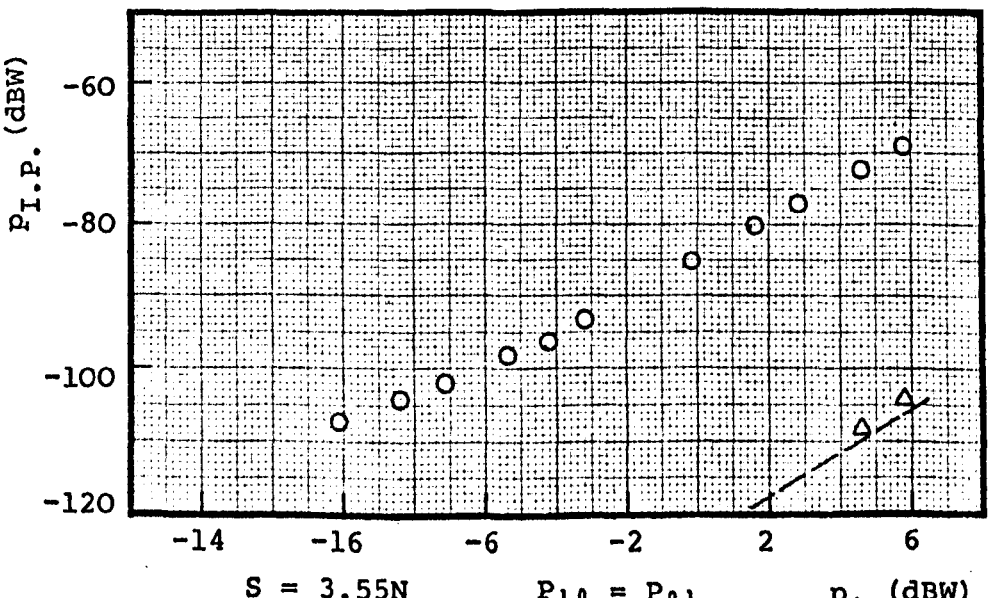

(c)

L-Band

Graph 6.13 Steel-to-Steel, Cast No. 3716, Mechanical Polished

□ 3rd-Order I.P. with Increasing Incident Power
○ 3rd-Order I.P. with Decreasing Incident Power
△ 5th-Order I.P. with Decreasing Incident Power
---Residual level

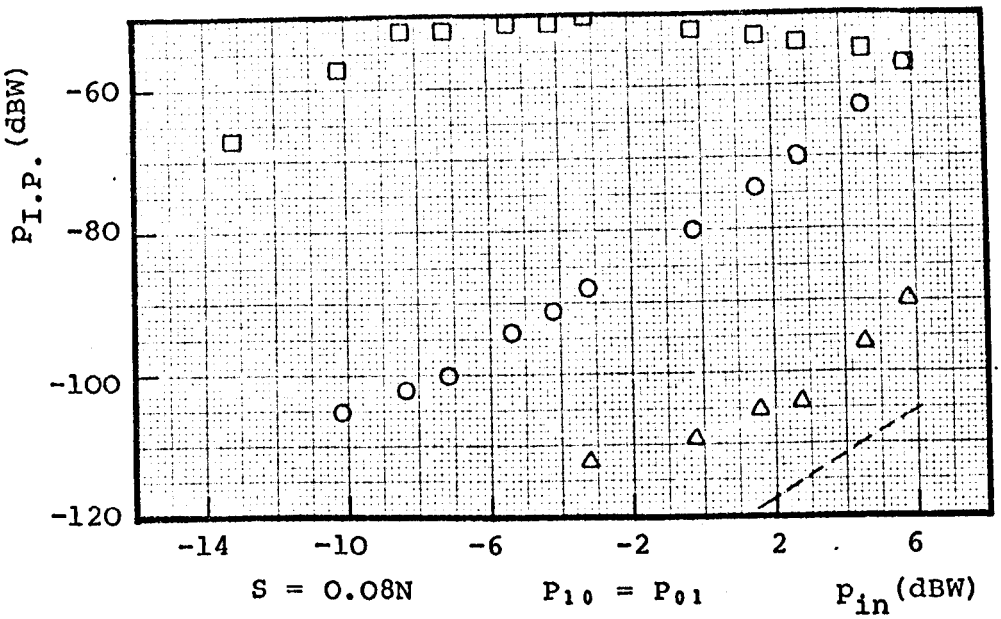

(a)

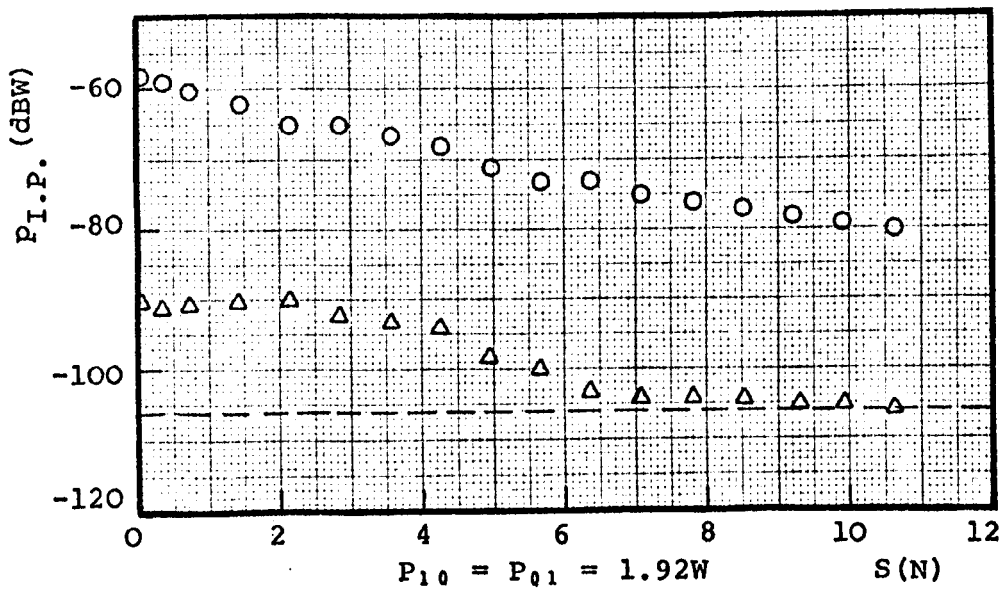

(b)

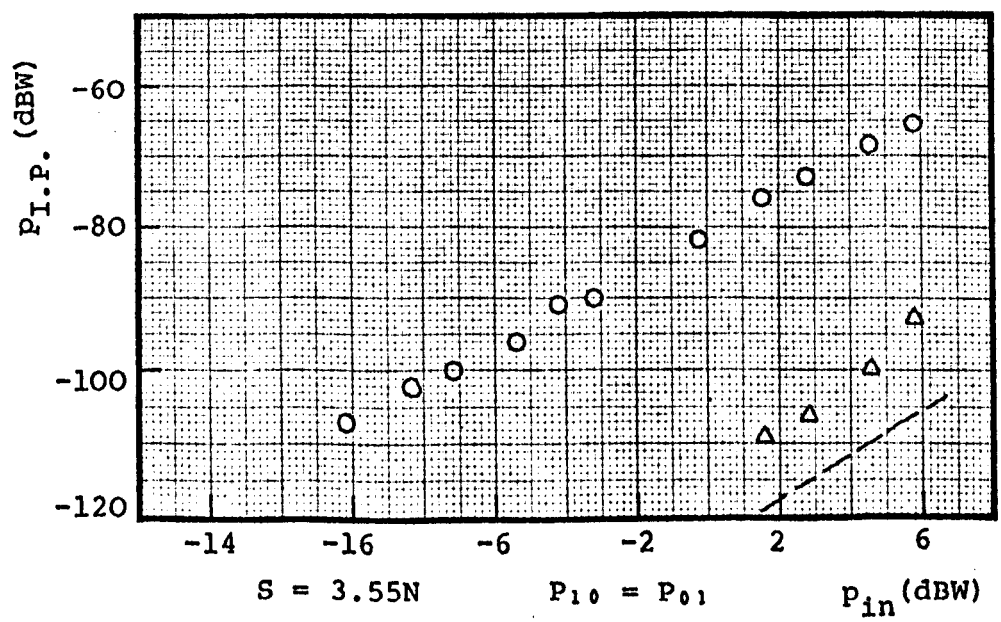

(c)

L-Band

Graph 6.14 Steel-to-Steel, Cast No. 3717, Mechanical Polished

□ 3rd-Order I.P. with Increasing Incident Power
○ 3rd-Order I.P. with Decreasing Incident Power
△ 5th-Order I.P. with Decreasing Incident Power
---Residual level

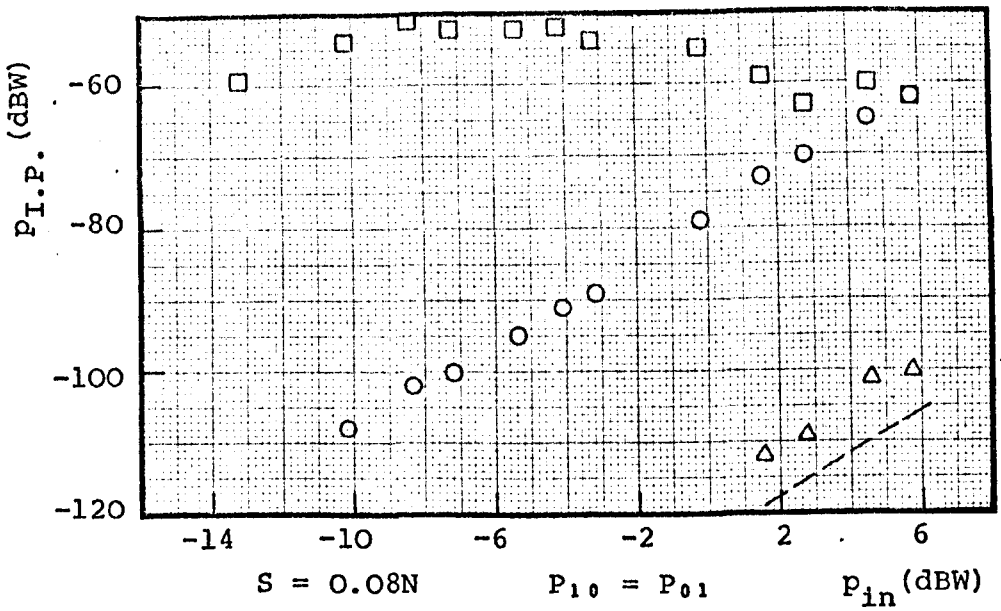

(a)

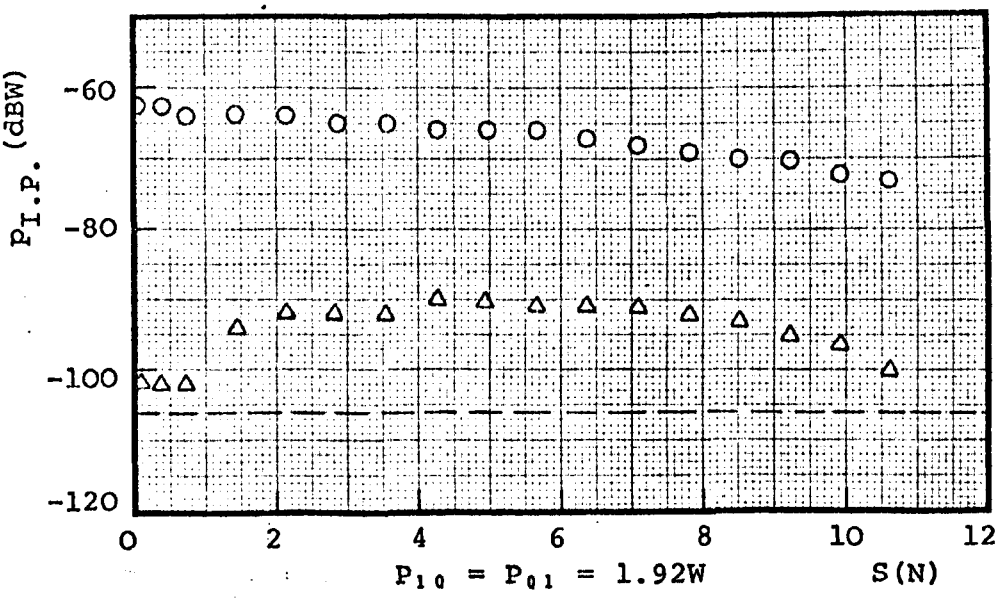

(b)

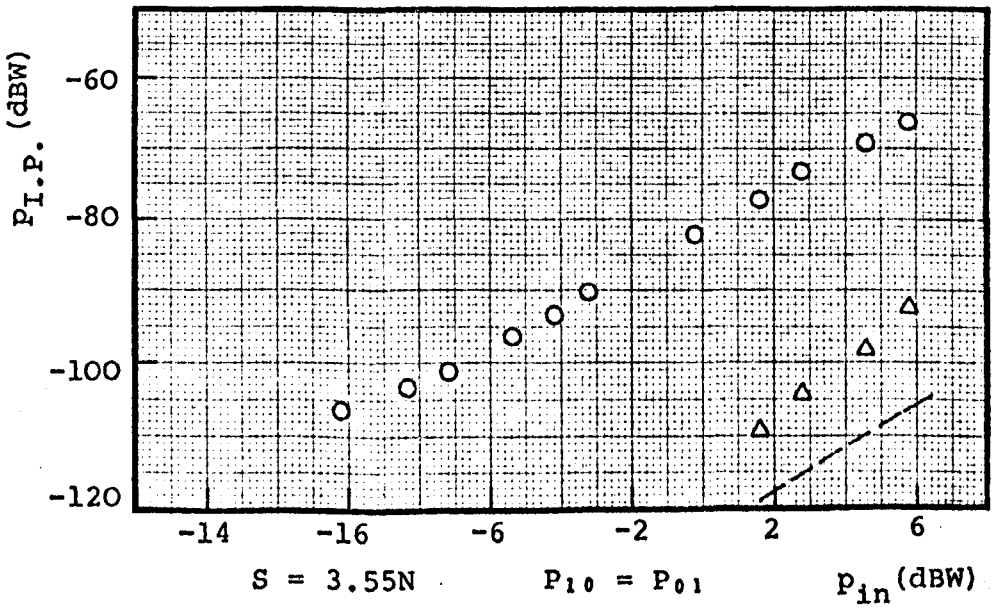

(c)

be responsible for higher strength of oxidized layers against electrical deformation as a result of thicker oxide layers. Both the slope of 3rd-order I.P. level with decreasing incident power level (see Graph 6.11a, 6.12a, 6.13a and 6.14a), and difference between 3rd- and 5th-order I.P. levels for steels 3714, 3715, 3716 and 3717 have increased. Probably as the Cr content increases in the steel composition, after an electrical deformation a better contact has been established. It can be seen from Graph 6.12, 6.13b and 6.14b that the maximum available axial force was not able to produce a perfect metal-to-metal contact but an axial force of about 9N was sufficient for mechanical breakdown of the oxide layers on the contact surface of steel 3714 (see Graph 6.11b). The highest I.P.'s level were obtained at zero axial force. The almost constant difference of about 25dB between 3rd- and 5th-order I.P. level over the whole range of available axial force again indicates that the surface property of the contact surface has an important role for I.P. generation. Both the 3rd- and 5th-order I.P. levels decrease with decreasing incident power at a constant axial force of 3.55N (see Graphs 6.11c, 6.12c, 6.13c and 6.14c) and the slope of 3rd-order I.P. level for all four steels was about 2.5.

6.2.10 Steel-to-steel, 3718, 3719 and 3720

Graphs 6.15, 6.16 and 6.17 show the results obtained for similar steel-to-steel made of steels with cast Nos. 3718, 3719 and 3720 respectively. Comparing Graphs 6.15 and 6.16 show very little difference between results obtained from steel 3718 and 3719, as was expected since there is little difference between compositions of these two steels, therefore only results shown in

L-Band

Graph 6.15 Steel-to-Steel, Cast No. 3718, Mechanical Polished

□ 3rd-Order I.P. with Increasing Incident Power

○ 3rd-Order I.P. with Decreasing Incident Power

△ 5th-Order I.P. with Decreasing Incident Power

———Residual level

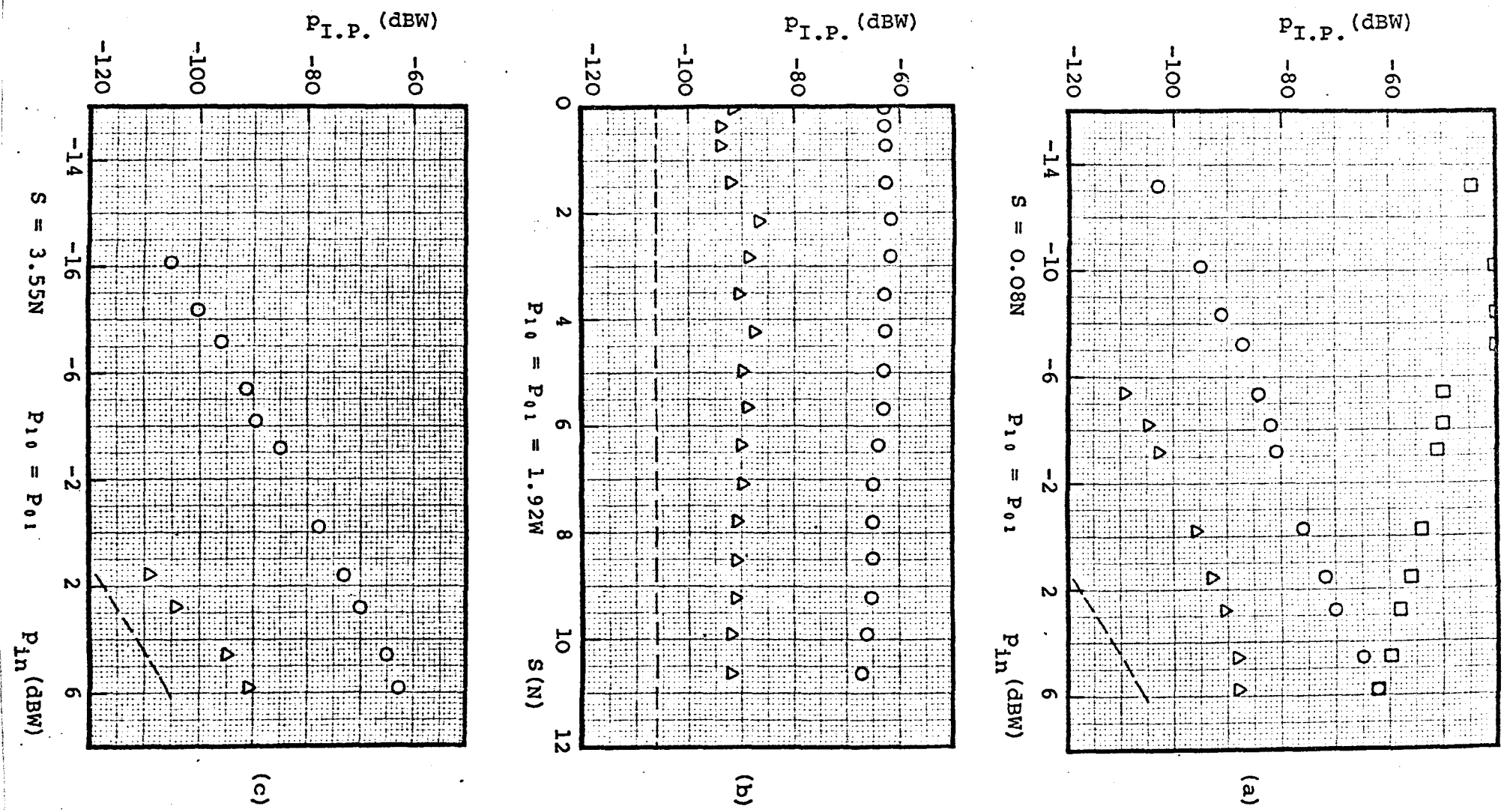

L-Band

Graph 6.16 Steel-to-Steel, Cast No. 3719, Mechanical Polished

□ 3rd-Order I.P. with Increasing Incident Power
○ 3rd-Order I.P. with Decreasing Incident Power
△ 5th-Order I.P. with Decreasing Incident Power
---Residual level

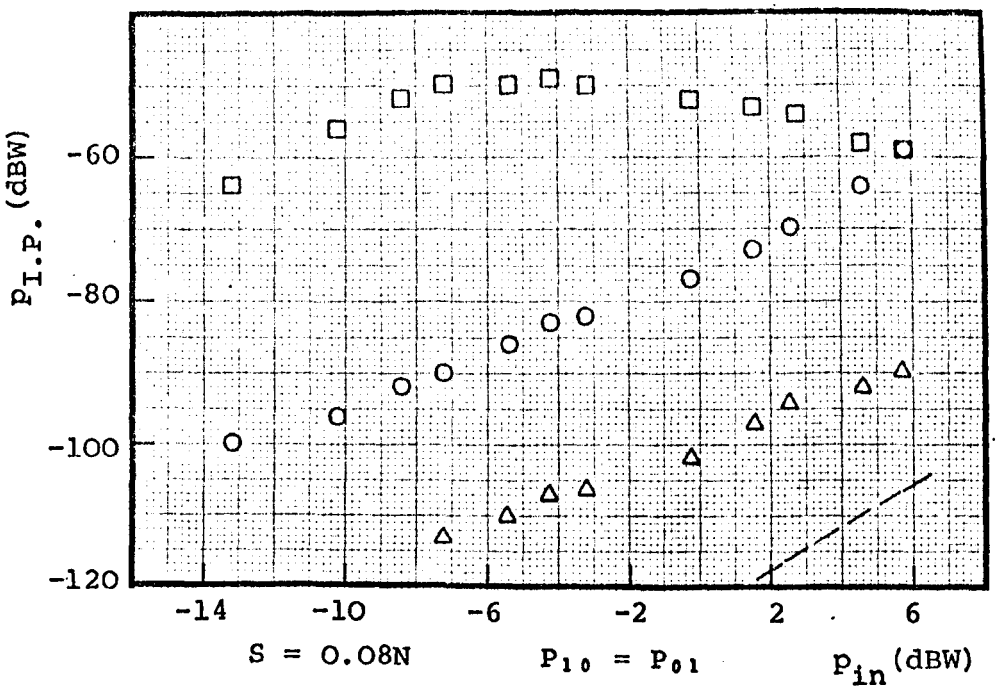

(a)

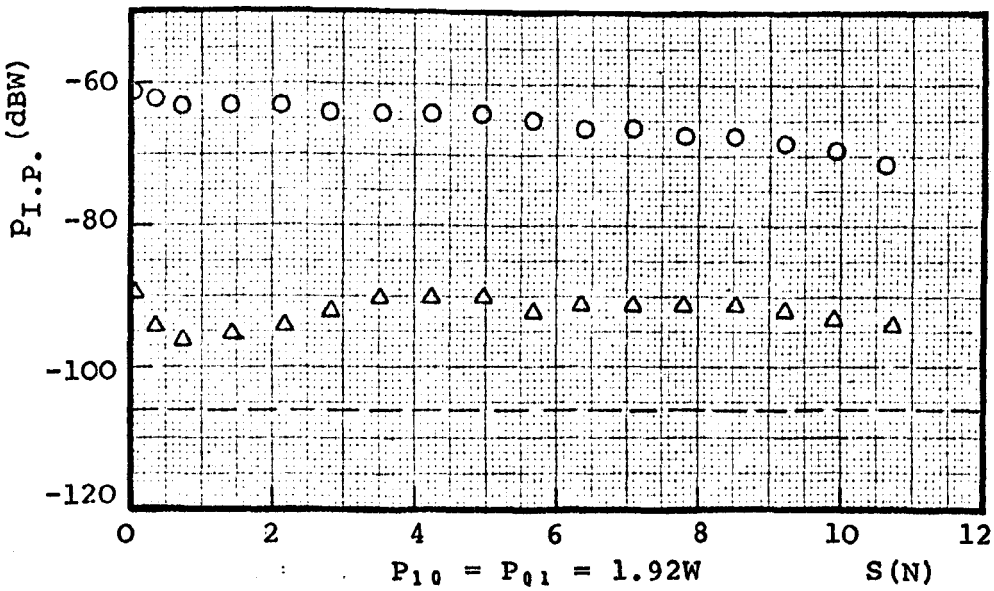

(b)

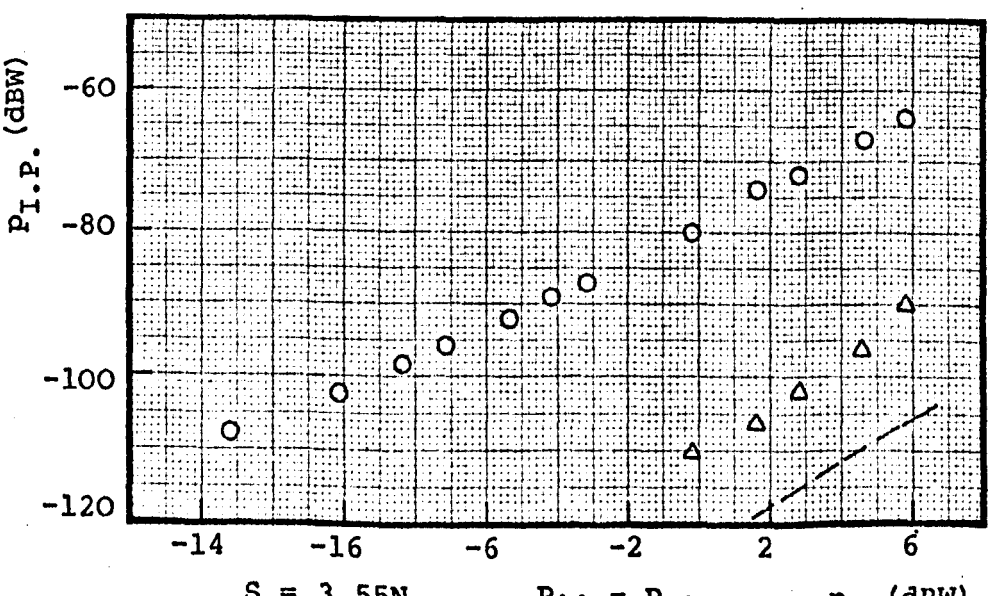

(c)

L-Band

Graph 6.17 Steel-to-Steel, Cast No. 3720, Mechanical Polished

□ 3rd-Order I.P. with Increasing Incident Power

○ 3rd-Order I.P. with Decreasing Incident Power

△ 5th-Order I.P. with Decreasing Incident Power

———Residual level

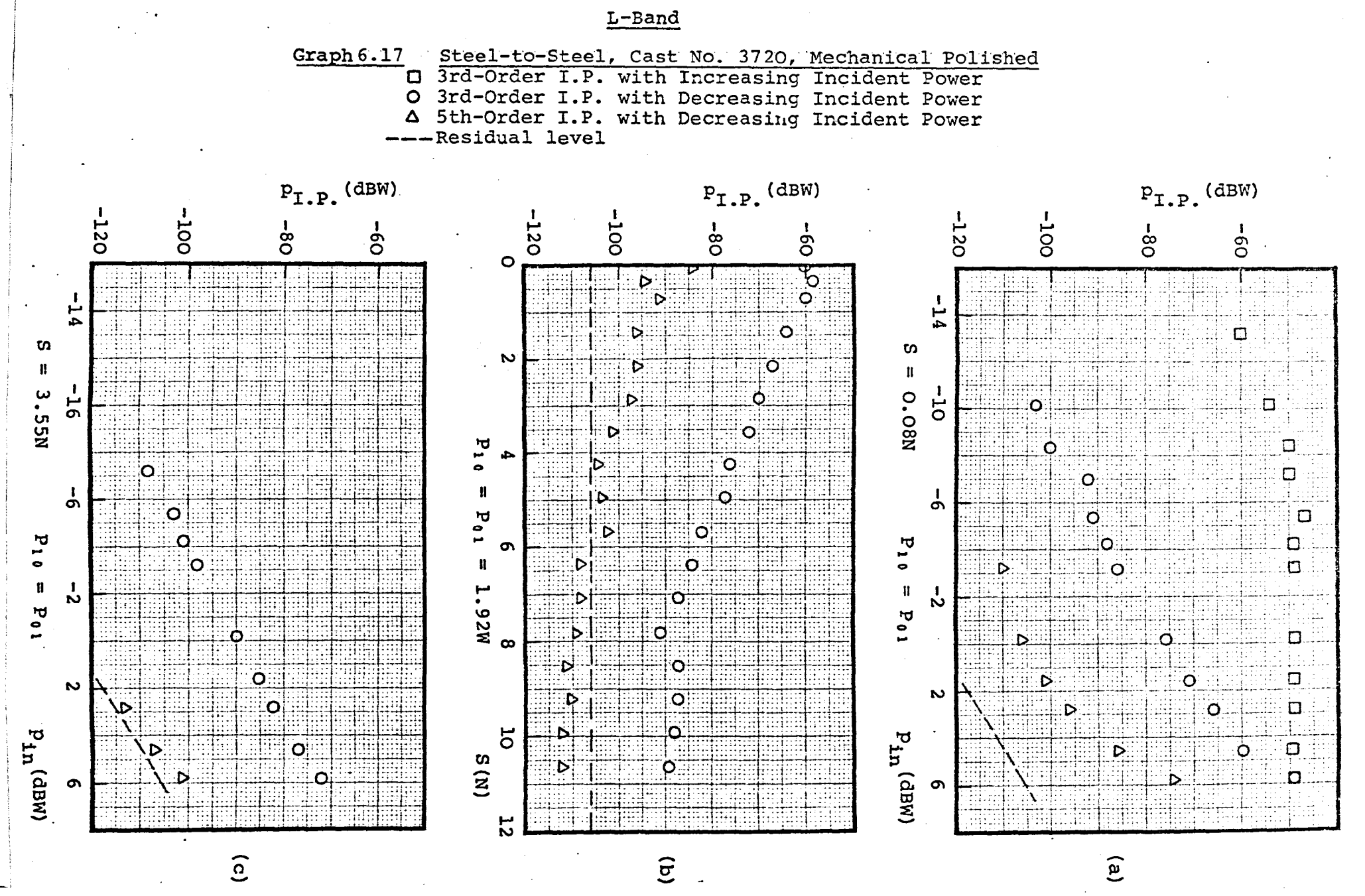

Graphs 6.16 and 6.17 are discussed in this section. The 3rd-order I.P. level increased with increasing incident power level up to $P_{in} \simeq 0.2W$, then an electrical deformation occurred (see Graphs 6.16a and 6.17a) and the 3rd-order I.P. level reached to about -70dBW and -60dBW at an incident power level of 3.84W for steels 3719 and 3720 respectively. By decreasing the incident power at a constant axial force of 0.08N both the 3rd- and 5th-order I.P. levels decrease almost linearly at both steels. The maximum 5th-order I.P. levels of -90dBW and -75dBW were recorded for a maximum incident power of 3.84W for steels 3719 and 3720 respectively. In Graphs 6.16b and 6.17b the variation of 3rd- and 5th-order I.P. levels are given for both steel with increasing axial force. While 3rd- and 5th-order I.P. levels for 3719 remain almost constant, they decrease slowly for steel 3720. The probable reason may be the smaller carbon content in 3720 than in 3719 (see Table 5.1) and the addition of a small amount of Al i.e. 0.17% so that the thickness of the oxidized film will be decreased. Therefore the amount of required axial force for mechanical deformation decreases. This slow breakdown of oxide layers has caused smaller 3rd- and 5th-order I.P. levels for steel 3720 than those for steel 3719 with decreasing incident power level at a constant axial force of 3.55N (see Graphs 6.16c and 6.17c). The slope of the 3rd-order I.P. level being the same for both steels of about 3.

6.3 Similar Metal-to-Metal Contacts with Electropolished Surface

To study the effect of surface finish on generation of I.P. levels, the contact surface of six test sample pairs made of stainless steel (EN58B), mild steel, duraluminium, oxygen free nickel and copper were electropolished (see Section 5.3)

to give a surface roughness less than 0.35μ (C.L.A.).

6.3.1 Stainless steel-to-stainless steel (EN58B), electropolished

Graph 6.18 shows the results obtained from similar metal-to-metal contacts of electropolished stainless steel (EN58B). The variation of 3rd- and 5th-order I.P. levels with increasing and decreasing incident power level at a constant axial force of 0.08N (see Graph 6.18a) were very erratic indicating the presence of oxide layers which could not be electrically deformed. The I.P. levels produced by electropolished stainless steel at a low axial force (≈0.1N) were higher than those obtained from mechanically polished stainless steel. But as the axial force increases at a constant incident power of 3.84W (see Graph 6.18b), both the 3rd- and 5th-order I.P. decrease slowly so that at an axial force of about 7N, the 3rd-order I.P. level falls down to the residual level. It seems that mechanical breakdown can take place at a lower axial force as the contact surface becomes smoother. The slope of the 3rd-order I.P. level with decreasing incident power at an axial force of 3.55N, i.e. after breakdown has started, is about 2.5 (see Graph 6.18c).

6.3.2 Mild steel-to-mild steel, electropolished

The results for electropolished similar metal-to-metal contacts recorded for mild steel are shown in Graph 6.19. Very high 3rd- and 5th-order I.P. levels were obtained at an axial force of 0.08N over the whole range of incident power (see Graph 6.19a). In other words while 3rd-order I.P. levels with increasing and decreasing incident power levels are almost repeatable, the oxide layers at contact point are not damaged and responsible for I.P. generation. The levels of 3rd- and 5th-order I.P. in this test were about 10dB higher than those for mechanically polished mild

L-Band

Graph 6.18 Stainless Steel-to-Stainless Steel, EN58B, Electropolished

□ 3rd-Order I.P. with Increasing Incident Power

○ 3rd-Order I.P. with Decreasing Incident Power

△ 5th-Order I.P. with Decreasing Incident Power

---Residual level

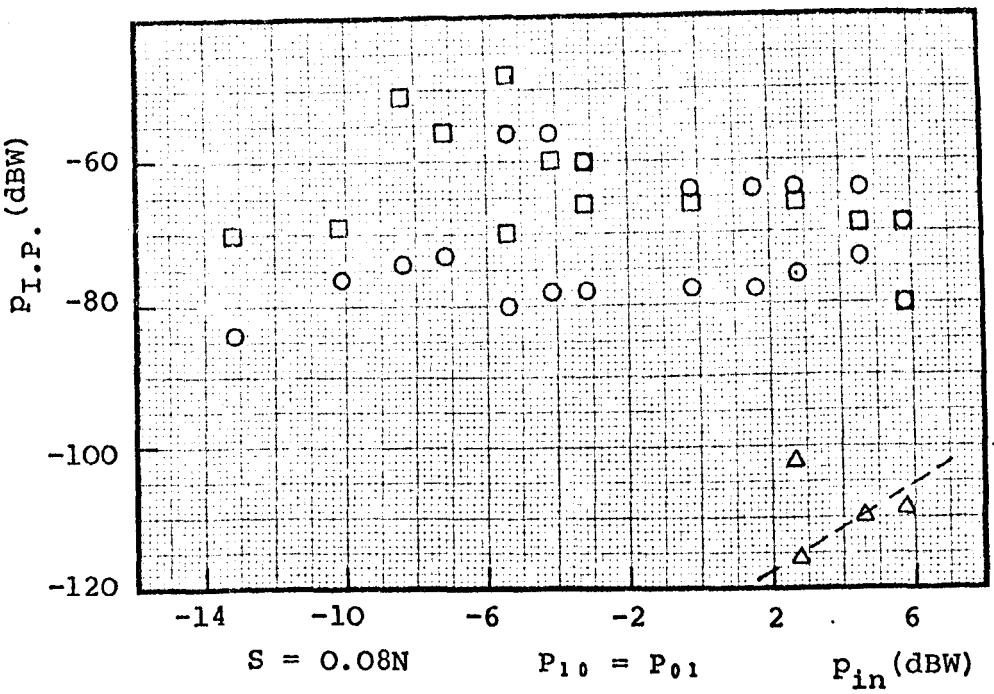

(a)

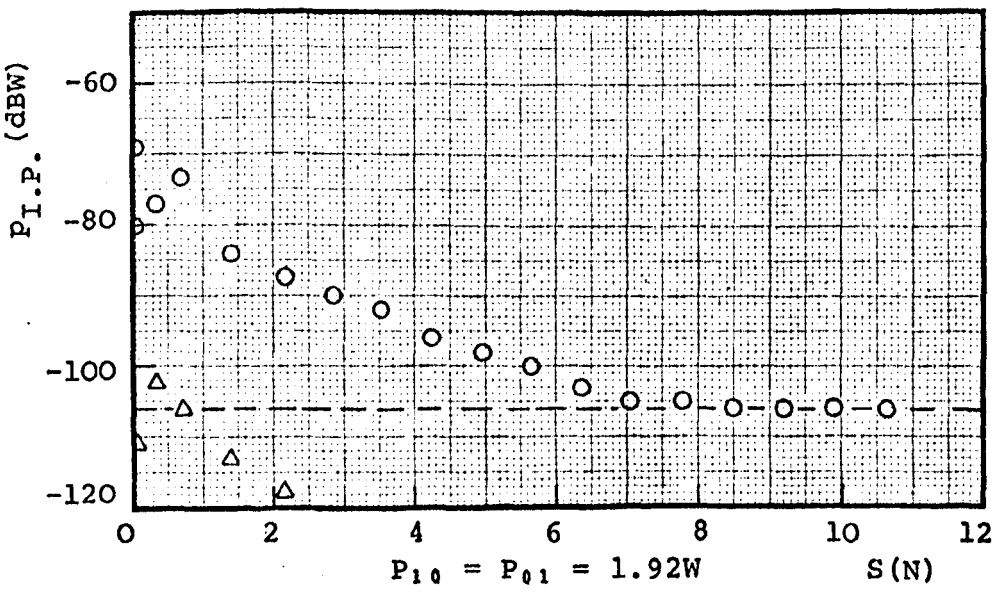

(b)

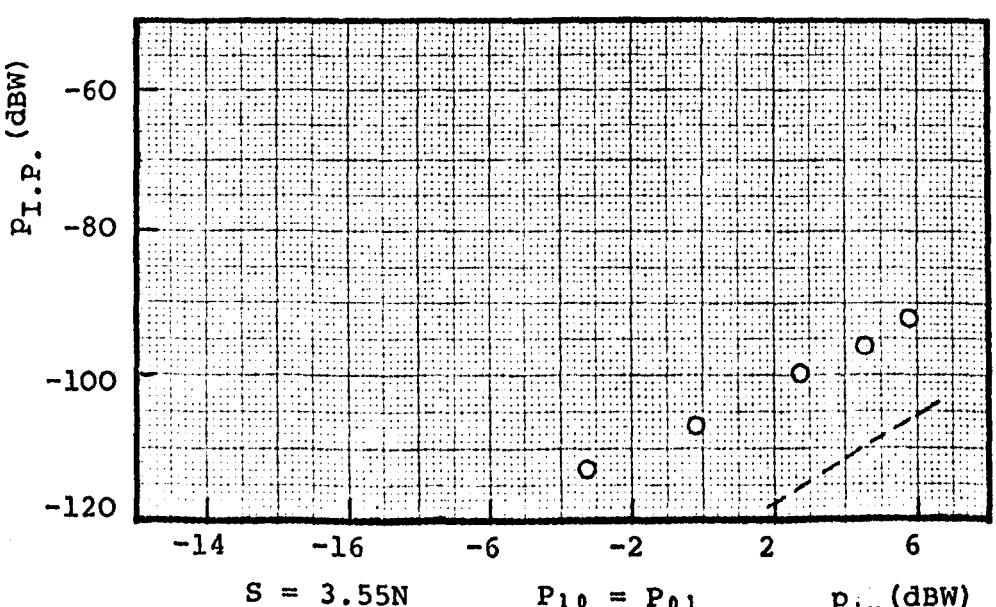

(c)

L-Band

Graph 6.19 Mild Steel-to-Mild Steel, Electropolished

□ 3rd-Order I.P. with Increasing Incident Power

○ 3rd-Order I.P. with Decreasing Incident Power

△ 5th-Order I.P. with Decreasing Incident Power

---Residual level

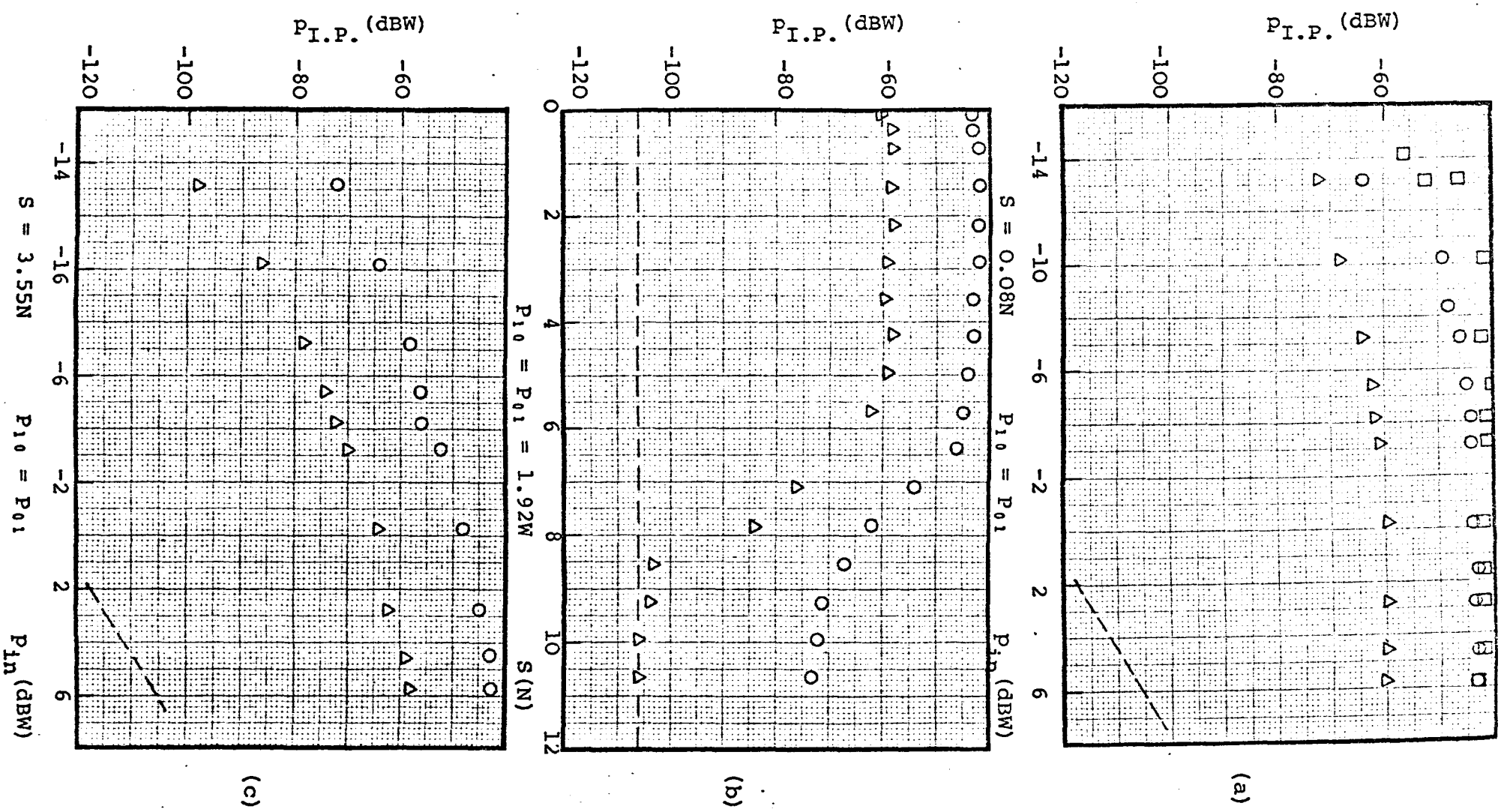

steel at a lower axial force (lower than 6N) as illustrated in Graph 6.19b. The maximum available axial force was not sufficient for perfect breakdown of the oxide layers but at S = 6N some deformation had occurred so that both the 3rd- and 5th-order I.P. levels had fallen down to -75dBW and -110dBW respectively from their original value of -40dBW and -60dBW. It can be seen that when a better contact has been established not only the I.P. levels fall down to lower levels but also the gap between I.P. levels increases. By comparing Graph 6.19b in this test with results obtained for mechanically polished mild steel (Graph 6.2b) it may be concluded that, as the contact surface becomes more smoother, the lower level becomes the axial force necessary for mechanical deformation or breakdown. The variation of 3rd- and 5th-order I.P. levels with decreasing incident power at an axial force of 3.55N, where deformation has not occurred yet, seems almost linear with a slope of 1.5 which is greater than the slope of those at an axial force of 0.08N.

6.3.3 Duraluminium-to-duraluminium, electropolished

The results for electropolished test sample pairs made of duraluminium are given in Graph 6.20. The maximum 3rd- and 5th-order I.P. levels of about -50dBW and -80dBW were observed with a maximum incident power of 3.84W at a constant axial force of 0.08N (Graph 6.20a). The 5th-order I.P. level pronounced itself in this test at a higher level than that obtained for mechanically polished but the 3rd-order I.P. decreases with decreasing the incident power more slowly than that of mechanically polished at the same condition. The slope of the 3rd-order I.P. level in this test is about 2.5. Both the 3rd- and 5th-order I.P. levels remain almost constant with increasing axial force up to 8N where

L-Band

Graph 6.20 Duraluminium-to-Duraluminium, Electropolished
□ 3rd-Order I.P. with Increasing Incident Power
○ 3rd-Order I.P. with Decreasing Incident Power
△ 5th-Order I.P. with Decreasing Incident Power
---Residual level

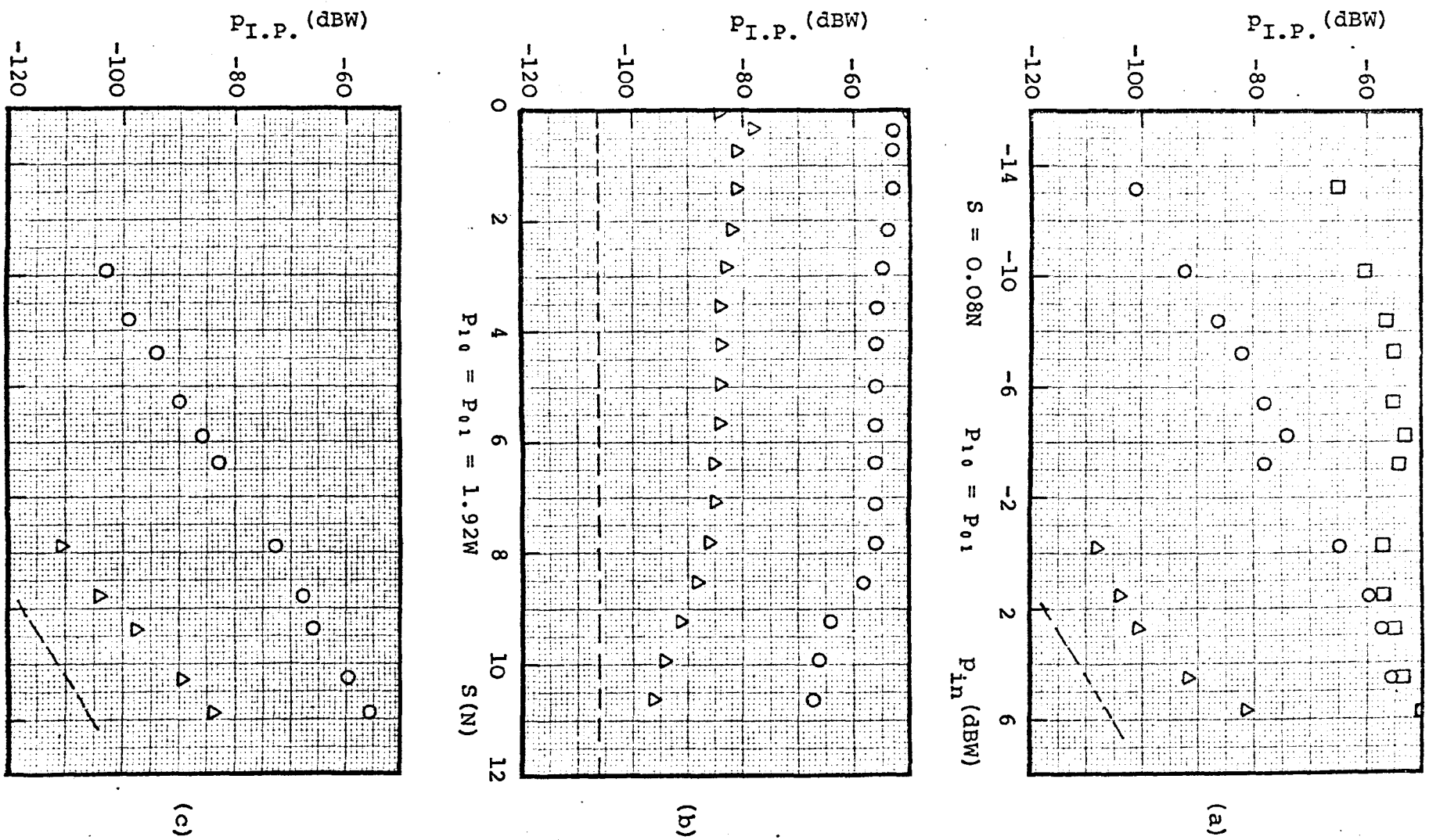

mechanical deformation of oxide layers has started but it seems for electropolished duraluminium, axial force much higher than the maximum available axial force in this test (12N) is required for a complete breakdown. When it is expected that the oxide layer on a spherical contact break sooner than that on a flat contact as axial force is increasing and it was the case for electropolished stainless steel and mild steel, but it seems in this test the smooth flat contact has squeezed the oxide layer on the spherical contact rather than rupturing it. This may be why the 3rd- and 5th-order I.P. levels with decreasing incident power at axial force of 3.55N (Graph 6.20c) have higher levels than those obtained from mechanical polished duraluminium.

6.3.4 Oxygen free nickel-to-oxygen free nickel, electropolished

Graph 6.21 shows the results obtained for electropolished test sample pair made of oxygen free nickel. The 3rd-order I.P. level increases with increasing incident power up to $P_{in} \approx 0.5W$ at constant axial force of 0.08N and then remains almost constant up to maximum incident power 3.84W having the level of about -50dBW. By decreasing incident power both the 3rd- and 5th-order I.P. levels decrease linearly with a slope of 3.5 and 5.5 respectively (Graph 6.21a). The 5th-order level at maximum incident power at axial force of 0.08N was about -75dBW. By increasing axial force, the 3rd-order I.P. level decreases and falls down to residual level at axial force of 3.5N (Graph 6.21b). Therefore the I.P. levels at axial force of 3.55N with decreasing incident power were not measured. Comparing the results of electropolished and mechanical polished of nickel test sample pairs once more it suggests that the smoother the surface finish the lower is the axial force for mechanical breakdown of oxide layers.

6.3.5. Copper-to-copper and oxygen free copper-to-oxygen free copper, electropolished

Graph 6.22 shows a typical result for electropolished copper and oxygen free copper test sample pairs. By comparing these results with those for mechanical polished strongly suggests that cleanliness of contact surfaces is much more important than surface roughness. In other words when the contact surfaces are free of oxide layers or are covered with very thin oxide layers only a little increase in axial force is sufficient for a perfect metal-to-metal contact which is expected to produce a 3rd-order I.P. level much less than the residual level at maximum incident power level.

6.4 Similar-Metal-to-Metal Contacts with Electroplated Surface

To study the electroplated metal contacts, five test sample pairs made of brass were electroplated with nickel, cadmium, copper, silver and gold (see Section 5.4) and an investigation was carried out for similar metal-to-metal contacts.

6.4.1 Nickel-to-nickel, electroplated

Graph 6.23 shows the results recorded for similar metal-to-metal contacts made of nickel electroplated brass. While the 3rd-order I.P. level with increasing incident power at constant axial force of 0.08N (Graph 6.23a) showed an erratic variation, it became more stable under the same condition with decreasing incident power level. At maximum available incident power P_{in} = 3.84W, the 3rd- and 5th-order I.P. levels were about -60dBW and -110dBW respectively. It was not possible to increase axial force above 6.5N (Graph 6.23b) because of the total length of this sample being shorter than 10mm, but it was observed that by

L-Band

Graph 6.21 Oxygen free nickel-to-oxygen free nickel, electropolished

□ 3rd-Order I.P. with Increasing Incident Power
○ 3rd-Order I.P. with Decreasing Incident Power
△ 5th-Order I.P. with Decreasing Incident Power
---Residual level

L-Band

Graph 6.22 Typical graph for electropolished similar metal-to-metal contacts of copper and oxygen free copper

L-Band

Graph 6.23 Nickel-to-Nickel, Electroplated

□ 3rd-Order I.P. with Increasing Incident Power

○ 3rd-Order I.P. with Decreasing Incident Power

△ 5th-Order I.P. with Decreasing Incident Power

---- Residual level

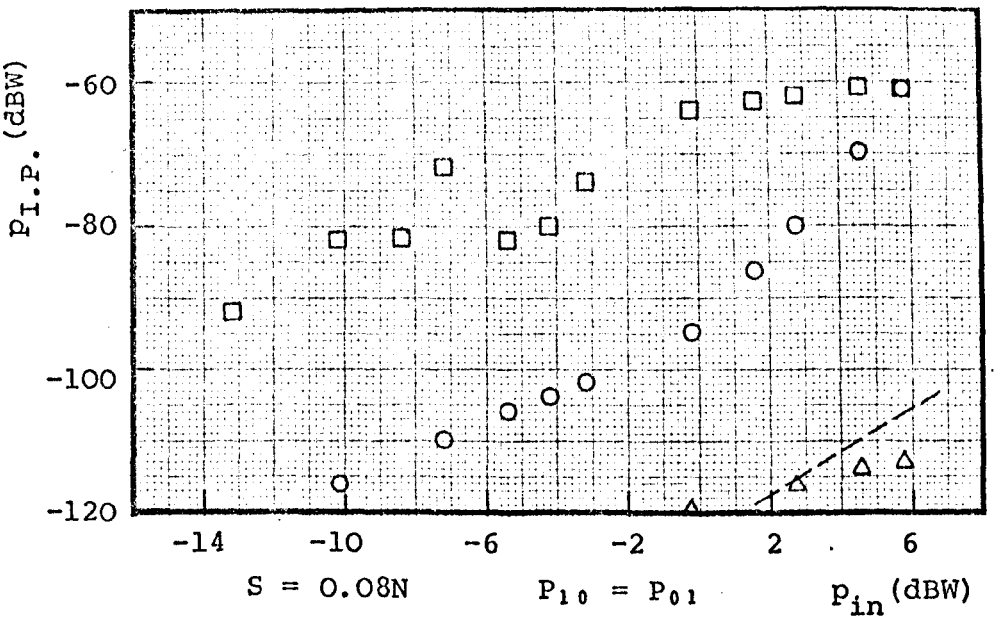

(a)

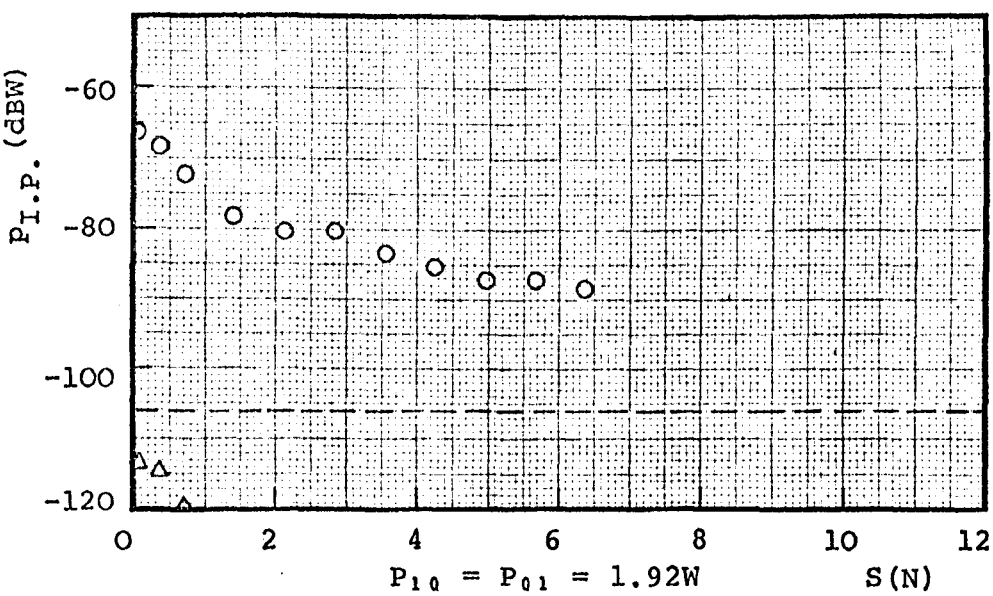

(b)

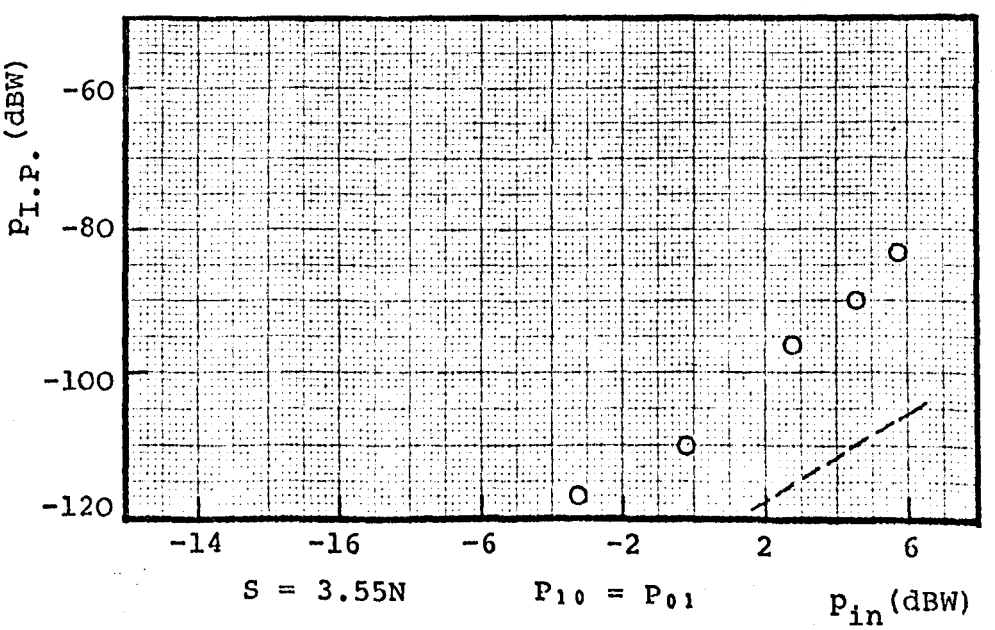

(c)

increasing axial force at a constant incident power of 3.84W, both the 3rd- and 5th-order I.P. levels decreased. Decreasing of the 3rd-order I.P. level with decreasing incident power level at a constant axial force of 3.55N was much more linear than of that at 0.08N axial force. It can be seen that over the whole range of available axial force, as far as I.P. generation is concerned, the nickel plated contact is similar to the test sample pair made of nickel as the base material.

6.4.2 Cadmium-to-cadmium, electroplated

The results obtained for the test sample pair made of cadmium electroplated brass are shown in Graph 6.24. In this test no 5th-order I.P. levels were detectable even at maximum incident power. The reproducible measurements of 3rd-order I.P. levels indicate that the oxide layers on the contact surface are responsible for generation of I.P.'s and the available incident power was insufficient for electrical deformation (see Graph 6.24a) but mechanical breakdown was achieved at an axial force of 1N bringing the 3rd-order I.P. level from about -80dBW at P_{in} = 3.84W down to the residual level.

6.4.3. Copper-to-copper, silver-to-silver and gold-to-gold, electroplated

The I.P. levels generated by similar metal-to-metal contact of test sample pairs made of copper plated brass, silver plated brass and gold plated brass were almost the same, i.e. at zero axial force they generate 3rd-order I.P. levels of about -60dBW at maximum incident power of 3.84W, but a little increase in axial force up to 0.08N is sufficient for mechanical breakdown and a perfect metal-to-metal contact. Therefore no graph has been plotted. This result was expected

L-Band

Graph 6.24 Cadmium-to-cadmium, electroplated
□ 3rd-Order I.P. with Increasing Incident Power
○ 3rd-Order I.P. with Decreasing Incident Power
△ 5th-Order I.P. with Decreasing Incident Power
---- Residual level

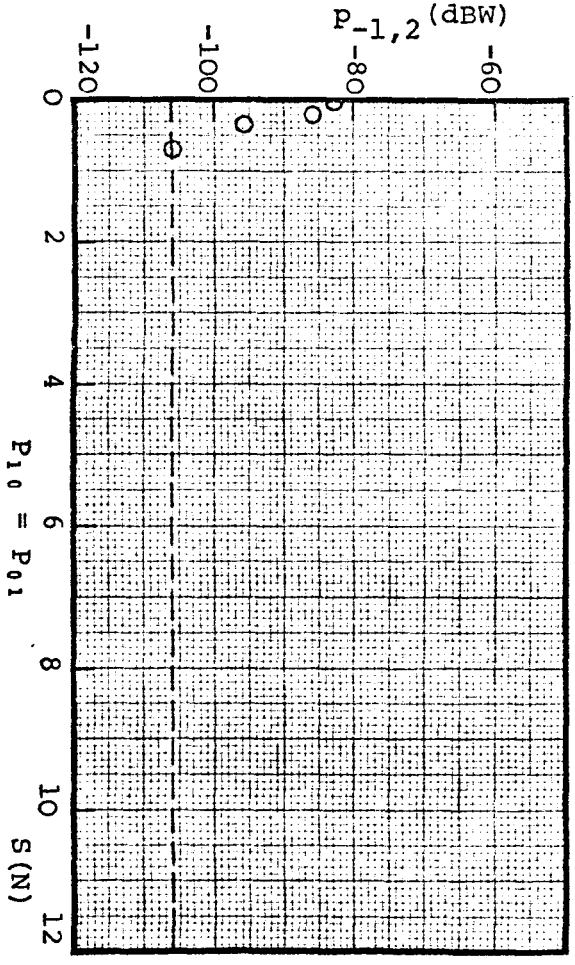

(b)

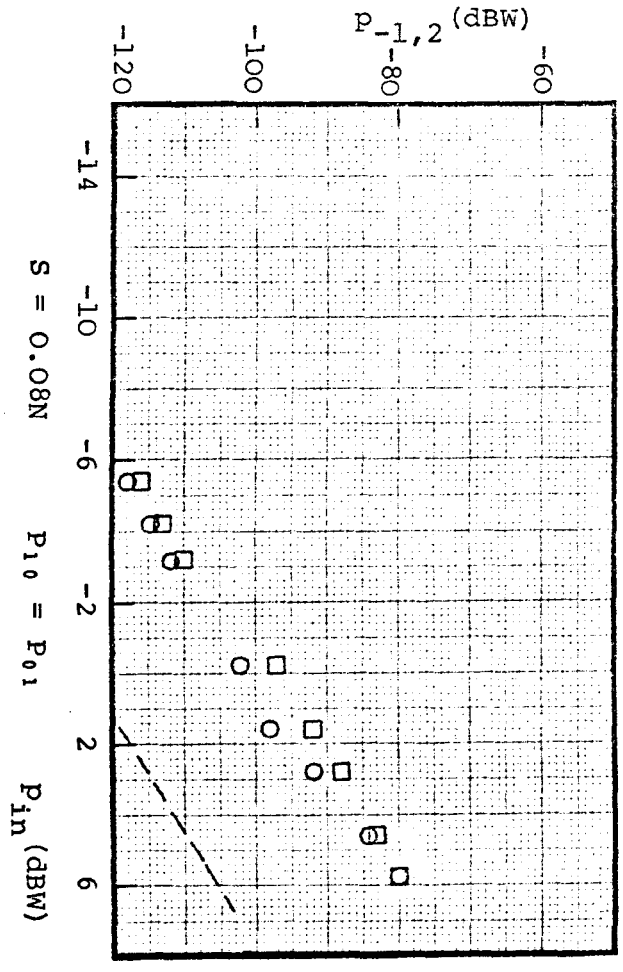

(a)

because gold and silver are resistant against corrosion and copper plated was electrically clean so that the thickness of the oxide layers was too thin to bear an axial force of 0.08N.

6.5 Effect of Corroded Contact Surface on I.P. Generation

Three test sample pairs, mechanically polished copper, electropolished copper and copper electroplated brass were allowed to corrode inside the laboratory for about 200 days after the intial results mentioned before were taken. Graphs 6.25, 6.26 and 6.27 show the results obtained for similar metal-to-metal test sample pairs of corroded mechanically polished, electropolished and electroplated copper respectively. The 3rd-order I.P. level increases with increasing incident power at three test samples (Graphs 6.25a, 6.26z and 6.27a) but it increases more rapidly in mechanically polished copper than that in the two other cases. The 3rd-order I.P. observed at maximum incident power was about -68dBW, -52dBW and -58dBW for these test sample pairs at a constant axial force of 0.08N and also the 3rd- and 5th-order I.P. levels for the mechanically polished copper decrease with decreasing incident power more rapidly than those in two others indicating the presence of more stable oxide layers at the contact surfaces of the corroded electropolished and electroplated copper than that at mechanically polished copper. On the contrary by increasing axial force the oxide layers on the electroplated copper breakdown at about $S = 0.1N$ and that on the electropolished one deform at $S \approx 0.7N$ and completely breakdown at $S = 9N$ while the maximum available axial force was not sufficient to break down the oxide layer on mechanically polished copper (see Graphs 6.25b, 6.26b and 6.27b). It can be concluded that again the smoother the

L-Band

Graph 6.25 Corroded Copper-to-Copper, Mechanical Polished

□ 3rd-Order I.P. with Increasing Incident Power

○ 3rd-Order I.P. with Decreasing Incident Power

△ 5th-Order I.P. with Decreasing Incident Power

---- Residual level

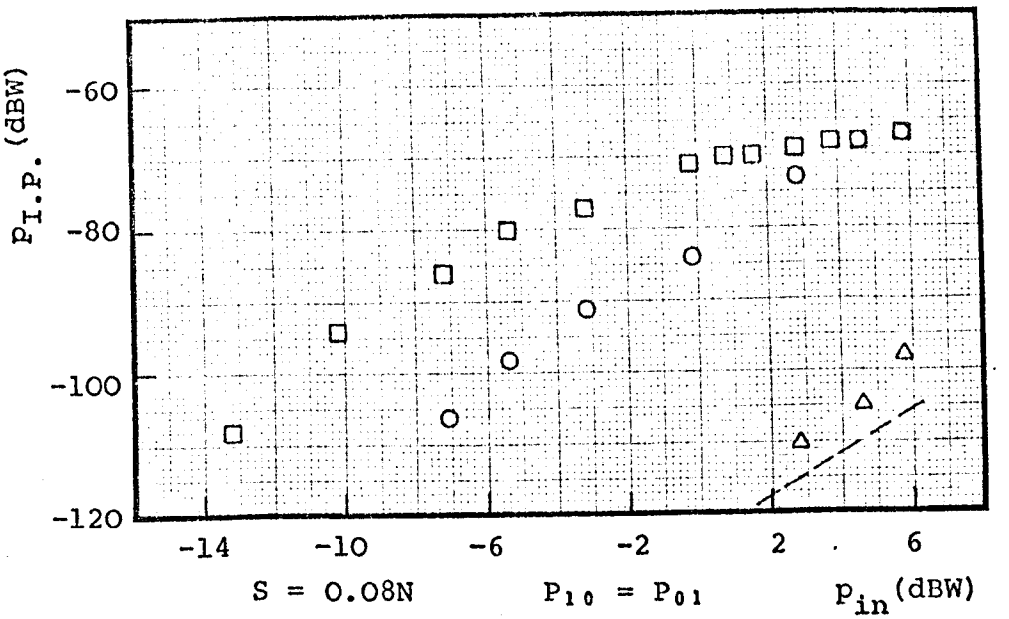

(a)

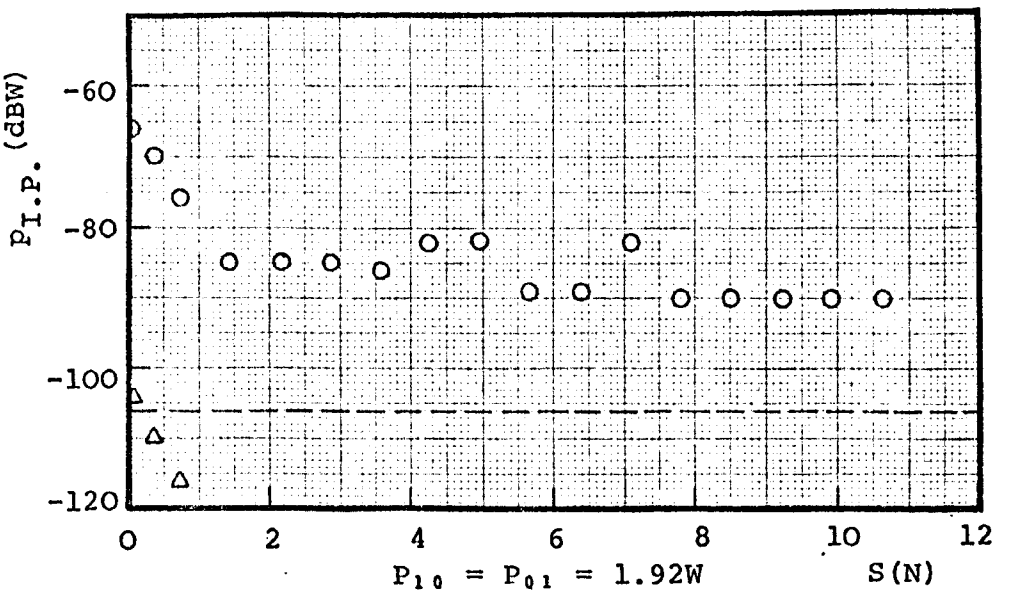

(b)

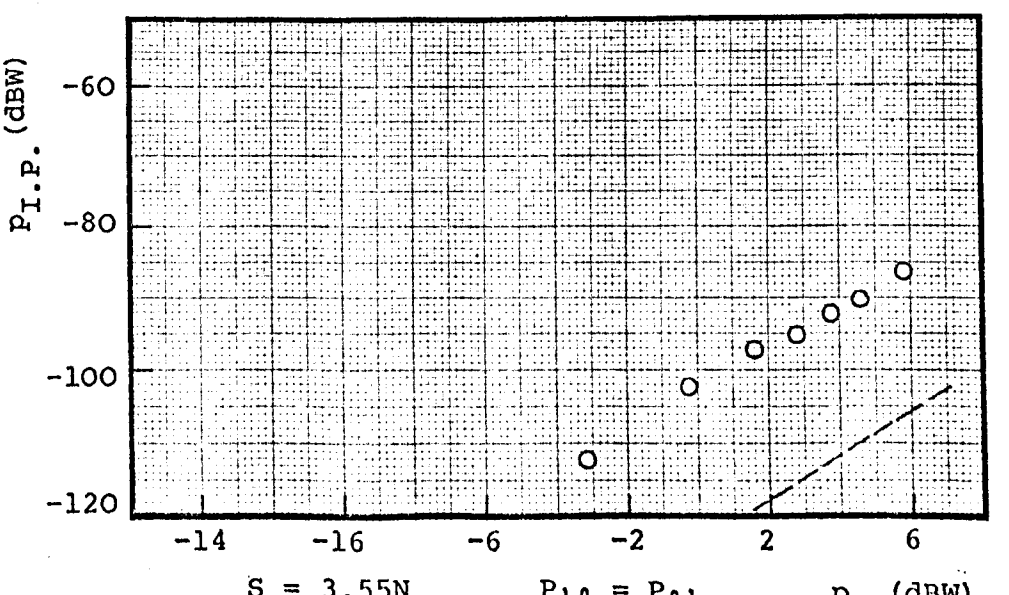

(c)

L-Band

Graph 6.26 Corroded Copper-to-Copper, Electropolished

□ 3rd-Order I.P. with Increasing Incident Power

○ 3rd-Order I.P. with Decreasing Incident Power

△ 5th-Order I.P. with Decreasing Incident Power

---Residual level

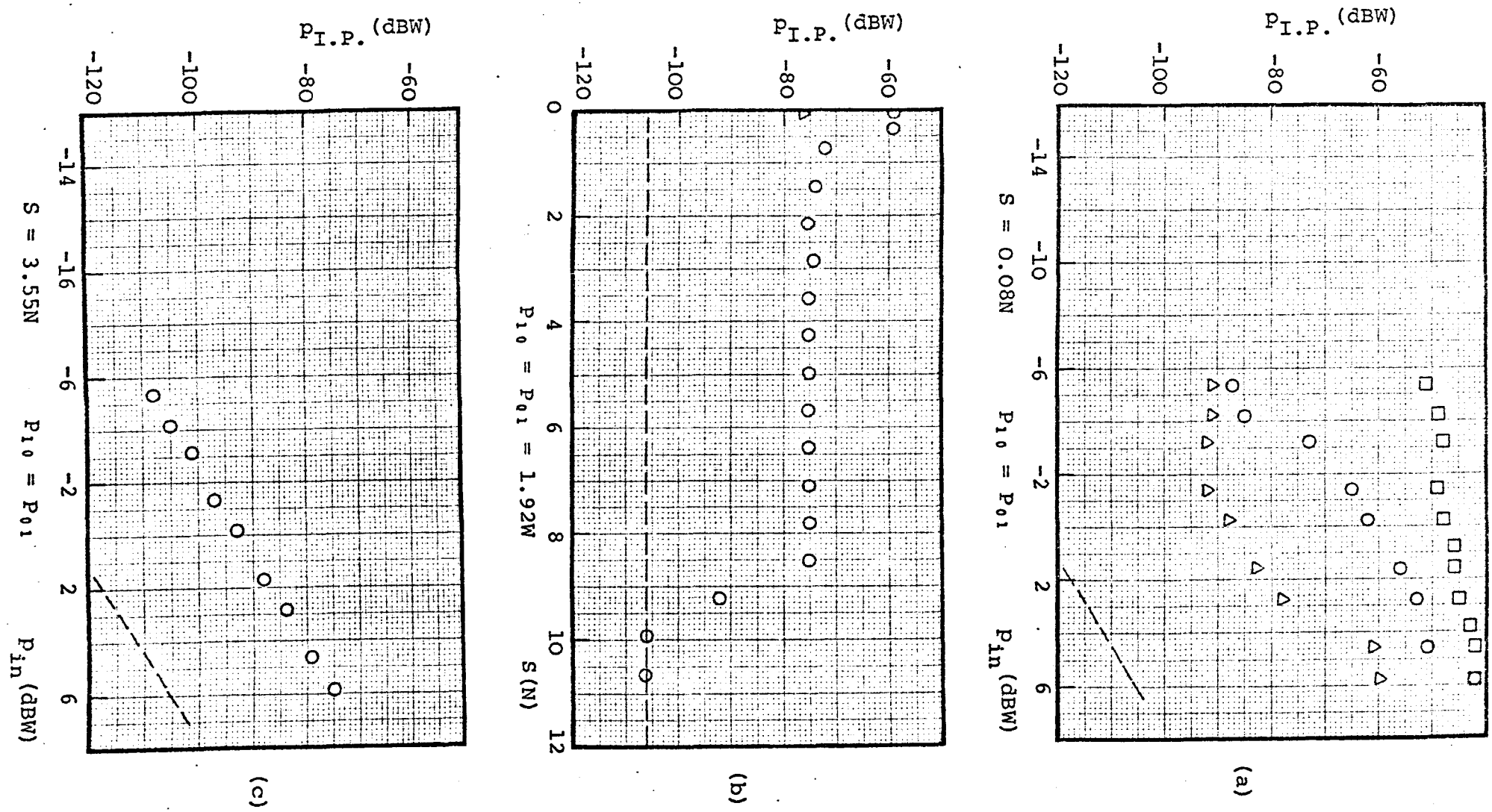

L-Band

Graph 6.27 Corroded copper-to-copper, electroplated

□ 3rd-Order I.P. with Increasing Incident Power
○ 3rd-Order I.P. with Decreasing Incident Power
△ 5th-Order I.P. with Decreasing Incident Power
--- Residual level

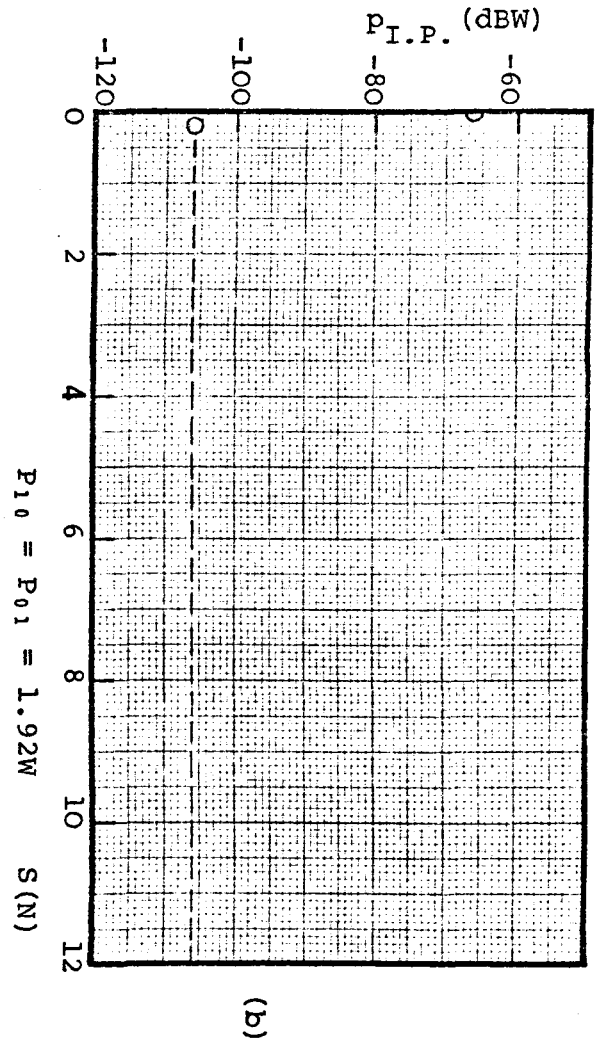

(b)

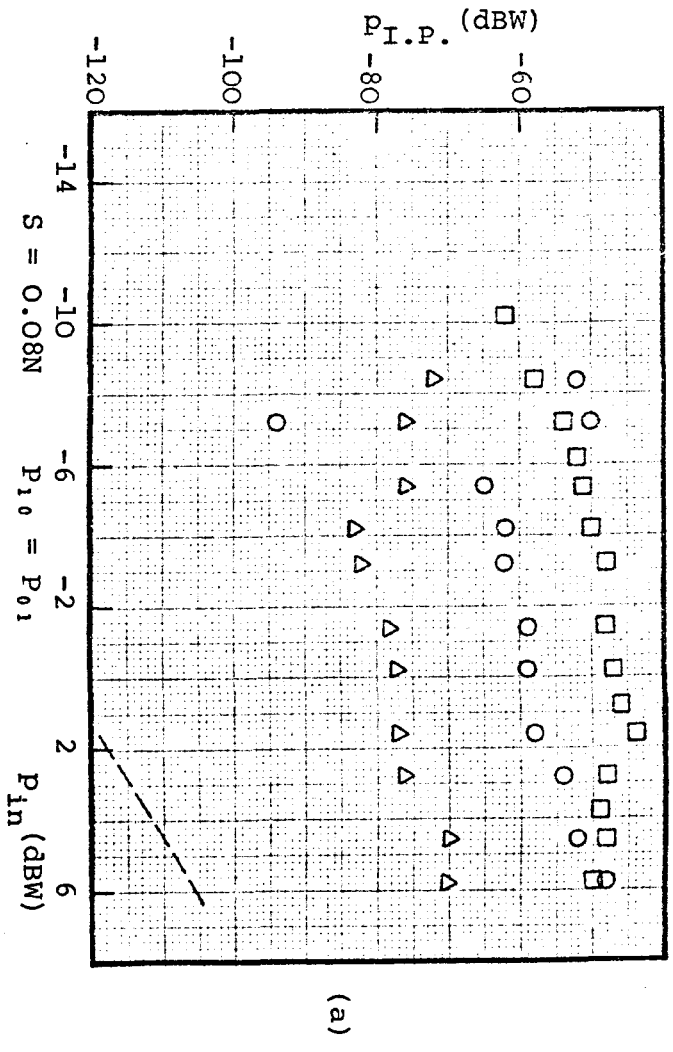

(a)

surface finish the lower the axial force for breakdown. Before mechanical break down of oxide layers occurs the smoother the surface finish and consequently the more stable the oxide layer, the more the surface is resistant to electrical breakdown. The two steps, deformation and breakdown in corroded electropolished copper could be caused because of breakdown of oxide layers on spherical and flat samples respectively. Variation of 3rd-order I.P.'s with decreasing incident power, when a mechanical deformation has occurred for corroded mechanically polished and electropolished copper test samples, at a constant axial force of 3.55N are linear as illustrated in Graphs 6.25c and 6.26c with the slope of almost 3.

6.6 Statistical Measurements

When two metallic conductors are brought together, the contact surfaces are sufficiently rough on the microscopic scale that the magnified profiles of the contact surfaces for a point contact may be illustrated as Fig.6.1.

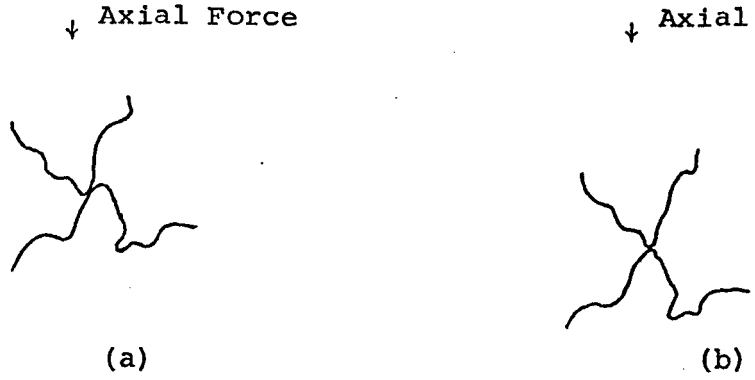

Fig.6.1 Magnified profile of contact surfaces

As the force builds up on the contacting surfaces, deformations are expected to take place at contact. If the profile curves of the contact surfaces are known, for a certain

axial force, both the elastic and plastic deformations may take place depending on the location of asperities. If the distribution function of the asperities and the probability density function and mechanical properties of the oxide layers are known, then the constriction resistance[31,32,33] and of course contact resistance can be calculated. In other words the nature of deformations not only depends on the mechanical properties of the oxide films and base material but also on the position of the contact point(s) which can be defined by a certain probability. For instance, if the position of the contact point is similar to that shown in Fig.6.1a, the oxide film would be expected to rupture at a lower axial force than that shown in Fig.6.1b as it is squeezed between the metal electrodes. Therefore statistical measurements were found to be necessary. The statistical measurements were carried out for similar and dissimilar metal-to-metal contacts and only the 3rd-order I.P. levels were recorded at maximum available incident power of 3.84W ($P_{10} = P_{01} = 1.92W$) at six discrete axial forces of 0.08N, 0.35N, 0.71N, 3.55N, 7.1N and 10.65N (see Section 4.2).

6.6.1 Similar metal-to-metal contacts with mechanically polished surface

Five test sample pairs from each different base material mentioned in Section 5.1 (except oxygen free copper) were tested. The test results obtained for similar metal-to-metal contacts of stainless steel (EN58B), mild steel and duraluminium are illustrated in Graphs 6.28a, b and c respectively. In each graph the spread of 3rd-order I.P. level and the average value are shown. When the 3rd-order I.P. level fell down into the residual level, the value of -106dBW

L-Band

Graph 6.28 Similar Metal-to-Metal Contacts

⊢—⊣ Spread of results from 5 different sample pairs

O Average value

– – – Residual level

(a) Duraluminium-to-duraluminium

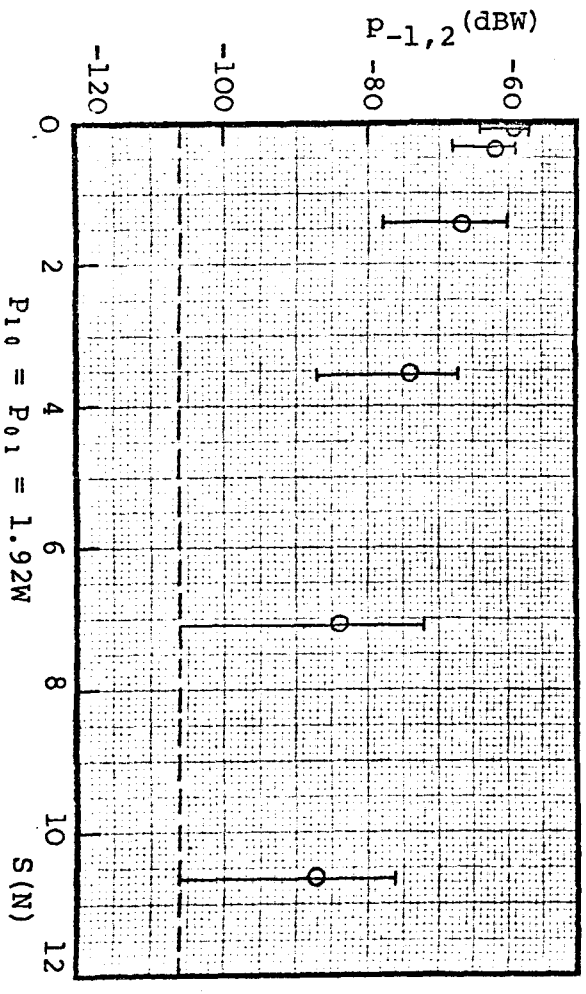

(b) Mild steel-to-mild steel

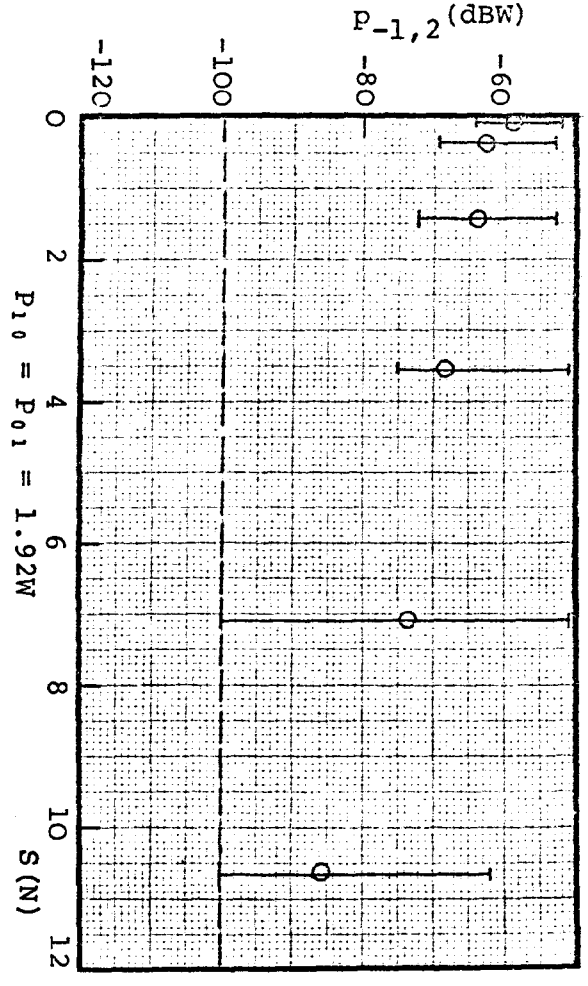

(c) Stainless steel-to-stainless steel

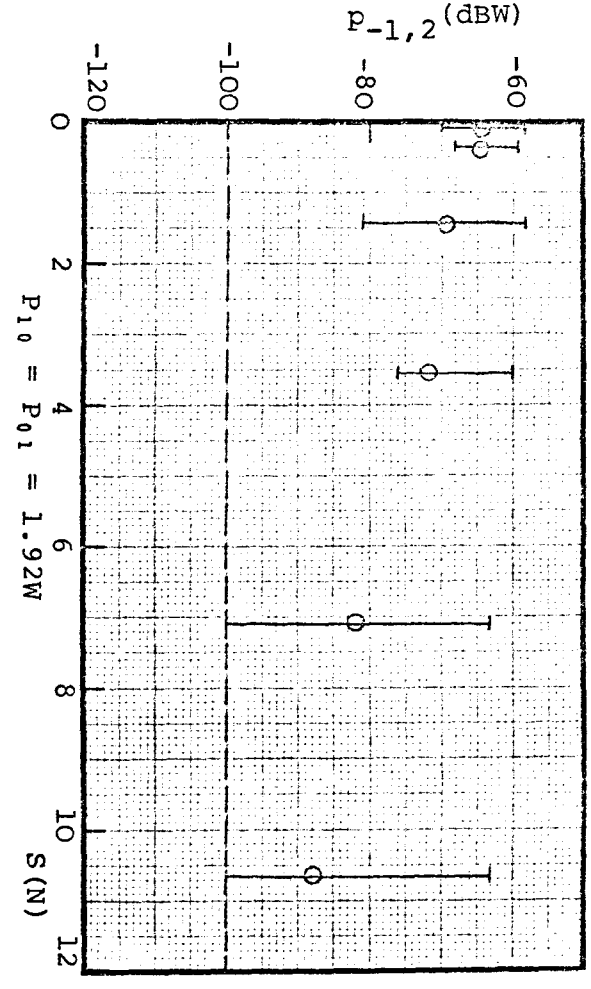

(residual level) was considered as the measured value for that sample in taking the average. The other four base materials, i.e. copper, beryllium copper, oxygen free nickel and brass generate maximum 3rd-order I.P. levels at zero axial force but at S = 0.08N all of them fell down into the residual level, therefore no graphs are provided. These results were not surprising, because mechanical polishing was done immediately after machining down to size the test sample pairs and then the 3rd-order I.P. levels were measured, therefore an axial force of 0.08N was sufficient to break down the very thin oxide layers.

6.6.2 Dissimilar metal-to-metal contacts with mechanically polished surface

For the statistical investigations of dissimilar metal-to-metal contacts, all the possible combinations of dissimilar metal-to-metal (M_1-to-M_2) contacts resulting from seven different materials mentioned in Section 6.6.1 except the combination of mild steel to duraluminium, beryllium copper, copper, brass and oxygen free nickel were studied. The test sample pairs were mechanically polished and Graphs 6.29 to 6.34 show the variation of 3rd-order I.P. levels with discrete axial force at maximum available incident power of 3.84W. For each dissimilar M_1-to-M_2 contacts measured, six test sample pairs were prepared. In three test sample pairs the spherical halves were made of material M_1 and flat halves were of M_2. In the other three test sample pairs the spherical halves were M_2 and the flat ones were made of M_1. In the graphs the spread and mean value of all six test sample pairs are shown and when the 3rd-order I.P. levels had fallen into the residual level, the residual level itself was considered when

taking the average. Referring to the results of similar metal-to-metal contacts given by Graph 6.28, it is clear that the test sample pairs which generated the strongest I.P. levels were made of mild steel, duraluminium and stainless steel. Considering the results of dissimilar metal-to-metal contacts of seven materials tested given in Graphs 6.29 to 6.34, if the results obtained from stainless steel-to-copper, beryllium copper and brass are neglected, it could be concluded that :

(i) The dissimilar metal-to-metal contacts of mild steel, stainless steel and duraluminium produced comparable results over a wide range of axial force (Graphs 6.29a and 6.29b).

(ii) The dissimilar metal-to-metal contacts of copper, beryllium copper, oxygen free nickel and brass produced low I.P. levels over a correspondingly narrow band of axial force (Graphs 6.32b, 6.32c, 6.33 and 6.34).

(iii) The dissimilar metal-to-metal contacts when one of the contact halves is made from stainless steel and duraluminium and the other half is made from copper, brass, beryllium copper and oxygen free nickel then this generated I.P. levels of an intermediate value (Graphs 6.29c, 6.31 and 6.32a).

The condition (ii) mentioned above is always true if the test sample pairs are electrically clean (free of oxide film) but conditions (i) and (iii) depend on the configuration of the contact halves and mechanical properties of the bulk material and oxide film. For this purpose the results obtained for

metal-to-metal contacts of stainless steel-to-duraluminium, copper and mild steel are shown in another form in Graphs 6.35, 6.36 and 6.37 respectively. In each graph the spread of the results for the three test sample pairs where the spherical contact half is made of M_1 and the flat half is made of M_2 and also the spread of results for another three test sample pairs where the spherical contact half is made of M_2 and the flat half is made of M_1 are given for comparison. The test results obtained for stainless steel-to-beryllium copper and brass also are similar to Graph 6.36, therefore no graphs are produced for them. From Graph 6.35, it can be seen that the spread of results when the spherical half is made of duraluminium and the flat half is made of stainless steel over a wide range of axial force is lower than the spread of results when the spherical half is of stainless steel and the flat half is of duraluminium. It can be concluded that, the mechanical breakdown leading to a perfect metal-to-metal contact at first occurs on the oxide film over the sharper (spherical) contact and then on the oxide film over the flat contact. As the hardness of the bulk material of the contact halves become more closer the probability of overlapping the results over a wide range of axial force increase (see Graph 6.36 and 6.37).

6.6.3 Similar steel-to-steel contacts with corroded contact surface

Three mechanically polished test sample pairs from each different steel mentioned in Table 5.1 were allowed to corrode inside the laboratory for about 200 days and Graphs 6.38 to 6.41 show the statistical measurements of 3rd-order I.P. levels with axial force at a constant incident power of 3.84W ($P_{10} = P_{01} = 1.92W$). All the steels produce very high I.P.

L-Band

Graph 6.29 Dissimilar Metal-to-Metal Contacts

|——| Spread of results from 6 different sample pairs

o Average value

---- Residual level

(c) Stainless steel-to-oxygen free nickel

(b) Stainless steel-to-duraluminium

(a) Stainless steel-to-mild steel

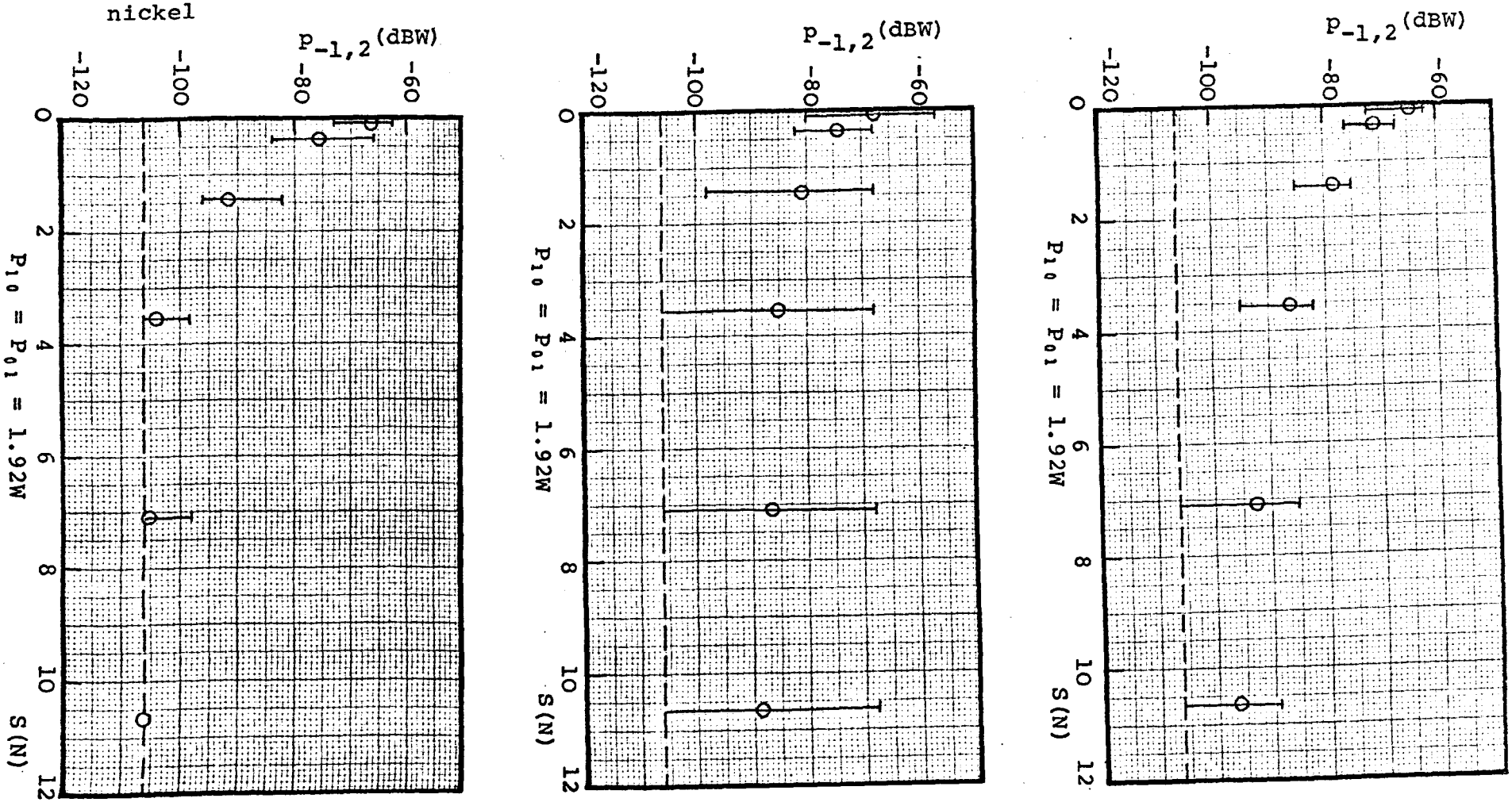

L-Band

Graph 6.30 Dissimilar Metal-to-Metal Contacts

⊢——⊣ Spread of results from 6 different sample pairs

O Average value

---- Residual level

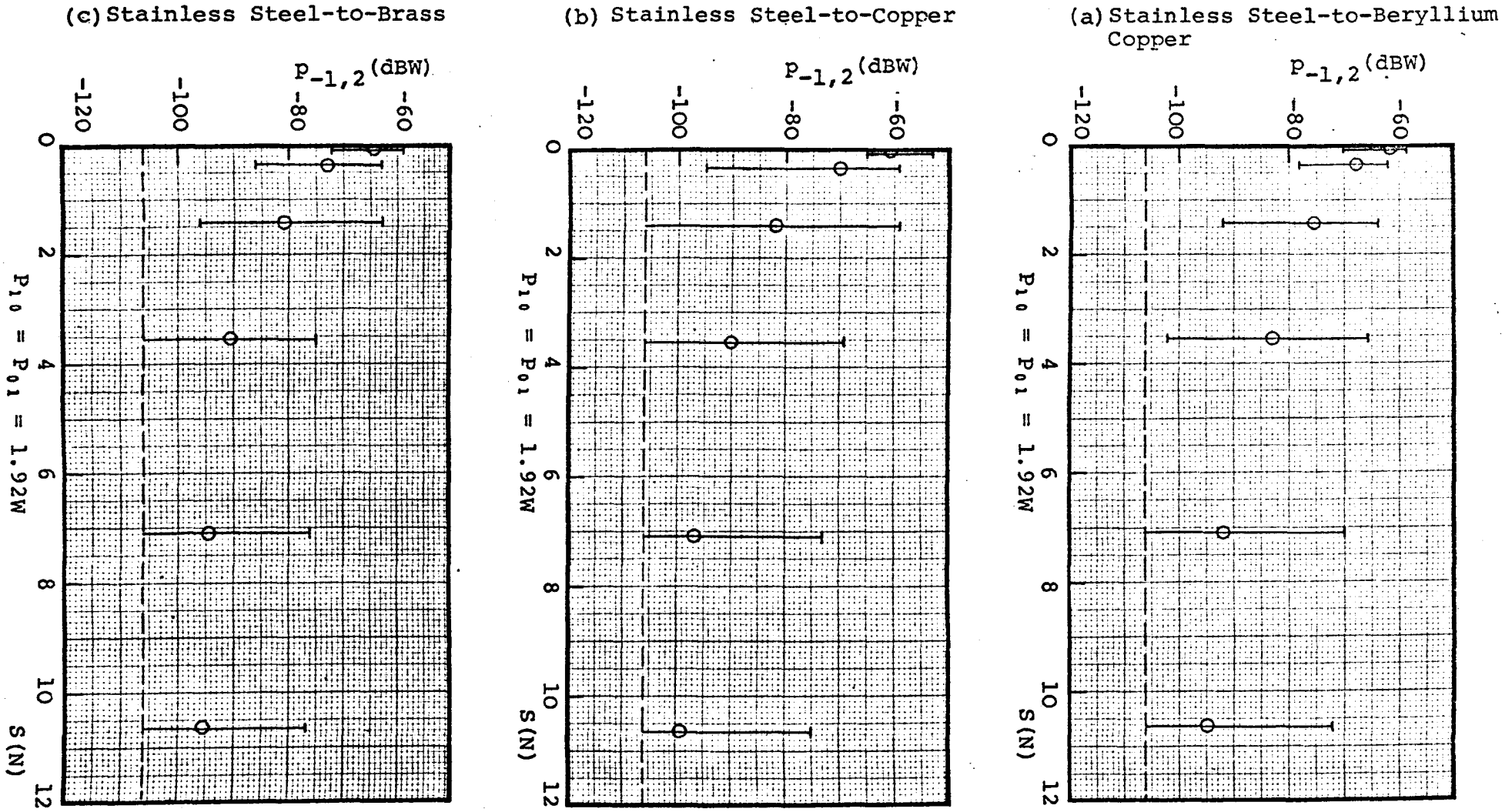

L-Band

Graph 6.31 Dissimilar Metal-to-Metal Contacts

Spread of results from 6 different sample pairs

o Average value

---- Residual level

(c) Duraluminium-to-Copper

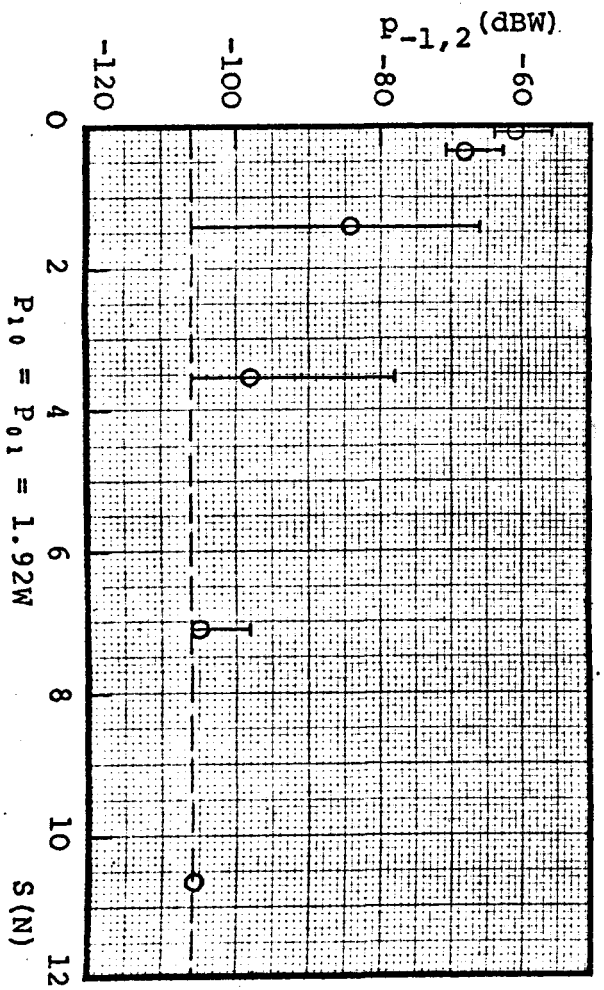

(b) Duraluminium-to-Beryllium copper

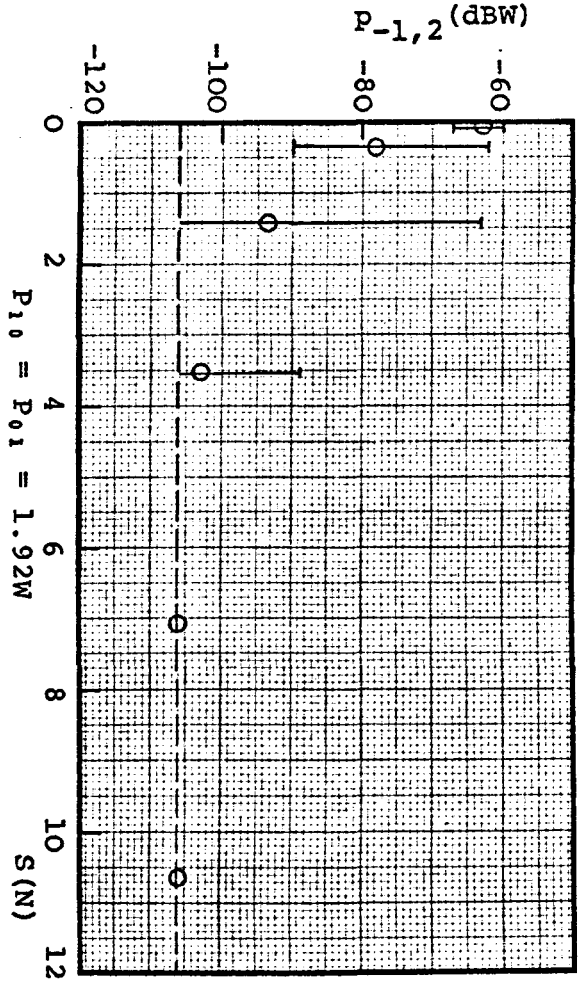

(a) Duraluminium-to-Oxygen free Nickel

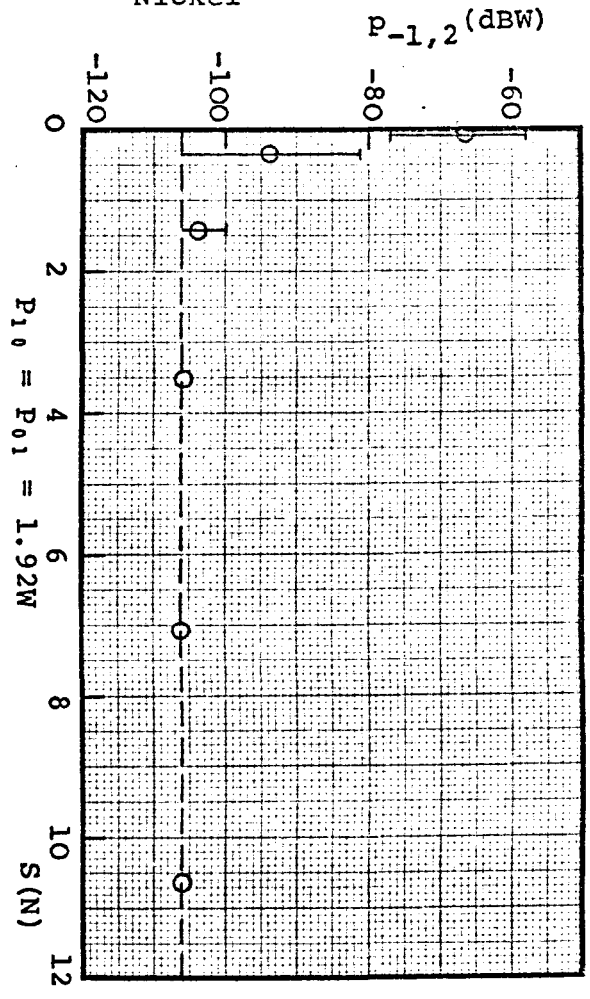

L-Band

Graph 6.32 Dissimilar Metal-to-Metal Contacts

⊢—⊣ Spread of results from 6 different sample pairs

O Average value

---- Residual level

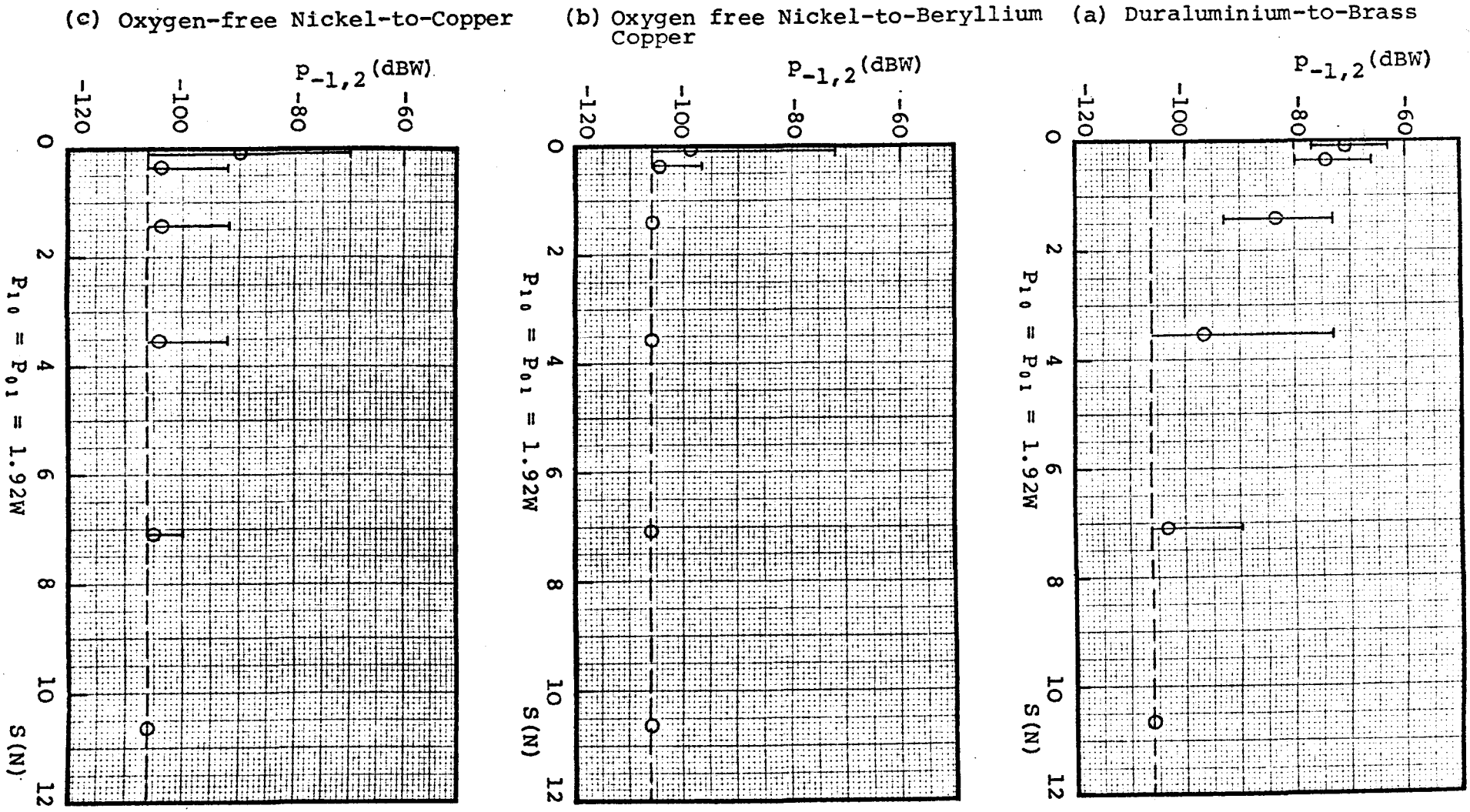

L-Band

Graph 6.33 Dissimilar Metal-to-Metal Contacts

|——| Spread of results from 6 different sample pairs

O Average value

---- Residual level

(c) Beryllium Copper-to-Copper

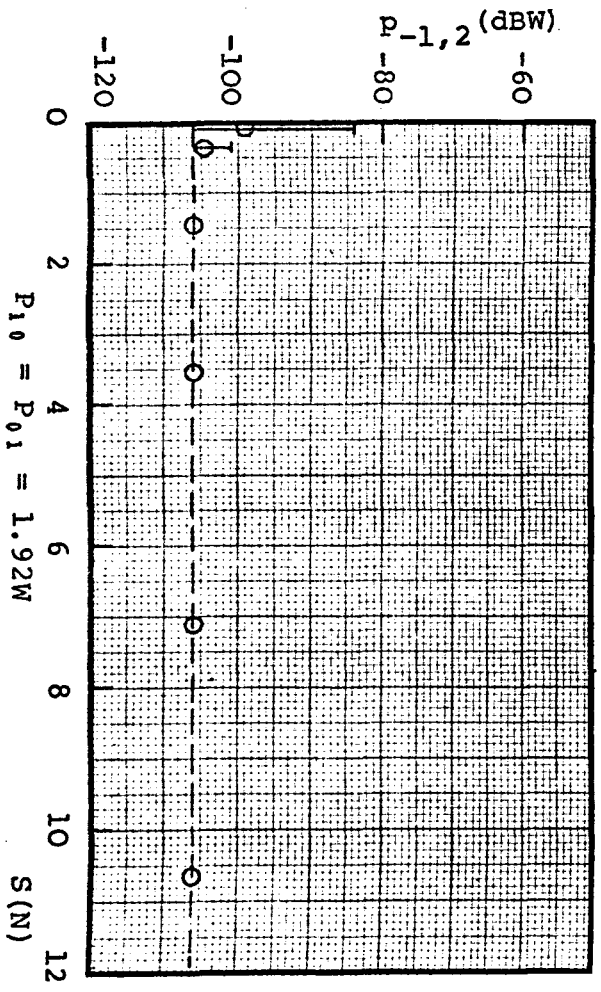

(b) Beryllium Copper-to-Brass

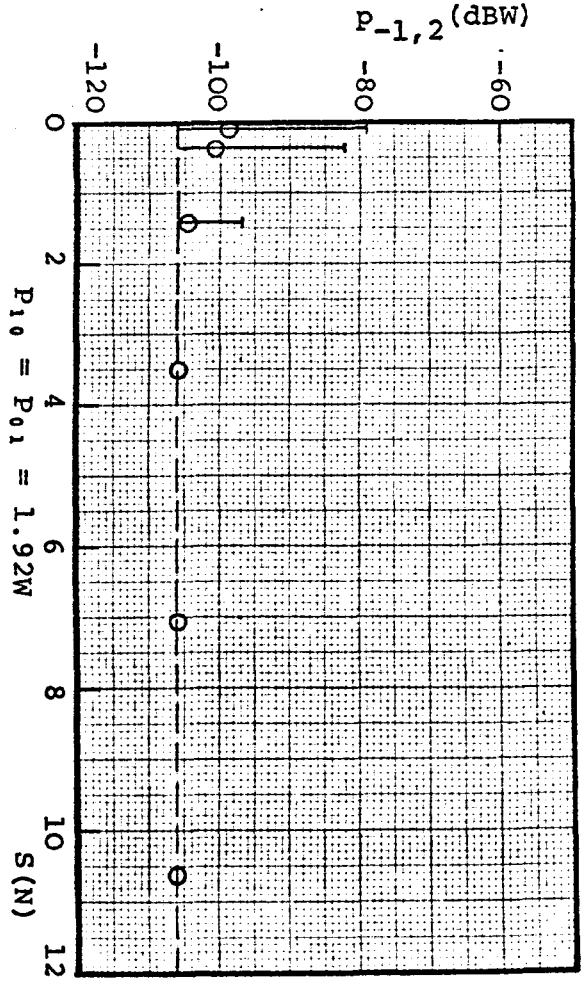

(a) Oxygen-free Nickel-to-Brass

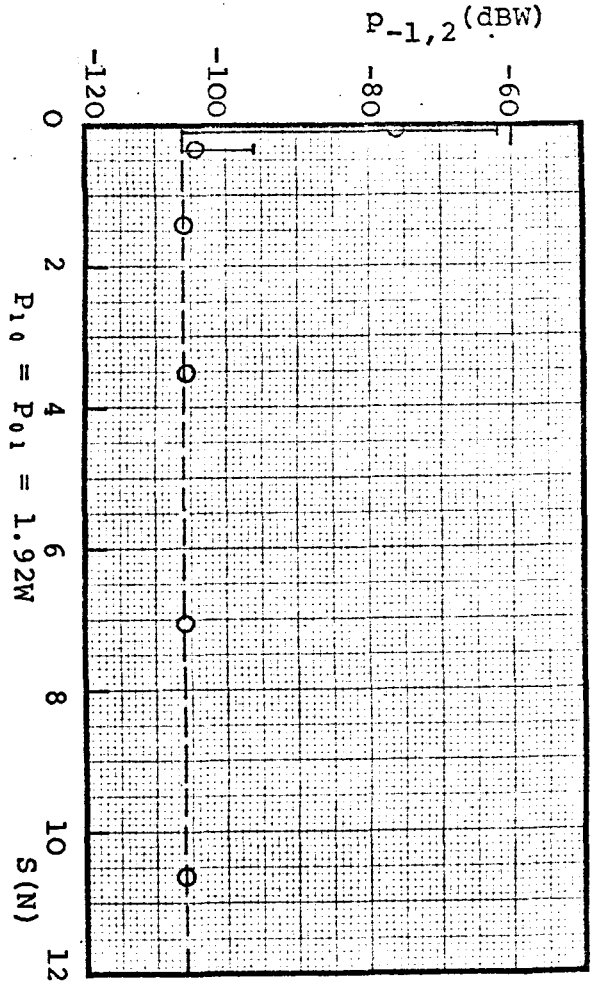

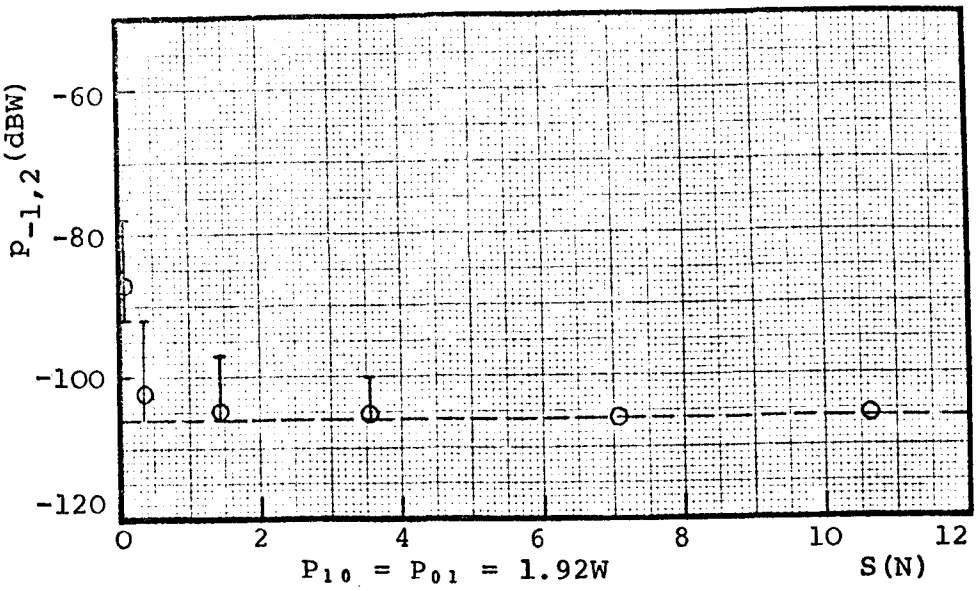

Graph 6.34 Copper-to-Brass

⟷ Spread of results from 6 different sample pairs

O Average value

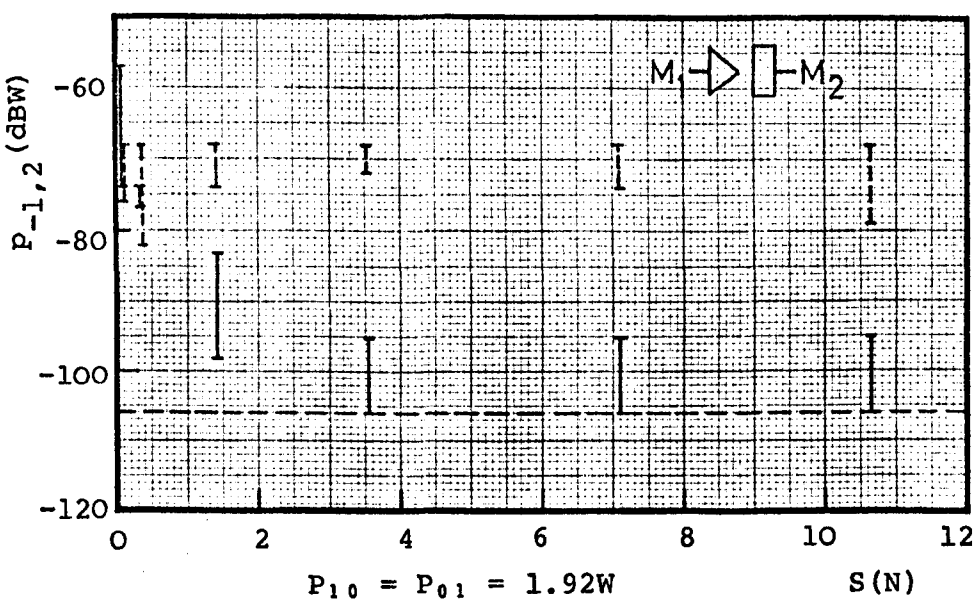

Graph 6.35

⟷ Spread of results from 3 different sample pairs
M_1 = Duraluminium M_2 = stainless steel

⟷ Spread of results from 3 different sample pairs
M_1 = stainless steel M_2 = Duraluminium

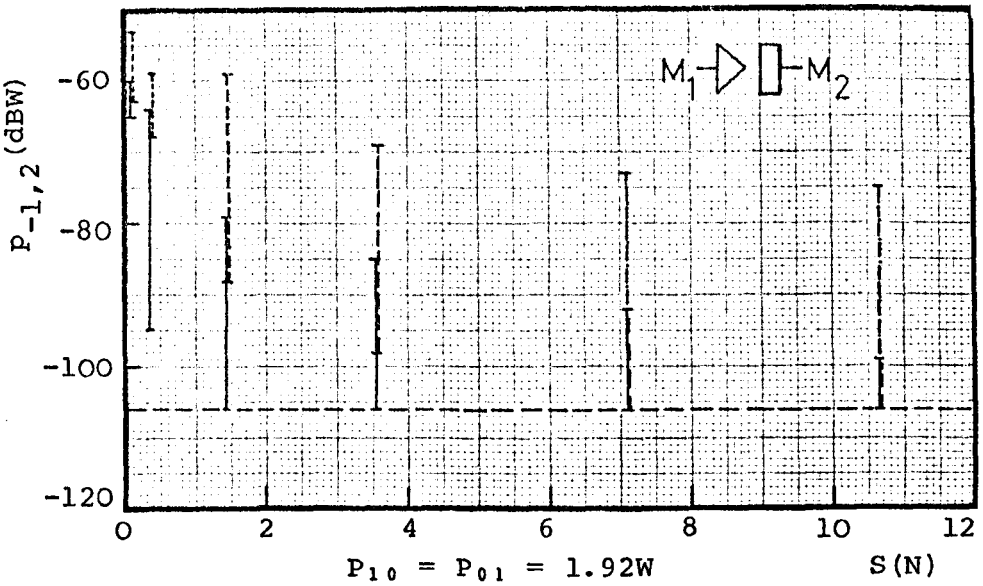

Graph 6.36

Spread of results from 3 different sample pairs
M_1 = copper M_2 = stainless steel

Spread of results from 3 different sample pairs
M_1 = stainless steel M_2 = copper

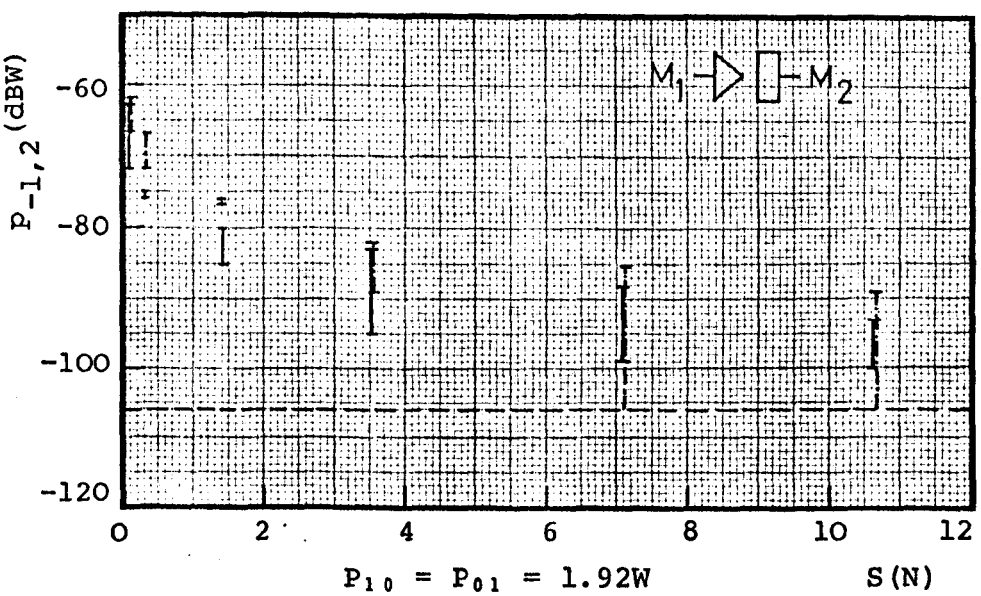

Graph 6.37

Spread of results from 3 different sample pairs
M_1 = mild steel M_2 = stainless steel

Spread of results from 3 different sample pairs
M_1 = stainless steel M_2 = mild steel

L-Band

Graph 6.38 Similar Corroded Steel-to-Steel

|——| Spread of results from 3 different sample pairs

O Average value

---- Residual level

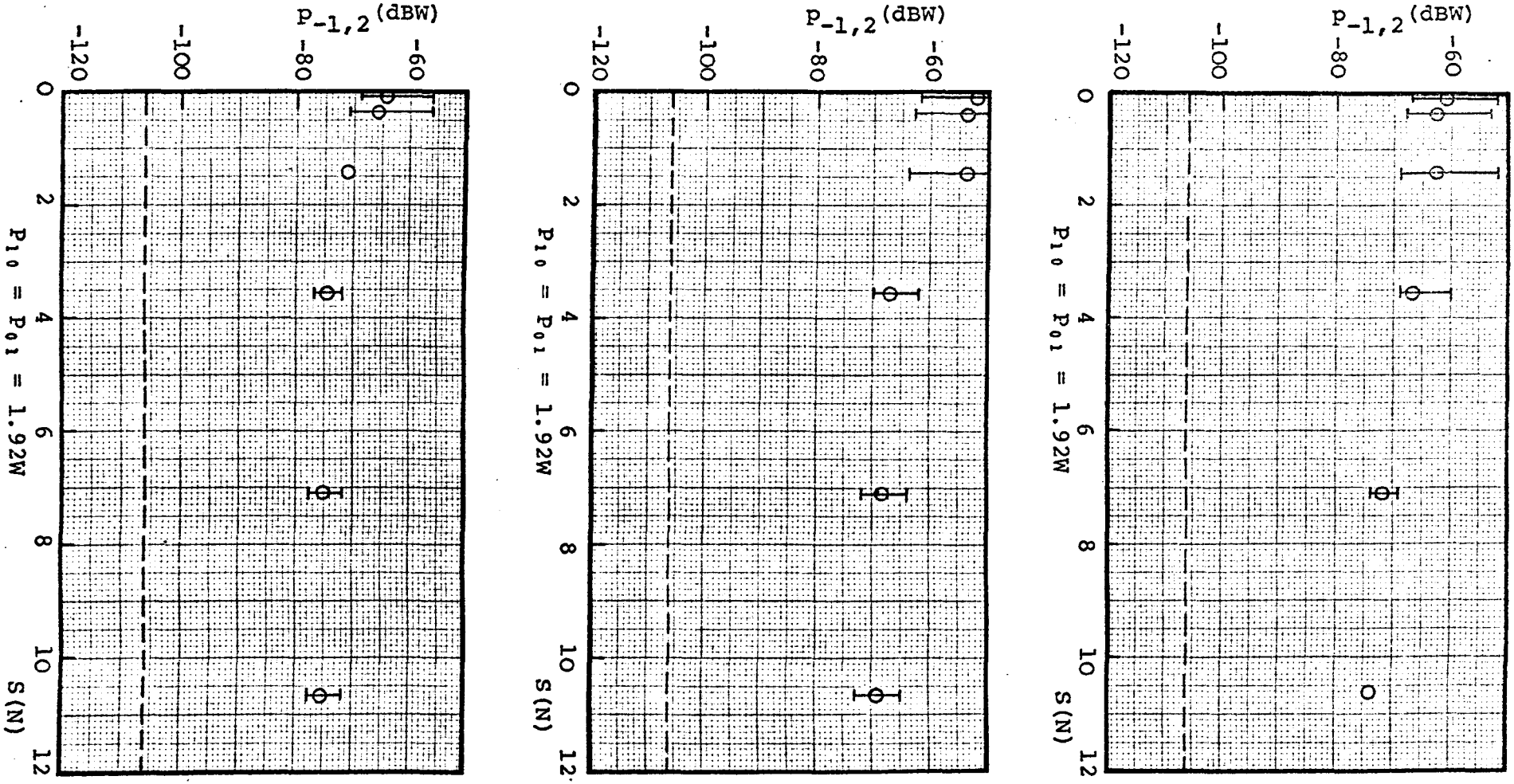

L-Band

Graph 6.39 Similar Corroded Steel-to-Steel

—I— Spread of results from 3 different sample pairs

O Average value

---- Residual level

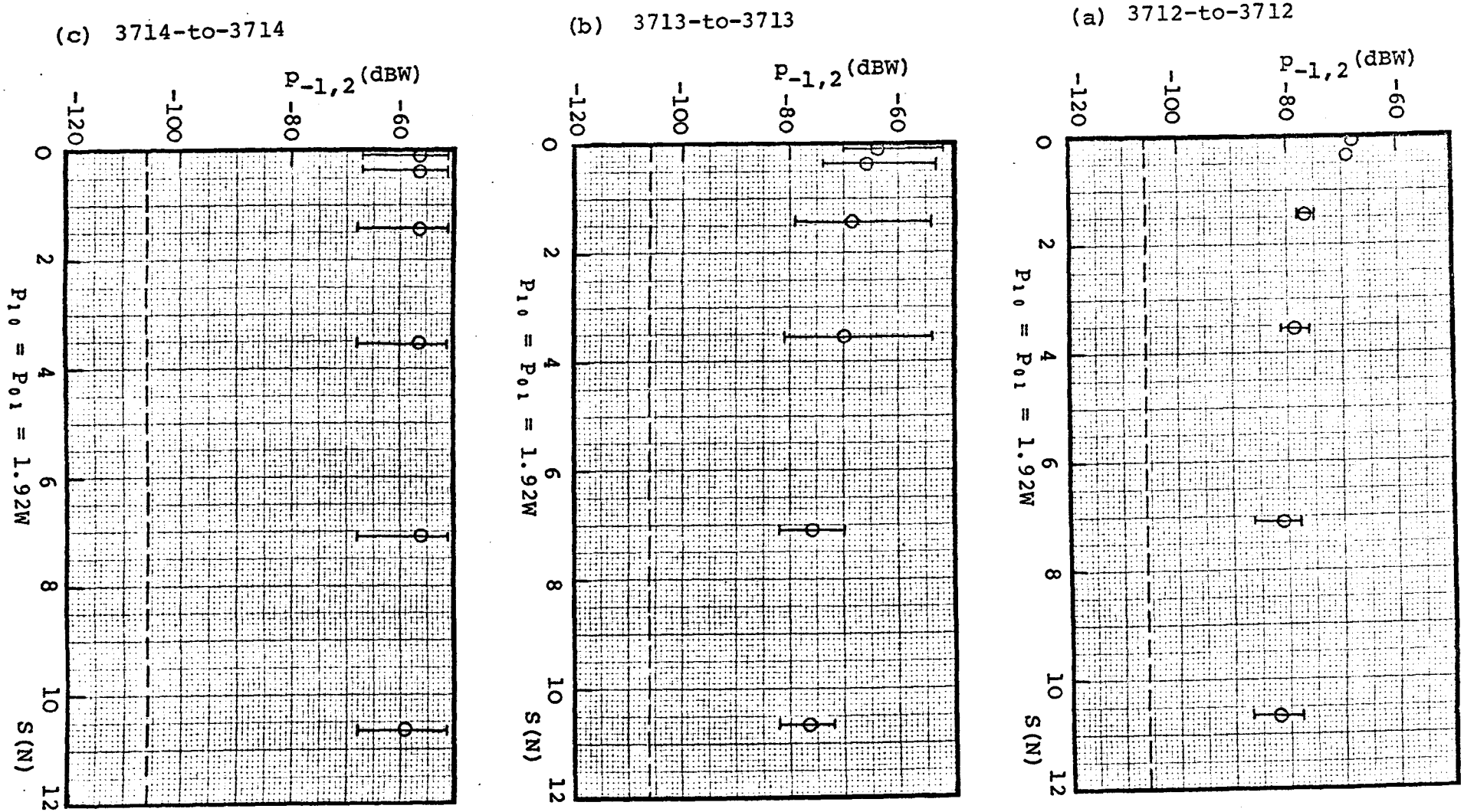

L-Band

Graph 6.40 Similar Corroded Steel-to-Steel

⊢—⊣ Spread of results from 3 different sample pairs

O Average value

---- Residual level

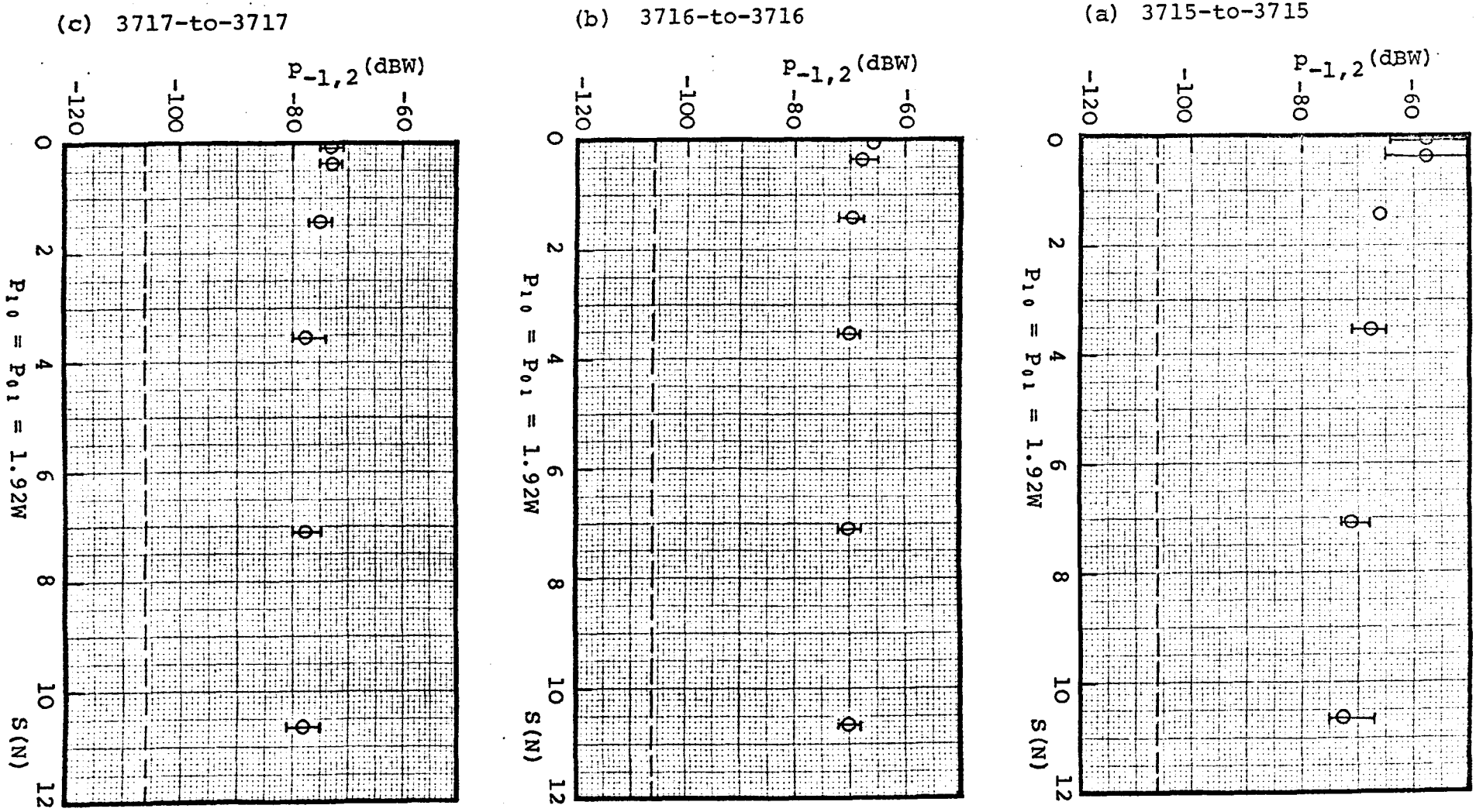

L-Band

Graph 6.41 Similar Corroded Steel-to-Steel

⊢——⊣ Spread of results from 3 different sample pairs

O Average value

---- Residual level

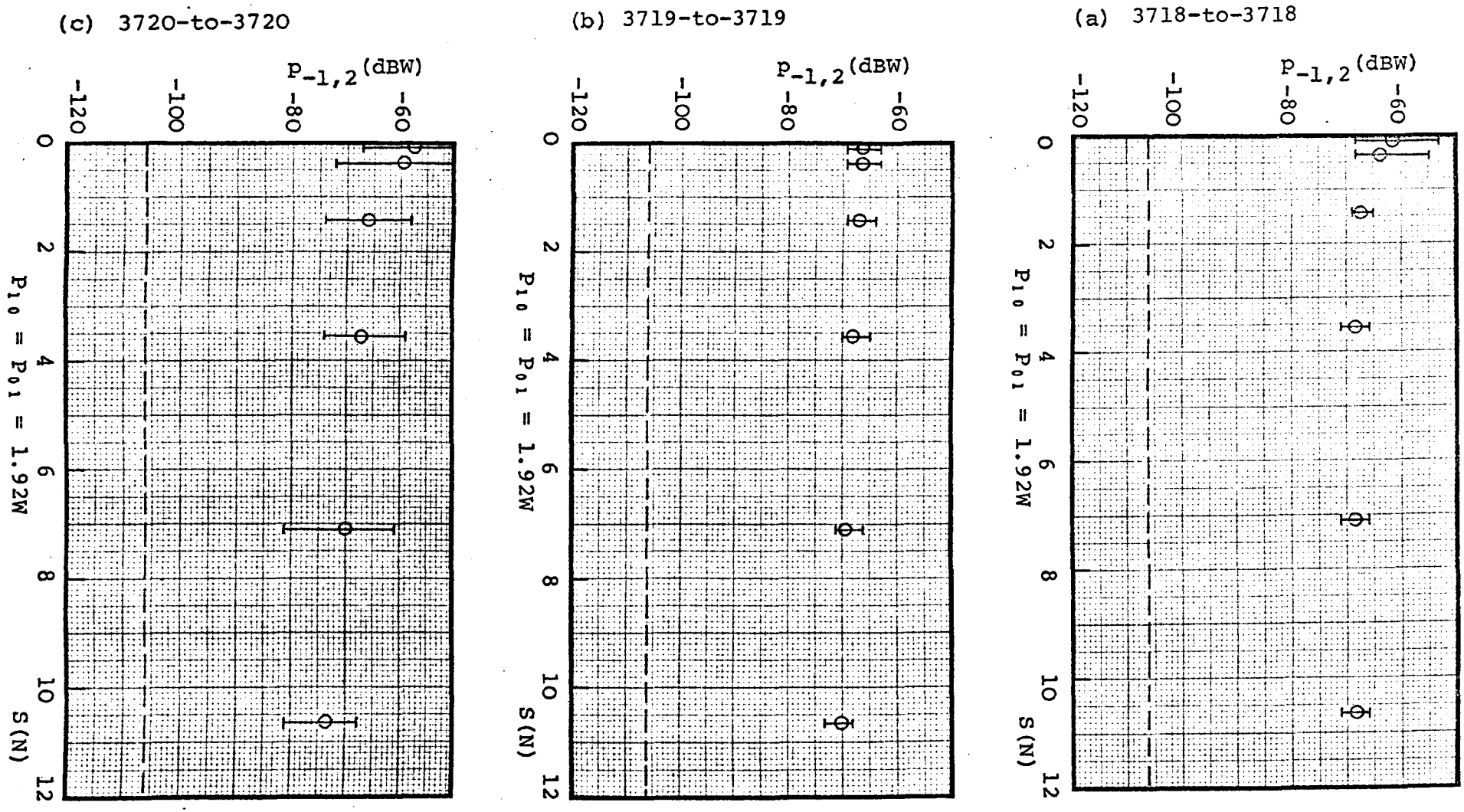

levels through the whole range of axial force or in other words the maximum available axial force was not sufficient for a complete mechanical breakdown. The differences between graphs are not considerable while most of the spreads overlap but it can be seen that the spread of results obtained from those sample pairs which contain Ni and Cr in their composition, especially, steels 3712, 3713 and 3717, are almost lower than those of other steels. This could be because of an anti-corrosion effect of these two compositions (i.e. Ni and Cr) which produces thinner oxide films allowing more electrons to tunnel through its barrier.

6.7 Effect of a Thin P.T.F.E. on the Contacting Metal Surfaces

The contacting surfaces of contact halves of several test sample pairs were sprayed with P.T.F.E. dielectric producing an insulator film on the surfaces less than 0.2mm thick. The 3rd-order I.P. levels with these sample pairs were equal to the residual level and also no 5th-order I.P. levels were detected. In spite of capacitive coupling between contact halves, there was no generation of I.P.'s at the contact surfaces or in other words if there is a capacitive coupling in an actual metal-to-metal contact, it is linear. It also can be concluded that if the oxide films on an actual metal-to-metal contact are thick enough then electrons cannot tunnel through them, and the contact is linear. By increasing axial force rupturing of the oxide films occurs producing a thinner oxide layer and therefore generating I.P. levels, but as the axial force builds up at the contact surface the perfect breakdown of oxide films may occur leading to a perfect metal-to-metal contact and therefore again 3rd-order I.P. levels drop down

into the residual level. This experiment would show that the non-linear resistance between metal-to-metal contact is responsible for I.P. generation.

6.8 Explanatory Measurement with Copper-to-Copper Contact

In previous sections, the relationship between 3rd-order I.P. level and the total incident power was measured with increasing and decreasing the incident power. The 3rd-order I.P. level increased with incident power and at some points it reached to a saturation curve or it decreased with increasing the incident power, however, its variation with decreasing incident power was not the same with increasing incident power.

Therefore it was reasonable to expect that some kind of deformation can happen by increasing incident power. The aim of this section is to examine how true this situation could be. For this purpose one pair of mechanically polished test samples made of copper were allowed to corrode inside the laboratory for about 50 days, then the 3rd-order I.P. level was measured with increasing and decreasing the total incident power in several mid-step sequences, i.e. each step of increase in incident power followed by several steps in decreasing the incident power at a constant axial force. Graph 6.42 shows the results obtained for corroded copper-to-copper contact. The arrows in this graph show the direction in which the measurement has been carried out. At $p_{in} = -16.2$dBW ($P_{in} = 0.025$W) the value of -65.5dBW was recorded for 3rd-order I.P. level at $p_{in} = -14.2$dBW, the decrease in incident power to initial value, does not produce a repeatable 3rd-order I.P. level of the original levels and so was the case for $p_{in} = -13.2$, -11.4, -9.2 and -1.4dBW. In the mid-range of incident power, i.e. from

p_{in} = -9.2dBW to -4.2dBW, the power sources were not stable, so no measurements were carried out in this range. An increase in the incident power from -1.4dBW to -0.2dBW resulted in a constant 3rd-order I.P. level but by decreasing the incident power from -0.2dBW to -1.4dBW caused an enormous change of about 25dBW in the 3rd-order I.P. level, bringing it down to -83dBW. At this point the 3rd-order I.P. level was almost repeatable in a range of incident power from -4.2dBW to 1.6dBW. This fact was confirmed after several increases and decreases in the incident power and then recording the 3rd-order I.P. level as is shown in Graph 6.42. The average slope in this case was about 2.5. But at p_{in} = -0.2dBW when the incident power increased to 0.8dBW another drop occurred in the 3rd-order I.P. level, bringing its level down to -88dBW at p_{in} = 0.8dBW from -82dBW at p_{in} = -0.2dBW. In this new situation again the 3rd-order I.P. was repeatable in the range of the maximum available incident power p_{in} = 5.8dBW down to p_{in} = -4.2dBW. At this stage the power sources were switched off without removing the test sample pairs and changing other conditions and 5 hours later the 3rd-order I.P. level was measured with increasing and decreasing the incident power, again a repeatable curve was obtained with a slope of about 2.7. In the same situation a direct current of about 30mA was passed through the contact and the 3rd-order I.P. level was measured. It was observed that no change in the I.P. level occurred. Again power sources and the dc source were switched off and 2 days later the 3rd-order I.P. level was measured with I_{dc} = 0 and no other change in the measuring condition. This time the 3rd-order I.P. level was repeatable with increasing and decreasing incident power with a slope of about 3. Finally, by

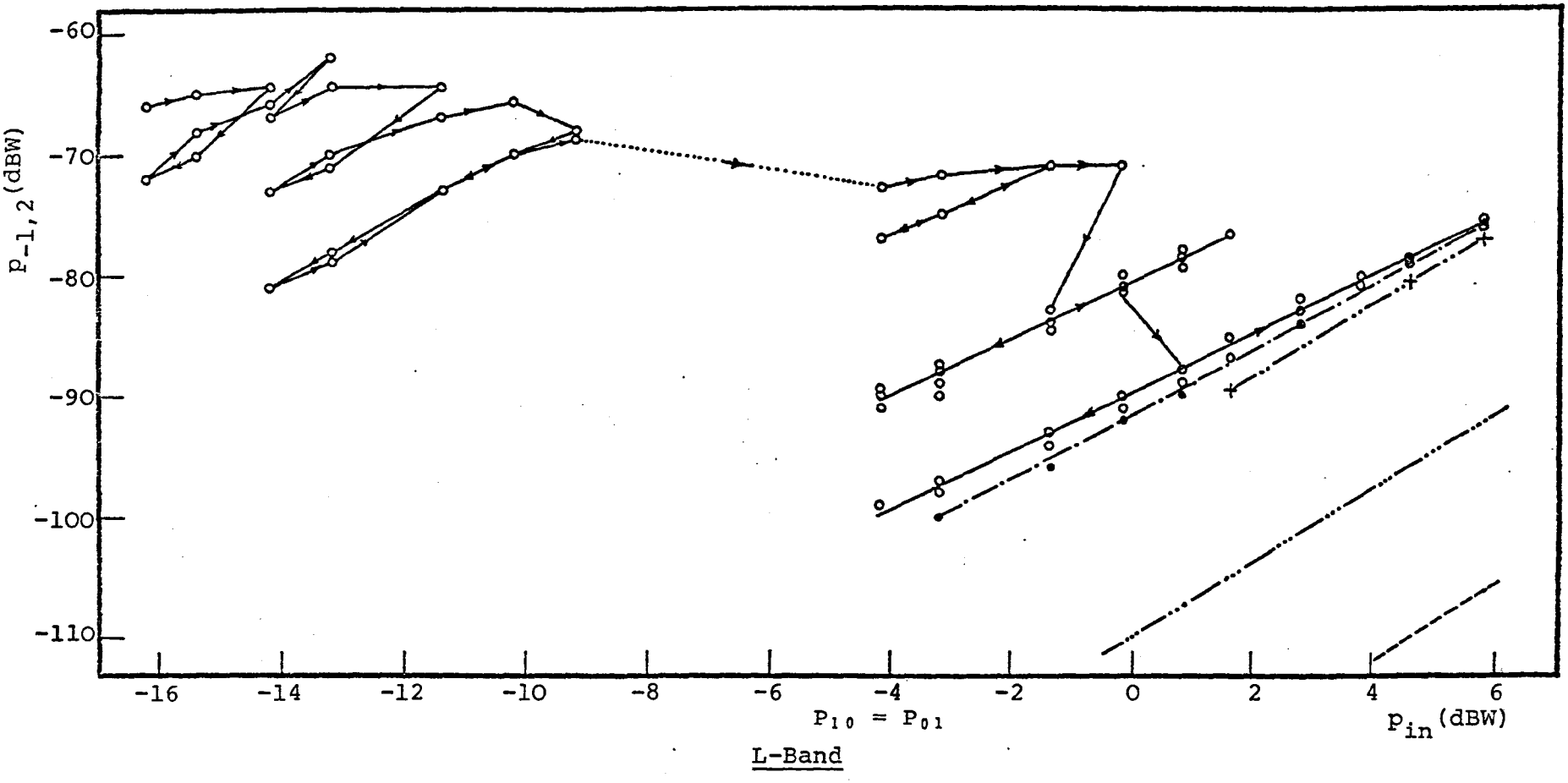

Graph 6.42 Similar to Copper-to-Copper Contact, Explanatory Measurement

- First Reading, S = 0.08N, $I_{d.c.}$ = 0.0
- Second Reading, 5 hours after First Reading, S = 0.08N, $I_{d.c.}$ = 0 and $I_{d.c.}$ = 30mA
- Third Reading, 2 days after First Reading, S = 0.08N, $I_{d.c.}$ = 0
- Fourth Reading, 2 days after First Reading, S = 3.55N, $I_{d.c.}$ = 0
- Residual Level

increasing the axial force to a constant value of 3.55N, the 3rd-order I.P. level was measured. It was observed that the 3rd-order I.P. level decreased with increasing the axial force to 3.55N and the slope of the 3rd-order I.P. level with the incident power was about 3. At a maximum available incident power and axial force the 3rd-order I.P. level was about -100dBW. At an axial force much higher than 12N, (it was not possible to specify the amount of axial force beyond the rating of bellows), the 3rd-order I.P. level dropped down into the residual level indicating a perfect metal-to-metal contact at that axial force.

CHAPTER 7

7. DISCUSSION OF RESULTS AND CONCLUSIONS

7.1 Introduction

The results presented in Chapter 6 showed that the surface properties of the contact surfaces of metal are the prime factors for high I.P. level generation. Therefore the explanation of results could well be followed by a general survey of corrosion of metal surfaces in open air.

There are two kinds of thin film : (i) physisorbed and (ii) chemisorbed.

(i) When a clean surface of a metal is exposed to air, oxygen deposits on it as physically adsorbed molecules which are bound to the metal surface by relatively feeble, so called Van Der Walls force of the order of 0.05eV. They are easily rubbed away when contact is made at room temperature.

(ii) Chemisorbed atoms are bound to valences of the metal surface atoms by covalent bonds. These atoms may be ionically bound with a bonding strength of about 1 to 8eV. Chemisorbed films endure some friction and elevated temperature without being removed from the metal surface. However, they are not thicker than about 10Å and therefore easily penetrated by means of the tunnel effect (see Section 3.1).

The physisorbed and chemisorbed films can be categorized as microfilms, as they are one or a few atoms thick. With respect to the thickness there is another type of film,

protective or passivating films which stop growing at a small thickness, for example, the films that make stainless steel resistant against chemical attack. The third type of film is a tarnish film. Such films are visible and continue to grow. In many cases the affinity between the metal and oxygen is strong enough to loosen metal atoms or ions from the solid metal and group them together with the oxygen in an oxide lattice. This is the beginning of tarnishing. With respect to the composition, a pre-tarnish film can be distinguished which can develop to tarnish and a chemisorbed film can be categorized with this type of film as well. The fourth type of film is an alien film such as a water film.

7.2 Variation of I.P. Levels with Axial Force

All the metals tested, with a clean surface or with an oxide layer on it, in similar or dissimilar metal-to-metal contact, without exception produce the highest and an erratic I.P. level at zero axial force. In spite of observing this fact, the I.P. levels at zero axial force were not recorded because of the contact being unstable at this force. If the metal surfaces are free of oxide film, the non-linear constriction resistance should be responsible for I.P. generation, then by expanding equation (3.5-8) in a series, according to equation (3.6-22) at $T_o = 293K$ with $L = 2.4 \times 10^{-8} (\frac{V}{K})^2$ (see eqn. (3.5-7)) it is easy to obtain :

$$p_{-1,2} = 3p_{in} + 40 \log \frac{\rho}{2a} - 4.32 \quad (dBW)$$

$$p_{-2,3} = 5p_{in} + 80 \log \frac{\rho}{2a} - 2.64 \quad (dBW) \qquad (7.2\text{-}1)$$

where a is the radius of the actual contact area of a single spot. At zero axial force a is very small therefore I.P.

levels become very high, of course a practical limit is $P_{I.P.} < P_{in}$.

In general, a curve of the I.P. level vs axial force displays three distinct regions. Firstly, the lower axial force range where the I.P. level is affected very little if at all by variation in axial force. Secondly, a "breakdown region" where a sharp decrease in the I.P. level is observed. Finally, in the higher axial force range, the I.P. level flattens out. The range of these three regions differs from metal to metal.

7.2.1 Similar metal-to-metal conctact

(a) GOLD: Gold does not oxidize in air. It is attacked by chlorine at 180°C forming a water-soluble $AuCl_3$ [26]. A chemisorbed monolayer of oxygen is deposited on gold in air as on every metal but does not grow beyond this layer. Such a layer is well penetrable for tunnelling electrons generating very low I.P. levels and thus is harmless in contact.

(b) SILVER: Silver oxidizes at room temperature only in the presence of ozone forming Ag_2O. This oxide is soft, easily removed mechanically and decomposes at 200°C [26]. In a normal atmosphere silver obtains a dark, resistive film of Ag_2S. The Ag_2S layer on silver is not a protective film. It grows slowly because the concentration of the attacking gas usually is small. A concentration of H_2S in the ratio of $1/10^9$ in the air is considered to be harmelss for contacts. Of course, contamination of the atmosphere by industrial activity considerably enhances tarnishing of silver. Dry H_2S does not attack silver, but H_2S or SO_2 does. The resistivity of Ag_2S at room temperature lies between 10^5 and $10^{10}\Omega$-m. This is the resistivity range of copper oxide. Visible films with such resistivity are

practically insulating if they cover the contact points. The Ag_2S is softer than the bulk material which is unlike almost all known tarnish products. Its hardness is about $1.5 \times 10^8 N/m^2$ which is almost half that of pure silver. When silver is gold-plated, the plating must be poreless, otherwise the Ag_2S can creep over the gold surface. No such creepage appears on rhodium and palladium. The number of chemisorbed atomic layers of oxygen on the initially clean metallic surface of silver after 1 to 2 minutes exposure to the air is about 0.3 (fractional layer does not cover the total conducting area). The growth of the oxide beyond this thickness is very slow. Because the Ag_2O is soft, thin and easily mechanically removed, the generation of the I.P. levels above the axial force of 0.08N dropped down into the residual level.

(c) COPPER: Cu_2O formed on copper. The thickness of the first oxide film that is develped in air in about 30 minutes is about $25\mathring{A}$[26]. The number of chemisorbed atomic layers of oxygen after exposure to air in about 2 days could be something between 2 to 10. The oxide layer beyond this thickness grows very slowly. This thin film is well penetrable for tunnelling effect and can be ruptured easily by applying very small axial force. The test results obtained from clean copper-to-copper contacts (Graph 6.22) show that this value is less than 0.08N. The cuprous oxide (Cu_2O) is a p-type semiconductor with an electrical conductivity between $10^{-6} \sim 10^{-7} mho/m$[34]. It is believed that another type of corrosive oxide, CuO, having a very poor conductivity of about $1 - 0.1 mho/m$[34] at room temperature could not be developed on the test sample surface below $400^{\circ}C$. Electrically clean test sample pairs made of

copper produce low I.P. levels at an axial force higher than 0.08N. The oxides on the copper do not really stop growing but grow slowly and therefore serve to some extent as a protective film. The forbidden band of Cu_2O is about 3eV (i.e. a barrier height of 1.5eV). When the copper is corroded, it has properties similar to its oxide[35] so that by increasing the axial force there are the combined effects of penetrating the oxide film and of deforming the metal beneath the oxide. Therefore the oxide layer will deform with the metal under an applied axial force until the heavy load is used for a perfect metal-to-metal contact. The contact hardness of copper is about 4×10^8 to $7 \times 10^8 N/m^2$. The axial force necessary for the breakdown depends on the mechanical property of the underlying metal of the test sample pairs (see Section 7.4). For mechanically polished corroded copper the maximum available axial force was not sufficient for breakdown of the oxide layers (see Graph 6.25). The rsults obtained from oxygen free copper were similar to those of copper when it was mechanically or electrically polished.

(d) NICKEL: The oxide on nickel, NiO, is to some extent a protective film because it does not really stop growing but grows slowly. The initial film of a few atom layers (2 atom layers after 2 hours) is considerably protective in a dry atmosphere[26]. The oxidation is much more rapid in a humid atmosphere. Hygroscopic dust on nickel in a humid atmosphere may promote electrolytic attack by means of local cells. Nickel with its protective oxide film is attacked very little by H_2S. NiO formed on the nickel even after 2 days is so thin and penetrable for tunnelling electrons generating low I.P. levels but it is as strong as the nickel (contact hardness of

nickel is about 7×10^8 to $20 \times 10^8 N/m^2$). Therefore after several weeks, it scarcely ruptures when contact is made in spite of its slow growth and causes a high level of I.P. generation. The statistical measurement on electrically clean nickel-to-nickel showed that at an axial force, the 3rd-order I.P. level dropped down into the residual level but mechanically polished nickel-to-nickel (Graph 6.4b) showed that even maximum available axial force is not sufficient for a mechanical breakdown indicating that the mechanical polishing of the old test sample pairs of nickel has not perfectly ruptured the NiO film. NiO is a p-type conductor[36]. Addition of nickel to steels, increased the resistance of steels against corrosion by producing a thin layer of oxide. Addition of chromium to steels has a similar effect to that of nickel. The statistical measurement on similar corroded steel-to-steel showed that, in general, the steels with Ni and Cr content produce lower I.P. levels (see Graphs 6.39a, 6.39b and 6.40c). Cr_2O_3 is also a p-type conductor. If the oxide film on steel is controlled by the Ni and Cr content in the steel (i.e. NiO-Cr_2O_3 mixed oxide layer) while both NiO and Cr_2O_3 are p-type conductors, the addition of a higher-valent oxide Cr_2O_3 to a lower-valent oxide NiO decreases the conductivity of the NiO-Cr_2O_3 mixed oxide[36]. Increasing the electric resistivity of an oxide layer on the surface of the samples by increasing the Cr_2O_3 content means an increase in the absorbed power and consequently an increase in the I.P. levels. By comparing the results obtained from the statistical measurements of a similar corroded metal-to-metal of 3712 and 3711 with a Cr to Ni content ratio of 0.44 and 0.92 respectively (see Table 5.1) to

some extent showed this fact (see Graphs 6.38c and 6.39a).

(c) ALUMINIUM: Al_2O_3 formed on aluminium is of an n-type conductor. This oxide film stops growing at a thickness of about 60Å at room temperature[26]. Cessation of the growth of a tarnish film means that the film protects the metal against further attack by oxygen. The protection usually is far reaching. Alumina film is very resistant against chemical action and it is also mechanically strong while aluminium itself is soft and highly reactive. The initial thickness of the film of about 20Å is attained in a few seconds, and very quickly, even at room temperature the thickness becomes too great for conduction by the tunnel effect. The alumina film is practically insulating and the aluminium electric contacts can be used only when the film is ruptured. If the oxide is hard and brittle and the underlying metal soft and ductile, then the oxide will fracture easily and the metallic contact will occur at the lightest axial load. This is the case with tin and to a lesser extent with aluminium. The results obtained by Bayrak with a similar tin-to-tin at S-band (13 - Section 5.1.1.6) showed that at the range of an axial force greater than 0.08N, the 3rd-order I.P. level dropped down into the residual level. The oxide film on the aluminium remains intact but as the axial force is increased a crack pattern is produced with cracks at an angle of about 45° to the track. As the axial force is further increased the cracks spread to the centre of the track and finally the oxide is penetrated and disrupted at an axial force of 21N[35]. The results obtained for mechanically polished duraluminium-to-duraluminium (Graph 6.3) showed that the maximum available axial force

(10.65N) was not sufficient for a perfect metallic contact. Statistical measurements showed that only one sample out of five samples produce a metallic contact at S = 7N (Graph 6.28c).

(f) BRASS: On brass chemisorbed layers begin to develop similar to those on copper. The number of chemisorbed atomic layers on the initially clean brass surface after exposure to air about 1 to 2 minutes, is something between 1 to 4[26]. But the rate of growth continues unchanged and does not slow down as on copper. The statistical measurements on similar fresh brass-to-brass showed the 3rd-order I.P. level was not detectable at an axial force greater than 0.08N. However Graph 6.5b shows that the mechanical breakdown has occurred at an axial force of about 4N. This is probably because the brass sample pairs had not been properly mechanically polished so there were still some oxide films on them. This could happen since a proper mechanical polishing on the spherical half of the test sample pairs was not easy if no geometrical change of sample was desired. It should be also mentioned that zinc which is as soft as gold is covered by a protective film which usually insulates in contacts. This metal has no ultimate rigidity but steadily creeps under the force, and the load bearing spots become larger with the consequence that the pressure diminishes on the initial metallic spots. Tarnishing of zinc can be accelerated by raising the temperature at the contact spot. ZnO is an n-type conductor.

(g) BERYLLIUM COPPER: The results obtained from similar fresh beryllium copper-to-beryllium copper and also statistical measurements showed that as far as the I.P.'s are concerned,

beryllium copper behaved similar to copper and brass. An increase in axial force i.e. S > 0.08N produced a perfect metallic contact.

(h) MILD STEEL AND STAINLESS STEEL: Stainless steel has a very effective protective film. When the stainless steel and mild steel have similar properties to their oxides, then the oxides will deform with the metal under the applied axial force until heavy loads are used. Graphs 6.1b and 6.2b obtained from similar metal-to-metal contact of stainless steel and mild steel respectively show that even at the maximum available axial force a perfect metallic contact could not be established. Protective film on the stainless steel increases the resistance of the metal against further attack by oxygen and usually against various other chemicals, therefore it is expected that the thickness of the oxide film on stainless steel is thinner than that on mild steel with the consequence that the I.P. levels generated at mild steel-to-mild steel be higher than those at stainless steel-to-stainless steel. This was the case at an axial force less than 10N for mechanically polished test sample pairs made of these two steels. Statistical measurements also showed that in spite of overlapping the spread of the 3rd-order I.P. levels obtained from these two steels over a whole range of axial force, the spread of results from mild steel occupied higher ranges of I.P. levels than those obtained from stainless steel (Graphs 6.28a and 6.28b).

(i) HOME MADE STEELS: In the last column of Table 5.1 the old cast numbers of home-made steels are mentioned which correspond to the cast numbers of steels used in the

literature[12]. The initial aim was to compare the I.P. levels generated at similar steel-to-steel contacts at L-band with those obtained by the University of Southampton at lower frequencies. It was concluded that with respect to the composition of steels there is no similarity in the results, therefore comparison looks meaningless. The reason is quite obvious, because they deal with the bulk material itself and non-linear B-H characteristic causing I.P. generation while in metal-to-metal contact the surface property and non-linear I-V characteristic of contacts have responsibility for the generation of I.P.'s. For a meaningful comparison two single pieces (see Fig.4.1) made of nickel and mild steel were put at the test sample location in the coaxial measuring device (see Figs.2.5, 2.6 and 2.7) and the 3rd-order I.P. levels were measured. It was observed that the 3rd-order I.P. level lies on the residual level of about -125dBW at a maximum incident power ($P_{10} = P_{01} = 1.92W$) for both these magnetic materials. Therefore the non-linear B-H characteristic of the test sample pairs, had no effect on the results. All the similar steel-to-steel contacts produce more or less similar and high I.P. levels (Graphs 6.6 to 6.17b) so that a reasonable comparison between results and drawing some conclusion was difficult. The presence of different oxides and various individual behaviour of each oxide on the surface of each steel make this comparison very complicated.

7.2.2 Dissimilar metal-to-metal contact

For the statistical results obtained from dissimilar metal-to-metal contact surfaces of seven bas materials, shown

in Graphs 6.29 to 6.34, the behaviour is straightforward. It is mentioned in Section 7.2.1(h) that if the metal has similar properties to its oxides, as is the case for stainless steel and mild steel and corroded-copper and nickel, then by increasing the axial force the oxide will deform with the metal under the applied load until the heavy loads are used for a perfect metal-to-metal contact with the consequence of decreasing the I.P. levels. If the oxide is hard and brittle and the underlying metal soft and ductile, as is the case with tin and to a lesser extent with duraluminium (as mentioned in Section 7.2.1(e)), then the oxide will fracture easily and metallic contact should occur at the lightest axial force. Statistical measurements on similar mechanically polished fresh metal-to-metal (Section 6.6.1) indicate thatmild steel, duraluminium and stainless steel produced high I.P. levels over the whole range of axial force (Graph 6.28) while copper, beryllium copper, nickel and brass produce low I.P. levels. It has been reported[13] that :

(i) Any combination of dissimilar metal-to-metal contact of the first group (copper, beryllium copper, nickel and brass) produce low I.P. levels. This was found to be true in so far as the metallic surfaces are almost free of oxides (Graphs 6.32b, 6.32c, 6.33 and 6.34).

(ii) Any combination of dissimilar metal-to-metal contact surface of the second group (mild steel, duraluminium and stainless steel) produce high I.P. levels.

(iii) A combination of the first group to the second group of metals produce, high or intermediate I.P. levels over the whole range of axial force.

The conditions of (ii) and (iii) were found to be dependent on the geometrical configuration of the contact halves and their mechanical properties. If the spherical half is soft and flat half hard the experiments indicate that (see Graph 6.35 for contact halves made of stainless steel and duraluminium) the oxide film on soft material will be cracked or penetrated readily whereas the oxide on a flat surface will often remain intact, i.e. it is expected that the oxide film on the spherical contact breaks down at earlier stages. On the other hand if the spherical half is hard and the flat one soft, the hard metal tends to break down the oxide film on the soft surface but there is no reliable means of assessing what will happen to the oxide on the harder metal. Mild steel-to-stainless steel contacts produce high I.P. levels (Graphs 6.29a and 6.37) because they both have almost similar properties. Stainless steel-to-oxygen free nickel (Graph 6.29c) and duraluminium-to-oxygen free nickel, -beryllium copper, -copper, and -brass produce intermediate I.P. levels (Graphs 6.31 and 6.32a respectively), i.e. metallic contact occurs at a lower range of the axial force (less than 8N in general). Stainless steel-to-duraluminium, -beryllium copper, -copper and -brass produce high and slighly lower I.P. levels (Graphs 6.29b, 6.30, 6.35 and 6.36) depending on whether the spherical half is made of stainless steel or the other four metals respectively.

7.3 Variation of I.P. Levels with Incident Power

Experimental data represented in Chapter 6 indicates that before a perfect metallic contact between two halves of the test sample pairs, the electrical property such as the dielectric constant of oxide, the width of the forbidden gap, etc. is of prime importance for the generation of I.P.'s. Therefore as it has been mentioned in Section 3.9 the non-linear I-V characteristic which is not a simple exponential curve (see also eqn.(3.2-1)) is responsible for the I.P.'s. It has been reported[24] for an insulator thickness of less than 40Å the tunnel effect is predominant while for a thicker insulator film, thermionic effect and space charge effect will affect the non-linearity. It is also reasonable to expect that for a thicker oxide layer, its non-linear semiconducting property should be taken into account. Variation of the 3rd-order I.P. level with the incident power for similar metal-to-metal contacts (Graphs 6.1 to 6.17) at an axial force of 0.08N indicate that there is some kind of electrical deformation in contact by increasing the incident power. It can possibly be explained by raising the temperature at the contact in consequence of increasing the current at the contact and therefore a change in the surface property of the contact surfaces. This was not the case with mild steel (Graph 6.2a) indicating that the maximum available incident power ($P_{10} = P_{01} = 1.92W$) was not sufficient for this kind of deformation on the surface of this sample. Variation of the 3rd- and 5th-order I.P. level with decreasing the incident power at an axial force of 0.08N and 3.55N (5.68N for a few samples which are indicated at the bottom of each graph)

allowing for experimental errors, were linear. The slope of the 3rd-order I.P. levels vary, except for mild steel, from approximately 2.2 to 4.6 at S = 0.08N. But the slope of the 3rd-order I.P. level, including mild steel, vary between 2.4 to 3.2 at S = 3.55N (or 5.68N). This may indicate that for a better contact situation the slope tends to be about 3. Similarly, for the 5th-order I.P. corresponding values of the slope vary from about 1.5 to 6. The average slope of the 3rd-order I.P. levels for the steel-to-steel contact was 2.5.

A comparison of the sequential readings between the 3rd- and 5th-order I.P's recorded under the same set conditions, shows that the 3rd-order I.P. level is always greater than the corresponding 5th-order I.P. level over the whole range of the incident power.

As far as the I.P. generation at the contacts are concerned, because of their short length (10mm) compared with the length of the rest of the transmission line, the non-linear I-V characteristic is more important than the resistance at the contact. In other words if the I-V characteristic is linear, no matter what slope it has got, there is no generation of the I.P.'s.

It has been reported[37,p.213] that corrosion can be introduced by soldering which arises from hygroscopic residues from the flux, particularly chlorides. These, in turn, may introduce a non-linear effect causing I.P.'s at the soldered junctions. Therefore a single piece made of three discs with a thickness of 2mm and a diameter of 10.5mm was soldered together and then finally soldered to two flat half samples making a rigid single piece (see Fig.4.1) was tested. This

specimen was made and tested by Bayrak[13] about five years ago at S-band. Neither when it was fresh at S-band nor when it was five years old at L-band was this effect observed. This could possibly be because of good soldering. However it may be serious enough in the case of cable-connector assemblies, where less care may be involved.

By increasing current through the contact point (increasing the incident power), the temperature at the contact point which is higher than that of the bulk material will increase. It is known that chemical reactions are strongly dependent on temperature, which effectively controls the rate of oxidation on the metal contact. Formation of oxide layers around the contact point on one hand may increase the area of contact for the tunnelling current and on the other hand may decrease the area of contact by forcing the test sample pairs apart. In spite of some observable electrical deformation occurring at the contact point with increasing incident power, the above mentioned phenomena could be responsible for changeable behaviour of the contacts. The electrical deformation also could possibly be explained by raising the temperature at the contact point and therefore softening the oxide film, or in other words increasing the load area bearing with the result of the decreasing I.P. levels. If this is the case it is expected to have an electrical breakdown followed by the electrical deformation at a very high incident power instead of a maximum available incident power of 3.84W on the samples.

7.4 Effect of Electropolished Contact Surface

Both similar metal-to-metal contacts of the test sample pairs made of copper and oxygen free copper with mechanically polished and electrically polished surfaces produce very low I.P. levels at an axial force greater than 0.08N indicating electrical cleanliness is more important than surface roughness.

Contact resistance (constriction resistance) between a palladium surface and a silver surface with Ag_2S tarnish of a thickness of 1400Å against load has been measured by Hisakado[33]. He has reported that "during plastic deformation of the contact asperities with the film the broken area of the film on a rough surface may be greater than that for the smooth surface". His measurements show that constriction resistance with increasing surface roughness has decreased.

Comparing the 3rd- and 5th-order I.P. levels with decreasing incident power at a constant axial force of 0.08N obtained from similar electropolished metal-to-metal contacts of stainless steel, mild steel, duraluminium and oxygen free nickel (Graphs 6.18a, 6.19a, 6.20a and 6.21a) with those obtained from corresponding mechanically polished ones (Graphs 6.1a, 6.2a, 6.3a and 6.4a) indicate that I.P. levels obtained from electrically polished surfaces are higher than those obtained from corresponding mechanically polished surfaces. This may confirm the rougher the metal surface the greater the area of contact. But as the axial force builds up it seems the probability of mechanical breakdown of oxide films on electropolished surfaces is higher than that on mechanically polished surfaces. This can be seen from Graphs 6.18b, 6.19b, 6.20b and 6.21b with corresponding Graphs of

6.1b, 6.2b, 6.3b and 6.4b. This could possibly be because of perturbation of the structure of the test sample surfaces caused by mechanical polishing.

Smoothed contact surfaces caused by repeated make and break of contact, such as connectors after being used several times, are usually an unwelcome phenomenon. Metallic contact members may be shaped to each other by repeated make and break of the contact, without current in the same position, resulting in flattening of the surfaces by elimination of the protuberances. When further contact is made the members meet at the points with a relatively small curvature and the contact spots may be produced merely by elastic yielding. In this state their films endure the deformation without rupturing. This fact was investigated by recording the 3rd-order I.P. levels obtained from an old (50 days) test sample pair made of copper with axial force at a constant incident power of 3.84W. A constant I.P. level of about -75dBW over a range of axial force less than 4N was recorded. At S = 4N mechanical breakdown occurred resulting in the I.P. level dropping down into the residual level. Then the power sources were switched off and finally after several times of repeating the make and break of contact again the 3rd-order I.P. level was recorded at an incident power of 3.84W with axial force. This time an almost constant level of about -70dBW was recorded over a whole range of axial force.

7.5 Electroplated Metal Contacts

Gold- and silver-plated brass produce very low I.P. levels at an axial force greater than 0.08N at P_{in} = 3.84W. Similar results were obtained from copper plated brass which

is certainly because of its electrical cleanliness.

It is evident when discussing the metallic coatings that in so far as these coatings are continuous the behaviour of the coated surface is practically identical with that of the metal coating in solid form. When, as is more often the case, the coating contains or develops pores, galvanic corrosion* of dissimilar metals arise. An important reason for using nickel plating on brass articles is to prevent season cracking[37]. Nickel and chromium fall into the class of cathodic coatings** when applied to such base metals as steel, brass, copper, zinc, aluminium or magnesium[37]. No important influence has been demonstrated with the many nickel plating processes[38]. It is true that the quality, cleanliness and smoothness of the base metal surface influence the porosity developed in the coating, but the effect of these variables themselves become less important as the thickness of the deposit is increased. The choice of the base metal may be influenced by the thickness of the coating required for satisfactory protection, e.g. a coating thickness of 30μ on steel was about equivalent to one of 25μ on zinc alloys or 10μ on the brasses[37]. The thickness of nickel on the brass test sample pairs was 30μ (this thickness was chosen with the consideration of skin effect) which gives a degree of

---

* Corrosion associated with the current of a galvanic cell (a cell made up of two dissimilar conductors in contact with an electrolyte or two similar conductors in contact with dissimilar electrolytes) made up of dissimilar electrodes.

** In terms of galvanic couples (galvanic corrosion), the metallic coatings fall into two general classes: those of which the metal coating is an anodic member of the couple, and those in which the metal coating is cathodic.

protection of about 80. It seems the results obtained from similar electroplated nickel-to-nickel (Graph 6.23) are to some extent similar to those obtained for oxygen free nickel-to-oxygen free nickel (Graph 6.4).

Cadmium coatings depend largely on the fact that cadmium combines to some extent the anodic behaviour** of zinc with a basic metal such as iron and protects the exposed areas of an iron surface by sacrificing itself[38]. Its ability to protect steel, particularly indoors, solder easily with non-corrosive flux (which may increase the non-linearity of the junctions) and its high chemical resistance against sea water[37] are important factors of cadmium coatings. The results obtained from similar electroplated cadmium-to-cadmium show that there was no electrical deformation at P_{in} = 3.83W but the film was broken at S = 1N (Graph 6.24). This could be expected because the rate of corrosion for cadmium is small.

7.6 Effect of Corrosion

An axial force of less than 0.08N was sufficient for a complete breakdown of an oxide film on the test sample pairs made of copper in three states, i.e. mechanically polished, electropolished and electroplated surfaces. However, Graphs 6.25, 6.26 and 6.27, the results of which were obtained from the corresponding similar metal-to-metal contacts, show the I.P. levels to be as high as those for stainless steel. In the light of the above observation an important conclusion which can be drawn is that the surface properties of the metal contact

---

** In terms of galvanic couples (galvanic corrosion), the metallic coatings fall into two general classes: those of which the metal coating is an anodic member of the couple, and those in which the metal coating is cathodic.

are of prime importance and responsible for the generation of I.P.'s. In other words any change in the surface properties such as corrosion, surface roughness of the oxide layer, electrical and mechanical deformation affect the non-linearity governed at the contact resulting in the changes of the I.P. levels.

Comparing the results obtained from the mechanically polished and electropolished test sample pairs (Graphs 6.25 and 6.26 respectively) also indicate that at a lower range of axial force (less than 8N) the rougher the surface is the lower the I.P. level, probably because more points are in contact, but the smoother the surface is the higher the probability of mechanical breakdown of the oxide film at a lower axial force which is probably caused by perturbances at the underlying layer of the base metal surface.

The statistical results obtained from the corroded steel-to-steel (Graphs 6.38 to 6.41) also indicate the importance of corrosion or surface properties on the metal contacts (see corresponding results, Graphs 6.6 to 6.17). It also indicates that, in general, an increase of Ni and Cr in the steel composition produces a lower I.P. level throughout the whole range of axial force, probably because of the protective characteristic of these two metals which may result in the formation of thinner oxide films on the steel surfaces.

7.6.1 Some explanation about frequency effect and explanatory measurement discussion

Graph 6.42 shows the variation of the 3rd-order I.P. level with the incident power at an axial force of 0.08N (see Section 6.8). The test sample pair which was made of copper,

was allowed to corrode inside the laboratory. It was therefore expected that an oxide film (Cu_2O) with a thickness of about 30Å could form on it[26]. By increasing the incident power some electrical deformation had occurred probably because of the reasons mentioned in Section 7.3. Finally, the repeatable variations were observed. These variations indicated the presence of oxide layers, because at higher axial forces (higher than 12N), the 3rd-order I.P. dropped down into the residual level indicating a mechanical breakdown of the oxide layers and therefore a perfect metal-to-metal contact. Furthermore, since the thickness of the oxide layer is less than 40Å, the non-linear tunnel resistance is responsible for the generation of I.P.'s (see Section 3.9).

When the power sources were switched off and the contact was allowed to cool down for about 5 hours, the variation of the 3rd-order I.P. level with the incident power was again repeatable at nearly the same levels. This indicated that the local temperature at the contact point(s) responds to the incident power very quickly otherwise it should not be repeatable at the same level.

Biasing the contact with a direct current of about 30mA did not change the surface properties and again a repeatable variation of the 3rd-order I.P. level, similar to that when it was not biased, was recorded. This could be expected by comparing the actual alternative current (about 0.4A total) at a maximum incident power with a 30mA bias current. But at a lower incident power level, the bias direct current is comparable with the high-frequency current and therefore the 3rd-order I.P. has a larger slope.

Because the rat-races used for the I.P. measurements are frequency sensitive (see Section 2.2.6), it was not possible to observe the effect of frequency on the same measuring set. Also, Graph 6.42 indicates that, comparison between the results obtained at L-band and those obtained at other frequency bands by other investigators[13,14,15] are complicated because of the effect of surface property to a large extent on the generation of I.P.'s which will mask the effect of frequency. Therefore a histogram in Graph 7.1 is produced for some spherical contact test sample pairs. In this graph, the spreads of the 3rd-order I.P. levels at L-, S- and C-bands at $P_{10} = P_{01} = 1.6W$ ($P_{in} \sim 3.2W$) and at an axial force of S = 10.65N for similar metal-to-metal contacts are illustrated. The spread of results at L-band at $P_{in} = 3.2W$ are obtained by extrapolating the results measured statistically (see Section 6.6.1) at $P_{in} = 3.84W$. The spread of results at S-band are obtained directly from the literature[13] and it represents the difference between first and second readings. The results at C-band have been obtained from unpublished results measured by H. Sanli*.

An attempt was made to compare the results at L-band with those obtained by R.H. Martin at E.R.A.[40,41] in the frequency range of 225-400MHz. He carried out measurements on a number of materials similar to those tested at L-band such as stainless steel (EN58B), beryllium copper, oxygen free copper, mild steel, brass, copper, aluminium and gold and nickel plating. Lack of sufficient information in his reports such as apparent areas of contact and also introducing the

---

* To be published in a Ph.D. Thesis at the University of Sheffield in 1978.

Graph 7.1 Spread of 3rd-Order I.P. Level at L, S and C bands
Spherical contacts $P_{in} \approx 3.2W$, $S \approx 10.65N$,
Residual level ≈ -106dBW

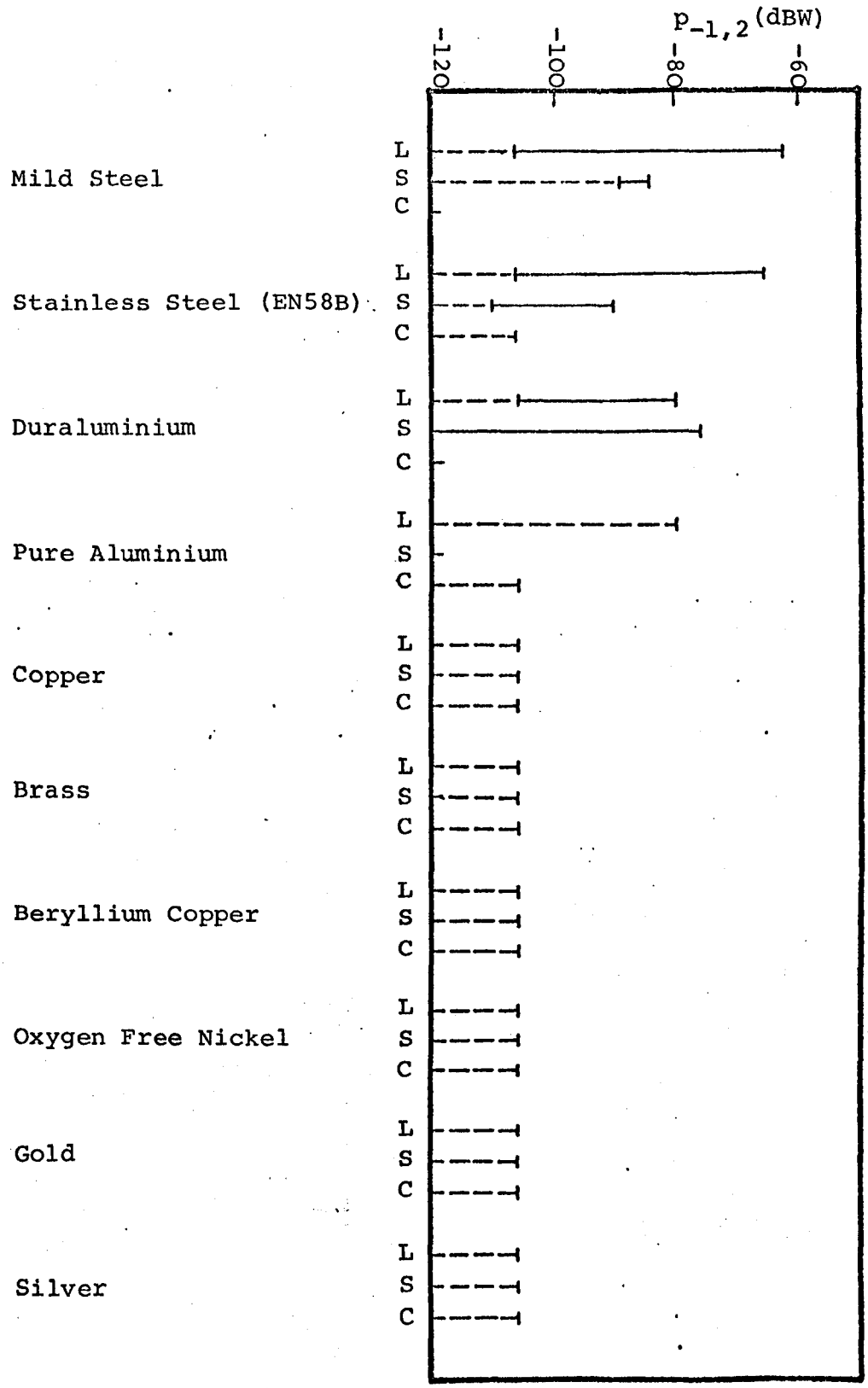

axial force applied on the contact as the pressure in Kg/mm^2 or MPa makes the quantitative comparison very difficult. Nevertheless, in spite of difficulties in quantitative comparison, there is a close qualitative agreement between some of his results and the present investigation at microwave frequencies e.g. mild steel, stainless steel and duraluminium produce high I.P. levels compared to copper and gold.

The generation of I.P.'s in a vast number of coaxial cables has been investigated by M.B. Amin and F.A. Benson[42,43] at L-, S- and C-bands. In their studies, the effect of frequency could easily be observed since the I.P. levels generated by a certain piece of a particular coaxial cable could be measured with different frequency band set ups. They have reported that the higher the frequency of the two fundamental signals, the higher will be the I.P. levels, probably because the currents crossing at the braid contacts increase with frequency. They also have reported that the composition of the materials of the braid-conductors is the most important parameter in the generation of I.P.'s in the coaxial cable at microwave frequencies. Braids with aluminium, stainless steel or nickel-plated copper wire were reported to generate the strongest 3rd- and 5th-order I.P.'s.

7.7 Conclusions

1. At perfect metal-to-metal contacts, the I.P. levels are within the residual level. This substantiates the argument that the thin insulating films (e.g. oxide films) are responsible for the generation of higher I.P. levels (higher than residual level).

2. The level of the I.P.'s depends on the surface properties of the contact metals.
3. At zero contact load, all the similar or dissimilar metal-to-metal contacts produce the highest level of I.P.'s independent of the surface roughness of the metal contacts.
4. The 3rd-order I.P. level was always higher than the 5th-order I.P. level at corresponding conditions (i.e. for a certain test sample pair measured at a corresponding incident power and applied axial force).
5. Electrical cleanliness is more important than surface roughness for the generation of low I.P. levels.
6. It seems that for thin insulating films (less than 40Å) the non-linear tunnel resistivity results in the generation of I.P.'s. Other effects such as the thermionic effect, space charge effect and semi-conducting property of the oxide film can be taken into account for the thicker oxide film. A thick perfect insulator (such as P.T.F.E. with a thickness of 0.1mm) behaved linearly although there was a capacitive coupling between the contact halves of the test sample pair.
7. As far as only the generation of I.P.'s is concerned, it seems that the non-linear I-V characteristic of the contact is more effective than the magnitude of the electrical contact resistance of the test sample pair.
8. An aged single piece (about 5 years inside the laboratory) of soldered-joints in cascade did not produce any detectable I.P. levels.

9. Single pieces of magnetic metals such as nickel and mild steel did not generate measurable I.P. levels.

10. Gold and silver produced very low I.P. levels which was probably because of their anti-corrosion characteristic and oxide films being very easy to remove by axial force.

11. The materials used for similar metal-to-metal contacts can be split into two groups :

Group I : Electrically clean copper, brass, oxygen-free copper, beryllium copper and oxygen-free nickel produce low I.P. levels.

Group II : Mild steel, stainless steel and duraluminium produce high I.P. levels.

The histogram in Graph 7.2 shows the relative levels of the I.P.'s produced by different test sample materials under a variety of contact surface conditions.

12. Dissimilar metal-to-metal contacts show that :

(i) any combination of metals of Group I as a test sample pair produce low I.P. levels.

(ii) any combination of Group II or Group I and II depends on the mechanical property of the base material and geometrical configuration of the contact halves. If both metals are hard such as mild steel and stainless steel, they produce a high I.P. level. If the spherical half is soft such as duraluminium and the flat half is hard such as stainless steel, the probability of mechanical breakdown at a lower range of axial force will increase and vice versa.

The histogram shown in Graph 7.3 compares the 3rd-order I.P. levels generated at the contact surfaces of some dissimilar metal-to-metal contacts.

13. Corroded test sample pairs, such as corroded-copper and nickel produced high I.P. levels which were comparable with those obtained from stainless steel (see Graph 7.2).

14. The smoother the surface, the higher the probability of mechanical breakdown at a lower range of axial force, although before breakdown they produce higher I.P. levels than those of rougher surfaces.

15. It seems that so far as the I.P. generation is concerned, the behaviour of cadmium- and nickel-electroplated brass are practically identical with those of electroplating metals in a solid form (both were 30μ thick)

16. All the steels tested produced high and comparable results.

17. It seems that the corroded steels with Ni and/or Cr content generated comparatively lower I.P. levels through the whole range of axial force (see histogram shown in Graph 7.4).

18. Whilst a theoretical approach might have clarified, some of the behaviour of the I.P.'s, because of the changeable behaviour of the contact point and extreme complexity of the I.P.'s generation, it was therefore considered prudent to base the proposed work on experimental observation.

L-Band

Graph 7.2 Similar Metal-to-Metal Contacts
Relative 3rd-Order I.P. Level at $P_{10} = P_{01} = 1.92W$
and S = 10.65N

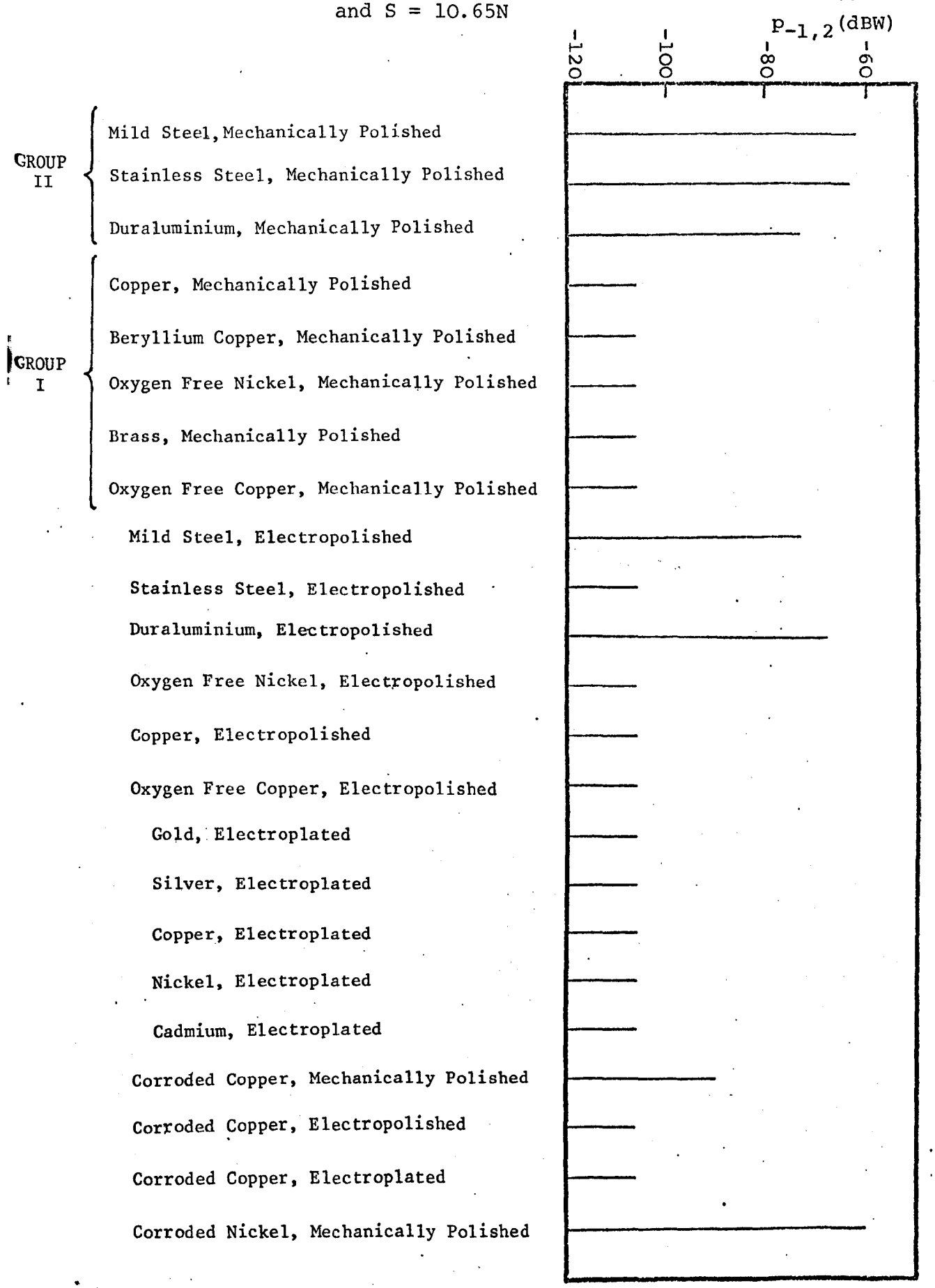

L-Band

Graph 7.3 Dissimilar Metal-to-Metal Contacts
Spread of 3rd-Order I.P. Level at
$P_{10} = P_{01} = 1.92W$ and S = 10.65N
(residual level = -106dBW)

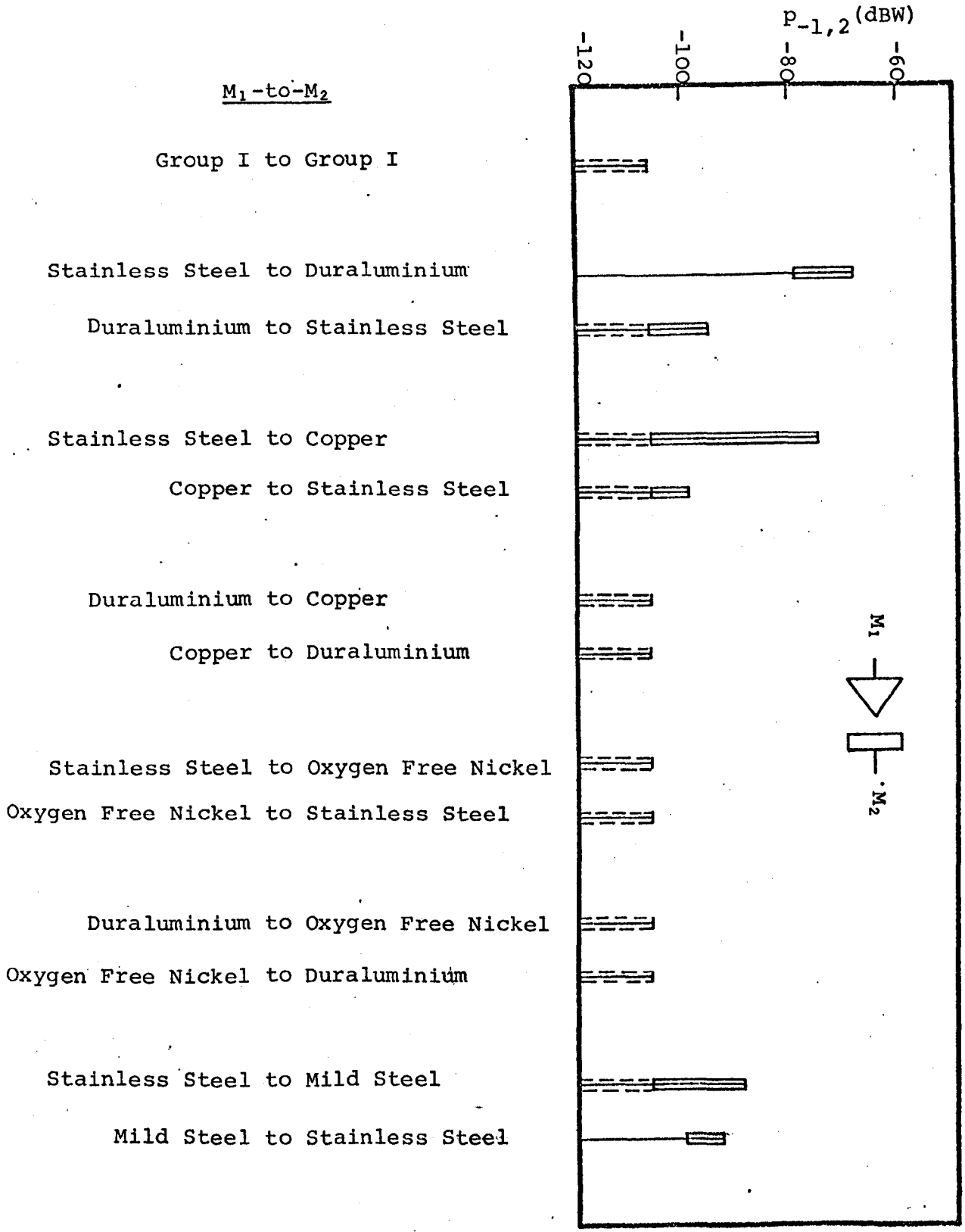

L-Band

Graph 7.4 Similar Corroded Steel-to-Steel

Spread of 3rd-Order I.P. Level at $P_{10} = P_{01} = 1.92W$ and $S = 10.65N$

----- Residual Level

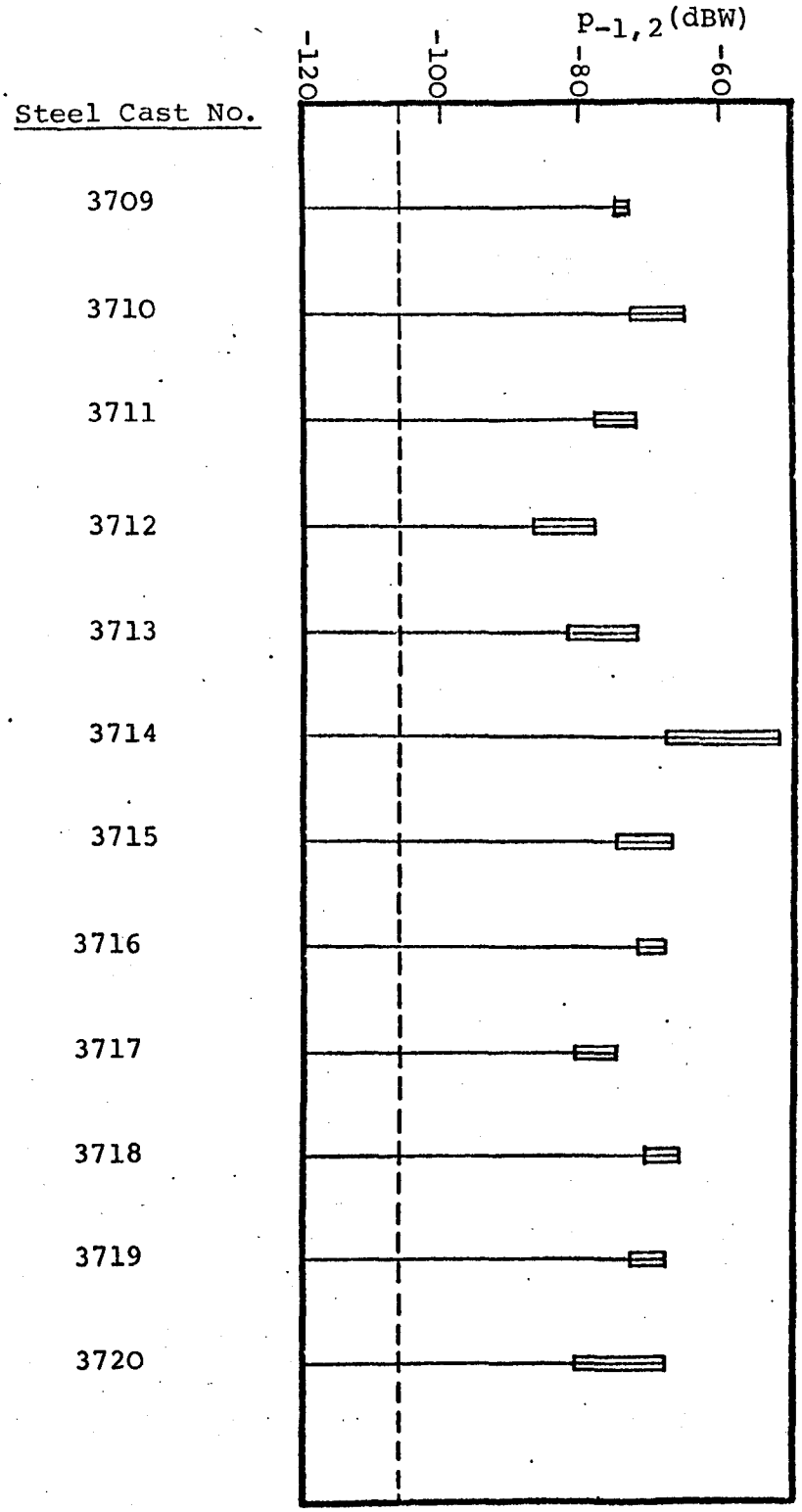

7.8 Suggestions for Future Work

It has been firmly established from the present study that an ideal metal contact should have the following characteristics: strength against the formation of any oxide layer on it (anti-corrosive), high electrical and thermal conductivities (to spread out the high local temperature produced at the contact point to prevent any further oxidation of the contact) and resistant to corrosion at a high temperature. If this attempt is hard to achieve, the oxide film should be very protective, thin and easily removed mechanically (one attempt could be soft metal with a ductile oxide film on it such as tin). Again, if this is also too difficult to achieve, the oxide layer should be thin, with a low dielectric constant, narrow forbidden bandwidth and low electrical resistivity. Therefore future work could be carried out to these statements.

Long term experiments on bright acid tin plating, because of its reasonably good corrosion resistance and solderability, on palladium 60% - silver 40% contact, whose movable contacts are gold overlayed which was reported[39] to have a contact performance (i.e. contact resistance and corrosiveness) as good as palladium, can be suggested.

In theoretical treatment of the problem of I.P. generation caused by surface films, several parameters related to the electrical and mechanical properties (e.g. semi-conductor properties, forbidden band, dielectric constant and hardness) of such films appear, making a detailed study of the surface properties of the contact material necessary.

One drawback experienced with the present measuring circuit is the high transmission path loss (≈15dB) of the I.P. signal which in effect means approximately a 15dB decrease in the sensitivity of the measuring circuit. The measuring circuit illustrated in Fig.7.1 where a multiplexor is used instead of a power combining unit (rat-races) and associated filters is suggested to overcome the above problem. The multiplexor is used to combine the fundamental signals, transmit them to the test location and direct the generated I.P. frequency to the detector. The multiplexor should have high isolation (more than 60dB) between ports 1-2, 1-3 and 2-3 to ensure that no power crosses from one signal source to another and to stop excessive power entering into the sensitive detector.

The sensitivity of the circuit can be increased by using the spectrum analyser with a parametric front-end amplifier where the I.P. measurements at a very low incident power (where the oxide layer is electrically undamaged) is necessary.

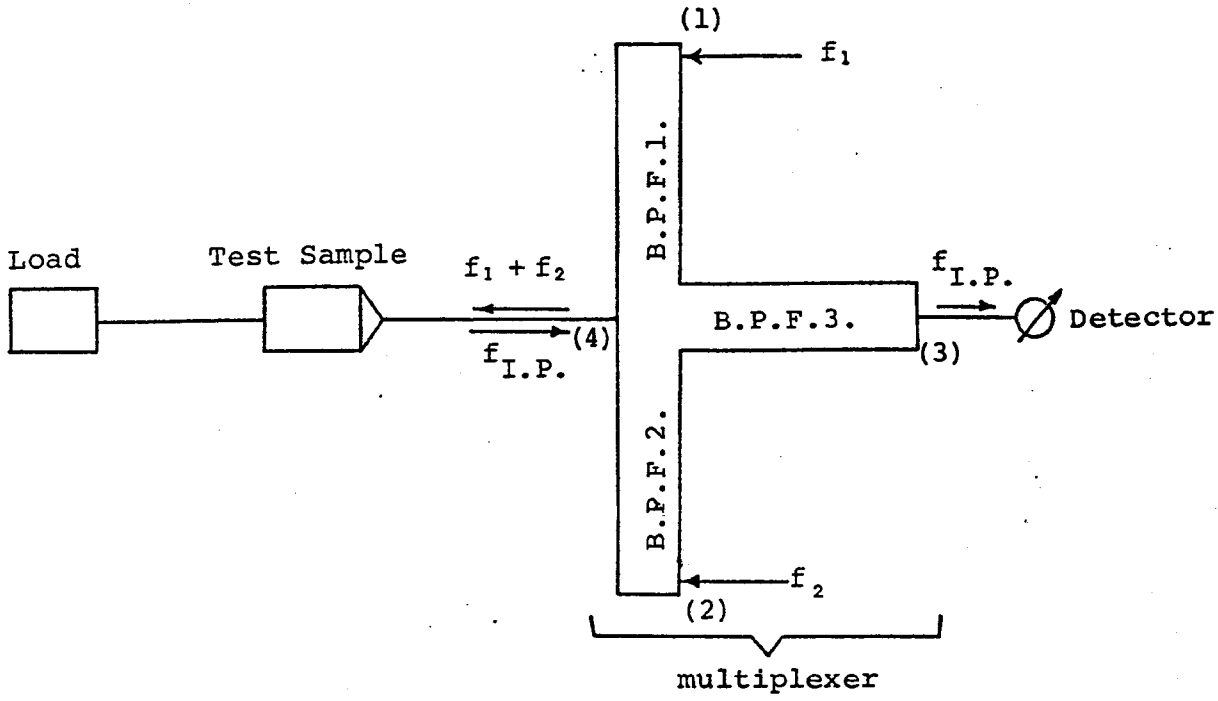
(1)
f_1
B.P.F.1.
Load
Test Sample
$f_1 + f_2$
$f_{I.P.}$
B.P.F.3.
$f_{I.P.}$
Detector
(4)
(3)
B.P.F.2.
f_2
(2)
multiplexer

Fig.7.1

APPENDIX I

Polynomial Non-Linearities[1] (see 1.2.1-1)

A non-linear device with input x and output y can be described by the power series

$$y = \sum_{k=0}^{\infty} a_k x^k \qquad (I.1)$$

The input is given by $x = x_1 + x_2 + \ldots + x_n$ where $x_i = E_i \cos\theta_i$ and $\theta_i = \omega_i t$ so eqn.(I.1) can be written as

$$y = \sum_{k=0}^{\infty} a_k \left(\sum_{m=1}^{n} x_m \right)^k \qquad (I.2)$$

The intermodulation of order N can be produced only by terms in eqn.(I.1) for which the degree k is greater than or equal to N, and that k must be odd or even as N is odd or even. It can be shown that the total intermodulation amplitude is :

$$V = \sum_{L=0}^{\infty} \frac{a_{N+2L}(N+2L)!}{2^{N+2L-1}} \sum_{q_1, q_2, \ldots q_n} \prod_{p=1} \frac{E_p^{|C_p| + 2q_p}}{(q_p + |C_p|)!\, q_p!} \qquad (I.3)$$

Equation (I.3) holds for $\theta = \sum_{i=1}^{n} C_i \theta_i \neq 0$ where C_i is an integer. For $\theta = 0$ (i.e. $N = \sum_{i=1}^{n} |C_i| = 0$) the formula becomes

$$V_{d.c.} = \sum_{L=0}^{\infty} \frac{a_{2L}(2L)!}{2^{2L}} \sum_{q_1, q_2, \ldots q_n} \prod_{p=1}^{n} \frac{E_p^{2q_p}}{(q_p!)^2} \qquad (I.4)$$

In either case, the multiple summation is over all non-negative integers q_i, such that $q_1 + q_2 + \ldots + q_n = L$. This summation may be represented more formally as :

$$\sum_{q_1, q_2, \ldots q_n} = \sum_{q_n=0}^{L} \sum_{q_{n-1}=0}^{L_{n-1}} \cdots \sum_{q_2=0}^{L_2}$$

where $L_i = L - q_n - q_{n-1} \cdots - q_{i+1}$ for $i = 1, 2, \ldots, n$ and $q_1 = L_1$.

For example assume an input of the form $x = E_1\cos\theta_1 + E_2\cos\theta_2$ and suppose that the amplitude of the output component $V\cos(-\theta_1 + 2\theta_2)$ is desired. In this case $n = 2$, $N = 3$, $C_1 = -1$, $C_2 = 2$.

So eqn.(I.3) becomes

$$V = \sum_{L=0}^{\infty} \frac{a_{3+2L}(3+2L)!}{2^{2+2L}} \sum_{\substack{q_1 \\ (q_1+q_2=L)}} \sum_{q_2} \frac{E_1^{1+2q_1} E_2^{2+2q_2}}{(q_1+1)!q_1!(q_2+2)!q_2!} \qquad (I.5)$$

APPENDIX II

Discontinuous non-linearities[2] (See 1.2.1-2)

A half-wave linear rectifier forms a simple rectifying characteristic. The behaviour of the rectifier can be elegantly represented as

$$v_{out} = \frac{v_{in}}{2} + \frac{v_{in}}{\pi} \int_0^\infty \frac{\sin(v_{in}\lambda)}{\lambda}\, d\lambda \qquad \text{(II.1)}$$

where v_{in} and v_{out} are input and output voltage respectively which satisfy the condition :

$$\left.\begin{aligned} v_{out} &= v_{in} \qquad v_{in} \geqslant 0 \\ &= 0 \qquad\quad v_{in} \leqslant 0 \end{aligned}\right\} \qquad \text{(II.2)}$$

when two frequencies are applied, substitution of $v_{in} = E_1 \sin\theta_1 + E_2 \sin\theta_2$ yields an integral which may be simplified by the relation :

$$\sin(\lambda\sin\theta) = 2 \sum_{k=0}^{\infty} J_{2k+1}(\lambda)\, \sin(2k+1)\theta \qquad \text{(II.3)}$$

It can then be routinely shown that the amplitude of intermodulation product, V_{mn} is:

$$V_{mn} = \frac{2}{\pi}(-1)^{\frac{m+n+2}{2}} \int_0^\infty \frac{J_m(\lambda E_1)\, J_n(\lambda E_2)\, d\lambda}{\lambda^2} \qquad m+n \text{ even} > 0$$

$$= 0 \qquad\qquad m+n \text{ odd} > 0$$

The case of $m+n = 0$ requires a special treatment which the reader can refer to the original paper.

Similarly when four frequencies are applied, i.e. $v_{in} = \sum_{i=1}^{4} E_i \cos\theta_i$, the amplitude of I.P. V_{mnpq} is :

$$V_{mnpq} = \frac{2}{\pi} (-1)^{\frac{m+n+p+q+2}{2}} \int \frac{J_m(\lambda E_1) J_n(\lambda E_2) J_p(\lambda E_3) J_q(\lambda E_4)}{\lambda^2} \, d\lambda$$

$$= 0 \qquad m+n+p+q \text{ odd except } m+n+p+q = 1$$

where $J_i(z)$ represents the Bessel function of the first kind.

APPENDIX III

Power Conversion in non-linear resistive element[8] (See 1.2.2.6)

In general, the current-voltage characteristic of a non-linear resistive element can be approximated by an exponential function (see Fig.3.7).

$$i(t) = I_o\left[e^{\gamma v(t)} - 1\right] \qquad \text{(III.1)}$$

where i(t) and v(t) are the current through the non-linear resistor and the voltage across it respectively. Then the relation between current and generator voltage follows from Eq. III.1 and Fig.3.7 :

$$i(t) = I_o\left[e^{\gamma(e(t)-2R_o i(t))} - 1\right] \qquad \text{(III.2)}$$

An explicit relation between current and generator voltage in the form of a power series is given by :

$$i(t) = \sum_{k=1}^{\infty} \frac{1}{K!} H_k(z)\, e^k(t) \qquad \text{(III.3)}$$

where $z = \frac{di}{de} = \frac{\gamma I_o}{1+2R_o\gamma I_o}$ evaluated at $e(t) = 0$

and $$H_k(z) = \frac{\gamma^{k-1}}{2R_o} \sum_{m=0}^{2K-1} \alpha_{k,m}(2R_o z)^m \qquad \text{(III.4)}$$

where $\alpha_{k,m} = m\,\alpha_{k-1,m} - 2(m-1)\alpha_{k-1,m-1} + (m-2)\alpha_{k-1,m-2}$

note $\alpha_{k,m} = 0$ for $m < 0$ and $m > 2k-1$

By expanding e^k when $e = \sum_{i=0}^{n} E_i \cos\theta_i$, it is simple to realize that i(t) which is a periodic function of time can be represented by the Fourier series. In a simplified case when

$e = E_{10}\cos 2\pi f_1 + E_{01}\cos 2\pi f_2 t$ we have

$$i(t) = \frac{1}{2} \sum_{r=-\infty}^{\infty} \sum_{s=-\infty}^{\infty} I_{rs}\, e^{j2\pi(rf_1+sf_2)t}$$

Then the power at the intermodulation frequency rf_1+sf_2 is

$$P_{rs} = \frac{1}{2} U_{rs} I_{rs} = R_o I_{rs}^2 \qquad \text{(III.5)}$$

As an example 3rd-order peak I.P. current, $I_{-1,2}$ is

$$I_{-1,2} = 0.75 \frac{H_3(z)}{3!} E_{10}E_{01}^2 + (\frac{15}{8} E_{10}^2 + \frac{5}{4} E_{01}^2) E_{10}E_{01}^2 \frac{H_5(z)}{5!}$$

$$+ (\frac{210}{64} E_{10}^4 + \frac{105}{16} E_{10}^2 E_{01}^2 + \frac{105}{64} E_{01}^4) E_{10}E_{01}^2 \frac{H_7(z)}{7!} + \ldots. \qquad \text{(III.6)}$$

APPENDIX IV

Design and Assembly Procedure of the Power Combining Unit (see Section 2.2.6)

Fig.2.2 illustrates the construction of the power combining unit. Two sheets of 2oz copper clad on both sides, single registration ⅛" polyguide* were sensitized and then photo-etched to form the cascaded hybrid rings (shown by broken lines) of the power combining unit.

Referring to Fig.IV-1 the following expressions were used

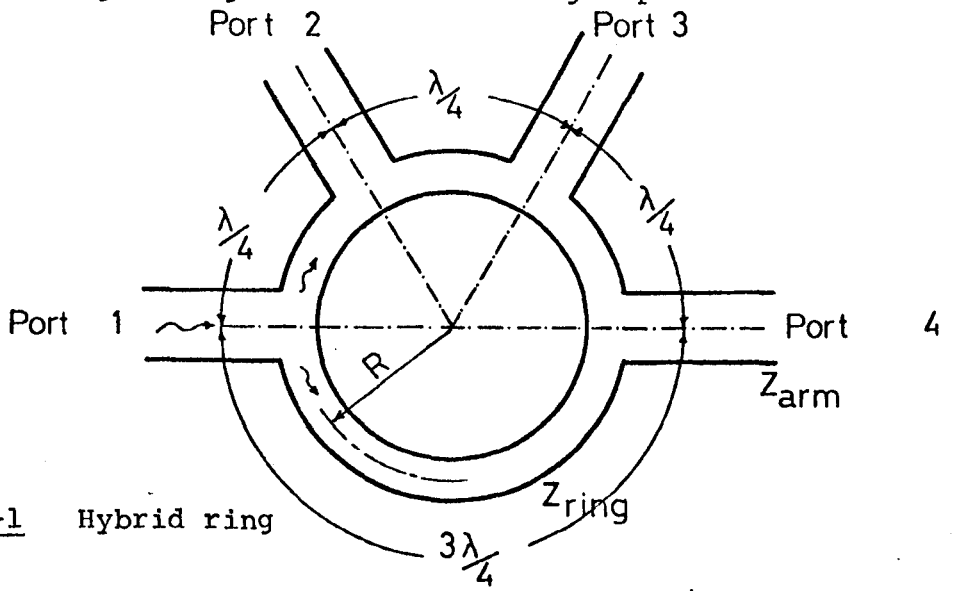

Fig.IV-1 Hybrid ring

to calculate the mean radius, R of the rat-races at a centre frequency of 1.5GHz.

$$2\pi R = (3/2)\lambda$$

$$\lambda = \lambda_{air}/\sqrt{\varepsilon_r}$$

where λ = wavelength in the dielectric medium

λ_{air} = free space wavelength = 0.2m (at f = 1.5GHz)

ε_r = relative dielectric constant of the medium

---

* Purchased from "Auriema Ltd."

Hence for polyguide (ε_r = 2.32) at a centre frequency of 1.5GHz, R = 31.35mm.

For good matching, the impedance of the ring and the impedance of the arm of the rat-race should be related by the following expressions[18] :

$$Z_{ring} = \sqrt{2}\, Z_{arm}$$

where the characteristic impedance of the arm, Z_{arm} = 50Ω.

Graph IV-1 obtained from Cohn's paper[19] can be used to calculate the width, W of the triplate transmission line where :

$t = 7.112 \times 10^{-2}$mm (0.0028"), $\frac{b}{2}$ = 3.175mm (0.125")

Doing so we obtain :

$$W_{arm} = 4.92\text{mm}$$

$$W_{ring} = 2.68\text{mm}$$

The power combining unit was then assembled as follows : Two sheets of polyguide having appropriate dimensions were photo-etched on each side. One of the sheets was completely etched of copper on one side and the other sheet was etched so that strips of copper forming the arms and rings of the rat-races remained. The etched faces of the two sheets of polyguide were then brought together so that unetched sides formed the grounded conducting planes. The unit was then cut to the shape and dimensions as shown in Fig.2.2, so that each arm of the rat-races intersects a side at a right angle. The unit was then sandwiched between the two brass plates.

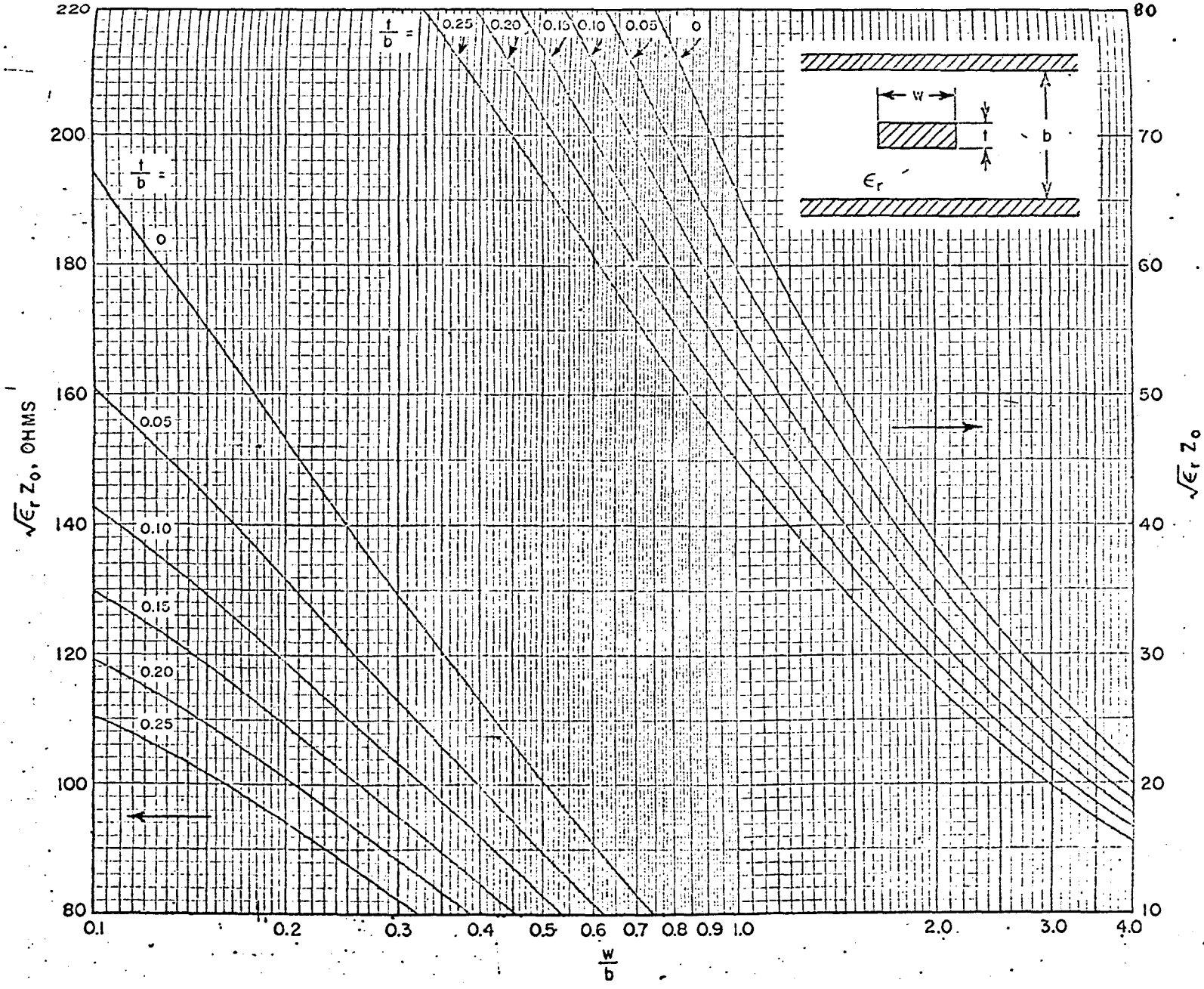

Graph IV.1 Z_0 vs w/b for various of t/b

APPENDIX V

Calculation of d.c. Constriction Resistance[27,p.13]

(see Section 3.4-1)

If "a" is the radius of the circular and single spot metal-to-metal contact, since it is very small compared with the contact member dimension we can approximate the semi contact as in Fig.V-1.

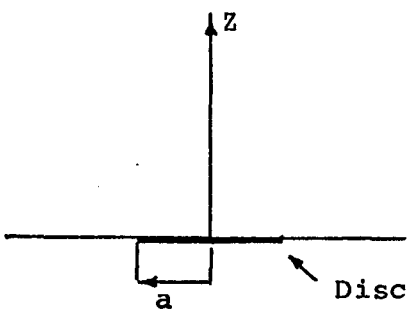

Fig.V-1

i.e. assuming a circular disc with radius "a" at Z = 0 of the contact member.

In the metal the potential satisfies Laplace's equation. Then in cylindrical coordinates because of symmetry with respect to ϕ we have, $V = V(r,Z)$ then :

$$\nabla^2 V = \frac{\partial^2 V}{\partial r^2} + \frac{1}{r}\frac{\partial V}{\partial r} + \frac{\partial^2 V}{\partial Z^2} = 0 \qquad \text{(V-1)}$$

Using Hankel transform, i.e. multiplying both sides of eqn.(V-1) by $r\,J_o(pr)$ and integrating with respect to r from 0 to infinity we get :

$$\frac{\partial^2 V}{\partial Z^2} - p^2 \frac{\partial^2 V}{\partial r^2} + \left| r\,J_o(pr)\,\frac{\partial V}{\partial r}\right|_{r=0}^{\infty} + p\left| r\,J_1(pr)\,V\right|_{r=0}^{\infty} = 0$$

Since V is not infinite at r = 0, the last two terms are equal to zero, then :

$$\frac{\partial^2 \bar{V}}{\partial Z^2} - p^2 \bar{V} = 0 \qquad \text{(V-2)}$$

where $\bar{V} = \int_0^\infty V\, r\, J_o(pr)\, dr$ (V-3)

From eqn. (V-2) we have :

$$\bar{V} = A(p)e^{-pZ} + B(p)e^{pZ}$$

since V and consequently $\bar{V}$ should vanish at infinity ($Z = \infty$), $B = 0$, then :

$$\bar{V} = A(p)e^{-pZ} \qquad \text{(V-4)}$$

Using the inverse Hankel transform :

$$V = \int_0^\infty A(p)e^{-pZ}\, p\, J_o(pr)\, dp \qquad \text{(V-5)}$$

The boundary condition is

$$\left.\begin{aligned} V &= V_o \qquad 0 \leqslant r < a \\ E_z &= -\frac{\partial V}{\partial Z} = 0 \qquad a < r \end{aligned}\right\} \text{ at } Z = 0$$

or

$$\left.\begin{aligned} &\int_0^\infty A(p)\, p\, J_o(pr)\, dp = V_o \qquad 0 \leqslant r < a \\ &\int_0^\infty A(p)\, p^2\, J_o(pr)\, dp = 0 \qquad r > a \end{aligned}\right\} \qquad \text{(V-6)}$$

If we select $pA(p) = \frac{2}{\pi} V_o \frac{\sin ap}{p}$ both boundary conditions of eqn. (V-6) are satisfied then :

$$V = \int_0^\infty J_o(rp) \frac{\sin ap}{p} e^{-pZ}\, dp \qquad \text{(V-7)}$$

and the current density is :

$$i_z = \frac{E_z}{\rho} = -\frac{1}{\rho}\frac{\partial V}{\partial Z} = -\frac{1}{\rho}\frac{2}{\pi} V_o \int_o^\infty J_o(rp) \sin ap\, e^{-pZ}\, dp$$

current density at Z = 0 is :

$$i_z = -\frac{1}{\rho}\int_o^\infty J_o(rp) \sin ap\, dp \qquad \text{(V-8)}$$

Integrating i_z over the surface of the disc gives the total current, I_t.

$$I_t = \int_o^\infty i_z \Big|_{z=0} 2\pi r\, dr = \frac{4a}{\rho} V_o \qquad \text{(V-9)}$$

From eqn.(V-9) we can obtain $\frac{V_o}{I_t} = \frac{\rho}{4a}$ which is half of the constriction resistance, therefore :

$$R_{d.c.} = \frac{\rho}{2a} \qquad \text{(V-10)}$$

Furthermore if I(r) is the total current from r = 0 to r of the disc then :

$$I(r) = \frac{4V_o\, a}{\rho}\left[1 - \sqrt{1 - (r/a)^2}\right] \qquad \text{(V-11)}$$

Therefore the variation of $I(r)/I_t$ vs $\frac{r}{a}$ is a circle with a centre at x=0, y=1 and a radius of 1. It is quite obvious that most of the direct current passes through the outer rim of the contact spot, e.g. when $\frac{r}{a} = 0.87$, the $\frac{I(r)}{I_t}$ is equal to 0.5, or in other words 50% of the total current passes through 13% of the outer part of the radius.

APPENDIX VI

1) Amplitude of the 3rd-Order I.P.'s Current (see Section 3.6)

$$I_{-1,2} = a_3(0.75V_{10}V_{01}^2)+a_5(1.25V_{10}V_{01}^4+1.875V_{10}^3V_{01}^2)+a_7(1.6406V_{10}V_{01}^6+6.5625V_{10}^3V_{01}^4+3.2812V_{10}^5V_{01}^2)+a_9(1.9687V_{10}V_{01}^8+14.7656V_{10}^3V_{01}^6+19.6875V_{10}^5V_{01}^4+4.9218V_{10}^7V_{01}^2)+a_{11}(2.2558V_{10}V_{01}^{10}+27.0703V_{10}^3V_{01}^8+67.6757V_{10}^5V_{01}^6+45.1172V_{10}^7V_{01}^4+6.7676V_{10}^9V_{01}^2)+a_{13}(2.5137V_{10}V_{01}^{12}+43.9892V_{10}^3V_{01}^{10}+175.957V_{10}^5V_{01}^8+219.9463V_{10}^7V_{01}^6+87.9785V_{10}^9V_{01}^4+8.7978V_{10}^{11}V_{01}^2)+a_{15}(2.7493V_{10}V_{01}^{14}+65.9838V_{10}^3V_{01}^{12}+384.906V_{10}^5V_{01}^{10}+769.812V_{10}^7V_{01}^8+577.359V_{10}^9V_{01}^6+153.9624V_{10}^{11}V_{01}^4+10.9973V_{10}^{13}V_{01}^2)+a_{17}(2.9675V_{10}V_{01}^{16}+93.4772V_{10}^3V_{01}^{14}+747.8174V_{10}^5V_{01}^{12}+2181.134V_{10}^7V_{01}^{10}+2617.3608V_{10}^9V_{01}^8+1308.6804V_{10}^{11}V_{01}^6+249.2724V_{10}^{13}V_{01}^4+13.3539V_{10}^{15}V_{01}^2)+a_{19}(3.1715V_{10}V_{01}^{18}+126.8619V_{10}^3V_{01}^{16}+1332.0497V_{10}^5V_{01}^{14}+5328.1989V_{10}^7V_{01}^{12}+9324.348V_{10}^9V_{01}^{10}+7459.4784V_{10}^{11}V_{01}^8+2664.0994V_{10}^{13}V_{01}^6+380.5856V_{10}^{15}V_{01}^4+15.8577V_{10}^{17}V_{01}^2)+a_{21}(3.3637V_{10}V_{01}^{20}+166.5062V_{10}^3V_{01}^{18}+2220.0829V_{10}^5V_{01}^{16}+11655.435V_{10}^7V_{01}^{14}+27973.044V_{10}^9V_{01}^{12}+32635.218V_{10}^{11}V_{01}^{10}+18648.696V_{10}^{13}V_{01}^8+4995.1864V_{10}^{15}V_{01}^6+555.0207V_{10}^{17}V_{01}^4+18.5009V_{10}^{19}V_{01}^2)+a_{23}(3.5459V_{10}V_{01}^{22}+212.7579V_{10}^3V_{01}^{20}+3510.506V_{10}^5V_{01}^{18}+23403.373V_{10}^7V_{01}^{16}+73720.626V_{10}^9V_{01}^{14}+117953.0V_{10}^{11}V_{01}^{12}+98294.168V_{10}^{13}V_{01}^{10}+42126.072V_{10}^{15}V_{01}^8+87762.65V_{10}^{17}V_{01}^6+780.1124V_{10}^{19}V_{01}^4+21.2758V_{10}^{21}V_{01}^2)+a_{25}(3.7195V_{10}V_{01}^{24}+265.9474V_{10}^3V_{01}^{22}+5318.9485V_{10}^5V_{01}^{20}+43881.325V_{10}^7V_{01}^{18}+175525.3V_{10}^9V_{01}^{16}+368603.13V_{10}^{11}V_{01}^{14}+421260.72V_{10}^{13}V_{01}^{12}+263287.95V_{10}^{15}V_{01}^{10}+87762.65V_{10}^{17}V_{01}^8+14627.108V_{10}^{19}V_{01}^6+1063.7897V_{10}^{21}V_{01}^4+24.177V_{10}^{23}V_{01}^2)+ \ldots\ldots\ldots$$

2) Amplitude of the 5th-Order I.P.'s Current (see Section 3.6)

$$I_{-2,3} = a_5(0.625V_{10}^2V_{01}^3)+a_7(1.6406V_{10}^2V_{01}^5+2.1875V_{10}^4V_{01}^3)+$$
$$a_9(2.9531V_{10}^2V_{01}^7+9.8437V_{10}^4V_{01}^5+4.9218V_{10}^6V_{01}^3)+a_{11}(4.5117V_{10}^2V_{01}^9+$$
$$27.0703V_{10}^4V_{01}^7+33.8379V_{10}^6V_{01}^5+9.0234V_{10}^8V_{01}^3)+$$
$$a_{13}(6.2842V_{10}^2V_{01}^{11}+58.6523V_{10}^4V_{01}^9+131.9678V_{10}^6V_{01}^7+87.9785V_{10}^8V_{01}^5+$$
$$14.6631V_{10}^{10}V_{01}^3)+a_{15}(8.2479V_{10}^2V_{01}^{13}+109.9731V_{10}^4V_{01}^{11}+$$
$$384.906V_{10}^6V_{01}^9+461.8872V_{10}^8V_{01}^7+192.453V_{10}^{10}V_{01}^5+21.9946V_{10}^{12}V_{01}^3)+$$
$$a_{17}(10.3863V_{10}^2V_{01}^{15}+186.9543V_{10}^4V_{01}^{13}+934.7717V_{10}^6V_{01}^{11}+$$
$$1744.9072V_{10}^8V_{01}^9+1308.6804V_{10}^{10}V_{01}^7+373.9087V_{10}^{12}V_{01}^5+31.159V_{10}^{14}V_{01}^3)+$$
$$a_{19}(12.6862V_{10}^2V_{01}^{17}+296.011V_{10}^4V_{01}^{15}+1998.0746V_{10}^6V_{01}^{13}+5328.1989V_{10}^8V_{01}^{11}+$$
$$6216.232V_{10}^{10}V_{01}^9+3196.9193V_{10}^{12}V_{01}^7+666.0248V_{10}^{14}V_{01}^5+42.2873V_{10}^{16}V_{01}^3)+$$
$$a_{21}(15.1369V_{10}^2V_{01}^{19}+444.0166V_{10}^4V_{01}^{17}+3885.145V_{10}^6V_{01}^{15}+$$
$$13986.522V_{10}^8V_{01}^{13}+23310.87V_{10}^{10}V_{01}^{11}+18648.696V_{10}^{12}V_{01}^9+6993.261V_{10}^{14}V_{01}^7+$$
$$1110.0414V_{10}^{16}V_{01}^5+55.5021V_{10}^{18}V_{01}^3)+a_{23}(17.7298V_{10}^2V_{01}^{21}+$$
$$638.2738V_{10}^4V_{01}^{19}+7021.012V_{10}^6V_{01}^{17}+32764.723V_{10}^8V_{01}^{15}+73720.626V_{10}^{10}V_{01}^{13}+$$
$$84252.144V_{10}^{12}V_{01}^{11}+49147.084V_{10}^{14}V_{01}^9+14042.024V_{10}^{16}V_{01}^7+1755.253V_{10}^{18}V_{01}^5+$$
$$70.9193V_{10}^{20}V_{01}^3)+a_{25}(20.4575V_{10}^2V_{01}^{23}+886.4914V_{10}^4V_{01}^{21}+11967.634V_{10}^6V_{01}^{19}+$$
$$70210.12V_{10}^8V_{01}^{17}+204779.52V_{10}^{10}V_{01}^{15}+315945.54V_{10}^{12}V_{01}^{13}+263287.95V_{10}^{14}V_{01}^{11}+$$
$$117016.87V_{10}^{16}V_{01}^9+26328.795V_{10}^{18}V_{01}^7+2659.4743V_{10}^{20}V_{01}^5+$$
$$88.6491V_{10}^{22}V_{01}^3)+ \ldots\ldots$$

3) Amplitude of the 3rd-Order I.P.'s Current When $V_{10} = V_{01} = V$
(see Section 3.6)

$$I_{-1,2}(V) = 0.75a_3V^3+3.125a_5V^5+11.48437a_7V^7+41.34375a_9V^9+$$
$$148.88672a_{11}V^{11}+539.18262a_{13}V^{13}+1965.77a_{15}V^{15}+$$
$$7214.0637a_{17}V^{17}+26634.651a_{19}V^{19}+98871.054a_{21}V^{21}+$$
$$368801.71a_{23}V^{23}+1381624.8a_{25}V^{25}+ \ldots\ldots$$

4) Amplitude of the 5th-Order I.P.'s Current When $V_{10} = V_{01} = V$
(see Section 3.6)

$$I_{-2,3}(V) = 0.625a_5V^5+3.828125a_7V^7+17.71875a_9V^9+74.44336a_{11}V^{11}+$$
$$299.5459a_{13}V^{13}+1179.462a_{15}V^{15}+4590.7678a_{17}V^{17}+$$
$$17756.434a_{19}V^{19}+68449.191a_{21}V^{21}+263429.79a_{23}V^{23}+$$
$$1013191.5a_{25}V^{25}+ \ldots..$$

APPENDIX VII

Calculation of U_{mn} and W_{mn} (see Section 3.7)

The U_{mn} and W_{mn} coefficients can be found by the integration of eqn.(3.7-9) throughout the rectangle bounded by $x = \pm\pi$, $y = \pm\pi$. From eqn.(3.7-7) it is clear that the function $U(x,y)$ may be represented by a surface which crosses the xy-plane through the curve,

$$\cos x + k \cos y = 0 \qquad \text{(VII-1)}$$

Since the function $U(x,y)$ is symmetric about the x and y axes, the boundaries of integration for a fixed value of k and several values of C according to eqns. (3.7-5) and (3.7-6) are shown in Graph VII-1 for only a quadrant of the rectangle bounded by $x = \pm\pi$ and $y = \pm\pi$. From the symmetry of the regions about the x and y axes we deduce at once that the sine coefficients, $W_{\pm mn}$ must vanish and that the cosine coefficients, $U_{\pm mn}$, may be obtained by integrating throughout one quadrant only and multiplying by four. We therefore obtain, on substitution of proper limits :

$$U_{mn} = \frac{2}{\pi^2} \int_0^{\pi} \int_0^{\pi} U(x,y) \cos mx \cos ny \, dx \, dy \qquad \text{(VII-2)}$$

From eqn.(VII-2), considering that

$$U(x,y) = U(\pi - x, \pi - y) \qquad \text{(VII-3)}$$

we deduce that

$$U_{mn} = 0 \quad \text{for } m+n = \text{even}$$

and for m+n odd the eqn.(3.7-10) can be obtained.

The integration of eqn.(3.7-10) for m+n odd by referring to Graph VII-1 can be simplified as two following cases :

(a) $0 \leqslant c \leqslant 1-k$

$$U_{mn} = \frac{4E_{10}}{\pi^2}\{c\int_{y=0}^{\pi}\cos ny\,dy\int_{x=0}^{\beta_1}\cos mx\,dx + \int_{y=0}^{\pi}\cos ny\,dy\int_{x=\beta_1}^{\beta_2}(\cos x + k\cos y)\cos mx\,dx\} \qquad \text{(VII-4)}$$

(b) $1-k < c \leqslant 1+k$

$$U_{mn} = \frac{4E_{10}}{\pi^2}\{c\int_{y=0}^{\beta}\cos ny\,dy\int_{x=0}^{\beta_1}\cos nx\,dx + \int_{y=0}^{\beta}\cos ny\,dy\int_{x=\beta_1}^{\beta_2}(\cos x + k\cos y)\cos mx\,dx$$
$$+ \int_{y=\beta}^{\pi}\cos ny\,dy\int_{x=0}^{\beta_2}(\cos x + k\cos y)\cos mx\,dx\} \qquad \text{(VII-5)}$$

where $\beta_1 = \cos^{-1}(c - k\cos y)$ (VII-6)

$\beta_2 = \cos^{-1}(-k\cos y)$ (VII-7)

$\beta = \cos^{-1}(\frac{c-1}{k})$ (VII-8)

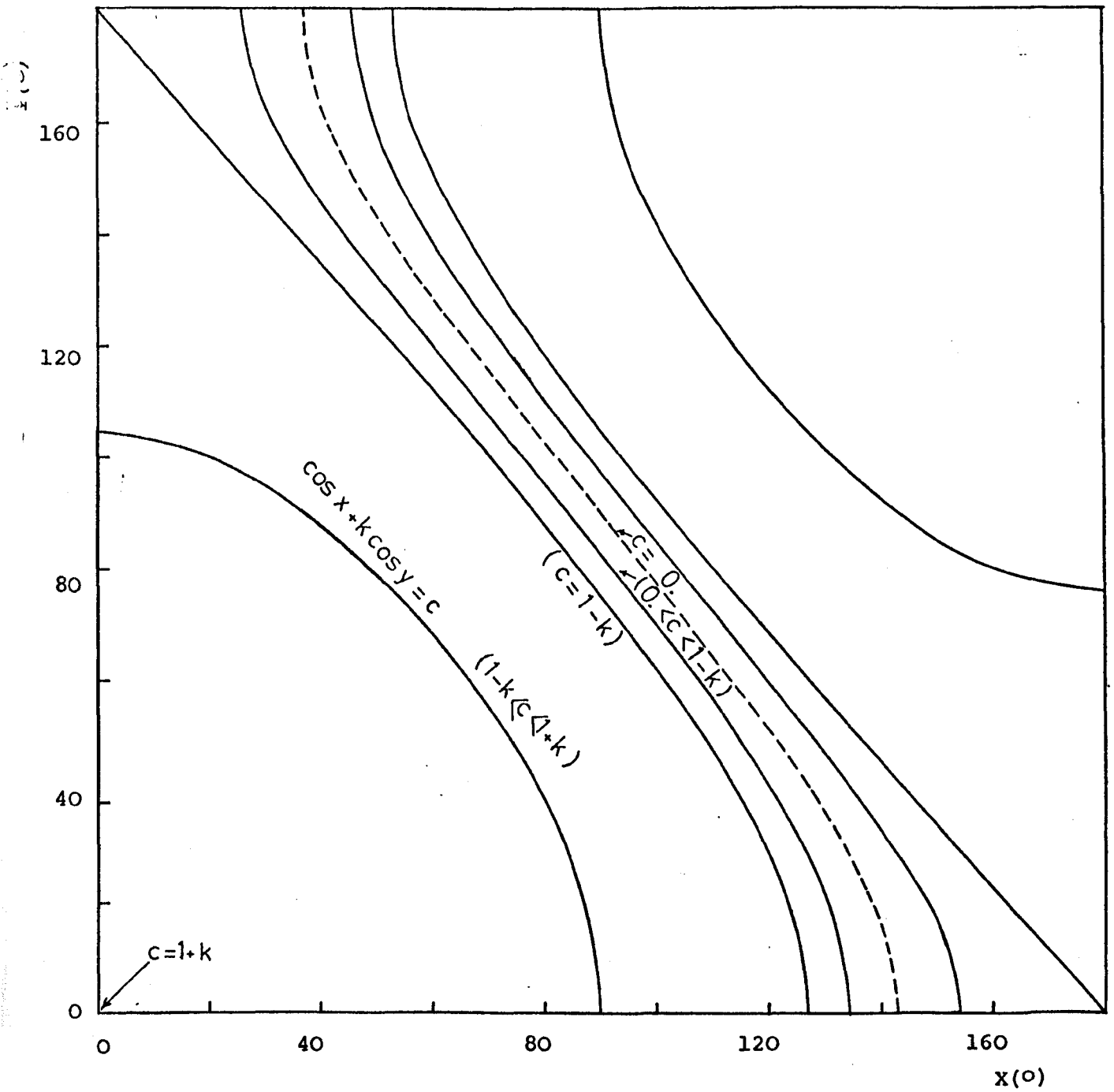

Graph VII-1 Region of integration for determination of the coefficients in the double Fourier series expansion of U(x,y).

APPENDIX VIII

Approximate Formula for Calculation of 5th-Order from the 3rd-Order I.P. (see Section 3.8)

By applying $I_{-1,2}(E)$ and $I_{-2,3}(E)$ from Appendix VI parts 3 and 4 into eqn.(3.8-2) one can obtain :

$$\begin{aligned} \sum_{m=1}^{n} f_m e_m &= g_1 \\ \sum_{m=1}^{n} f_m e_m^2 &= g_2 \\ \sum_{m=1}^{n} f_m e_m^3 &= g_3 \\ &\vdots \\ \sum_{m=1}^{n} f_m e_m^{2n} &= g_n \end{aligned} \qquad \text{(VIII-1)}$$

where b_ms and c_ms coefficients are related to f_ms and e_ms as follows :

$$\begin{aligned} b_m &= \frac{f_m}{\sqrt{e_m}} \\ c_m &= \sqrt{e_m} \end{aligned} \qquad \text{(VIII-2)}$$

and g_i can be calculated by dividing the coefficients of the same degree of E in expansion of $I_{-1,2}(E)$ and $I_{-2,3}(E)$ in Appendix VI parts 3 and 4.

The e_ms are the roots of a polynomial equation of the form :

$$e^n + \sum_{k=1}^{n} c_k e^{k-1} = 0 \qquad \text{(VIII-3)}$$

where

$$g_{i+n} + \sum_{k=1}^{n} c_k g_{i+k-1} = 0 \quad (i=1,2,\ldots,n) \qquad \text{(VIII-4)}$$

The C_k coefficients can be obtained by solving the set of simultaneous linear equations in eqn.(VIII-4). The f_ms are then found by inserting the roots of eqn.(VIII-3) into eqn.(VIII-1) and solving.

APPENDIX IX

The compositions of electropolishing, the electric current I, applied potential v, time of operating t and the initial temperature T necessary for electropolishing the test sample pairs were as follows :

Material	Composition	v(V)	I(A)	t(min.)	T(oc)
Copper	700ml orthophosphoric acid 350ml distilled water	1	0.17	15	20
Oxygen free Copper	"	1	0.15	17	20
Oxygen free Nickel	196ml H_2SO_4 15ml H_2PO_3 90ml H_2O	10	1.45	5	15
Stainless Steel EN58B	5% perchloric acid 95% glacial acetic acid	90(initially) 70(after inserting sample inside electrolyte)	3	1	14
Mild Steel	"	90	3	0.5	14

Table IX-1

The electropolishing of the aluminium alloy was done by local electrolytic polishing[30] (P.A. Jaquet method) with the Ellopol, Model APM.

Electrolyte: Bupac with Ogipol or preferably Sharpol plug. The applied voltage is v = 39V, quick dabs at first, then shower (contact is 1 to 4 seconds at intervals of 1 to 3 seconds), at t = 30 ∿ 60 seconds.

REFERENCES

1. Sea, Ronald G. :"An Algebraic Formula for Amplitudes of Intermodulation Products Involving an Arbitrary Number of Frequencies". Proc. I.E.E.E., Vol.56, p.1388, Aug. 1968.

2. Bennett, W.R. :"New Result in the Calculation of Modulation Products". B.S.T.J., Vol.12, p.228, 1933.

3. Foster, D.E. :"A New Form of Interference-External Cross Modulations". R.C.A. Review, Vol.1, No.4, p.18, 1937.

4. Ebel, A.J. :"A Note on the Sources of Spurious Radiation the Field of Two Strong Signals". Proc. I.E.R.E., Vol.30, p.81, 1942.

5. Blake, K.W. :"External Cross-Modulation in the 100MHz Band". Journal I.E.E., Vol.94, Part IIIA, p.659, 1947.

6. Reiffen, B., and Grayzel, A.I. :"A Non-linear Effect in Passive U.H.F. Transmission Systems". Massachusetts Institute of Technology, Lincoln Laboratory, Lexington, Massachusetts, p.511-523.

7. Löw, V.W. :"An Investigation of the Production of Combination Frequencies when Waveguides and Coaxial Components are used with more than one Transmission Frequency". Frequency, Vol.17, No.3, p.94, March 1963.

8. Rutz-Philip, E.M. :"Power Conversion in Non-linear Resistive Element Related to the Interference Phenomena". I.B.M. Journal, p.550, September 1967.

9. Cox, R.D. :"Measurements of Waveguide Components and Joint Mixing Products in 6GHz Frequency and Diversity System". I.E.E.E. Trans. on Communication Technology, Vol. Com-18, No.1, p.33-37, February 1970.

10. Mason, H.P. :"Multiple Channel U.H.F. Reception on Naval Ships". The Radio and Electronic Engineering, Vol.43, No.5, p.299-311, May 1973.

11. Ebenzer, D.R. :"A study of the Generation of Intermodulation Products". MOD Contract report N/C, p.48/47268/67/4B. 201, University of Southampton, September 1972.

12. Betts, J.A., and Ebenezer, D.R. :"Intermodulation Interference in Mobile Multiple-Transmission Communication Systems Operating at High Frequencies (3 ∿ 30MHz)". Proc. I.E.E., Vol.120, No.11, p.1337, November 1973.

13. Bayrak, M. :"Non-linearities in Transmission Lines and Connectors at Microwave Frequencies". Ph.D. Thesis, University of Sheffield, 1973.

14. Bayrak, M., and Benson, F.A. :"Intermodulation Products from Non-linearities in Transmission Lines and Connectors at Microwave Frequencies". Proc. I.E.E., Vol.122, No.4, p.361-367, April 1975.

15. Sanli, H. :"Non-linear Effects in Contacts and Coaxial Cables at Microwave Frequencies". M.Eng. Thesis, University of Sheffield, 1975.

16. Levy, R. :"Hybrid Junctions". Electronic and Radio Engineering, Vol.36, p.308-312, 1959.

17. Maloratskiy, L.G. :"Analysis of a Hybrid-ring". Telecommunication and Radio Engineering, Vol.22, No.9, p.95-99, Sept. 1967.

18. Blackband, W.T. :"Intersheaths Between Cable Braids". Royal Aircraft Establishment, Technical Report 72151, September 1972.

19. Cohn, S.B. :"Characteristic Impedance of the Shielded Strip Transmission Line". I.R.E. Trans., Vol. MTT-2, No.2, p.52-57, July 1954.

20. Harvey, A.F. :"Microwave Engineering" Hand Book, Academic Press, 1963.

21. Simmons, J.G. :"Generalized Formula for the Electric Tunnel Effect between similar Electrodes separated by a Thin Insulating Film". Journal of Applied Physics, Vol.34, No.6, June 1963, p.1793.

22. Simmons, J.G. :"Electric Tunnel Effect between Dissimilar Electrodes Separated by a Thin Insulating Film". Journal of Applied Physics, Vol.34, No.9, p.2581, September 1963.

23. Reark, R.J. and Young, W.C. :"Formulas for Stress and Strain", 5th-Edition. McGraw-Hill Book Company, 1975.

24. Simmons, J.G. :"Potential Barriers and Emission-Limited Current Flow Between Closely Spaced Parallel Metal Electrodes". Journal of Applied Physics, Vol.35, No.8, p.2472, August 1964.

25. Whinnery, J.R. and Jamieson, H.W. and Theo, Eloise Robbins :"Coaxial-Line Discontinuities". Proceedings of the I.R.E., p.695, November 1944.

26. Holm, R. :"Electric Contacts Handbook". 3rd-Edition, Springer-Verlag, Berlin, 1958.

27. F. Llewellyn Jones, :"The Physics of Electrical Contacts", Oxford at the Clarendon Press, 1957.

28. Fisher, J.C. and Gizever, I. :"Tunnelling Through Thin Insulating Layers". Journal of Applied Physics, Vol.32, No.2, p.172, February 1961.

29. Medhurst, R.G. and Harris, R.A. :"Calculation of Non-linear Distortion Products". Proc. I.E.E., Vol.115, No.7, July 1968.

30. Jacquet, P. :"Non-destructive Techniques for Macro- and Micrographic Surface Examination of Metallic Specimens (Electrolytic Local Polishing and Replica Technique)". Proc. A.S.T.M., Vol.57, p.1290, 1957.

31. Greenwood, J.A. and Williamson, J.B.P. :"Contact of Nominally Flat Surfaces". Burndy Corporation Research Div., Norwalk, Connecticut, U.S.A., April 1966.

32. Harda, S. and Mano, K. :"Constriction Resistance of Electric Contact between Rough Flat Surface and Smooth Flat Surface Considering Surface Roughness". The Journal of the Institute of Electronic and Communication Engineers of Japan, Vol.50, No.9, p.5, Sept. 1967.

33. Hisakado, T. :"Effect of Surface Roughness and Surface Film on Contact Resistance", Wear, Vol.44, pp.345-359, 1977.

34. Samsonov, G.V. Translated from Russian by : C. Nigel Turton and Tatiana I. Turton :"The Oxide Handbook". IFI/Plenum Publishing Corporation, 1973.

35. Bowden, F.B., and Tabor, D. :"Friction and Conduction of Metals. The Role of Surface Films". Proceeding of the 2nd International Symposium on Electric Contact Phenomena, Graz, Austria, pp.469-491, May 4, 5, 6, 1964.

36. Hauffe, K. :"Oxidation of Metals" (Book). Based on the German edition of 'Oxydation Von Metallen & Metallegierugen', Plenum Press, New York, 1965.

37. Evans, Ulick, R. :"The Corrosion and Oxidation of Metals: Scientific Principles and Practical Applications". Hand Book. Edward Arnold Ltd., 1960.

38. Burns, R.M. and Bradley, W.W. :"Protective Coatings for Metals". Reinhold Publishing Corporation, New York, 1955, second edition.

39. Takuya, Tanii, Yuji Otsuka, Kozo Toma and Masaji Takahashi: "Development of Palladium-Silver Contacts". The Transactions of The IECE of Japan, Vol.E59, No.10, p.41, October 1976.

40. Martin, R.H. :"Non-linearity in RF Cables and Connectors". ERA Report 2885, under MOD(PE), CVD Contract N/CP 541/73, Reference RP 34-11, April 1976.

41. Martin, R.H. :"Non-linearity in RF Cables and Connectors Supplementary Results at UHF". ERA Report 77-2022, under MOD(PE), CVD Contract N/CP 541/73, Reference RP 34-17, October 1977.

42. Amin, M.B. :"Generation of Intermodulation Products in Coaxial Cables and Connectors at Microwave Frequencies". Ph.D. Thesis, University of Sheffield, 1977.

43. Amin, M.B. and Benson, F.A. :"Non-linear effects in coaxial cables at microwave frequencies". Electronic Letters, Vol.13, No.25, pp.768-770, 8 Dec. 1977.